Development of an Integrated System for the Simulation and Assessment of Produced Water Discharges from Offshore Platforms

Lin Zhao

A Thesis

In the Department

of

Building, Civil and Environmental Engineering

Presented in Partial Fulfillment of the Requirements

For the Degree of

Doctor of Philosophy (Civil Engineering) at

Concordia University

Montreal, Quebec, Canada

April 2012

CONCORDIA UNIVERSITY
SCHOOL OF GRADUATE STUDIES

This is to certify that the thesis prepared

By: Lin Zhao

Entitled: Development of an Integrated System for the Simulation and Assessment of Produced Water Discharges from Offshore Platforms

and submitted in partial fulfillment of the requirements for the degree of

Doctor of Philosophy (Civil Engineering)

complies with the regulations of the University and meets the accepted standards with respect to originality and quality.

Signed by the final examining committee:

Dr. Christopher W. Trueman	Chair
Dr. Sebastien Sauve	External Examiner
Dr. Mingyuan Chen	External to Program
Dr. Tarek Zayed	Examiner
Dr. Fariborz Haghighat	Examiner
Dr. Zhi Chen, Dr. Kenneth Lee	Thesis Supervisor

Approved by

_____
Chair of Department or Graduate Program Director

April 19, 2012

_____
Dean of Faculty

ABSTRACT

Development of an Integrated System for the Simulation and Assessment of Produced Water Discharges from Offshore Platforms

Lin Zhao, Ph.D.

Concordia University, 2012

Techniques for modeling of marine pollution have been studied for decades. Specialized modeling methods have been used to simulate the dispersions of pollutants from offshore outfalls. Produced water, the largest volume waste stream discharged from offshore oil and gas production activities, is a complex mixture of dissolved and particulate organic and inorganic chemicals including metals and hydrocarbons. In recent years, the growing importance and interest in the ocean environment assessment has urged further evaluation of produced water impacts on the marine ecosystem. This thesis study describes an integrated system for the modeling and assessment of produced water discharges in coastal area. The system integrates ocean circulation simulation, pollutant fate and transport modeling that couples near field mechanisms and far field processes, and risk assessment approaches where exposure risks and probabilistic risks are evaluated.

A literature survey is first introduced to review and present capabilities and limitations of the most widely used methods and models associated with assessment of the impact of marine pollution. This review identified the need for an integrated system with configurations of numerical schemes of Princeton Ocean Model (POM) for ocean circulation simulation, a Lagrangian method to simulate near field transport processes in three dimensional cross flows, and a numerical solution for far field transport modeling. The physical models are dynamically integrated to ensure mass and energy conservation.

Furthermore to assess risks, a modified Monte Carlo method which uses a statistical model to establish the relationship between uncertainty parameters and output concentrations is integrated with physical modeling system along with risk characterization approaches to map risk levels.

Evaluation and field validations are conducted for each individual sub-models and for the overall integrated modeling results. Specifically, the near field model is validated against a field study performed in USA platform located about 100 miles of New Orleans Louisiana. The computational efficiency and accuracy of the far field model are evaluated through test cases in comparison with concentration distribution results generated from an exact analytical solution and a RWPT (Random Walk Particle Tracking) method. Validations of ocean circulation results and the integrated produced water dispersion results are conducted in a case study carried out on the Grand Banks of Newfoundland, Canada. Validations show good performance of the developed modeling system which is used to provide satisfactory 3D simulation of marine pollutant dispersion for effective assessment and management of offshore waste discharges. Finally, a risk assessment is carried out to predict risks associated with predicted lead and benzene concentration resulting from potential future produced water discharges in the East Coast of Canada. This research study provide a tool for the modeling of complex transport processes in the coastal area, and improved methods for risk assessment of produced water impacts on the regional water environment.

ACKNOWLEDGEMENTS

I would like to express my sincere thanks and appreciation to my advisor, Dr. Zhi Chen, for his patience, guidance and ensuring financial support throughout my studies in Concordia University. His constant inspiration has encouraged me to furnish my best effort, leading to the successful completion of the present study and submission of the thesis in the present form.

My deepest gratitude goes to my co-supervisor, senior research scientist at the COOGER research centre at the Fisheries and Oceans Canada, Dr. Kenneth Lee, who contributed to the present research and supported me extensively including financial support, field cruises to the Hibernia site, and field data for model validations. It was a great opportunity to work with specialists with a vast knowledge of research and with enormous practical and real site experiences, which improved my scientific knowledge tremendously.

I would like to acknowledge the professional sample analysis work by Prof. Renata Bailey at the University Regina. I am also very grateful to Ms. Susan Cobanli and Dr. Haibo Niu from the Fisheries and Oceans Canada for their professional sample analysis work, insightful remarks, and continuous support of my research studies.

This study was funded part by the National Sciences and Engineering Research Council of Canada (NSERC), Fisheries and Oceans Canada (DFO), and Natural Resources Canada's (NRCan) program of Energy Research and Development (PERD).

TABLE OF CONTENTS

CHAPTER 1: INTRODUCTION

CHAPTER 2: LITERATURE REVIEW

CHAPTER 3: DEVELOPMENT OF THE THREE DIMENSIONAL NUMERICAL

MODELING AND RISK ASSESSMENT SYSTEM

CHAPTER 4: STUDY CASE AND FIELD INVESTIGATION

CHAPTER 5: 3D OCEAN CIRCULATION MODELING IN THE STUDY AREA

CHAPTER 6: EVALUATION AND FIELD VALIDATION OF POLLUTANT

FATE AND TRANSPORT MODELS

CHAPTER 7: MODELING AND ASSESSMENT OF POLLUTANT DISPERSION RESULTING FROM PRODUCED WATER DISCHARGES AT STUDY SITE

CHAPTER 8: DISCUSSION

CHAPTER 9: CONCLUSION AND RECOMMENDATION

List of Figures

xiii

List of Tables

List of Symbols

x, y, z conventional Cartesian coordinates

σ sigma vertical coordinate

H bottom depth (L)

η surface elevation (L)

U, V horizontal velocities (L/t)

$W(\omega)$ vertical velocity (L/t)

D equals $H + \eta$ is the total elevation of the surface water (L)

t time (t)

K_M vertical kinematic viscosity (L^2/t)

T temperature (ºC)

S salinity (M/L^3)

f Coriolis parameter (/t)

g gravitational acceleration (L/t^2)

ρ' equals $\rho - \rho_{mean}$ before the integration is carried out

ρ_{mean} generally the initial density field which is area averaged on z-levels and then transferred to sigma coordinates in the exact same way as the initial density field

F_x, F_y horizontal diffusion terms (L^2/t^2)

K_H vertical diffusivity (L^2/t)

q^2 twice the turbulence kinetic energy (L^2/t^2)

ℓ turbulence length scale (L)

$wu(0)$, $wv(0)$	surface turbulence momentum flux (L^2/t^2)
el	surface elevation
ua and va	vertically integrated velocities
ϕ	represents U, V, η
c	phase speed value (L/t)
C_d	drag coefficient (dimentionless)
K	equals 4 is the von Karman's constant
z_0	roughness parameter (L)
x_j, y_j, z_j	location of jth plume element (L)
u_j, v_j	horizontal velocity of jth plume element (L/t)
w_j	vertical velocity of jth plume element (L/t)
V_j	magnitude of the velocity of jth plume element (L/t)
h_j	thickness/length of jth plume element (L)
b_j	radius of of jth plume element (L)
ρ_j C_j	density and solute concentration of jth plume element (M/L^3)
$\emptyset_j$	angle of the jet axis with the horizontal plane of jth plume element
θ_j	angle between the x-axis and the projection of the jet axis on the horizontal plane of jth plume element
M_j	mass of the jth plume element (M)
Δt	time step (t)
S_m, S_{ave}	centerline dilution and average dilution
C_m, C_{ave}	maximum concentration and average concentration (M/L^3)
λ	ratio of concentration to velocity width

ΔU	relative jet velocity in the direction of the jet axis (L/t)
α_s	entrainment coefficient
F_{pe}	local jet densimetric Froude number
g'	reduced gravity (L/t^2)
ΔM	incremental mass of the plume element (M)
ΔM_s	shear entrainment (M)
ΔM_f	forced entrainment (M)
$\Delta M_{fx}, \Delta M_{fy}, \Delta M_{fz}$	forced entrainments in three dimensional cross flow conditions (M)
$V_r(\max)$	radial entrainment velocity (L/t)
ΔU_g	centerline excess velocity (L/t)
C	pollutant concentration (M/L^3)
D_x, D_y, D_z	directional dispersion coefficients (L^2/t)
k	reaction rate constant (/t)
$t_{1/2}$	chemical half-life (t)
Q_s	volumetric source or sink term (/t)
SS	source and sink terms (M/L^{3}t)
C_{MLR}	predicted output concentration using MLR model (M/L^3)
β_i (i = 0, …, n)	regression coefficient to be determined
P_i (i = 1, …, n)	uncertainty parameter
n	number of the uncertainty parameters.
ε	random error
$f_L(L)$	associated probability density function
$P(L>C_0)$	probability of concentration L larger than C_0

q	discharge rate (M/t)
R_x, R_y, R_z	random numbers
m	mass of each particle (M)
C_{pb}	predicted lead concentration (M/L^3)
$C_{benzene}$	predicted benzene concentration (M/L^3)
Q_{prw}	produced water emission rate (L^3/t)
C_B	background concentration (M/L^3)
D_h	horizontal dispersion coefficient (L^2/t)

List of Acronyms

ASA	Applied Science Associates
BASIN	Offshore Eastern Canada hydrocarbon database
BBL	Benthic Boundary Layer
BIO	Bedford Institute of Oceanography
BMT	British Maritime Technology
BOSS	Benthic Organic Seston Sampler
BTEX	Benzene, Toluene, Ethylbenzene, and Xylenes
CCGS	Canadian Coast Guard Services
CFD	Computational Fluid Dynamics
CFL	Courant-Friedrich-Lewy stability condition
C-NLOPB	Labrador Offshore Petroleum Board
COOGER	Centre for Offshore Oil and Gas Environmental Research
CORMIX	Name of a software for mixing zone simulation
CTD	Conductivity, Temperature, Pressure
DFO	Department of Fisheries and Oceans Canada
DREAM	Dose Related Risk and Effect Assessment Model
ECOM-SI	Estuarine, Coastal & Ocean Model
EEM	Environmental Effects Monitoring
EFDC	Environmental Fluid Dynamics Code
EIF	Environmental Impact Factor
FDM	Finite Difference Method

FEM	Finite Element Method
FVM	Finite Volume Method
GBS	Gravity Base Structure
GUI	Graphical User Interface
JETLAG	Name of a model for buoyant jet simulation
MC	Monte Carlo method
MIKE21/3	Name of a software for river and ocean water simulation
MLR	Multiple Linear Regression
MMS	Minerals Management Service
MUDMAP	Combined Drilling Muds and Produced Water Model
NOAA	National Oceanic and Atmospheric Administration
OBCs	Open Boundary Conditions
OOC	Offshore Operators Committee
PAH	Polycyclic Aromatic Hydrocarbons
PERD	Program of Energy Research and Development
PLUMES	Name of a software for pollutant discharge plume simulation
PEC	Predicted (modeled) Environmental Concentration
PNEC	Predicted No Effect Concentration
POM	Princeton Ocean Model
PROFS	Princeton Regional Ocean Forecast System
PROMISE	Name of a probabilistic-based steady-state model
PROTEUS	Pollution Risk Offshore Technical EvalUation System
ONR	Office of Naval Research

RSB	Roberts, Snyder, and Baumgartner
ROMS	Regional Ocean Model System
RPC	Research & Productivity Council
RQ	Risk Quotient
RWPT	Random Walk Particle Tracking
SCRUM	the S-coordinate Rutgers University Model
SEOM	Spectral Elements Ocean Model
TAF	Trace Analysis Facility
USEPA	U.S. Environmental Protection Agency
VISJET	Name of a software for buoyant jet simulation
WAD	Wetting and Drying

CHAPTER
1

INTRODUCTION

1.1 Background and Problem Statement

Produced water represents the largest volume waste stream generated along with oil and gas production on most offshore platforms (Neff *et al.*, 2011). World production and disposal of produced water in offshore areas was estimated to have reached 667×10^6 tons (about 800×10^6 m^3) in 2003 (OGP, 2004). On a volumetric basis, produced water has also been classified as the largest contributor to the offshore waste stream (Krause, 1995). Treated produced water that is discharged to the ocean bears various hydrocarbons, other organic chemicals, metals, and production chemicals (Neff, 2002; Lee *et al.*, 2005).

The complex chemical ingredients in the produced water may have adverse effects on the marine environment. With anticipated increases in new offshore platforms, produced water discharge has been identified as an issue of concern by both regulators and environmental groups.

After matching the regulatory compliance concentrations, treated produced water may be released above or below the sea surface. The location of subsurface discharge pipes may range from 10 to 100 m in depth (Neff *et al.*, 2011). Disposal of produced water in the ocean has relied on the dispersive capacity of the sea to rapidly dilute and flush away contaminants. Factors that affect the dispersion of produced water may include discharge rate and depth, ambient current, turbulent mixing regime, water column stratification, water depth, and difference in density and chemical composition between the produced water and ambient water (Reed and Rye, 2011; Niu *et al.*, 2011; Neff *et al.*, 2011). Inadequate dilution due to excessive waste discharges in offshore areas may negatively impact aquatic life and human health (Lewis, 1997). In order to be able to predict the spatial and temporal distribution of produced water discharges under a variety of conditions, it is important to understand complex pollutant dispersion processes which combine the effects of molecular and turbulent motion.

For outfalls located in offshore waters such as produced water discharges, the pollutant dispersion patterns of the liquid effluent plume are often very complex varying with time and space. In order to properly simulate the mixing and dispersion processes of a continuous discharge, the effluent plume is generally divided into three zones according to the mechanisms dominating the mixing process: (i) near field zone, dominated by the effluent dynamics and the interactions with ambient conditions, is tens to hundreds of

meters in length and operates on a time scale on the order of minutes (Li and Hodgins, 2004), (ii) the far field zone, dominated by advection and diffusion with ocean currents, can be kilometers in length and operates on a time scale on the order of hours (Martin and McCutcheon, 1998; Choi and Lee, 2007), while between these two regions, is an intermediate region, or zone of waste field establishment. (Martin and McCutcheon, 1998; Davis, 1999; Ridge, 2002).

Because of the significant differences in dispersion processes and length and time scales among different zones, near field models and far field simulations require different spatial and temporal resolutions. In the near field, density differences between discharges and the receiving water body causes the effluent to rise or fall in the water column, meanwhile, a large amount of ambient water continuously entrains the near field plume. Near field modeling (e.g. Roberts, 1999; Jirka *et al.*, 1996; Lee and Cheung, 1990; Baumgartner *et al.*, 1994) normally ends when the plume reaches physical boundaries or its final trapping level at neutral density, beyond which the model is generally not able to accurately simulate the pollutant dispersion beyond the near field zone. Far field models solve the dispersion process via the advection and diffusion mechanisms controlled by ocean circulation and turbulence on a large scale and over a long period of time. An approach designed for large-scale flow simulations in the far field may not adequately resolve the effects of discharges in the near-field either (Davis, 1999).

Since factors, such as the ocean current (in strength and direction), the density along the plume and of the receiving water body, and the pollutant concentrations, changes with time as the waste water releases continuously, the modeling problem becomes finding a solution which integrates all the modeling components to fully account

for the interactions between effluent plume and the receiving waters. The coupling of the necessary modeling components should be carefully handled to ensure the conservation of mass, momentum, and energy.

The most widely used coupling approach is the so called "one-way" coupling technique (Hillebrand, 2003; Choi and Lee, 2007), where the scalar concentration predicted by near-field models at the transition zone is introduced to far-field models. However, such coupling method does not fully consider the interaction between discharged fluids and receiving waters. Li and Hodgins (2004) introduced a dynamically coupled outfall plume-circulation model to predict three dimensional circulation and effluent dispersions. In their study, the scalar concentration at the end of the near field as predicted in the near field plume model was introduced to the far field grids. The ambient velocity and density field from the far field model were updated continuously, serving as input to the near field model. In this simple coupling approach, it was assumed that the near field flow pattern does not have significant effect on the far field flow. Choi and Lee (2007) further extended Li and Hodgins' coupling approach. Except for updating the ambient conditions at each timestep of the near field model, the entrainment flow into plume elements is excluded from the far-field flow, whereas the dilution flow from the source plume is applied as a source term to the far field model grid cell at the terminal level of near-field simulation. Such that, the coupling approach ensures conservation of mass and takes account of the interaction between two water bodies. Choi and Lee (2007) conducted comparisons between model predictions and basic laboratory data, in which only a uniform horizontal ambient condition is considered. In order to simulate pollutant dispersion behaviour in field studies of offshore areas where varying three dimensional

currents are anticipated, both near field and far field models should be able to apply in varying spatial and temporal ambient conditions.

For decades, studies have been conducted on modeling techniques to estimate the potential adverse effects of contaminants released into the ocean. The efforts of developing new and specialized modeling methods have been made, such as employing empirical methods (Lee and Neville-Jones, 1987; Roberts *et al*., 1989a), Eulerian-Lagragian methods (Koziy *et al*., 1998; Li and Hodgins, 2004), particle tracking techniques (Nakano and Povinec, 2003; Periáñez and Elliott, 2002; Rye *et al*., 1998), and integral methods (Frick *et al*., 1997; Lee and Cheung, 1990). Single discipline and multidiscipline modeling packages have been developed over the years, such as VISJET, which is based on the Lagrangian formulation to simulate the plume and jet behaviors (Lee and Cheung, 1990; Lee and Chu, 2003); Delft3D includes the ocean circulation and pollutant transport simulation (Delft3D, 2009).

However, while most of the existing models have tackled single part or parts of the necessary modeling components, more studies are still required to establish a functional modeling and assessment system for the simulation of offshore wastewater discharge problems. The accuracy of the modeling results still requires extreme attention in future studies. Analysis from model inter-comparisons has highlighted the existing level of variance between the outputs (James, 2002; Stolwijk *et al*., 1998). Extensive model comparisons and validations against results from experiments and field measurements are required.

Therefore, inspired by pioneer studies, a modeling and assessment system for produced water discharges from offshore platforms is established in this thesis. The

system includes both physical modeling and risk assessment functions. In the physical modeling, it dynamically integrates ocean circulation simulation, pollutant fate and transport modeling which includes both near field and far field mixing and dispersion processes. The risk assessment approaches where exposure risks and probabilistic risks are evaluated are also integrated with the physical modeling system. In order to evaluate the accuracy of the system, validations against field data associated with produced water discharges in offshore areas and model inter-comparison are performed. In the end, risk assessments are carried out to predict potential long-term environmental impacts associated with individual chemicals resulting from produced water discharges on the Grand Banks of Newfoundland, Canada.

1.2 Objectives of the Study

The objectives of the study are summarized as follows:

- To develop a modeling and assessment system for the evaluation of pollutant fate and transport resulting from produced water discharges from offshore platforms. The primary features of the system will include:

  ✓ Integrated ocean hydrodynamics, pollutant fate and transport and risk assessment approaches;

  ✓ Dynamic coupling of ocean circulation, near field dispersion and far field transport modeling;

  ✓ Ability of simulating multi-sources and different chemicals;

  ✓ Characterization and plotting of exposure and probabilistic risk levels;

  ✓ Development of a Graphical User Interface system.

- To validate the modeling system with field observation data collected at the site associated with offshore production platforms for both current modeling results and pollutant dispersion simulation results;

- To simulate and assess the potential impacts of produced water discharged from offshore oil and gas production activities in Atlantic Canada.

1.3 Organization of the Thesis

The following chapters of this thesis are organized as follows:

Chapter 2 provides an extensive literature review of the capabilities and limitations of the most widely used methods and models for simulating ocean circulation and pollutant dispersion associated with offshore discharges, and of risk assessment studies of produced water discharges in offshore areas.

Chapter 3 describes the methodology developed in the present research, including the integration of the modeling and assessment system, the dynamic coupling of ocean circulation, near field mixing and far field transport, integration of the risk assessment method with physical models, and numerical algorithms for each component of the system. At the end, a graphical user interface system is briefly presented.

Chapter 4 introduces the information of the case study performed in Atlantic Canada, including field sampling information for use in validation, and for modeling input information.

Chapter 5 presents the ocean current modeling results in the study area, such as the modeling setup, the consideration of the boundary conditions in the study area, and validation of the ocean current with field data.

Chapter 6 presents evaluation and field validation results of pollutant fate and transport models. The efficiency of far field models is evaluated through test cases by model inter-comparisons. Both near field modeling results and the overall integrated modeling results are validated using field experimental data. Concentration plumes of

two substances - lead and benzene are evaluated to present both conservative and non-conservative substances associated with produced water discharges in the study area.

Chapter 7 presents the predicted three dimensional produced water pollutant dispersion patterns and risk assessment results for the study area. Again, the risk assessment is implemented for both lead and benzene simulations.

Chapter 8 discusses the factors that may affect the physical modeling predictions and risk assessment results.

Chapter 9 presents the conclusions, contributions, and recommendations for future work.

CHAPTER
2

LITERATURE REVIEW

To improve the existing methods and modelling packages, and to design a better system, it is necessary to understand the various approaches and methods currently being used and to know their strengths and limitations. Inappropriate use of these techniques may lead to unreliable information for the assessment of environmental problems. In this chapter, the capabilities and limitations of the most widely used methods and models, when used to assess the impact of marine pollution, are reviewed and presented. The literature survey establishes the need for the development of the integrated modeling and risk assessment system for the management of large volume of produced water discharges in the marine environment.

2.1 Modeling the Dispersion of Wastewater Discharges from Offshore Outfalls

Techniques for modeling marine pollution have been studied for decades. Specialized modeling methods have been used to simulate pollutant dispersion resulting from offshore outfalls. These include empirical and analytical methods, particle tracking methods, numerical solutions for solving the advection diffusion equations, and jet integral methods. This section reviews modeling techniques associated with simulation of wastewater dispersion discharged from offshore outfalls based on type of methods and physical process of ocean discharge, such as near field and far field modeling. Advantages and limitations of the major mathematical methods are analyzed, as well as their functionality and the availability of modeling software. Development of numerous modeling approaches and software, both commercial and academic, reflects the growing importance and interest in ocean environmental assessment.

2.1.1 Description of mixing and dispersion processes of wastewater discharges

Increasingly, offshore outfalls are being used for the disposal of wastewater in marine environment. Because the discharged effluents generally exhibit different velocity, temperature, and density characteristics compared with the receiving water body, waste discharges form plumes and jets of high momentum and different densities (Jirka *et al*., 1996; Martin and McCutcheon, 1998). The mixing and dispersion processes of a continuous discharge into a receiving water body can be divided into near field, far field,

and intermediate regions according to length and time scales (Martin and McCutcheon, 1998; Davis, 1999; Ridge, 2002).

In the vicinity of the discharge point, the jet trajectory and mixing are dominated by the momentum of the discharges and density differences between discharges and the receiving water body. This region is referred to as the near field, where the typical time and length scales of the plume are in the order of minutes and tens to hundreds of metres, respectively (Choi and Lee, 2007). After some time, or some distance from the discharge point, the influence of the inflow characteristics dissipates and ambient flow conditions then control transport and mixing of the discharges. This region, where the diluted effluents are advected and diffused with ocean currents, is referred to as the far field, where the typical time and length scales are in the order of hours and kilometres (Martin and McCutcheon, 1998; Choi and Lee, 2007). Between these two regions, there is a zone called the intermediate field, which starts at the end of the jet regime. The intermediate field may extend over distances greater than the water depth under conditions of weak ambient flow (Jirka, 1982); however, under strong ambient conditions, intermediate field processes can be far less significant than far field dispersion processes (Bleninger, 2006). Thus, the effects of the intermediate field are often negligible unless weak ambient flows are present.

Near field models and far field simulations require different spatial and temporal resolutions. The effect of a jet or buoyant plume can be transient over a limited distance. Time scales of near field mixing are also significantly different from far field dispersion. A model designed for large-scale ambient flow conditions will not adequately resolve the effects of discharges in the near field; conversely, near field models will not be suitable

for far field simulations (Davis, 1999). The following sections provide a comprehensive view of current modelling techniques that are used to analyze wastewater discharges resulting from offshore outfalls and for simulation of pollutant dispersion in offshore areas.

2.1.2 Modeling methods of pollutant dispersion from offshore outfalls

A number of different methods that address the advection and diffusion mechanism have been studied towards providing a better understanding of the behaviour of wastewater discharges into the complex aqueous environment. Four major modelling techniques that are widely used for the simulation of offshore outfall discharges are discussed in the following sections: empirical and analytical solutions; numerical methods for directly solving the advection–diffusion equation; random walk particle tracking (RWPT) models; and jet-type integral methods.

2.1.2.1 Empirical and analytical solutions

Empirical solutions (or length-scale approaches) are used mainly in near field simulations to develop empirical expressions of the governing plume parameters. The final variable of interest in this kind of solution is the average dilution rate or centreline dilution rate. The basic idea is to use dimensionless analyses to form dimensionless groups that can be used in scaling the results of laboratory studies to full-sized field processes. The results of experimental data are used to determine empirical relationships between the dimensionless groups.

Early studies have used empirical models to simulate offshore outfalls since the 1980s. One example is the RSB (Roberts, Snyder, and Baumgartner) model, developed by Roberts et al. (1989*a*, 1989*b*, 1989*c*), which is based on an empirical length-scale method for ocean outfalls. The general idea of the RSB model is that four dimensionless dependent ratios can be expressed as functions of four independent values as follows:

$$\frac{S_m q N}{b^{2/3}}, \frac{z_e}{l_b}, \frac{h_e}{l_b}, \frac{z_m}{l_b} = f(\frac{l_m}{l_b}, \frac{s}{l_b}, F, \Theta) \qquad (2.1)$$

where S_m is the minimum dilution at the point of maximum concentration in the plume, $S_m = S/1.15$; S is the mean dilution, $S = Q/Q_0$; Q is the total discharge rate in the diffuser ($L^3 T^{-1}$, where L, length; T, time); N is the Brunt–Vaisalla frequency (T^{-1}); q is the discharge in unit diffuser length ($L^2 T^{-1}$); Z_e is the height to the top of the waste field layer (L); s is the port spacing (L), h_e is the thickness of the waste field after trapping (L); z_m is the height above discharge to the point of minimum dilution (L); $F = U_a^3/b$ and is known as Robert's F. Similarly, Lee and Neville-Jones (1987) developed formulas for estimation of buoyancy-dominated horizontal plumes in unstratified ambient seawater.

The advantage of empirical models is that the equations are easy to evaluate and often include the main physical effects such as boundary interactions that are not easily included in numerical models. However, limitations of empirical models include: (*i*) there is always a range where the original data were taken (extrapolation) and when using the equations to predict behaviour beyond that range, large errors will occur; (*ii*) empirical expressions for different regions of the same plume may not be continuous (as shown in Figure 2-1), and thus predictions in the intersection area will not fit the two sides of the boundary; and (*iii*) conditions in the laboratory are limited and it is usually impossible for these to be the same as those in the field (Davis, 1999).
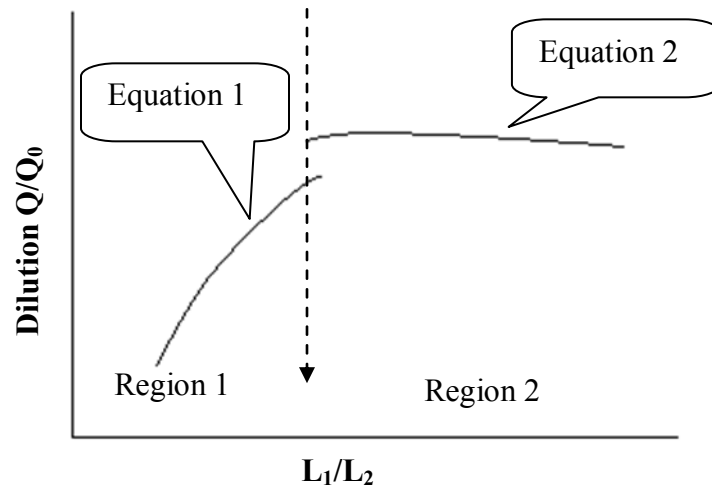
Figure 2-1 Sample graph showing the inconsistency of the analytical expression for different regions of the same plume (modified from Davis (1999))

Analytical solutions are often referred to as a closed-form solution that uses simplified derivations to solve governing equations (McCutcheon, 1990). Because of the complex nature of fluid hydrodynamics, many assumptions (e.g., flow, geometry, water-quality situations, etc.) have to be made during the derivations to obtain analytical solutions. The major disadvantages of analytical solutions are the very limited applications where they can be used, e.g., special cases involving regular, symmetrical geometry for flow solutions and limited water-quality situations (Martin and McCutcheon, 1998). In such cases, analytical solutions are not suitable for field simulation of offshore outfalls because of the complexity of the ocean environment. However, analytical solutions normally have very simple formulations and are useful for checking and validating conceptual and numerical solutions. For example, Riddle *et al.* (2001) used an analytical solution to compare results from the random walk model. Israelsson *et al.*

(2006) used analytical solutions to verify three Lagrangian approaches for extending near field mixing calculations.

2.1.2.2 Numerical solutions to the advection-diffusion equation

In modelling the fluxes of pollutants in offshore waters, the corresponding general solute transport or advection-diffusion equation can be written as (Daily and Harleman, 1966)

$$\frac{\partial C}{\partial t} + \vec{V} \bullet \nabla C = \nabla \bullet (D \nabla C) + Q - R \qquad (2.2)$$

where C is the pollutant concentration in space (x, y, z) at each timestep (M L^{-3}); $\vec{V}$ presents the flow field (L T^{-1}); D is the diffusivity, which may also vary in space and time (L^2 T^{-1}); ∇ is the gradient operator; while Q and R represent the sources and sinks in the model (M L^{-3} T^{-1}), respectively.

To solve the previous partial differential equation (Equation 2.2), three major numerical methods that have been extensively developed in fluid dynamics can be adopted, *i.e.*, finite difference methods (FDMs), finite element methods (FEMs), and finite volume methods (FVMs). Many textbooks document these numerical methods in computational fluid dynamics (CFD) (Chung, 2002; Date, 2005; Wendt, 2009; amongst others):

- FDMs, historically, have dominated CFD applications because of the simplicity of their formulations and computations, and the ease of implementation. With proper configuration of grid resolutions and the timestep, FDMs can generate results reasonably close to the exact solutions. However, finite difference equations must be constructed on structured Cartesian meshes.

- FEMs are versatile in applications involving multidimensional, complex, irregular geometries because they can be written in unstructured grids as well as in structured grids. It is easier for FEMs to handle complicated land boundaries and grid refinements in regions of interest. The study domain is divided into a group of elements; variables are described by basic functions over the local element and then, by the union of all elements, the global finite element equations can be obtained. Underlying principles and formulations from FEMs are more rigorous and complicated than those of FDMs. However, FEMs may provide more accurate solutions than FDMs because FEMs include more consistent interpolation procedures over the spatial domain.

- FVMs are formulated by tracking fluxes through the surfaces of control volumes resulting in the spatial integration of the governing equations where the integrated terms are approximated by either finite differences or finite elements. Because the formulation itself physically conserves the mass, momentum, and energy, FVMs can be constructed on unstructured grids. This is one of the most important features of FVMs compared with FDMs.

Among these numerical methods, FDMs are perhaps the most frequently used technique in ocean water simulation. For instance, Koziy *et al*. (1998) developed an explicit– implicit scheme to solve the advection–diffusion equations for temperature and salinity, and the suspended sediment and radionuclides transport in estuaries and shelf seas. Abbaspour *et al*. (2005) used MIKE21 software that solved the advection–dispersion equation by a third-order finite difference scheme to simulate thermal pollution in the Persian Gulf. The FVMs resemble FDMs in certain ways and they can

often be interpreted as a finite difference approximation to the differential equations (LeVeque, 2002). However, the starting point of FVMs is the integral formulation of the conservation law that gives FVMs many advantages over FDMs, especially for problems involving flow or flux boundaries (Yang, 2008).

The FEMs became popular for solving transport equations in the early 1970s (Noye, 1987). Previous studies showed that FEMs usually yield more accurate solutions than finite difference solutions (van Genuchten, 1976; Croucher and O'Sullivan, 1998). FEMs can be used with irregular meshes of triangular or quadrilateral elements, and therefore, they have more advantages for modelling complex irregular domains. However, the irregularity gives rise to a set of irregular algebraic equations, and solving the irregular matrix system is very time consuming (FAO, 1997; Wai and Lu, 2000).

Previous studies prove that FDMs or FEMs are well suited for far field modelling (e.g., Koziy *et al.*, 1998; Li and Hodgins, 2004; Ilyina *et al.*, 2006). However, the spatial and temporal resolutions of the near field mixing process can limit the application of such numerical methods. The length scale of the near field has dimensions of tens to hundreds of metres (bounded by diffuser length and water depth). The base of the plume, controlled by momentum and buoyancy associated with the individual ports, has diameters in the order of 10 cm, which would require grid sizes of 1 cm (Zhang, 1995). Numerical methods such as FDMs or FEMs, are usually applied in the length scale of tens to hundreds of kilometres with typical grid sizes of hundreds to thousands of metres. Time scales of the initial mixing process in the near field often take place in a few minutes, while the numerical methods usually run from days to years with a timestep of minutes to hours. Thus, the spatial and temporal resolutions of these numerical methods

can be limited by stability or accuracy considerations, to small values of the dimensionless Courant number or CFL (Courant–Friedrichs–Lewy) condition (Courant *et al.*, 1967), which makes these methods difficult to resolve near field mixing processes.

An advantage of FDMs and FEMs is the possibility of calculating long time periods and the interacting hydrodynamics for the whole domain. Also, it can easily incorporate second- and higher-order equations to describe chemical kinetics. Previous studies have verified that methods of directly solving advection–diffusion equations can achieve results in good agreement with measurements for far field modelling. A disadvantage of these approaches is that the solutions generated by FDMs and FEMs typically contain excessive numerical dispersion and artificial oscillation for advection-dominated problems, resulting in overshoot, undershoot, or negative values in the vicinity of high gradients of scalar values (Gray and Pinder, 1976; Glass and Rodi, 1982; Westerink and Shea, 1989).

2.1.2.3 Random walk particle tracking methods

The random walk particle tracking (RWPT) method is a Lagrangian-based approach that has been diversely applied in marine pollutant dispersion simulations in recent years. These diverse applications include simulations for drilling mud and produced water discharges (Rye *et al.*, 1998; Riddle *et al.*, 2001), river discharges (Korotenko *et al.*, 2004), sediment transport in coastal areas (Argall *et al.*, 2003), radionuclide dispersion (Periáñez and Elliott, 2002; Periáñez, 2006), coastal biophysical problems related to zooplankton or fish larvae (Batchelder, 2002), as well as other areas (Suh, 2006; Boufadel *et al.*, 2007).

In contrast with solving the advection–diffusion equation (Equation 2.2) directly, the particle tracking approach solves the transport equation by following individual particles as they move through space and time. Using this method, the advection is simulated by a translation of the individual particles in the local fluid velocity field. Turbulent diffusion is simulated by a random walk technique that displaces each particle a certain distance derived from the variance of a given distribution function (Periáñez and Elliott, 2002; Israelsson *et al.*, 2006; Suh, 2006). A typical particle tracking equation is expressed as

$$\Delta x = \left[u + \frac{\partial D_{xx}}{\partial x} \right] \Delta t + \sqrt{2 D_{xx} \Delta t}\, Z_1$$

$$\Delta y = \left[v + \frac{\partial D_{yy}}{\partial y} \right] \Delta t + \sqrt{2 D_{yy} \Delta t}\, Z_2 \qquad (2.3)$$

$$\Delta z = \left[w + \frac{\partial D_{zz}}{\partial z} \right] \Delta t + \sqrt{2 D_{zz} \Delta t}\, Z_3$$

where *Δx, Δy and Δz* represent the movement of a particle from the start to the end of a model timestep (L); *Δt* is the timestep (T); and *u*, *v*, and *w* are three-dimensional (3D) components at time *t* (L T^{-1}), respectively; D_{xx}, D_{yy}, and D_{zz} are the *x*, *y*, and *z* directional diffusivities (L^2 T^{-1}); *Z* is a random number with mean 0 and variance 1.

Conversion of particle locations into concentrations is straightforward. If the number (*N*) of particles is moved simultaneously according to Equation 2.3, and a number (N_g) of particles are inside a small volume (V_g), then the concentration can be expressed as

$$C(\mathrm{X}, t) = m \frac{N_g}{V_g} \qquad (2.4)$$

where m is the mass of each particle (M). The concentration distribution generated can be smoothed by using projection functions in which the mass of each particle is partially distributed over adjacent grid cells (Bagtzoglou *et al*., 1992; Moeller and Adams, 1994).

The RWPT method treats the transport of a solute mass via a large number of particles, which avoids solving the transport equation numerically. Therefore, it is virtually free of numerical dispersion and artificial oscillations, *i.e*., giving less numerical errors and maintaining the physics in the tracking and identification of particle locations (Banton *et al*., 1997; Salamon *et al*., 2006; Suh, 2006). Each particle can be tagged with its characteristics, therefore, allowing the simulation of multi-component effluents. In addition, because of the use of particles as discrete mass parcels, conservation of mass is automatically satisfied.

A drawback of the RWPT method is that when concentration data are required rather than particle locations when projecting particles onto a grid, the quality of the resulting concentration field depends on the particle density per grid cell, which decreases with increasing distance from the source. This effect can prevent the application of the RWPT method in long-term simulations in large domains, indicating that the RWPT method is more effective for dealing with problems where high-concentration gradients are involved, such as in the vicinity of point sources (Periáñez and Elliott, 2002; Israelsson *et al*., 2006). Concentration-dependent chemical processes, such as reactions between different chemical species or sequential decay reactions, are either not easily incorporated or have to be implemented with a trade-off with respect to the amount of system uncertainties (Tompson *et al*., 1996; Abulaban *et al*., 1998; Suh, 2006; Israelsson *et al*., 2006). The RWPT method can also be very time consuming. The

particle number must be restricted because storing and tracking the history characteristics of every particle requires large amounts of memory and computing time. While there is no stability criterion equivalent to the CFL condition for the RWPT method, the grid resolution and timestep must also be reasonably chosen to maintain the accuracy of the first-order advection scheme (Equation 2.3) that is used to compute particle movement (Periáñez and Elliott, 2002).

2.1.2.4 Buoyant jet-type integral methods

Integral methods are characterized by solving the ordinary differential equations along with the flow problem. Experiments and analytical analysis of jet behaviours started in the 1920s (Jirka, 2004). The groundwork for the jet integral theory, in which the overall properties of jet behaviour can be derived with the Gaussian profile, was proposed by Reichardt (1941). Later on, numerous experimental and numerical studies were carried out by various groups, including Jirka (2004, 2006, 2007), who introduced a jet integral model, CorJet, which was included in the CORMIX system to provide simulation of jet behaviours in unbounded stratified flow and in surface discharges. Lee and Cheung (1990) and Lee and Chu (2003) introduced the Lagrangian buoyant jet model, JETLAG, which used computer graphics techniques to give virtual reality simulations of merging jets.

Integral methods require that appropriate distribution profiles be assumed for velocity, temperature, and concentration (Davis, 1999). Many studies have shown that the Gaussian profile is a superior fit to the discharged flow profiles (Agrawal and Prasad, 2003). The jet integral model is based on conservation of mass, momentum, buoyancy, and concentration. By relating all the problem conditions to plume characteristics, the

overall behaviour may be calculated by a simple integration of ordinary differential equations, which describe the axial variation of plume width, velocity, and density difference (Kim *et al.*, 2002). There is also another type of jet integral model, written in a Lagrangian framework, in which a jet element is assumed to be advected with average local velocity along the trajectory (Jirka, 2004). One example of this is VISJET, developed by Lee and Cheung (1990) and Lee and Chu (2003).

Predictions of these integral models have compared well with basic laboratory experimental data; the models also correctly predicted the asymptotic behaviour of pure jets and plumes, and advected line puffs and thermals, proving that jet integral models produce very good approximations to jet and (or) plume behaviour. One drawback of all jet integral models is spatial restrictions, which become critical when integral models are applied to finite receiving domains in which jet boundary interactions either terminate or significantly alter the jet motion (Jirka, 2004). This suggests that integral methods have restricted application to more complex turbulent flows, where it is difficult to assign profile shapes and relate entrainment rates to local influences in complex environments (Webb and Mansour, 2000; Agrawal and Prasad, 2003).

2.1.3 Near field and far field modeling of pollutant transport in the marine environment

2.1.3.1 Near field modelling

The requirement for controlling contamination within the mixing zone by regulatory agencies led to many previous studies that focused on near field plume behaviour. A number of current public-domain and commercial models are available to aid in the

prediction of the initial dilution of offshore effluent discharge schemes; for example, the CORMIX system (Jirka *et al.*, 1996; Jirka, 2004, 2006), PLUMES (Baumgartner *et al.*, 1994; Frick *et al.*, 2003), and JETLAG (Lee and Cheung, 1990; Lee and Chu, 2003) (part of VISJET).

Other efforts have also been made to predict near field plume characteristics. For instance, Luhar and Britter (1992) used the random walk model for simulating buoyant plume dispersion in the convective boundary layer. Davidson and Pun (1998) developed a hybrid of the length scale and integral approaches for prediction of the initial dilutions from outfall discharges. Johansen (2000) presented a Lagrangian plume model for predicting the deep-water blowouts resulting from oil and gas production in the ocean.

Most of the previous studies of near field modelling have achieved reasonable results by comparing experimental data with field measurements using the jet integral and random walk methods (*e.g.*, Luhar and Britter, 1992; Lee and Chu, 2003; Jirka, 2006). These models have been intensively tested and compared for simulation of near field plume behaviours. However, if information beyond the mixing zone is desired (where near field models may not be able to provide accurate results), hydrodynamic and transport processes in the far field must be also considered in detail.

2.1.3.2 Far field modelling

In contrast to the near field mixing process, far field processes do not focus on the jet, plume, or waste field driven motions. Instead far field processes focus on the natural water body motions. In the far field, plume field characteristics can be transported and

dispersed by ambient currents and turbulence. Therefore, a full far field dispersion analysis, including a general flow model coupled with a transport model, is required.

Far field modelling requires a pollutant dispersion model coupled with or input with ocean circulation information. Therefore, the far field modelling approach should be able to (*i*) predict 3D hydrodynamics; (*ii*) generate a reasonable grid solution in the study area, such as fine resolution near the discharge point and flexible mesh along the shoreline; and (*iii*) provide accurate boundary conditions that exist along study area boundaries. For open boundary conditions, simulations of a large scale, in which the study area is nested inside, can be performed to establish the temporally and spatially variable boundary condition around the study site.

2.1.3.3 Near field and far field coupling techniques

Near field simulations need to consider the interactions between discharge momentum fluxes and receiving water turbulence. Most jet and (or) plume models generate jet and (or) plume trajectories and substance concentrations without involving grid resolutions. Far field modelling requires a high-resolution model to represent the ambient velocity field and further concentration distributions on structured or unstructured grid meshes. The transition between near field and far field should be handled to ensure the conservation of mass, momentum, and energy.

The most widely used coupling approach is to introduce the scalar concentration predicted by near field models at the transition zone (surface-bottom boundary or the equilibrium rise height) for far field models, where the dispersion plume can be determined based on different cases. This method considers the results from the near field

models as the source information for the far field models. It does not take into account the interactions between the discharge fluxes and receiving water flux turbulence. This coupling approach is called the ''one-way'' coupling technique (Hillebrand, 2003; Choi and Lee, 2007) and is commonly used to link near field and far field simulations. For example, Zhang and Adams (1999) coupled the RSB near field model and the ECOMsi 3D circulation model, to simulate the Boston outfall. Kim *et al*. (2002) employed a jet integral model together with a particle tracking model to simulate the mixing of a single buoyant jet discharge. Particles were introduced at the equilibrium rise height or at the end of the computed initial mixing zone, to conduct the simulation of far field transport. Bleninger and Jirka (2004) and Bleninger (2006) proposed a method to couple the near field mixing zone model CORMIX with the Delft3D circulation model to simulate the submarine outfalls.

However, one-way coupling does not take full consideration of the interaction between discharged fluids and receiving waters. When coupling near field and far field models, conservation of mass becomes an issue. Few studies described a fully dynamic coupling approach. One study reported integrating the JETLAG model with the environmental fluid dynamics code (EFDC) model (Hamrick, 1992; Choi and Lee, 2007). Except for updating the ambient conditions at each timestep, the entrainment flow into plume elements is excluded from the far field flow, whereas the dilution flow from the source plume is applied as a source term to the circulation model grid cell at the terminal level of near field simulation, ensuring conservation of mass. Such a dynamically coupled approach can only be implemented, however, when the near field models are similar to the JETLAG model, which calculates the entrainment flow into plume elements, and

where the entrainment flow can be used as the sink of the receiving waters. Improvement of coupling techniques used in different modelling methods is currently an active area study.

2.1.4 Modeling packages

The total ocean simulation system is extremely complicated and involves many variables and processes, including highly nonlinear interactions. In the past, a variety of modelling packages have been developed that fully or partially serve the purpose of simulating pollutant dispersion processes, and many have been applied in the ocean environment. It is not our intention to review every one of these models in this thesis, and only some of those most widely used for simulations of wastewater dispersion in marine environment are presented here. Table 2-1 shows the features of these modelling packages and more detailed descriptions follows.

2.1.4.1 Jet and plume models

Jet and (or) plume models are quite appealing and very important to governmental agencies because buoyant jet motions are a key feature in fluid waste disposal methods. These models provide fundamental knowledge for protecting and managing the ambient water quality. Most of these models favour empirical and (or) analytical solutions and jet integral methods because these methods are relatively simple and easy to implement and also can provide good approximations of jet or plume behaviours.

One of the most prominent jet models is CORMIX, which was initially developed in 1986 as a research project of the USEPA to demonstrate practical application of

artificial intelligence on desktop computers for environmental management (Doneker and Jirka, 2007). The CORMIX system mainly emphasizes the prediction of plume geometry and dilution within an initial mixing zone, including compliance with regulatory constraints. A flow classification system with a total of about 160 generic flow configurations or classes is at the heart of CORMIX, based on hydrodynamic criteria using length-scale analysis and empirical knowledge from laboratory and field experimentation. Once a flow has been classified, CORMIX assembles and executes a sequence of appropriate hydrodynamic simulation modules that are based on buoyant jet similarity theory, buoyant jet integral models, ambient diffusion theory, stratified flow theory, and simple dimensional analysis (Doneker and Jirka, 2007). The buoyant jet integral model CorJet is also included in CORMIX to predict jet trajectory and dilution characteristics of single port and multiport diffusers and to enhance the near field predictions provided by the flow classification systems. CorJet allows specification of varying ambient current speed and direction with arbitrary stable density profiles, but can only be used in unbounded environments.

Other jet models include VISJET, which simulates single or multiple buoyant jets discharged at different angles to the ambient current in three dimensions, using JETLAG, a Lagrangian formulation of integral models (details of the theory and computation can be found in Lee and Cheung (1990) and Lee and Chu (2003)), and Visual PLUMES, which is a collection of several jet–or plume models, including UM3 (based on a Lagrangian framework of integral method), DKHW (the Davis, Kannberg, Hirst model for Windows), and PDSW (Prych, Davis, Shirazi model for Windows) (based on the Eulerian integral method), and RSB (based on empirical solutions) (Frick et al., 2003).

Table 2-1 Existing modeling packages for simulation of pollutant dispersion processes

Category	Example Models	Corresponding Mathematical Approaches for Pollutant Dispersion	Major Functionalities/Capabilities Related to Pollutant Dispersion	Availability
Jet/Plume Models	CORMIX (Doneker and Jirka, 2007)	• Empirical solutions • Eulerian jet integral method	• Prediction of jet/plume geometry and dilution in the near field • Single or multiple jets	Commercial model
	VISJET (Lee and Cheung, 1990; Lee and Chu, 2003)	• Lagrangian jet integral method		Commercial model
	Visual PLUMES (Frick *et al.*, 2003)	• Empirical solutions • Eulerian and Lagrangian jet integral methods		Free package
Sophisticated Multi-disciplinary Models	MIKE 21/3 (DHI, 2007)	FVM; RWPT method	Predictions of • Ocean hydrodynamics • Pollutant fate and transport in the far field • Water quality • Sediment processes	Commercial package
	Delft3D (Delft3D, 2009)	FDM; RWPT method	Predictions of • Ocean hydrodynamics • Pollutant fate and transport in the far field • Water quality • Sediment processes	Commercial package
	EFDC-Hydro (Hamrick, 1992; USEPA, 2002)	FDM; RWPT method	Predictions of • Ocean hydrodynamics • Pollutant dispersion in the far field • Near field processes using the embedded jet model JETLAG • Suspended sediment transport	Free package
	HydroQual-ECOMSED (HydroQual, 2002)	FDM; RWPT method	Predictions of • Ocean hydrodynamics • Pollutant fate and transport in the far field • Sediment processes	Free package

Extensive validations against laboratory and field experimental data have been performed (see Frick *et al.*, 2003; Lee *et al.*, 2008; Doneker and Jirka, 2007; Jirka, 2004, 2006, 2007). Comparison of the results shows that these models can provide generally accurate and reliable representations of buoyant jet motions; however, they are limited to certain discharge and flow conditions. For example, Kikkert *et al.* (2007) reported that predictions from the CorJet and VISJET models were shown to be conservative for simulating the behaviour of inclined negatively buoyant discharges at the centreline maximum height and at the return point, or impact point.

2.1.4.2 Sophisticated multidisciplinary models

In recent years, there has been great interest in the development of multidisciplinary models to integrate flow, pollutant fate and transport, water quality, ecology, and sediment transport, etc. in one sophisticated system. Such models include MIKE 21/3, Delft3D, EFDC, HydroQual–ECOMSED, and many others. Some of these models are commercially available, such as MIKE 21/3 and Delft3D, while some are free packages, *e.g.*, EFDC, HydroQual–ECOMSED. Table 2-1 presents some of the features of these model packages. In the following section, MIKE 21/3 is briefly reviewed as an example of a multidisciplinary modelling package.

The marine MIKE products are professional engineering software packages, in which two major versions of coastal and marine modelling systems operate: MIKE21 for two-dimensional (2D) coastal and sea simulation and MIKE3 for 3D simulation. MIKE 21/3 consists of several simulation modules: hydrodynamic, transport, ecology and water quality (ECO-Lab), as well as sediment processes. The system has a wide range of

engineering and environmental applications in oceanography, environmental hydraulics, and sediment processes. For example, Tomicic *et al.* (2001) simulated the sewage system and receiving waters of the island of Ischia using MIKE 21. Lomborg and Windelin (2003) used MIKE 21 to simulate the hydrography and cohesive sediment in the Rømø Dyb tidal area. Vanderborght *et al.* (2007) also used the marine MIKE products to conduct reactive transport modelling of C, N, and O_2 in the Scheldt estuary.

Regarding the simulation of pollutant dispersion processes, the transport module in MIKE 21/3 is closely integrated with the hydrodynamic module and the ecology and water-quality module (ECO Lab) to simulate the fate and transport of dissolved or suspended substances in an aquatic environment under the influence of the fluid transport and associated dispersion processes. The numerical solution of the primitive transport equations is performed using a cell centred FVM for spatial discretization, and an explicit scheme for the time integration (DHI, 2007). A particle analysis module based on the RWPT approach is also included in MIKE 21/3 to simulate the transport and fate of dissolved and suspended substances.

With the development of advanced monitoring techniques, a larger number of field validation studies comparing field data and modelling results can be performed. Edelvang *et al.* (2005) verified and calibrated the MIKE3 modelling system using *in situ* measurements from various monitoring stations in Danish marine waters, and validated these against satellite images from SeaWiFS for modelling of phytoplankton biomass. The model was able to accurately simulate the spatial and temporal variation in the sea surface distribution of chl-*a* in Danish marine waters.

In relation to outfall discharge problems, MIKE 21/3 allows the simulation of pollutant dispersion processes under the influence of fluid motions in the far field, but cannot model the jet and (or) plume behaviour in the near field. This inability to simulate near field processes is found in most of the multidisciplinary models. Among the models listed in Table 2-1, only EFDC, developed by USEPA (2002), has been coupled with a near field buoyant jet model and far field model to simulate wastewater discharge problems. However, at the time of writing, only the hydrodynamic model of EFDC can be obtained from the USEPA website.[1] While Choi and Lee (2007) applied such coupled models in simple lab-scale experiments, this coupled technique has not been applied to field studies.

There are also many specialized pollutant dispersion models for the assessment of ocean environments, such as those used for oil spills, drilling muds, sediment modelling, etc. Since our focus is on produced water modelling and assessment, only those modelling packages associated with produced water simulations are reviewed (see Section 2.3), whereas other specialized models are not discussed.

2.1.5 Summary of advantages and limitations

Mathematical modelling can serve as an effective tool for the management of ocean discharges and provides useful information for decision makers. Considerable advances have been made in recent years in predicting the impact on the environment from marine discharges. Previous sections have provided a review of the techniques used during the last decade to model wastewater dispersion resulting from offshore outfalls. Table 2-2

[1] http://www.epa.gov/athens/wwqtsc/html/efdc.html (Access date: April 2012)

Table 2-2 Summary of modeling techniques for wastewater dispersion resulting from offshore outfalls

Methods	Formulation	Advantages	Limitations	Utilization	References
Empirical solutions	Dimensionless analysis	• Easy to evaluate and implement • Includes physical effects	• Limited applications • Discontinuous problems under certain flow conditions	• Near field mixing processes • Simple steady flow conditions	(Jirka *et al*., 1996; Davis, 1999; Bleninger, 2006)
Analytical solutions	Closed form solution	• Very simple formulations • Useful for validating numerical solutions	• Limited applications • Requires assumptions for flow, geometry, and water quality situations	• Simple steady flow conditions • Validating other methods and models	(McCutcheon, 1990; Martin and McCutcheon, 1998)
Numerical solutions for directly solving the advection-diffusion equation	FDMs, FEMs, FVMs	• Simulation of complex geometry, larger domain, long term simulations • Easily describes higher-order chemical kinetics • Assures conservation of mass, momentum, and energy	• Complicated formulations and computations • Stability problems • Excessive numerical dispersion	• Far field modeling • Complex flow and geometry conditions • Time series results	(Westerink and Shea, 1989; Zhang and Adams, 1999; Chung, 2002; Li and Hodgins, 2004; Ilyina *et al*., 2006)
RWPT method	Lagrangian-based particle tracking	• Free of numerical dispersion • Maintains physical dispersion processes • Assures conservation of mass • Easy implementation of multi-component effluents	• Accuracy depends on the particle density per grid cell • Time consuming, especially for long term and large domain simulations • Difficult incorporating higher-order chemical reactions	• Near field or intermediate field modelling • Variable time and flow conditions	(Abulaban *et al*., 1998; Periáñez and Elliott, 2002; Israelsson *et al*., 2006; Salamon *et al*., 2006; Suh, 2006)
Jet Integral methods	Eulerian formulation or Lagrangian formulation	• Good approximation of plume behaviour • Simple formulations and easy to implement	• Requires assumptions for distribution profiles • Spatial restrictions for applications • Requires termination conditions	• Near field simulation • Unbounded ambient condition	(Davis, 1999; Lee and Chu, 2003; Jirka, 2004; Li and Hodgins, 2004)

Note: RWPT, random walk particle tracking; FDMs, finite difference methods; FEMs, finite element methods; FVMs, finite volume methods

summarizes the advantages and limitations of different mathematical approaches and the application of these methods in the simulation of wastewater dispersion. Conclusions drawn from the review of these mathematical approaches are:

- Empirical and analytical models have inherently limited use in the simulation of offshore pollution (Martin and McCutcheon, 1998; Davis, 1999). The consistent use of dimensional analysis leads to a heavy reliance on experimental data to determine the numerous constants in these models.

- Numerical methods for directly solving the advection–diffusion equation are more suitable for far field modelling because it is possible to calculate long time periods and interacting hydrodynamics for large and complex domains. However, the use of these methods may be limited to certain grid resolutions, which may not allow the simulation of near field transport processes (Zhang and Adams, 1999).

- The RWPT method has been widely used for offshore discharge simulation in all physical dispersion regions. However, this method may be more suitable for areas with high substance concentration gradients (Periáñez and Elliott, 2002; Israelsson *et al.*, 2006; Suh, 2006). The accuracy of the results generated during the conversion from particles to concentrations depends on the particle density in each grid cell. In addition, it is time consuming to track the movements of each particle, especially for a large domain and a long period of time.

- Jet integral models are widely used and generally give good approximations for the presentation of dispersion of a dissolved substance for patches or jets and plumes. These models become less accurate when substance spreading is

restricted by the presence of a boundary, such as the seabed, although approximations can be made to account for boundary influences (Jirka, 2004).

Some of the most widely used modelling packages for simulations of wastewater dispersion in offshore and ocean areas are discussed in the previous sections, including jet and (or)plume models and multidisciplinary models. The main findings from an overview of the existing model packages are:

- Jet and plume models tend to use empirical and (or) analytical solutions and jet integral methods that have relatively simple formulations. All of these models can simulate the behaviours of both single and multiple buoyant jets, and extensive validations show that jet and (or) plume models can provide very good approximations of pollutant discharges resulting from offshore outfalls in the near field.

- Multidisciplinary models are becoming highly developed and a great many sophisticated commercial and academic systems have been developed that try to integrate many features in one system. In general, these models use FDMs and FVMs to predict pollutant dispersion processes. For solving outfall discharge problems, however, most of these models lack the ability to simulate near field jet and (or) plume behaviours, which may affect the accuracy of the modelling results.

Based on the previous review, each type of model provides a unique approach to predictions and assessment of waste discharges in offshore areas. However, more work still needs to be done to improve these models so that they can be employed to accurately model a greater variety of real problems, and research remains very active in each of the

various modelling technology areas. We still expect continual improvement in model functionality and in our scientific understanding of the underlying processes.

2.2 Ocean Circulation Models

The ocean's hydrodynamic conditions are a major factor affecting pollutant dispersion behaviors in marine environment. Local flows directly influence the simulation of pollutant fate and transport of wastewater discharges from offshore outfalls. Many ocean circulation models have been developed over the years (e.g. Princeton Ocean Model (POM), Estuarine, Coastal & Ocean Model (ECOM-SI), Regional Ocean Modeling System (ROMS), Spectral Elements Ocean Model (SEOM), etc.). Many of these have been tested and verified in a number of different studies. Therefore, using an existing ocean circulation model is considered for the current study. Since we aim at developing an integrated system in this research, in order to easily implement the integration, ocean circulation models with open source codes are of interest. Two of the most widely used open source ocean circulation models – POM (Princeton Ocean Model) and ROMS (The Regional Ocean Model System) are briefly reviewed in the following sections.

2.2.1 Princeton Ocean Model (POM)

The Princeton Ocean Model (POM) is a sigma-coordinate, free-surface, ocean model, which includes a turbulence sub-model for surface and bottom mixed layer dynamics. It was developed and first introduced by Blumberg and Mellor (1987), with subsequent

contributions from other researchers. The model has been used for the modeling of estuaries, coastal regions, and basin and global oceans (Hakkinen and Mellor, 1992; Ezer and Mellor, 1994; Ezer *et al*., 1995; Mellor and Ezer, 1995; Ezer, 1999, 2001; Oey *et al*., 2005). Support has been provided by ONR, NOAA, MMS, and other agencies. Publications, updates, and upcoming events related to the open source code model POM are available online.[1]

POM uses a sigma coordinate in the vertical and a structured finite difference grid in the horizontal. The model equations are discreted on the Arakawa C-grid, a commonly used staggered grid. Accurate second-order spatial differencing is used throughout. Leap-frog time differencing is used throughout, with the exception of the horizontal diffusion terms which are lagged in time and the vertical diffusion terms which are treated implicitly. The parameterization of vertical mixing follows the turbulence closure sub-model of Mellor and Yamada (1982) which includes prognostic equations for the turbulent kinetic energy and turbulence length scale. Horizontal mixing is parameterized using a Laplacian formulation with mixing coefficients proportional to the local grid spacing and velocity shears. The advective terms are treated with standard second-order-accurate differencing schemes in both time and space (Blumberg and Mellor, 1978, 1987; Mellor, 2004; Haidvogel *et al*., 2000a).

POM is well-tested and widely-used. As of 2011, POM had 3548 registered users from 71 countries.[1] One of the applications of POM occurs in the coastal ocean forecasting system. The Princeton Regional Ocean Forecast System (PROFS) is a hindcast, nowcast and forecast ocean model based on POM (Oey *et al*., 2005). PROFS has been in active development over the past decade. The quality of the model is

---

[1] http://www.aos.princeton.edu /WWWPUBLIC/htdocs.pom/ (Access date: April 2012)

monitored and reassessed by comparing the results with observations. Zhang *et al*. (2002) have developed an optimal adjoint variational data assimilation technique to assimilate subtidal water levels sampled along the US East Coast into the two-dimensional Princeton Ocean Model (POM). This technique has been used in the Experimental East Coast Water Level Data Assimilation Nowcast/Forecast Model System. The simulated results from POM are in good agreement with observed subtidal water levels at coastal water level gauge stations. Yao *et al*. (2000) have coupled a multi-category sea-ice model and POM to implement ice-ocean forecasts for the Labrador Sea and the surrounding continental shelves on the East Coast of Canada. Sea-ice behavior is coupled to POM using the coupling scheme devised by Mellor and Kantha (1989). This model has also been used by the Canadian Ice Service to provide daily digital ice maps (DFO-OES, 2007). Many of other systems and models based on or coupled with POM across the world can be found at the Princeton Ocean Model website.

Many studies have also made efforts to improve the present version of POM and enhance its application. For example, Oey (2005, 2006) has proposed and applied a wetting and drying (WAD) scheme to POM in its most general three-dimensional setting with stratification, bathymetry, and forcing. Ezer and Mellor (2004) have compared the behavior of bottom boundary layers when either terrain-following (sigma or combined sigma and z-level) or a z-level vertical grid is used, with most of the other numerical aspects remain unchanged. Such terrain-following ocean models provide reasonable climatology and water mass predictions. The Norwegian Meteorological Institute has developed a numerical model termed the Meteorological Institute's POM (MI-POM). Besides the production of daily forecasts on a routine basis, MI-POM has been applied in

several studies and assignments, *e.g.*, for public administration, oil companies engaged in offshore activities in Norwegian waters, and for climate change studies (Meteorological Institute, 2007).

2.2.2 The Regional Ocean Model System (ROMS)

ROMS (The Regional Ocean Model System) is a free-surface, terrain-following, primitive equation ocean model expanded from SCRUM (the S-coordinate Rutgers University Model) which was originally developed by Song and Haidvogel (1994). ROMS has been completely rewritten with a variety of new features including alternatives for high-order upstream-biased advection, for subgridscale parameterization, and for high-performance computing on SMP (symmetric multiprocessing) computer architectures, to improve both numerical schemes and efficiency in single and multi-threaded computer architectures (Haidvogel *et al.*, 2000b).

Numerically ROMS has several important features in common with POM. For instance, both models use a structured finite difference C-grid in space. Both of them have second-order numerical approximations and both use split-explicit time stepping of the external gravity mode. However, there are several important algorithmic differences between them as well, such as the availability of quasi-monotone advection schemes and higher order, constancy-preserving timestepping (Shchepetkin and McWilliams, 1998; Haidvogel et al., 2000b). The enhanced time stepping algorithm is very robust and stable. The algorithms that comprise ROMS computational nonlinear kernel are described in detail in Shchepetkin and McWilliams (2003, 2005), and the tangent linear and adjoint kernels and platforms are described in Moore *et al.* (2004).

ROMS has been widely used in a diverse range of applications. For example, Haidvogel *et al*. (2000a) applied ROMS to a decaldal-length simulation of the circulation in the North Atlantic Ocean. Their results were evaluated against those of other North Atlantic models used in previous multi-model comparison studies. Di Lorenzo (2003) investigated the seasonal dynamics of the Southern California Current using ROMS. Inputs of different wind forcing parameters were tested and results were verified against the mean and seasonal circulation inferred from long term *in situ* observations. Budgell (2005) coupled ROMS with a dynamic thermodynamic sea ice model to conduct ocean climate dynamical downscaling simulations for the Barents Sea region. Comparisons with available observations show good agreement in the simulation of the variability and distribution of the ocean temperature field.

ROMS is also an open source model, for which information and source code can be obtained online.[1]

2.2.3 Comparison of POM and ROMS

While both POMS and ROMS bear similarities in several important aspects (*e.g.* curvilinear orthogonal horizontal coordinates, a horizontal staggered "C" grid, a vertical staggered grid with either a sigma or a more general s-coordinate system), they have different numerical algorithms, code structure, and parameterization options (Ezer *et al*., 2002). The numerical schemes used in POM are simple and relative standard, while those used in ROMS are relatively complicated. For example, though both models use time splitting schemes where a short time step is used for solving two dimensional vertically

---

[1] http://www.myroms.org/index.php (Access date: April 2012)

integrated momentum equation and a longer time step for resolving fast moving barotropic waves and three dimensional momentum equations, the time stepping schemes and filtering techniques used in both models are very different. POM uses an explicit, second order "leap-frog" time stepping numerical scheme and a simple Asselin filter, while ROMS uses a predictor-corrector (PC) time stepping method and a Gaussian-like filter.

Several studies have conducted comparisons between results from POM and ROMS. For example, Robertson and Beckmann (2001) simulated internal tides using both ROMS and a modified version of POM for two different cases of stratification and topography. Though the numerical algorithms, model configuration, and code size between POM and ROMS are very different, both models are good at simulating the estuary and coastal ocean currents. While developing new numerical algorithms for a terrain-following ocean modeling systems, Ezer *et al*. (2002) comparatively evaluated several different numerical aspects of POM and ROMS. For simulations by the two models, sensitivity studies demonstrates that different behaviors may occur in terms of numerical errors, the stability condition and the computational efficiency. For example, while the new time stepping algorithms in ROMS may reduced numerical errors and allow using longer time steps than POM, the new schemes in ROMS may require more careful choices of time steps and advection schemes to maintain numerical stability.

The basic POM is a simple standalone code with a limited number of options and standard numerical schemes. Because of its simplicity and robustness POM quickly became very popular. On the other hand, ROMS provides users a large number of choices, such as different advection, diffusion and pressure gradient schemes, different boundary

conditions, and even data assimilation schemes, which provides it with greater flexibility than POM. Moreover, some of its advanced numerics may be more accurate and relatively more efficient than standard codes. However, the extra options make the ROMS code 20 times longer than the POM code, and requires users to have a greater knowledge of the behavior of the model under different parameterizations, and thus require a longer learning curve. Because both models can provide good simulations in ocean environment, and that the continuation of previous research (Zhao, 2007) was envisaged in this study, POM was chosen for the simulation of ocean circulations in the study area.

2.3 Produced Water Dispersion Modeling

Produced water has received a great deal of attention from both regulatory agencies and environmental research groups in recent years because of its continuous and worldwide discharge into the ocean, as well as the anticipated increase in new offshore platforms. Produced water releases low, but continuous amounts of dissolved pollutants and dispersed crude oil, contributing more than 90% of the inputs into the marine environment from extraction activities (Utvik, 1999). During the last two decades, researchers have put great efforts on the dispersion modelling studies with different approaches, different perspectives, and various degrees of sophistication. Some of the most recent studies and widely-used modelling packages are reviewed in the following sections.

2.3.1 Dispersion studies with single discipline in produced water modeling

Because of regulatory issues, near field mixing processes has been the focus in produced water dispersion studies. One of the earliest produced water models was the Offshore Operators Committee (OOC) Mud and Produced Water Discharge model, which was developed by the Offshore Operators Committee (OOC) and Exxon Production Research Company to predict the initial fate of drilling mud and cuttings in a marine environment (Brandsma and Sauer, 1983a, 1983b; O'Reilly *et al.*, 1988; Brandsma *et al.*, 1992). The model has been modified to allow the prediction of the initial dynamics and passive diffusion of produced water. Smith *et al.* (1994, 2004) verified the OOC model against field data on drilling mud and produced water dispersion at distances up to 103 m downcurrent from the discharge point. Though measured concentrations exhibited high variability, modeled results were in good agreement with field observations.

Brandsma (2001) studied the near field produced water plume discharged from platform Irene off Santa Barbara, California using the OOC model. Skåtun (1996) used a BJET model to study the near field mixing of a warm (32ºC), high salinity (84 ppt) produced water released from a platform in the Gulf of Mexico. These studies indicated rapid dilution of the discharge to non-acutely toxic levels within very short distances from discharge points. However, these single discipline models only estimate near field mixing and short term fate of produced water discharges. Long term and far field transport are equally important for the environmental assessment of produced water.

2.3.2 Multidiscipline models in produced water simulation and assessment

Currently, in modeling and assessment of produced water discharges, the most prominent model is DREAM (dose-related risk and effect assessment model). DREAM, developed by SINTEF (Trøndheim, Norway), has been widely used in the European oil industry to assess acute and chronic risks associated with long-term, low-level releases of produced water discharges into the marine environment from offshore oil platforms (Reed et al., 2001). The DREAM model simulates pollutant transport, effluent dilution, and general fate of chemicals resulting from single or multiple sources, and provides data based on total contaminant concentrations, without distinguishing between dissolved and particle-bound contaminants. This model includes a 3D dispersion model that consists of a near field release model based on buoyant plume equations developed by Koh and Chang (1973) and Brandsma *et al*. (1980), as well as a far field transport model based on RWPT methods (Durell *et al*., 2006). The DREAM model requires local hydrodynamic, meteorological, and discharge data to predict the dilution of contaminants and their concentration in the ocean. Durell *et al*. (2006) compared deployed mussels (*Mytilus edulis*), semipermeable membrane devices, and the DREAM model predictions to estimate the dispersion of polycyclic aromatic hydrocarbons (PAH). Their results showed that the predictions from the DREAM model indicated higher PAH dispersion than the field-based methods, particularly in the areas most influenced by tides. Field validation studies showed good agreement results between measured and modeled concentration of individual and total PAH, however, poor predictions occurred in certain fields because of lack of accurate physical oceanographic data for the period of the mussel deployment (Durell *et al*., 2006; Neff *et al*., 2006).

Similar produced water modeling and assessment system include the PROTEUS system developed by BMT (British Maritime Technology) Cordah Ltd. to support environmental risk assessments of discharges of produced water and drilling wastes from offshore oil and gas exploration and production activities. An extended random walk particle-based method has been adopted for the turbulent dispersion of buoyant discharges around the immediate zone of discharge and the dynamic collapse and passive turbulence stages in the far field zone (Sabeur *et al*., 2000; Sabeur and Tyler, 2004). Sabeur and Tyler (2004) showed a generally good agreement between PROTEUS model predictions and field observations; however, the model predictions appear to slightly underestimate the plume width at the near field zone.

Both the DREAM and PROTEUS systems have been widely used by the European oil industry (Sabeur and Tyler, 2004; Durell *et al*., 2006; Neff *et al*., 2006). DREAM is a commercial model, while the availability of PROTEUS is unknown.

Hodgins and Hodgins (1998, 2000) and AMEC (2006) both used the US EPA Visual Plume model coupled with a far field dispersion model to predict near and far field transport of produced water off the east coast of Canada. Burns *et al*. (1999) used the MUDMAP (Combined Drilling Muds and Produced Water Model) model to study the dispersion of produced water from the Harriet oil field on the Northwest Shelf of Australia. The MUDMAP model, developed by Applied Science Associates (ASA), includes a near field model whose governing equations are the same as those of the OOC model. Far field transport and fate of the discharge were calculated by a particle tracking random walk method. Niu *et al*. (2009) coupled a probabilistic-based steady-state model (PROMISE) with MIKE3 model to study dispersion of produced water over a wide range

of non-steady state discharge and environmental conditions. However, their study only assessed a hypothetical case for an outfall in Oresund, Denmark. Zhao *et al*. (2008) integrated a random walk particle tracking method with POM, enabling the fast prediction of future dispersion and risks of produced water discharges. Their results showed that an overestimation of dilution may occur at certain distances from the discharge points due to omission of near field buoyant jet behaviors.

Produced water dispersion models have advanced from single discipline models with only near field and short term predictions to comprehensive coupled models with different disciplines (e.g. near and far field dispersions). However, each model has its own advantages and limitations. Additional disciplines must still be added to these modeling systems. As is evident in previous overview, ocean hydrodynamic simulations are not included in most produced water models, but only treated as input information. It is also reported that poor predictions of produced water dispersion occurred because of the lack of available ocean circulation data. In addition, as discussed in Section 2.1, dynamic coupling of near and far field pollutant dispersion require simultaneous ocean circulation modeling to fully account for the interactions between the discharges and surrounding water body. The applicability of modeling methods in field studies requires further evaluation. Though most near field modeling results are in good agreement with basic laboratory experiments, which normally involve steady state one dimensional flow conditions, their behaviour in field studies with non-steady three dimensional environmental conditions still needs to be tested.

2.4 Risk Assessment Approach Related to Produced Water Discharges

Pollutant concentrations in the environment have generally received great attention because of the concern raised by their potential impacts on human health or ecosystem well-being. To study these effects, exposure assessments became one of the dominant risk assessment approaches in environmental assessment and management. One of the most common approaches for exposure risk characterization is the hazard quotient method which calculates the ratio of exposure concentration to a no-observed-adverse-effect-level. A risk-based produced water management tool based on such a method is the environmental impact factor (EIF) (Johnsen *et al*., 2000; Smit *et al*., 2003, 2011). The method is conservative in the sense of over-protecting rather than under-protecting the environment, and is intended to be used to quantify the comparative benefit to the environment of alternate management strategies (Reed and Rye, 2011).

The EIF method is based on the ratio of a predicted (modeled) environmental concentration (PEC) to a probable no-effect concentration (PNEC) of a single substance in produced water. Consequently, there may be a risk for ecological injury when the ratio exceeds 1, otherwise, the risk for injury from that single substance is considered to be acceptably near zero. The EIF calculation is performed in DREAM (dose-related risk and effect assessment model). First, the DREAM model predicts concentration fields for each produced water substance. The next step is to translate the exposure (modeled) concentration to a potentially affected fraction associated with a species sensitivity distribution described by Smit *et al*. (2008) for each substance. Finally, adding the risks as independent probabilities, the total risk at any given spatial point at any time can be

calculated (Johnsen *et al*., 2000). In the EIF methodology, the produced water composition is characterized by 14 groups of substances currently considered of potential hazard to the environment.

Other exposure risk assessment methods may involve modeling of the body burden of chemicals within a species body physiological compartment. For example, the PROTEUS system includes two toxic risk methods based on the toxicity predictions from the dynamic body burden of a specified species (Sabeur and Tyler, 2004).

Exposure risks account for the pollutant concentration exceeding a certain environmental threshold, with the result of potential ecological injuries occurring in the ecosystem. Toxicity studies are the major means to obtain the threshold concentration level. There are also statistical risk assessment methods to estimate the uncertainties resulting from modeling assumptions and configuring parameters, and then incorporating these uncertainties into the final expression of risk. The most widely used approach to characterize uncertainty in risk assessment studies is the Monte Carlo (MC) simulation (USEPA, 1996). Monte Carlo analysis is a combinatorial uncertainty propagation technique that can provide estimates of full probability distribution functions for model outputs and can accurately reflect any nonlinearity in a model (Ramaswami *et al*., 2005).

In a Monte Carlo analysis, a sample from the distribution of an input parameter is placed into a simulation run to interact in the model with samples from other input parameters. The downside of Monte Carlo analysis is that it can be computationally intensive, requiring hundreds or thousands of model runs in many cases. A number of previous studies on the risk assessment of produced water using the Monte Carlo method to conduct probabilistic analysis have been carried out. For example, Mukhtasor *et al*.

(2004) present an approach to evaluate the toxicity risk resulting from produced water in an offshore platform using the Monte Carlo simulation method correlated with the CHARM model. Riddle *et al*. (2001) have conducted a study on modeling the uncertainty in predicting produced water concentrations using a modified Monte Carlo (MC) approach. They considered that, owing partly to the CPU requirement and the size of the database, it was not possible to estimate uncertainties using traditional Monte Carlo (MC) simulations. Meinhold *et al*. (1996) employed Monte Carlo simulations to assess the human health risks of radium and lead in produced water. Chowdhury *et al*. (2004) used Monte Carlo simulations to predict the human health risks from radioactive materials in produced water. Though MC simulation has its limitations, *e.g*., insufficient or imprecisely informative data cannot be analyzed by MC (Lee, 1996), Mukhtasor *et al*. (2002) have suggested that MC simulation is still the best choice for environmental-failure analysis (exceeding probability on concentration) of ocean outfalls.

The uncertainty analysis based Monte Carlo method considers the randomness in data distribution. However, for uncertain parameters that cannot be expressed as probability distributions, such a stochastic risk assessment method is inapplicable (Brouwer and Blois 2008). Fuzzy set theory widely used to handle uncertainties associated with discrete and/or imprecise characteristic, can produced results of moderate acceptability (suitability) (Klir and Yuan, 1995; Zimmermann, 2001). Chen *et al*. (2010) applied a hybrid fuzzy-stochastic modeling approach to reflect uncertainties associated with produced water discharges and related regulated pollution criteria for the marine environment. Mofarrah and Husain (2010) used a fuzzy based approach to quantify the human health risk posed by produced water discharge from petroleum industries.

In the present thesis study, since most parameters can be presented by a probability distribution function, Monte Carlo method is used to quantify the modeling uncertainties. By the incorporation of probable no-effect concentrations (PNEC) obtained from EIF factor and local water quality guidelines, a probability risk and exposure risk ratio are characterized later in this thesis.

2.5 Summary

An extensive overview of the most widely used methods and models for modeling and assessment of marine environment was presented in this chapter. Though great efforts have been made to improve modeling techniques to assess potential adverse effects of contaminants released into the ocean, there remains a necessity for further improvement to existing methods and models, and to design a system better suited to specialized modeling conditions. Here, we suggest that a functional modelling and assessment system for produced water discharges into offshore waters could be developed. The system should consider following factors and include the following components:

- Ocean current hydrodynamic condition is the major factor affecting the dispersion of contaminants in ocean discharges. Therefore, a 3D high-resolution ocean circulation model that correctly simulates a combination of the key forces (*e.g.*, wind, Coriolis, hydraulic, stratification, and turbulent dispersion) is necessary. POM is a standalone code with standard numerical schemes. Because of its simplicity and robustness, POM has become very popular, especially when faced with limited computational resources. Since the system presented in this thesis

report was developed on a personal computer, POM was chosen for the ocean circulation simulation.

- Near field and far field conditions have different dispersion mechanisms; therefore, a 3D pollutant transport model that couples near field and far field dispersion processes is required. The coupling techniques still require further improvement, particularly regarding balance of mass and intermediate field simulation. The development of a near field and far field fate and transport model is described in Chapter 3. A dynamic integration of ocean circulation, near field and far field fate and transport is performed in order to ensure the mass balance and fully account for the transition from near field plume simulation to far field transport.

- Produced water is comprised of a mixture of components. The physio-chemical influence of speciation, the chemical characteristics and chemical reactions between the constituents following discharge into the ocean should be considered. However, many pollutants show complex and sometimes poorly understood physicochemical speciation; thus, in this study, only first order reactions of individual pollutant compounds are considered.

- Although equations for describing current flow, water stratification, and pollutant dispersion in a multidimensional water column are established, many model parameters (e.g., dispersion or diffusion coefficients) vary spatially and (or) temporally. The variation in these parameters, along with the lack of availability of monitoring data and difficulties in discretisizing an irregular spatial boundary condition, significantly affect simulation results (Poulter, 1998). Stochastic

analysis and fuzzy set theory could, therefore, be useful for quantifying some of these uncertainties in the modelling process (Bardossy and Duckstein, 1995). These uncertainties can be further employed in risk assessment. The Monte Carlo method is chosen for uncertain analysis involved in the risk assessment in this study.

- Creating a user-friendly graphical interface is also an important component in the development of the proposed modelling system.

DEVELOPMENT OF THE THREE DIMENSIONAL NUMERICAL MODELING AND RISK ASSESSMENT SYSTEM

Based on the previous review (Chapter 2), major components of the modeling and risk assessment system were identified and an integrated three dimensional numerical modeling and risk assessment system for produced water discharges in marine environment was developed in the present study. The system framework was introduced first, then detailed approaches to each component of the system are laid out consecutively in the order: (i) ocean circulation model, (ii) near field modeling approach, (iii) far field

transport modeling, (iv) pollutant fate simulation, (v) methods for system integration including physical model coupling and the integration of risk assessment approaches with physical models, and (vi) a graphical user interface to assemble all the components together.

3.1 System Framework

Figure 3-1 shows the system framework of the produced water modeling and assessment system developed, which integrates ocean circulation modeling, pollutant fate and transport simulation along with a risk assessment approach. Based on input information, sites of interest were selected and grid systems constructed for both ocean flow simulation and pollutant fate and transport modeling. The numerical schemes of the Princeton Ocean Model (POM) were used for the ocean circulation simulation, while pollutant transport modeling included both near field and far field dispersion processes. Near field processes were simulated by a Lagrangian jet model developed by Lee and Cheung (1990) and Lee and Chu (2003), extended to three dimensional cross flow conditions. Far field processes are primarily driven by ambient flow conditions. Such dispersion processes were simulated by a second-order explicit finite difference method solutions to the advection-diffusion equation.

Near field and far field models were dynamically coupled to simulate the pollutant dispersion behavior resulting from offshore outfalls. For the purpose of computational efficiency, choices were made for the integration of the ocean circulation model and pollutant transport simulation: a) "one-way" coupling - the ocean circulation model is

treated as a standalone model to provide ocean circulation data as input to the pollutant fate and transport model; b) "two-way" coupling - the ocean circulation model is dynamically integrated with the pollutant fate and transport model, which means source and sink terms are provided to the ocean circulation model from the pollutant transport models, and ocean circulation data are updated in the pollutant fate and transport model at each time step. The integration methods are introduced in Section 3.6.

After the generation of a pollutant concentration distribution, two risk quantification approaches can be used to evaluate the potential risk levels — exposure risks and probabilistic risks. Exposure risks are evaluated using the ratios of predicted environmental concentration (PEC) to a probable no effect concentration (PNEC) which is often computed based on toxicity information for marine organisms. Probabilistic risks are evaluated based on a modified Monte Carlo method. The entire system is conformed by a combination of file operations and a database system which stores and transfers data for system computations, comparisons and evaluation. Ultimately, a user interface was developed for users to graphically input information. Detailed formulations and approaches of the system are presented in the following sections.

3.2 Three Dimensional Ocean Circulation Model – POM

The ocean current is one of the most important factors determining the direction and rate at which produced water disperses. Implemented to provide ocean circulation information POM was dynamically integrated with the pollutant fate and transport models in the
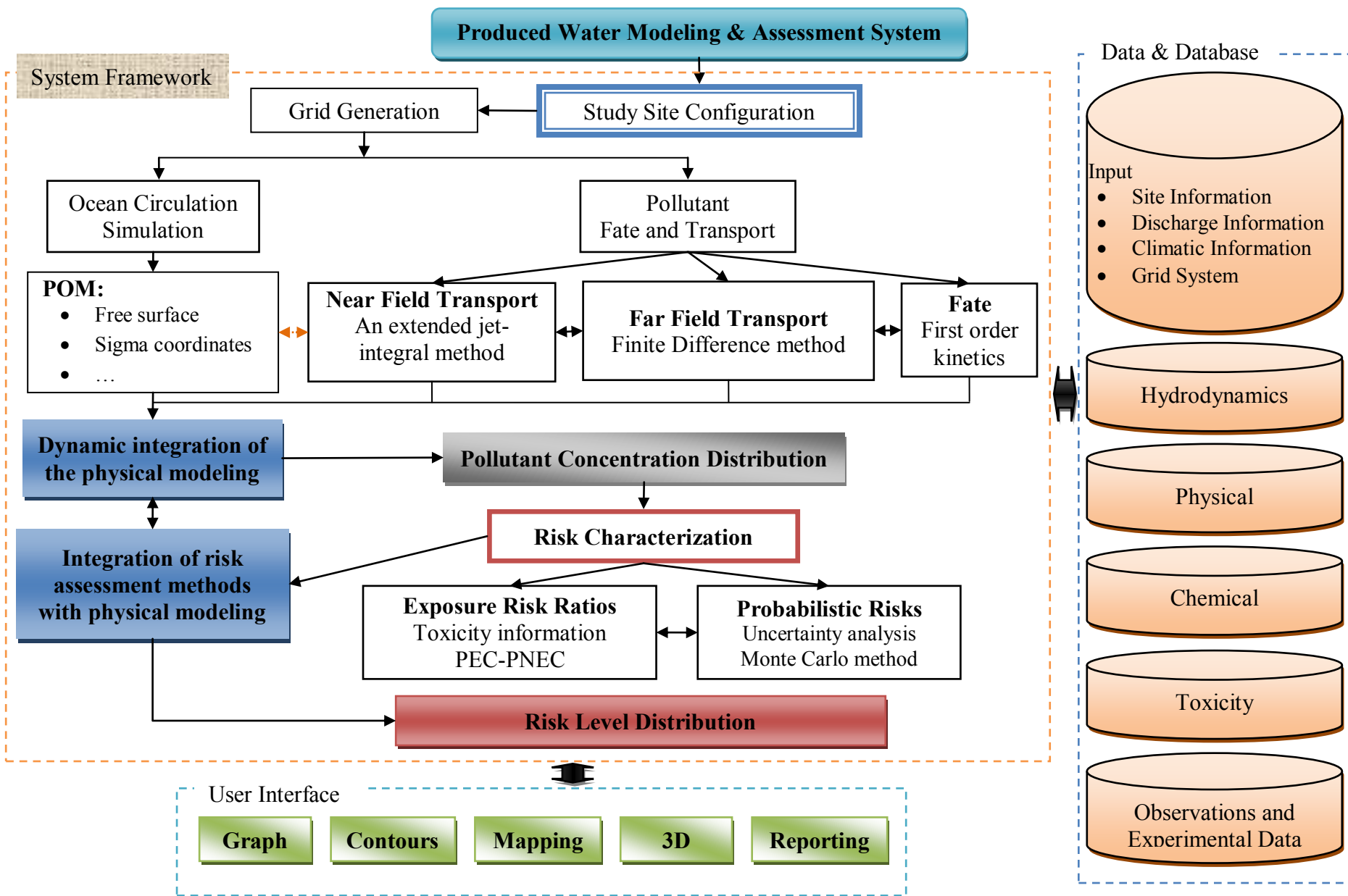
Figure 3-1 Framework of the produced water modeling and assessment system

system; it can also be separated from the dispersion simulations and run as a standalone model to provide ocean circulation. information (e.g., ocean currents, surface elevation, ocean water temperature and salinity). Horizontal grids were structured as Cartesian grids, while the vertical grids followed a sigma coordinate grid system. The grid generator provided on the POM website [1] was used for the system grid construction. The interpolations of topography, temperature, and salinity data were automatically completed once the grid information was provided.

3.2.1 Model description

A three-dimensional, primitive equation, time-dependent, sigma coordinate, free surface, estuarine and coastal ocean circulation model, POM is unique in having an imbedded turbulent closure submodel, which yields realistic Ekman surface and bottom layers (Blumberg and Mellor, 1987). The model represents ocean physics as realistically as possible and addresses large scale and long term phenomena, depending on the basin size and grid resolution. The principal attributes of the model are (Mellor, 2004):

- An imbedded second moment turbulence closure sub-model is included to provide vertical mixing dynamics between layers.

- It employs a sigma coordinate or a terrain-following transformation in the vertical dimension to provide a continuous representation of changing bathymetry.

- The horizontal grid uses curvilinear orthogonal or Cartesian coordinates and an "Arakawa C" differencing scheme.

- The horizontal time differencing is explicit whereas the vertical differencing is

---

[1] http://www.aos.princeton.edu/WWWPUBLIC/htdocs.pom/ (Access date: April 2012)

implicit. The latter eliminates time constraints for the vertical coordinate and permits the use of fine vertical resolution in the surface and bottom boundary layers.

- The model has a free surface and a split time step. The external mode portion of the model is two-dimensional and uses a short time step. The internal mode is three-dimensional and uses a long time step.

- Complete thermodynamics have been implemented.

3.2.2 Governing equations

Sigma coordinate transformation

The sigma coordinate equations are based on the transformation: (Blumberg and Mellor, 1978, 1987; Mellor, 2004)

$$x^* = x \ , y^* = y \ , \sigma = \frac{z - \eta}{H + \eta}, t^* = t \tag{3.1}$$

where *x, y, z* are the conventional Cartesian coordinates; *H* (*x, y*) is the bottom topography and *η* (*x, y, t*) is the surface elevation. The sigma coordinates are illustrated in Figure 3-2.
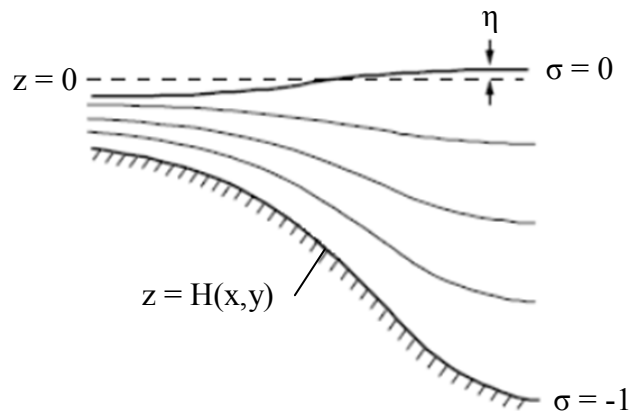
Figure 3-2 The sigma coordinate system (Mellor, 2004)

Continuity, momentum, turbulence closure, temperature and salinity equations were developed on the basis of the sigma coordinate system:

The continuity equation

$$\frac{\partial DU}{\partial x} + \frac{\partial DV}{\partial y} + \frac{\partial \omega}{\partial \sigma} + \frac{\partial \eta}{\partial t} = 0 \tag{3.2}$$

The momentum equations

$$\frac{\partial UD}{\partial t} + \frac{\partial U^2 D}{\partial x} + \frac{\partial UVD}{\partial y} + \frac{\partial U\omega}{\partial \sigma} - fVD + gD\frac{\partial \eta}{\partial x} + \frac{gD^2}{\rho_0}\int_\sigma^0 \left[\frac{\partial \rho'}{\partial x} - \frac{\sigma'}{D}\frac{\partial D \partial \rho'}{\partial x \partial \sigma'}\right]d\sigma' = \frac{\partial}{\partial \sigma}\left[\frac{K_M}{D}\frac{\partial U}{\partial \sigma}\right] + F_x \tag{3.3}$$

$$\frac{\partial VD}{\partial t} + \frac{\partial UVD}{\partial x} + \frac{\partial V^2 D}{\partial y} + \frac{\partial V\omega}{\partial \sigma} + fUD + gD\frac{\partial \eta}{\partial y} + \frac{gD^2}{\rho_0}\int_\sigma^0 \left[\frac{\partial \rho'}{\partial y} - \frac{\sigma'}{D}\frac{\partial D \partial \rho'}{\partial y \partial \sigma'}\right]d\sigma' = \frac{\partial}{\partial \sigma}\left[\frac{K_M}{D}\frac{\partial V}{\partial \sigma}\right] + F_y \tag{3.4}$$

The turbulence closure equations

$$\frac{\partial q^2 D}{\partial t} + \frac{\partial U q^2 D}{\partial x} + \frac{\partial V q^2 D}{\partial y} + \frac{\partial \omega q^2}{\partial \sigma} = \frac{\partial}{\partial \sigma}\left[\frac{K_q}{D}\frac{\partial q^2}{\partial \sigma}\right] + \frac{2K_M}{D}\left[\left(\frac{\partial U}{\partial \sigma}\right)^2 + \left(\frac{\partial V}{\partial \sigma}\right)^2\right] + \frac{2g}{\rho_0}K_H\frac{\partial \tilde{\rho}}{\partial \sigma} - \frac{2Dq^3}{B_1 l} + F_q \tag{3.5}$$

$$\frac{\partial q^2 lD}{\partial t} + \frac{\partial U q^2 lD}{\partial x} + \frac{\partial V q^2 lD}{\partial y} + \frac{\partial \omega q^2 l}{\partial \sigma} = \frac{\partial}{\partial \sigma}\left[\frac{K_q}{D}\frac{\partial q^2 l}{\partial \sigma}\right] + E_1 l\left(\frac{K_M}{D}\left[\left(\frac{\partial U}{\partial \sigma}\right)^2 + \left(\frac{\partial V}{\partial \sigma}\right)^2\right] + \frac{E_3 g}{\rho_0}K_H\frac{\partial \tilde{\rho}}{\partial \sigma}\right) - \frac{Dq^3}{B_1}\tilde{W} + F_l \tag{3.6}$$

The temperature equation:

$$\frac{\partial TD}{\partial t} + \frac{\partial TUD}{\partial x} + \frac{\partial TVD}{\partial y} + \frac{\partial T\omega}{\partial \sigma} = \frac{\partial}{\partial \sigma}\left[\frac{K_H}{D}\frac{\partial T}{\partial \sigma}\right] + F_T - \frac{\partial R}{\partial \sigma} \tag{3.7}$$

The salinity equation:

$$\frac{\partial SD}{\partial t} + \frac{\partial SUD}{\partial x} + \frac{\partial SVD}{\partial y} + \frac{\partial S\omega}{\partial \sigma} = \frac{\partial}{\partial \sigma}\left[\frac{K_H}{D}\frac{\partial S}{\partial \sigma}\right] + F_S \tag{3.8}$$

where U, V are the horizontal velocities (L T^{-1}); ω is the velocity component normal to sigma surfaces (L T^{-1}); T is the temperature (Θ); S is the salinity (M L^{-3}); η is the surface elevation (L); $D \equiv H + \eta$ is the total elevation of the surface water (L); x, y are the horizontal Cartesian coordinates (L); σ is the sigma vertical coordinate (L); t is time (T); f is the Coriolis parameter (T^{-1}); g is the gravitational acceleration (L T^{-2}); density $\rho' = \rho - \rho_{mean}$ before the integration is carried out (M L^{-3}); ρ_{mean} is generally the initial density

field which is area averaged on z-levels and then transferred to sigma coordinates in exactly the same manner as the initial density field (Mellor et al., 1994; Mellor et al., 1998); K_M is the vertical kinematic viscosity ($L^2 T^{-1}$); F_x, F_y are the horizontal diffusion terms ($L^2 T^{-2}$); K_H is the vertical diffusivity ($L^2 T^{-1}$); q^2 is twice the turbulence kinetic energy ($L^2 T^{-2}$); ℓ is the turbulence length scale (L).

3.2.3 Boundary conditions

Lateral boundary conditions

Ocean current modeling often involves open boundary conditions (OBCs), which play a crucial role in achieving the validity of the modeling outputs. Ideally, the numerical analysis of OBCs should allow fluid motions to be generated in the computational domain without affecting the interior solution. That is, waves can cross these boundaries unhampered without reflections (Tang and Grimshaw, 1996). A large number of OBCs has been studied and proposed over the years (Palma and Matano, 1998; Marsaleix *et al*., 2006; Marchesiello *et al*., 2001). One of the most popular OBCs is the radiation boundary condition which was derived from the radiation equation of Sommerfeld (1949). This type of OBCs can provide a simple and stable extrapolation of the interior solution, guided by the idea that interior disturbances approaching the boundary should propagate through it in a wave-like way (Marchesiello *et al.,* 2001).

Mellor (2004) included several possible open boundary conditions for POM characterized by external and internal modes. In the present study, the radiation boundary conditions are chosen for the flow simulations in the study area. The governing equations

for the radiation conditions stem from the one-dimensional Sommerfeld's equation (Orlanski, 1976; Chapman, 1985):

$$\frac{\partial \phi}{\partial t} \pm c \frac{\partial \phi}{\partial x} = 0 \tag{3.9}$$

where ϕ can represent U, V, or η; c is the phase speed of incoming waves (L T^{-1}), and x is the coordinate normal to the open boundary (L). One of the difficulties arises in the determination of the phase speed value (c). In the context of the shallow water equations the traditional choice is $c = \sqrt{gH}$, where H is the local water depth, which corresponds to the assumption that the waves approaching the boundary are surface gravity waves.

Table 3-1 shows the detailed solutions of the external and internal mode boundary conditions for the present study. In the external mode, the phase speed uses the equation $c_e = \sqrt{gH}$. In the internal mode, the speed c_i satisfies the Courant-Friedrich-Lewy stability condition (Tang and Grimshaw, 1996).

$$0 < \gamma \equiv c_i \Delta t_i / \Delta x < 1 \tag{3.10}$$

The finite difference expression can be written as (Mellor, 2004):

$$U_{im}^{n+1} = \gamma U_{im-1}^{n} + (1-\gamma) U_{im}^{n} \quad where \quad \gamma = \sqrt{\frac{H}{H_{max}}} \tag{3.11}$$

The boundary conditions determined are with a radiation condition on the u component in the east and in the west, and a v component in the north and in the south. The tangential velocities are set to the adjacent velocities on both boundaries.

Table 3-1 Open boundary conditions for the current model (modified from Mellor (2004))

Formula	Boundary	Calculations
External Mode Radiation Boundary $HU \pm c_e\eta = 0$	East	$u(im, j) = \sqrt{\dfrac{grav}{h(im-1, j)}}el(im-1, j)$ $v(im, j) = v(im-1, j)$
	West	$u(2, j) = -\sqrt{\dfrac{grav}{h(2, j)}}el(2, j)$ $v(1, j) = v(2, j)$
	North	$v(i, jm) = \sqrt{\dfrac{grav}{h(i, jm-1)}}el(i, jm-1)$ $u(i, jm) = u(i, jm-1)$
	South	$v(i,2) = -\sqrt{\dfrac{grav}{h(i,2)}}el(i,2)$ $u(i,1) = u(i,2)$
Internal Mode Radiation Boundary $\dfrac{\partial U}{\partial t} \pm c_i \dfrac{\partial U}{\partial x} = 0$	East	$gai = \sqrt{\dfrac{h(im, j)}{h_{max}}}$ $u(im, j, k) = gai \bullet u(im-1, j, k) + (1-gai) \bullet u(im, j, k)$ $v(im, j, k) = v(im-1, j, k)$
	West	$gai = \sqrt{\dfrac{h(2, j)}{h_{max}}}$ $u(2, j, k) = gai \bullet u(3, j, k) + (1-gai) \bullet u(2, j, k)$ $v(1, j, k) = v(2, j, k)$
	North	$gai = \sqrt{\dfrac{h(i, jm)}{h_{max}}}$ $v(i, jm, k) = gai \bullet v(i, jm-1, k) + (1-gai) \bullet v(i, jm, k)$ $u(i, jm, k) = u(i, jm-1, k)$
	South	$gai = \sqrt{\dfrac{h(i,2)}{h_{max}}}$ $v(i,2, k) = gai \bullet v(i,3, k) + (1-gai) \bullet v(i,2, k)$ $u(i,1, k) = u(i,2, k)$

Note: grav is gravity (g); h is water depth (H); el is surface elevation (η); im and jm are west and north boundary points, respectively.

Figure 3-3 shows the grid points calculated based on the open boundary conditions. The dotted line bounds the interior (non-boundary) grid points. "BC" indicates a line of points where the boundary conditions should be specified. Closed boundary conditions are automatically enabled through a specification of the masks, *dum, dvm* and *fsm*, in which the open conditions will be overwritten during computation.

Vertical boundary conditions

The vertical boundary conditions for Equation (3.2) are:

$$\omega\,(0) = \omega\,(-1) = 0 \tag{3.12}$$

The surface boundary conditions for Equations (3.3) and (3.4) are (Mellor, 2004):

$$\frac{K_M}{D}\left(\frac{\partial U}{\partial \sigma},\frac{\partial V}{\partial \sigma}\right) = -(<wu(0)>,<wv(0)>),\sigma \to 0 \tag{3.13}$$

where $wu(0)$, $wv(0)$ are the input values of the surface turbulence momentum flux ($L^2\,T^{-2}$).
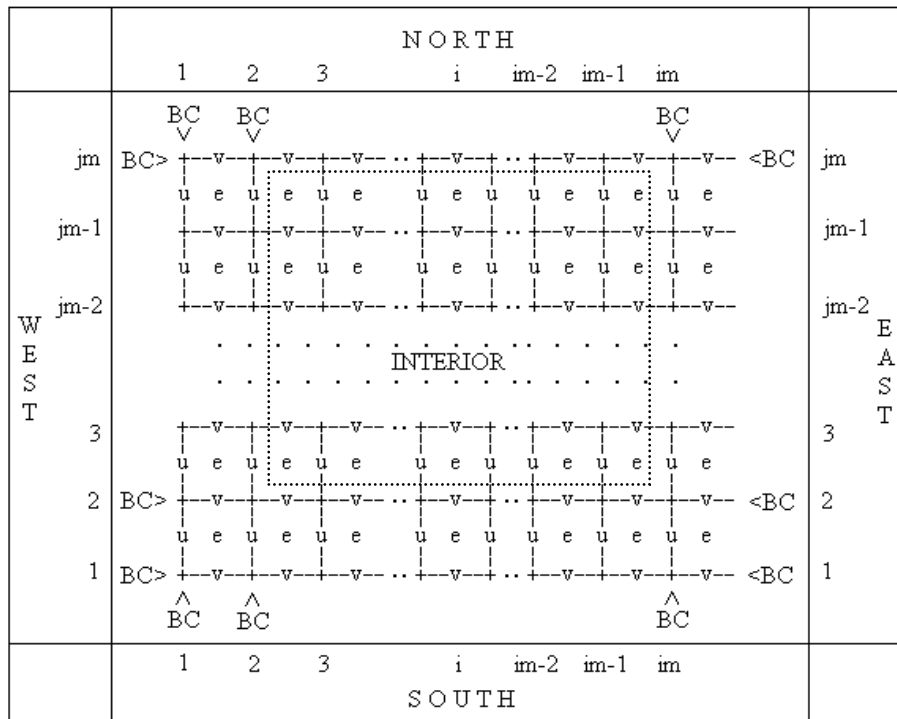
Figure 3-3 Grid points specified by open boundary conditions (modified from Mellor (2004))

In the present study, ocean surface forcing mainly considered the climatological wind stress fields, which were determined by surface-layer variables and the bulk aerodynamic formula (Hasse and Smith, 1996):

$$\tau = \rho C_d U^2 \tag{3.14}$$

where the drag coefficient C_d (dimensionless) represents the influence of the turbulence on the relation between wind and stress. Calculating C_d is based on the stability and the wind speed and/or the sea state, which can be expressed as (Wu, 1980):

$$C_d = \begin{cases} 1.2875 \times 10^{-3} & for \quad U < 7.5 \;\; m\;s^{-1} \\ (0.8 + 0.065U) \times 10^{-3} & for \quad U \geq 7.5 \;\; m\;s^{-1} \end{cases} \tag{3.15}$$

The bottom boundary conditions are:

$$\frac{K_M}{D}\left(\frac{\partial U}{\partial \sigma}, \frac{\partial V}{\partial \sigma}\right) = C_z \left[U^2 + V^2\right]^{1/2} (U,V), \sigma \to -1 \tag{3.16}$$

where $C_z = \max\,[\frac{k^2}{\ln\,(\frac{z}{z_0})}, \; 0.0025]$, $k = 0.4$ is the von Karman's constant and z_0 is the roughness parameter (L).

3.3 Near Field Dispersion Modeling Approach

3.3.1 General description

A large number of mathematical models have been developed to predict the behavior of the near field plume generated by an outfall (see Chapter 2). Some of the models are of the entrainment type, some are empirical, and some are based upon extrapolations from unstratified experiments to stratified fluids. In the present study, a buoyant jet-type

integral method which is based on the Lagrangian jet model JETLAG proposed by Lee and Cheung (1990) and Lee and Chu (2003), was employed for the near field modeling, with an extension to three dimensional cross flow conditions.
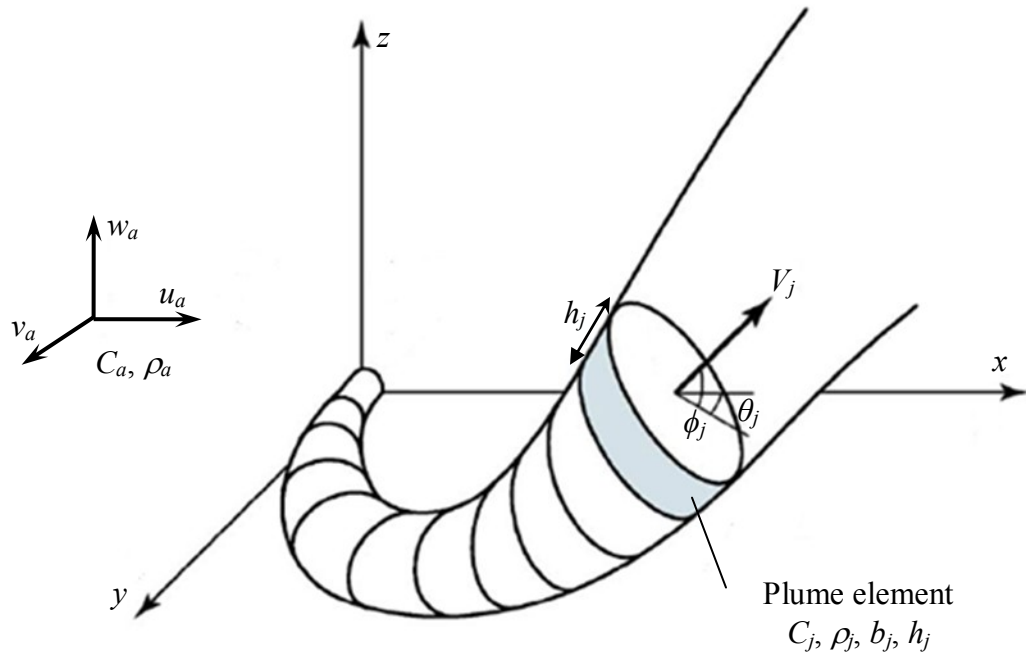
Figure 3-4 Schematic diagram of jet trajectory traced out by Lagrangian fluid parcels
(Modified from Choi and Lee (2007))

JETLAG is a well-proven robust jet model that predicts the mixing of an arbitrarily inclined round buoyant jet in a stratified cross flow, with a 3D trajectory. Figure 3-4 shows the basic concepts of the near field model. The predicted plume trajectory is embodied with a sequential series of plume elements which are characterized by their location, average velocity, pollutant concentration, density, width, and thickness. At each time step, on the basis of calculations of the incremental mass (turbulent entrainment of ambient fluid into the plume element), the momentum, energy, and tracer mass conservation equations can be solved in their integral form to give the velocity,

density, and concentration at the next time step. Then, by defining the thickness of a plume element as proportional to the local jet velocity, the Lagrangian method becomes similar to a time integration along the jet trajectory (Lee and Chu, 2003). The initial characteristics of the element at the source can be clearly related to the discharge parameters. A dtailed formulation is described in the following section.

3.3.2 Near field modeling formulation

Considering a plume element at the jth step (Figure 3-4), x_j, y_j, z_j represent the location of the element; u_j, v_j are the horizontal velocity, and w_j is vertical velocity of the plume element; $V_j = \sqrt{u_j^2 + v_j^2 + w_j^2}$ is the magnitude of the velocity; h_j is the thickness/length, defined as being proportional to the magnitude of the local jet velocity, $h_j \propto V_j$; b_j is the radius of the plume element; T_j, S_j, ρ_j C_j are the temperature, salinity, density, and solute concentration, respectively; $\emptyset_j$ is the angle of the jet axis with the horizontal plane; θ_j is the angle between the x-axis and the projection of the jet axis on the horizontal plane. The mass of the jth plume element is then given by $M_j = \rho_j \pi b_j^2 h_j$. After the next time step Δt, turbulent entrainment of the ambient fluid into the plume element causes an increase in mass ΔM_j, such that the characteristics of the plume element at next time step are calculated as follows (modified from Lee and Chu (2003)):

Mass:

$$M_{j+1} = M_j + \Delta M_j \tag{3.17}$$

$$M_{j+1} = \rho_{j+1} \pi b_{j+1}^2 h_{j+1} \tag{3.18}$$

Concentration and density:

$$S_{j+1} = \frac{M_j S_j + \Delta M_j S_a}{M_{j+1}}$$

(3.19)

$$T_{j+1} = \frac{M_j T_j + \Delta M_j T_a}{M_{j+1}}$$

(3.20)

$$\rho_{j+1} = \rho(S_{j+1}, T_{j+1})$$

(3.21)

$$C_{j+1} = \frac{M_j C_j + \Delta M_j C_a}{M_{j+1}}$$

(3.22)

Momentum:

$$u_{j+1} = \frac{M_j u_j + \Delta M_j U_a}{M_{j+1}}$$

(3.23)

$$v_{j+1} = \frac{M_j v_j + \Delta M_j V_a}{M_{j+1}}$$

(3.24)

$$w_{j+1} = \frac{M_j w_j + \Delta M_j W_a + M_{j+1}(\frac{\rho_a - \rho}{\rho})_{j+1} g \Delta t}{M_{j+1}}$$

(3.25)

$$(HVEL)_{j+1} = (u_{j+1}^2 + v_{j+1}^2)^{1/2}$$

(3.26)

$$V_{j+1} = (u_{j+1}^2 + v_{j+1}^2 + w_{j+1}^2)^{1/2}$$

(3.27)

Thickness/radius:

$$h_{j+1} = \frac{V_{j+1}}{V_j} h_j$$

(3.28)

$$b_{j+1} = (\frac{M_{j+1}}{\rho_{j+1} \pi h_{j+1}})^{1/2}$$

(3.29)

Jet orientation:

$$\sin\phi_{j+1} = (\frac{w}{V})_{k+1}$$

(3.30)

$$\cos\phi_{j+1} = \pm(\frac{HVEL}{V})_{k+1}$$

(3.31)

$$\sin\theta_{j+1} = (\frac{v}{HVEL})_{k+1}$$

(3.32)

$$\cos\theta_{j+1} = (\frac{u}{HVEL})_{k+1}$$

(3.33)

Location:

$$x_{j+1} = x_j + u_{j+1}\Delta t_n$$

(3.34)

$$y_{j+1} = y_j + v_{j+1}\Delta t_n$$

(3.35)

$$z_{j+1} = z_j + w_{j+1}\Delta t_n$$

(3.36)

In the above equations, U_a, V_a, W_a, T_a, S_a, ρ_a, C_a represent, respectively, the flow characteristics of velocities, temperature, salinity, density, and solute concentration in the ambient fluid. The initial location of the fluid parcel is set at the discharge location.

$(u,v,w)_0 = (V_0\cos\phi_0\cos\theta_0, V_0\cos\phi_0\sin\theta_0, V_0\sin\phi_0)$; $(b,h)_0 = (0.5D, 0.5D)$;

$\Delta t_0 = 0.1\times h_0/V_0$. The density is calculated based on temperature and salinity data for both discharge plume and the receiving waters (Martin and McCutcheon, 1998):

$$\begin{aligned}
\rho = {}& 999.842594 + 6.793952\times 10^{-2}\,T - 9.095290\times 10^{-3}\,T^2 + 1.001685\times 10^{-4}\,T^3 \\
& -1.120083\times 10^{-6}\,T^4 + 6.536332\times 10^{-9}\,T^5 + (0.824493 - 4.0899\times 10^{-3}\,T \\
& + 7.6438\times 10^{-5}\,T^2 - 8.2467\times 10^{-7}\,T^3 + 5.3875\times 10^{-9}\,T^4)S + (-5.72466\times 10^{-3} \\
& + 1.0277\times 10^{-4}\,T - 1.6546\times 10^{-6}\,T^2)S^{1.5} + 4.8314\times 10^{-4}\,S^2
\end{aligned}$$

(3.37)

Based on the equations presented above, only the average properties in the jet cross section can be represented. The centerline dilution (or maximum concentration in the jet cross section) is estimated based on:

$$S_m = \frac{C_{ave}}{C_m} = \frac{\lambda^2}{1+\lambda^2} S_{ave}$$

(3.38)

where S_m, S_{ave} are the centerline dilution and average dilution, respectively; C_m, C_{ave} are the maximum concentration and average concentration in the jet cross section, respectively; λ is the ratio of concentration to velocity width, where $\lambda \approx 1.2$ based on the experiments carried out by Lee and Cheung (1990) and Lee and Chu (2003).

3.3.3 Formulation of turbulent entrainments

The most difficult part of the model is the calculation of turbulent entrainment of the ambient fluid into the plume element in a crossflow as incremental mass at each time step. From there, the momentum, energy, and tracer mass conservation equations can be solved to provide the plume element characteristics at the next step. The incremental mass of the plume element at each time step, ΔM, consists of two components: the shear entrainment ΔM_s because of the difference between the plume element velocity and the ambient velocity in the direction of the jet axis; and the forced entrainment ΔM_f due to the ambient crossflow (Lee and Chu, 2003). The formulation of entrainments is presented as follows.

Shear entrainment

$$\Delta M_s = 2\pi\alpha_s b_{pe} h_{pe} \Delta U \Delta t_n \rho_a$$

(3.39)

$$\alpha_s = \sqrt{2}(0.057 + 0.554\sin\phi_{pe}/F_{pe}^2)(\frac{2V_{pe}}{\Delta U + V_{pe}})$$

(3.40)

where, V_{pe} is jet velocity (L T^{-1}), $\Delta U = |V_{pe} - U_{ajet}|$ is the relative jet velocity in the direction of the jet axis (L T^{-1}), b_{pe}, h_{pe} are the radius and thickness of the plume element (L), ρ_a is ambient density (M L^{-3}), α_s and F_{pe} are the entrainment coefficient and the local jet densimetric Froude number, respectively, $F_{pe} = \Delta U / \sqrt{g'b_{pe}}$, g' is the reduced gravity (L T^{-2}), Δt_n is time step of the near field model (t), the subscript pe presents plume elements at each time step.
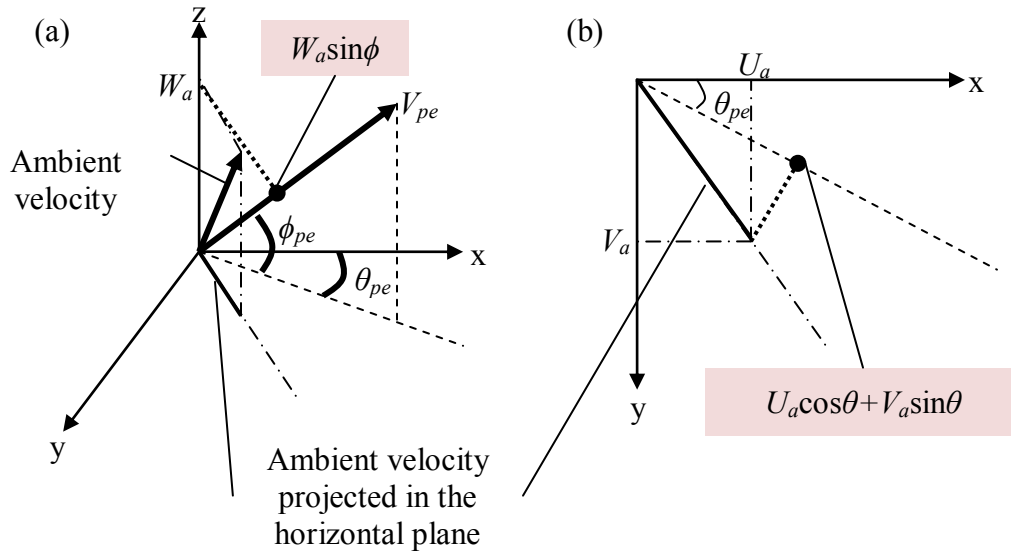
Figure 3-5 Ambient and jet velocity projections in a) the three dimensional coordinates, and b) the horizontal plane

U_{ajet} is the ambient velocity projected in the jet axis direction (L T^{-1}). The projections are depicted in the three dimensional coordinates (Figure 3-5a) and horizontal plane (Figure 3-5b). The projection of ambient velocity in the jet axis takes the form of

$$U_{ajet} = (U_{ape}\cos\theta_{pe} + V_{ape}\sin\theta_{pe})\cos\phi_{pe} + W_{ape}\sin\phi_{pe}$$

(3.41)

~ 70 ~

where U_{ape}, V_{ape}, and W_{ape} are the three components of ambient velocity in the plume element location, θ_{pe} is the angle between the x-axis and the projection of the jet axis on the horizontal plane, and ϕ_{pe} is the angle of the jet axis with the horizontal plane.

Forced entrainment

The forced entrainment is also further extended to formulations in three dimensional cross flow conditions based on Yapa and Zheng (1997), Cheung and Lee (1999), Lee and Chu (2003), and projections in Figure 3-5:

$$\Delta M_f = \Delta M_{fx} + \Delta M_{fy} + \Delta M_{fz} \tag{3.42}$$

$$\Delta M_{fx} = \rho_a |U_{ape}| \left[\underbrace{2b_{pe}h_{pe}\sqrt{1-\cos^2\phi_{pe}\cos^2\theta_{pe}}}_{A_p} + \underbrace{\pi b_{pe}\Delta b_{pe}\cos\phi_{pe}\cos\theta_{pe}}_{A_w} + \underbrace{\frac{\pi b_{pe}^2}{2}\Delta(\cos\phi_{pe}\cos\theta_{pe})}_{A_c} \right] \Delta t_n \tag{3.43}$$

$$\Delta M_{fy} = \rho_a |V_{ape}| \left[2b_{pe}h_{pe}\sqrt{1-\cos^2\phi_{pe}\sin^2\theta_{pe}} + \pi b_{pe}\Delta b_{pe}\cos\phi_{pe}\sin\theta_{pe} + \frac{\pi b_{pe}^2}{2}\Delta(\cos\phi_{pe}\sin\theta_{pe}) \right] \Delta t_n \tag{3.44}$$

$$\Delta M_{fz} = \rho_a |W_{ape}| \left[2b_{pe}h_{pe}|\cos\phi_{pe}| + \pi b_{pe}\Delta b_{pe}\sin\phi_{pe} + \frac{\pi b_{pe}^2}{2}\Delta(\sin\phi_{pe}) \right] \Delta t_n \tag{3.45}$$

where ΔM_{fx}, ΔM_{fy}, and ΔM_{fz} are the forced entrainments in three dimensional cross flow conditions (M).

The characteristics of the next plume element at step $pe+1$ are first calculated based on an initial estimation of ΔM_f using values at step pe and $pe-1$, and then an improved estimation $(\Delta M_f)_e$ using the newly calculated values at step $pe+1$ and pe is obtained based on Equations (3.42)-(3.45). The procedure is repeated at least twice until convergence (the relative difference of ΔM_f is less than 10^{-4}) is achieved. In the forced entrainment formulation, the projection term A_p is always positive, whereas the growth term A_w or curvature term A_c can be negative under some cross flow conditions (Cheung

and Lee, 1999). Therefore, under extreme cases, the values of ΔM_f based on Equations (3.42)-(3.45) could be negative; however, if such extreme flow conditions occurred, values of ΔM_f would be automatically set to zero.

Total entrainment

The maximum hypothesis $\Delta M = \max(\Delta M_s, \Delta M_f)$ is used for calculation of the total entrainment. However, the use of this hypothesis may give unreasonable predictions for a weak current (Lee *et al.*, 2008). The transition from the shear entrainment regime to the forced entrainment regime is handled based on an updated equation (Lee *et al.*, 2008) as

$$\Delta M = \Delta M_s \frac{\pi - \varphi_{pe}}{\pi} (1 - \sin^n \varphi_{pe}) + \Delta M_f \sin \varphi_{pe} \qquad n = 100 \qquad (3.46)$$

$$\cos(\varphi_{pe}) = \min(\frac{V_r(\max)}{V_{across}}, \ 1) \qquad (3.47)$$

where $V_r(\max) = 0.421\alpha_s \Delta U_g$, is the radial entrainment velocity (L T^{-1}), α_s is the shear entrainment coefficient (Equation 3.40), $\Delta U_g = 2\Delta U$ is the centerline excess velocity (L T^{-1}), and V_{across} is the ambient velocity in the plane of the jet cross-section (L T^{-1}).

3.4 Far Field Transport Modeling

3.4.1 Advection-diffusion equation

In contrast to the near field processes which are dominated by the discharge characteristics and the interaction between the discharge flows and the receiving water body, for far field processes, pollutant fluxes are mainly driven by ambient flow conditions. For far field modeling, the conservation of mass principle for chemical

species can often be well approximated by a parabolic partial differential equation — the advection-diffusion equation, and applies to one, two, or three dimensions (Gresho et al., 2000). The following equation is the three dimensional formulation of the traditional advection-diffusion equation (expanded from Equation 2.2):

$$\underbrace{\frac{\partial C}{\partial t}}_{local\ effects} = \underbrace{-\frac{\partial(UC)}{\partial x} - \frac{\partial(VC)}{\partial y} - \frac{\partial(WC)}{\partial z}}_{advection\ term} + \underbrace{\frac{\partial}{\partial x}\left(D_x\frac{\partial C}{\partial x}\right) + \frac{\partial}{\partial y}\left(D_y\frac{\partial C}{\partial y}\right) + \frac{\partial}{\partial z}\left(D_z\frac{\partial C}{\partial z}\right)}_{diffusion\ term} + \underbrace{SS}_{source/sink\ term}\ (3.48)$$

where C is the pollutant concentration in space (x, y, z) at each timestep $(M\ L^{-3})$; $U,\ V,\ W$ present three velocity components of the flow field $(L\ T^{-1})$; $D_x,\ D_y,\ D_z$ are the directional dispersion coefficients $(L^2\ T^{-1})$; t is the time (T); and, x, y, z are the coordinates.

As shown in Equation (3.48), the term on the left hand side represents the local effects or time derivative of substance concentrations. Terms on the right hand side of Equation (3.48) represent different physical processes: the first three terms describe advection while the following three corresponds to diffusion. SS represents both source and sink terms $(M\ L^{-3}\ T^{-1})$. detailed calculations for both source and sink terms are presented in Section 3.5 and 3.6.1. Equation (3.48) is mathematically and physically correct in all respects (Glover *et al.*, 2010). The following context presents the numerical methods applied in this study to solve the advection-diffusion equation for the far field simulation.

3.4.2 Three dimensional Finite Difference Method (FDM)

Computational fluid dynamics (CFD) usually require discretization of the problem into a large number of cells or grid points ($\geq$ millions), therefore the cost of the solution favors simpler, lower order approximations within each cell. Thus, most CFD problems tend to

use the finite difference method (FDM) because of its simple formulations and easy implementation in computer code. Moreover, FDM can provide accurate solutions if appropriate numerical schemes and resolutions are implemented (Chung, 2002).

Central finite difference formulas and a leap-frog time differencing scheme were used to derive Equation (3.48) in this study (*e.g.*, Chung, 2002). The detailed formulations are as follows:

Advection term:

$$\frac{\partial(UC)}{\partial x} \rightarrow \frac{(UC)_{i+1,j,k} - (UC)_{i,j,k}}{\Delta x} \rightarrow \frac{U_{i+1,j,k}(C_{i+1,j,k} + C_{i,j,k})/2 - U_{i,j,k}(C_{i,j,k} + C_{i-1,j,k})/2}{\Delta x} \tag{3.49}$$

$$\rightarrow \frac{U_{i+1,j,k}(C_{i+1,j,k} + C_{i,j,k}) - U_{i,j,k}(C_{i,j,k} + C_{i-1,j,k})}{2\Delta x}$$

$$\frac{\partial(VC)}{\partial y} \rightarrow \frac{V_{i,j+1,k}(C_{i,j+1,k} + C_{i,j,k}) - V_{i,j,k}(C_{i,j,k} + C_{i,j-1,k})}{2\Delta y} \tag{3.50}$$

$$\frac{\partial(WC)}{\partial z} \rightarrow \frac{W_{i,j,k+1}(C_{i,j,k+1} + C_{i,j,k}) - W_{i,j,k}(C_{i,j,k} + C_{i,j,k-1})}{2\Delta z} \tag{3.51}$$

Diffusion term:

$$\frac{\partial}{\partial x}\left(D_x \frac{\partial C}{\partial x}\right) \rightarrow \frac{D_x}{\Delta x^2}(C_{i+1,j,k} - 2C_{i,j,k} + C_{i-1,j,k}) \tag{3.52}$$

$$\frac{\partial}{\partial y}\left(D_y \frac{\partial C}{\partial y}\right) \rightarrow \frac{D_y}{\Delta y^2}(C_{i,j+1,k} - 2C_{i,j,k} + C_{i,j-1,k}) \tag{3.53}$$

$$\frac{\partial}{\partial z}\left(D_z \frac{\partial C}{\partial z}\right) \rightarrow \frac{D_z}{\Delta z^2}(C_{i,j,k+1} - 2C_{i,j,k} + C_{i,j,k-1}) \tag{3.54}$$

Local effects:

The Midpoint Leap-Frog time differencing scheme was used in this study, which is:

$$\frac{\partial C}{\partial t} \rightarrow \frac{C_{i,j,k}^{n+1} - C_{i,j,k}^{n-1}}{2\Delta t} \tag{3.55}$$

The complete difference equation can be expressed as:

$$
\begin{aligned}
C_{i,j,k}^{n+1} &= C_{i,j,k}^{n-1} - 2\Delta t (adv^n - diff^{n-1} - SS) \\
&= C_{i,j,k}^{n-1} - \frac{2\Delta t}{\Delta x}\{U_{i+1,j,k}^n (C_{i+1,j,k}^n + C_{i,j,k}^n)/2 - U_{i,j,k}^n (C_{i,j,k}^n + C_{i-1,j,k}^n)/2 - \\
&\qquad\qquad \frac{D_x}{\Delta x}(C_{i+1,j,k}^{n-1} - 2C_{i,j,k}^{n-1} + C_{i-1,j,k}^{n-1})\} \\
&\quad - \frac{2\Delta t}{\Delta y}\{V_{i,j+1,k}^n (C_{i,j+1,k}^n + C_{i,j,k}^n)/2 - V_{i,j,k}^n (C_{i,j,k}^n + C_{i,j-1,k}^n)/2 - \\
&\qquad\qquad \frac{D_y}{\Delta y}(C_{i,j+1,k}^{n-1} - 2C_{i,j,k}^{n-1} + C_{i,j-1,k}^{n-1})\} \\
&\quad - \frac{2\Delta t}{\Delta z}\{W_{i,j,k+1}^n (C_{i,j,k+1}^n + C_{i,j,k}^n)/2 - W_{i,j,k}^n (C_{i,j,k}^n + C_{i,j,k-1}^n)/2 - \\
&\qquad\qquad \frac{D_z}{\Delta z}(C_{i,j,k+1}^{n-1} - 2C_{i,j,k}^{n-1} + C_{i,j,k-1}^{n-1})\} + 2\Delta t SS
\end{aligned}
\tag{3.56}
$$

The leap-frog scheme is widely used in modeling advective processes, which achieves second-order accuracy with just one function evaluation per time step (Durran, 1991). One problem associated with the leap-frog scheme is the "time splitting" instability that increases the amplitude of computational mode (a numerical artifact of the finite difference scheme) with time. This time splitting can be solved by applying a Robert-Asselin time filter (Robert, 1966; Asselin, 1972), where the solution is smoothed at each time step according to:

$$C_s^n = C^n + \alpha(C^{n+1} - 2C^n + C^{n-1}), \ \alpha \sim 0.01. \tag{3.57}$$

Another problem with the leapfrog scheme is that in addition to the physical initial condition C^0, a computational initial condition C^1 is required to start the computation. In order to reduce the error introduced in the first time step, a method that

use half of the initial time step for the forward time step, followed by leapfrog time steps was used (Figure 3-6).

where
$$C^{1/2} = C^0 - \frac{\Delta t}{2}(adv^0 - diff^0 - SS)$$
$$C^1 = C^0 - \Delta t(adv^{1/2} - diff^0 - SS)$$
$$C^2 = C^0 - 2\Delta t(adv^1 - diff^0 - SS)$$
$$C^{n+1} = C^{n-1} - 2\Delta t(adv^n - diff^{n-1} - SS)$$
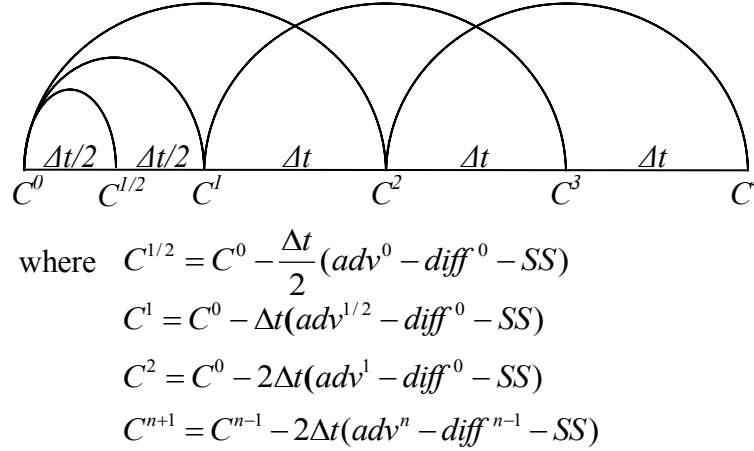
Figure 3-6 Schematic of the leapfrog scheme with half of the initial time step as starting step

The proposed FDM scheme solves the advection-diffusion equation (Equation 3.48) directly in the Cartesian coordinates system (Figure 3-7). The velocities are interpolated from the ocean circulation model (POM) and introduced at the center of the grid cell surface. Pollutant concentrations are presented in the center of the cell. The free surface at each time step is obtained from POM simulations. Bottom topography data are introduced as input information to POM and interpolated onto ocean circulation and pollutant transport model grids. Cells outside of the free surface and bottom lines (shaded cells in Figure 3-7) are abandoned from the computation. Open boundaries are considered in this study. When the grid points approach the lateral boundaries with open boundary conditions, the difference schemes in Equation (3.48) will not work. In this case, the

upstream advection schemes are adopted for modeling the lateral boundary conditions.

The surface and bottom boundary conditions are $D_z \dfrac{\partial C}{\partial z} = 0.$
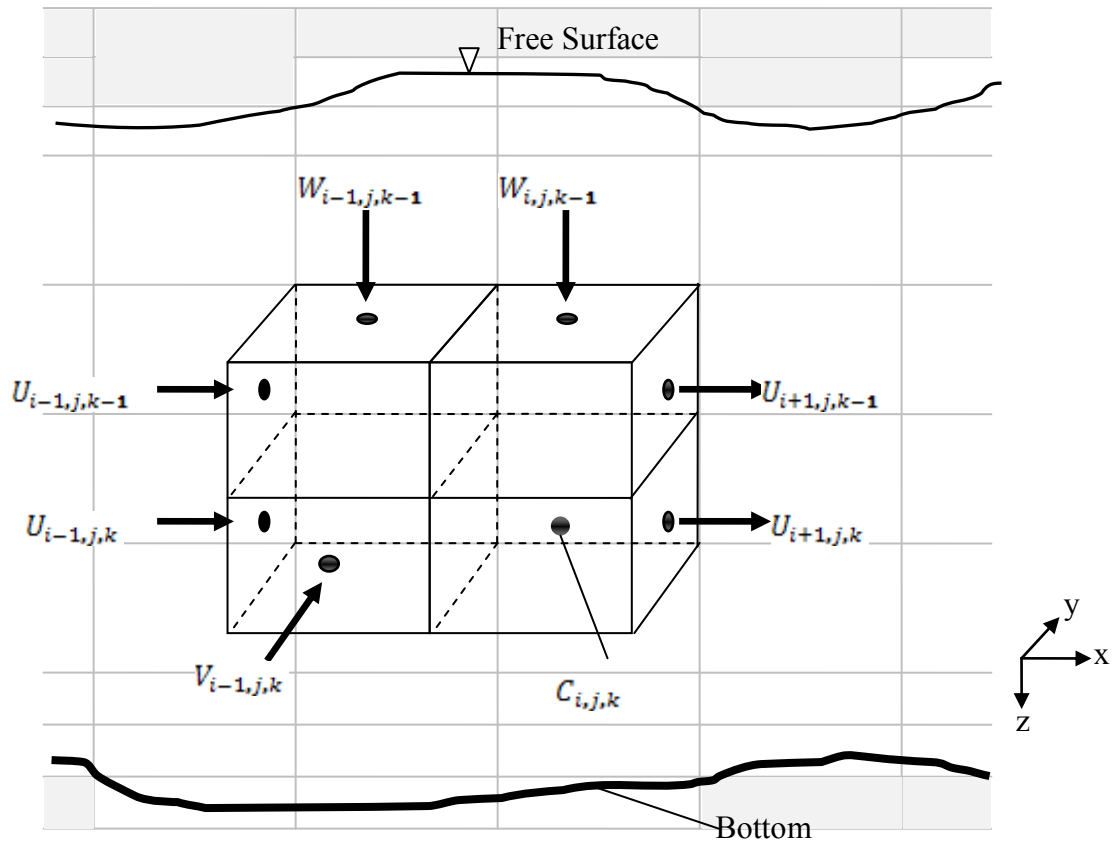
Figure 3-7 Cartesian coordinate system for the finite difference method (FDM) schemes. *x,y,z* are coordinates, *U,V,W* are the three components of current velocities, and *C* is the pollutant concentration, corresponding to each grid cell. The shaded cells are the cells abandoned to capture the free surface and bottom topography.

3.5 Pollutant Fate Simulation

Produced water is a complex mixture of dissolved and particulate organic and inorganic chemicals, which contains a variety of naturally-occurring compounds that are dissolved or dispersed from the geologic formations and migration pathways in which the produced water resided for millions of years (Neff *et al.*, 2011). These chemicals include inorganic salts, metals, radioisotopes, and a wide variety of organic chemicals.

In many environmental situations, especially in ocean waters with rapid dilution of the released waste streams, first order reactions are usually considered for the degradation of pollutant compounds. The mass-law expression for the first order decay rate of concentration C is written as:

$$\frac{-dC}{dt} = kC \tag{3.58}$$

and solved to yield the exponential decay equation:

$$C = C_0 e^{-kt} \tag{3.59}$$

where k is the reaction rate constant, and C_0 is the concentration at time $t = 0$. Equation 3.58 is used as one component of the sink terms *SS* (Equation 3.48). Note the rate constant k is related to the chemical half-life of the pollutant $t_{1/2}$ as:

$$t_{1/2} = \frac{-\ln(0.5)}{k} = \frac{0.693}{k} \tag{3.60}$$

where the half-life denotes the time it takes for the chemical concentration to be reduced to one half of its original value. Chemical transformation half-lives for many organic chemicals can be found in the *Handbook of Environmental Degradation Rates* (Howard *et al.*, 1991).

3.6 Integration of the System for the Modeling and Risk Assessment of Produced Water Dispersion

As presented above, the numerical schemes of the POM were used to simulate the ocean current. The near field plume was simulated by a Lagrangian method developed by Lee and Chu (2003) with an extension to three dimensional flow conditions, while far field dispersion was modeled via a finite difference method. These sub-models were dynamically coupled in the system, in addition to their integration with risk assessment approaches. Detailed integration methods are described in the following sections.

3.6.1 Dynamic integration of the physical models – "two-way" coupling

Coupling models means introducing flow quantities (e.g. momentum or mass) from one model into the other and vice-versa (Bleninger, 2006). Therefore, coupling techniques may raise concerns about such problems as (i) how to maintain the mass balance between fields; (ii) how to identify the transition area or transition boundaries; (iii) how to transform the predictions from one model to another. In the present study, as described in the previous sections, the near field model generates jet and (or) plume trajectories and substance concentrations without involving grid resolutions, whereas the ocean circulation and far field pollutant transport models are constructed on grid meshes. The integration of near and far field models should ensure the conservation of mass, momentum, and energy.

A dynamic coupling technique based on Choi and Lee (2007) was implemented in the present study, which introduces two factors in the ocean circulation and far field

transport modeling: 1) a series of entrainment sinks along the predicted plume trajectory; and 2) the diluted source flow and pollution loading at the predicted terminal level of plume rise. Immediate after produced water is discharged into the receiving water body, a buoyant plume is formed and entrainment processes continuously works between the two fluids. The ambient fluid penetrates the discharged fluid and the discharge fluid penetrates the ambient as well. Therefore, the plume mixing generates sink terms along the jet trajectory and source terms in the terminal level for both ocean circulation and far field transport model. Thus, the continuity equation (Equation 3.2) in POM becomes:

$$\frac{\partial DU}{\partial x} + \frac{\partial DV}{\partial y} + \frac{\partial \omega}{\partial \sigma} + \frac{\partial \eta}{\partial t} = Q_s \tag{3.61}$$

where Q_s is volumetric source or sink term representing the entrainment or diluted flow. Detailed calculations of source and sink terms (term Q_s in Equation 3.61 and term SS in Equation 3.48) are described as follows.

Sink terms

The entrainment flow described in Section 3.3.3 (Equations 3.39-3.47), from the ambient water into the plume element, is assigned to the corresponding POM and far field transport grid cell as sink terms based on the location of the center of computed elements (Figure 3-8), taking the form of,

$$Q_{sink} = -\sum (\frac{\Delta M_{pe}}{\rho_a \Delta t_n}) / (POM \quad cell \quad volume \quad \Delta x \Delta y) \tag{3.62}$$

$$SS_{sink} = -\sum (\frac{\Delta M_{pe}}{\rho_a \Delta t_n} C_a) / (far \quad field \quad transport \quad cell \quad volume \quad \Delta x \Delta y \Delta z) \tag{3.63}$$

where ΔM_{pe} is the entrainment flow mass of plume element pe assigned to the corresponding POM and far field model grid cell (M), Δt_n is the near field time step for

each plume element (T), ρ_a and C_a are the ambient density (M L^{-3}) and pollutant

concentration (M L^{-3}), respectively.

POM and far field transport grid cell
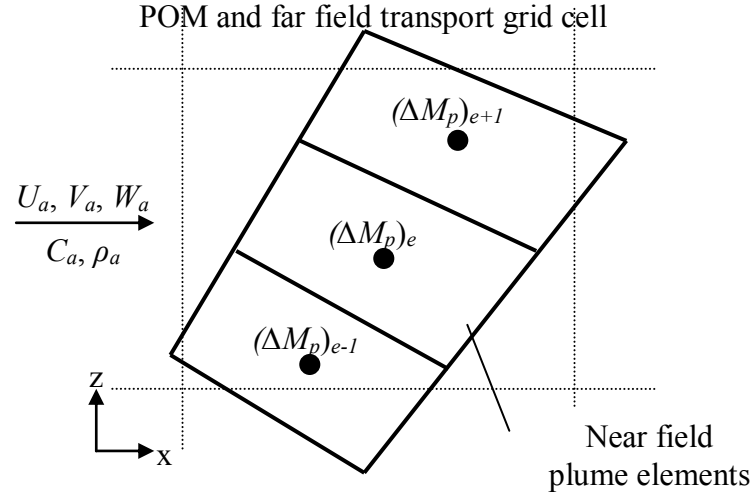
Figure 3-8 Conversion of sink terms from near field plume elements to ocean circulation

and far field transport grid cell (reproduced from Choi and Lee (2007))

Source term

If the surface, bottom boundaries or equilibrium condition are reached, the diluted source

flow is considered as a source term in POM and the far field transport model written as,

$$Q_{source} = \left[Q_0 + \sum_{total} (\frac{\Delta M_{pe}}{\rho_a \Delta t_n}) \right] / (POM \quad cell \quad volume \quad \Delta x \Delta y) \tag{3.64}$$

$$SS_{source} = \left[Q_0 C_0 + \sum_{total} (\frac{\Delta M_{pe}}{\rho_a \Delta t_n} C_a) \right] / (far-field \quad cell \quad volume \quad \Delta x \Delta y \Delta z) \tag{3.65}$$

where Q_0, C_0 are the discharge rate (L^3 T^{-1}) and discharge concentrations (M L^{-3}). Choi

and Lee (2007) introduced the source term the same way as the sink term presented

above which is the grid cell that contains the center of the dissipated plume element.

However, if the terminal plume element extends to cover multiple grid cells (e.g. Figure

3-9), one cell with the center of the plume element may not be able to fully capture the transition from near field to far field modeling. Therefore, in this study, projections of the terminal plume element are used to present the source zone in the far field modeling (Figure 3-9), where cells with over 2/3 length (e.g. line 1) inside the projection circle are considered as a transition zone.
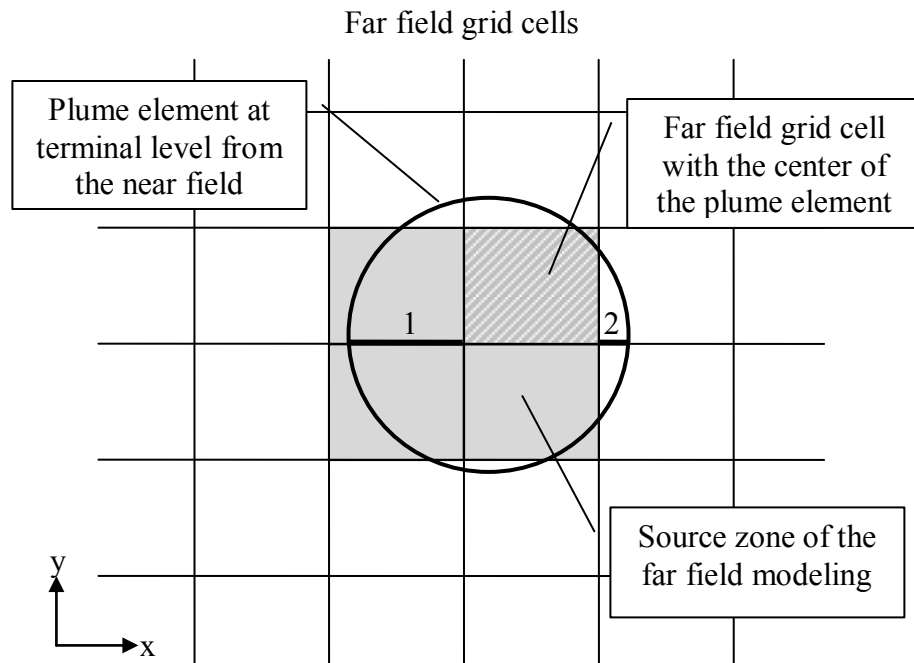
Figure 3-9 Transition zone of the source term from near field to far field models

Integration

Figure 3-10 summarizes the integration approach for the physical models. During each time step, POM provide velocity, density, and surface elevation profiles to the far field transport model, which, in turn, generates the spatial pollutant distribution in the study area. The ambient conditions generated from both POM and far field transport model are

then input into the near field model. Along with initial discharge information, the near

field model calculates the characteristics of each plume element which will be tested as to

whether the terminal level (free surface, bottom, or trap level in the presence of ambient

density stratification) is reached. If so, the near field modeling process stops and the

control will
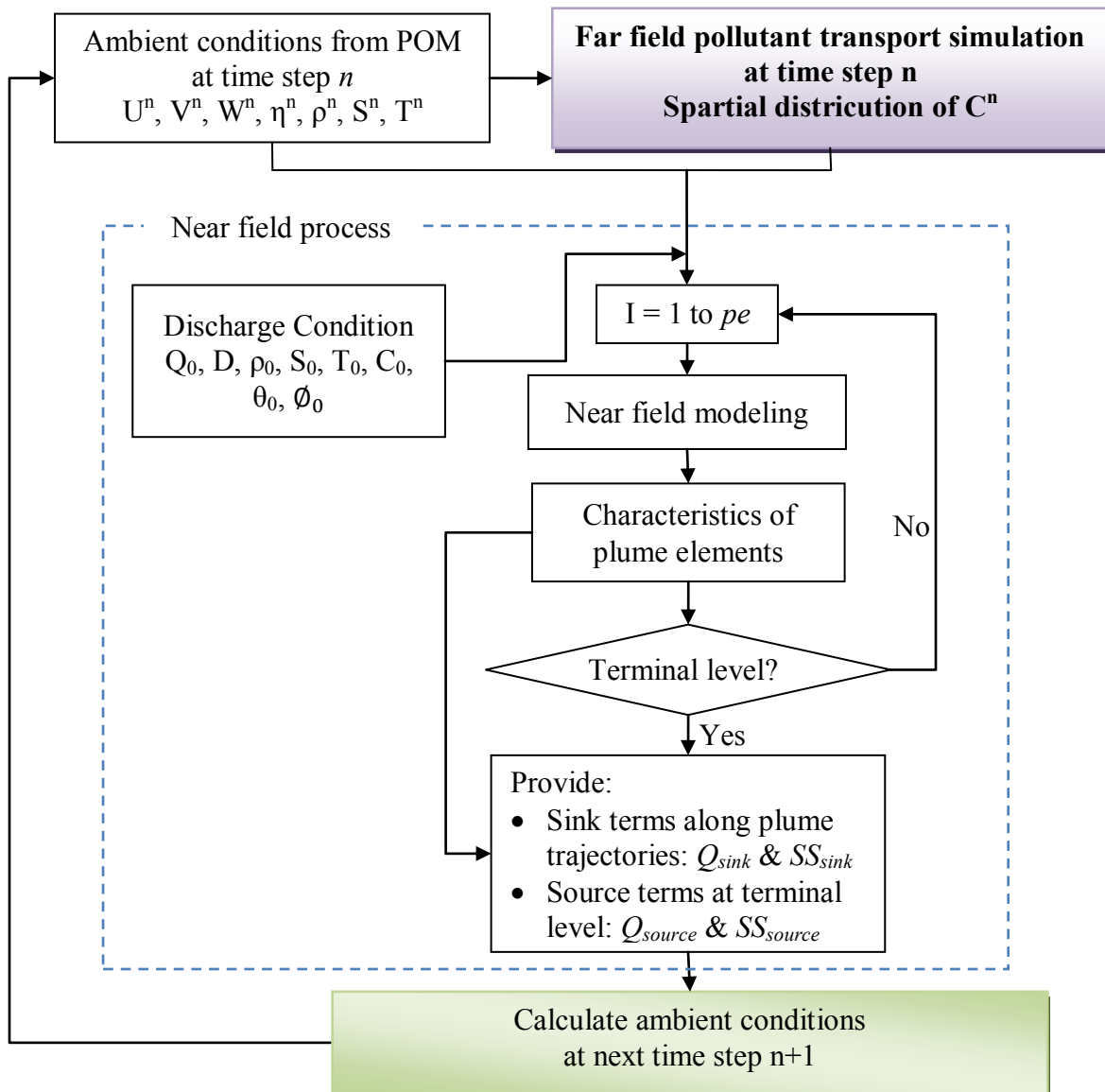
Figure 3-10 Schematic flow chart for dynamic coupling of ocean circulation, near field
plume, and far field transport models

turn back to the ocean circulation and far field transport model. At the same time, the near field model provides both sink and source terms to POM and the far field transport model. The computation procedure is repeated for the next time step until the predetermined total modeling time is reached.

As stated in Section 3.1, the near field and far field transport models were dynamically coupled. However, for the integration of POM and the transport model, a choice of "one-way" couplings can be made. If such case is chosen, only Q_s in Equation 3.61 equals zero, and the integration procedure described above remains unchanged, where velocity and density profiles generated from POM are still updated at each time step in the pollutant fate and transport model.

3.6.2 Integrated risk assessment

Lowrance (1976) defined risk as a measure of the probability and severity of adverse effects. In order to quantify risks, it is necessary to specify the spatial and temporal distribution of contaminants in the environment, the uncertainties in the system, and the method of risk evaluation. In the present study, the risk of environmental impacts arising from offshore oil/gas developments and production is quantified by using a related environmental threshold (e.g. environmental guidelines for protection of aquatic life), in concert with model predictions described in the previous sections of how produced water dispersion affected contaminant transport.

Figure 3-11 shows the computational structure of the integrated simulation and risk assessment system. A modified Monte Carlo method is used to analyze system uncertainties so as to quantify environmental risks. Two risk characterization methods are

integrated into the developed system to assess levels of potential risks associated with produced water discharges: probabilistic risks and exposure risks. The level of environmental risk arising from the release of a given produced water contaminant species into marine water is quantified, in a stepwise manner, on the basis of known regulatory toxic threshold limits/predicted no-effect concentrations. This is done by:

(1)   Identifying uncertainty parameters in the modeling system, and determine their probability distribution (e.g. normal distribution is commonly encountered in practice for variables which have a symmetric distribution about their mean).

(2)   A limited number of model runs are made based on a selected set of combination values of uncertainty parameters within their probability distribution range, i.e. the combination of maximum and minimum values of each uncertainty parameter.

(3)   Based on the modeling results from Step 2, a multiple linear regression model is used to obtain the relationship between uncertainty parameters and output concentration. The created regression equation is used for Monte Carlo simulation.

(4)   A random field is generated from the distribution function for each uncertainty parameter identified in Step 1 (i.e., based on the mean and standard deviation of uncertainty parameters, a random number subroutine is called to generate probabilistic distributions).

(5)   A vector of parameters is drawn at random as inputs to the regression model to predict the concentrations in each spatial location of the study area.

(6)   Step 4 and Step 5 are repeated until the chosen number of simulations is achieved.

(7)   Probability distribution functions of outputs are generated for each concern point in the study area.
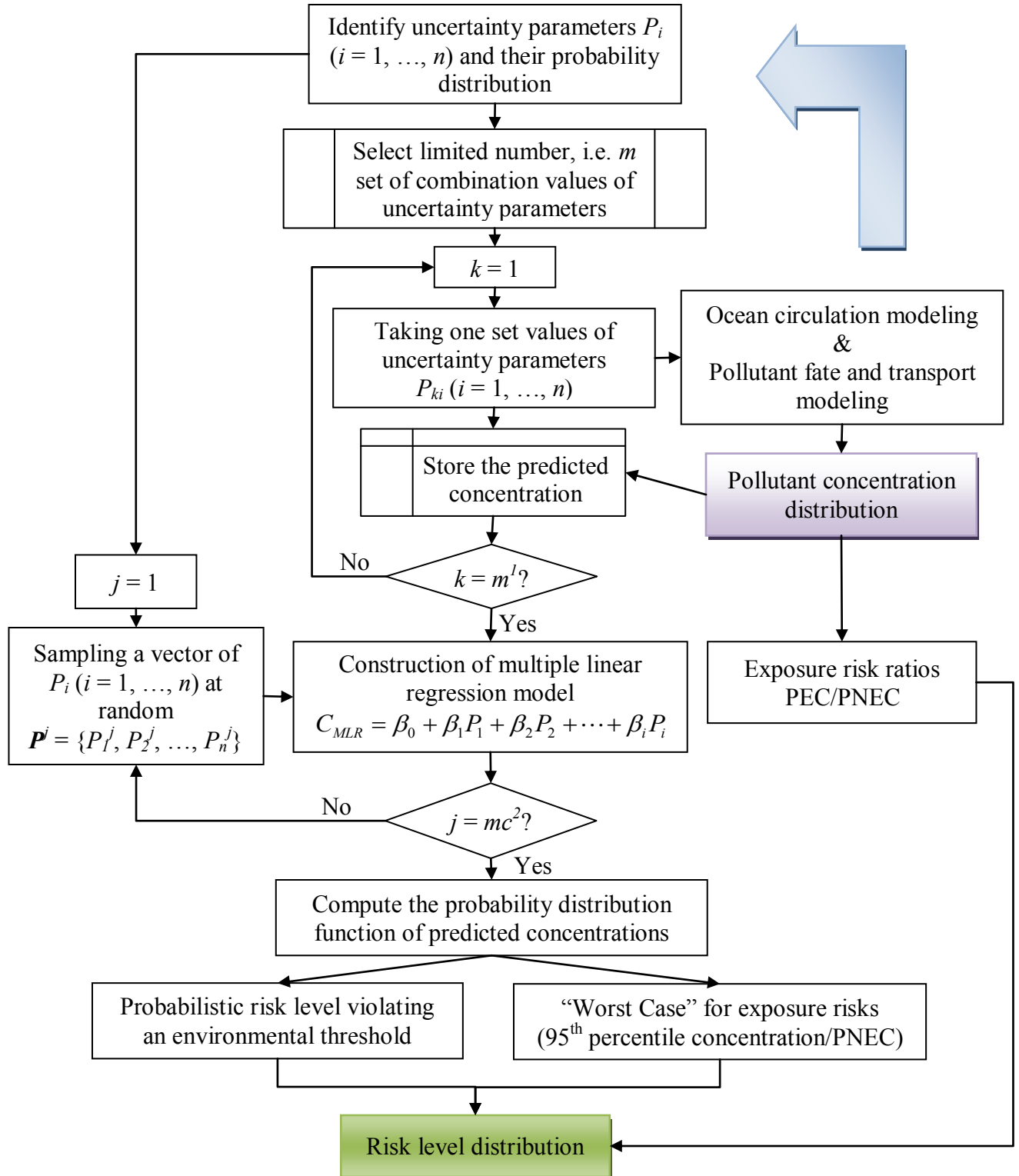
Figure 3-11 Integration of risk assessment methods with physical models

Note: [1] m is in the order of 10; [2] mc is normally in the order of over 10^3

(8)   Finally, having identified the chemical toxicity threshold standards, a complete set of risk-level predictions are obtained using risk characterization methods.

3.6.2.1 Modified Monte Carlo method for quantifying system uncertainty

Risk assessment requires that both model and data uncertainty be taken into account. Uncertainty analysis provides important information by considering the degree of uncertainty in model inputs and parameters and then estimating the effect of these uncertainties on model outputs. Monte Carlo simulation is a method by which repeated model runs are completed using sample vectors of input parameter values which are drawn from corresponding probability distribution functions assigned to the parameters. Thus, modeling uncertainties propagated from model inputs to model outputs can accurately reflect any nonlinearity in a model (Ramaswami *et al.*, 2005). A full set of probability distribution functions for modeling outputs can then be estimated from the results of the Monte Carlo method, and further serve as the basis for risk quantification. However, one drawback of Monte Carlo analysis is that the computational cost for modeling studies can be high, as hundreds or thousands of model runs may be required.

For the complex system as described in previous sections, a traditional Monte Carlo method is almost impossible to implement, especially using a personal computer. Thus, a modified Monte Carlo method, based on Riddle *et al.* (2001), which adopts a statistical method to interpolate the uncertainties from limited model runs, is integrated into the system developed. The steps for performing this modified Monte Carlo method include:

1)   Based on model input information, uncertainty parameters and their probability distribution functions are identified.

2)   Initially a small number of model runs are carried out using selected values of uncertainty parameters, i.e., the combination of values of each uncertainty parameter within their probability distribution range.

3)   Regression analysis is then performed to establish the proximate relationship between modeling output and uncertainty parameters using modeling results from Step 2. In the current study, a multiple linear regression (MLR) model to approximate the output concentrations from uncertainty parameters is constructed as:

$$C_{MLR} = \beta_0 + \beta_1 P_1 + \beta_2 P_2 + \cdots + \beta_i P_i \qquad i = 1, \ldots, n \tag{3.66}$$

where, C_{MLR} is the predicted output concentration using MLR model, β_i ($i = 0, \ldots, n$) is the regression coefficient to be determined based on simulation results from Step 2, P_i ($i = 1, \ldots, n$) is the uncertainty parameter, n is the number of the uncertainty parameters.

4)   After the regression equation (Equation 3.66) is created, the Monte Carlo method is carried out using Equation 3.66, with values of uncertainty parameters selected randomly from their statistical distributions, described in Step 1, to calculate output concentrations. The Monte Carlo results consist in a probability distribution of concentrations for each spatial position, which allows the uncertainty to be mapped.

3.6.2.2 Estimating regression models using least squares

Multiple linear regression is a method used to model the linear relationship between a dependent variable and one or more independent variables. The simplest and thus most common estimator for multiple linear regression models is the ordinary least squares (OLS) (Lai *et al*., 1978). Considering the multiple regression model constructed in Equation 3.66, the relationship between output concentration and uncertainty parameters is modeled through a random error ε, with n predictor variables (uncertainty parameters),

$$C = \beta_0 + \beta_1 P_1 + \beta_2 P_2 + \cdots + \beta_n P_n + \varepsilon \tag{3.67}$$

Based on the limited number of model runs carried out in Step 2 of Section 3.6.2.1, one can assume that if there are m model runs, then there are m levels of Equation 3.67 constructed, taking a vector form as

$$\{C\}=[X]\{\beta\}+\{\varepsilon\} \tag{3.68}$$

where {} and [] denotes column vector and matrix, respectively.

$$\{C\} = \begin{Bmatrix} C_1 \\ C_2 \\ \vdots \\ C_m \end{Bmatrix} \qquad [X] = \begin{bmatrix} 1 & P_{11} & P_{12} & \cdots & P_{1n} \\ 1 & P_{21} & P_{22} & \cdots & P_{2n} \\ & & \vdots & & \\ 1 & P_{m1} & P_{m2} & \cdots & P_{mn} \end{bmatrix} \qquad \{\beta\} = \begin{Bmatrix} \beta_0 \\ \beta_1 \\ \vdots \\ \beta_n \end{Bmatrix} \qquad \{\varepsilon\} = \begin{Bmatrix} \varepsilon_1 \\ \varepsilon_2 \\ \vdots \\ \varepsilon_m \end{Bmatrix}$$

Since vector $\{C\}$ and matrix $[X]$ are known based on the results from m model runs, to obtain the regression coefficients $\{\beta\}$, the ordinary least square method is used:

$$\{\beta\} = ([X]^T[X])^{-1}[X]^T\{C\} \tag{3.69}$$

The multiple linear regression model can now be estimated as:

$$\{C_{MLR}\}=[X]\{\beta\} \tag{3.70}$$

The random error $\{\varepsilon\}$ which is the difference between $\{C\}$ and $\{C_{MLR}\}$ is called the residual. Based on the residual sum of squares, the coefficient of determination which measures the global fit of the regression model can be determined.

3.6.2.3 Risk characterization

Two risk calculation methods are proposed in this study: probabilistic risks and exposure risk ratios.

Probabilistic risk assessment

This approach attempts to account for information from a range of sources and for the quality and relevance of that information (McDaniels *et al.*, 2004). The integrated risk simulation calculates numerous scenarios of a model by repeatedly picking values from a probability distribution for the uncertain variables and using those values for the model. These probabilities are propagated through the model, and an output distribution describing the probability of various outcomes is generated. The probabilistic risk may represent uncertainty or variability or both.

More specifically, environmental risk associated with the discharging of produced water could be expressed as the probability of a pollutant's concentration (denoted as random number L) exceeding an environmental threshold (denoted as C_0), i.e., $R = P(L>C_0)$, where P is the probability function and R denotes risk. Thus, the risk can be quantified as follows (Chen et al., 1998):

$$R = P(L > C_0) = \int_{C_0}^{\infty} f_L(L)dL \tag{3.71}$$

where f_L is the associated probability density function.

Exposure risk

This characterization of risks is carried out based on a risk quotient (RQ) factor which is the ratio of the predicted environment concentration (PEC) to the predicted no effect criteria (PNEC), *e.g.*, the local environmental guideline for a given species. The RQ factor is calculated as follows (Thatcher *et al*., 1999,. 2001):

$$RQ = \frac{PEC}{PNEC} \qquad (3.72)$$

where PNEC is often computed from the lowest-observed-adverse-effect level with appropriate uncertainty and modifying factors, while PEC represents the predicted pollutant concentration distribution from the system.

This exposure risk ratio can be viewed as a measure of the severity of risk. When the risk ratio is greater than 1, ecological injury, such as fish growths or mortality, may be expected. The greater the value of the risk above 1, the greater the possibility of environmental risks.

These two risk evaluation methods can be coupled together as shown in Figure 3-11. The probabilistic distribution of exposure risks for each assessment point derived through the Monte Carlo method is taken into account in the quantification of the potential exposure risks. The "worst case" scenario (e.g. the potential exposure risks under 95th percentile concentrations) can be constructed and severity risk levels can be quantified.

3.7 Development of Graphical User Interface

Designing the visual composition and temporal behaviour of the GUI (Graphical User Interface) is an important part of the system. Its goal is to enhance the efficiency and ease of use for the underlying logical design of a stored program. Source codes of the main system are written by FORTRAN language, while the interface is written by Visual Basic 2008. The entire system is developed to run on a personal computer. Though the user interface requires further improvement along with future applications, major functions are developed to fulfill the requirement of performing modeling study cases. Major functions of the user interface are briefly described as follows.
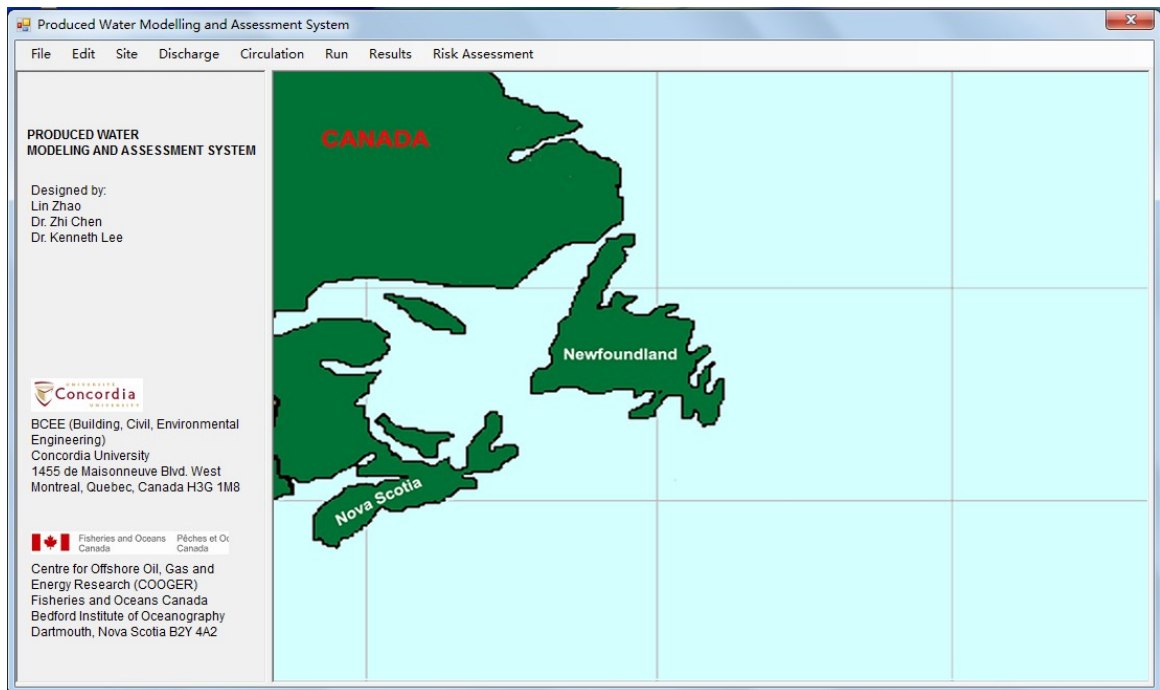
Figure 3-12 Main entry of the produced water modeling and assessment system

3.7.1 Interface development

Figure 3-12 shows a snapshot of the main entry of the developed interface system. Major functions include: <Site>, <Discharge>, <Circulation>, <Run>, <Results>, and <Risk Assessment> as shown on the menu of Figure 3-12.

Site menu

The <Site> menu allows users to input information required for the study area. Under this menu, multiple locations of offshore platforms involving produced water discharges can be selected. Once the coordinates of the study area and grid configurations for both ocean circulation and pollutant dispersion are inputted, the grid system will be automatically
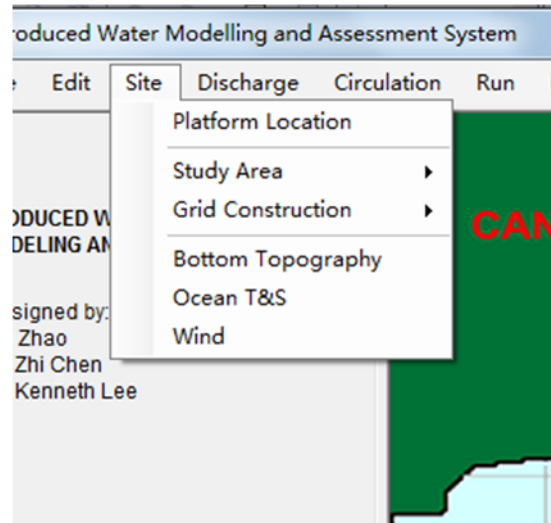
Figure 3-13 Site menu

constructed and ready for use of simulation. The study area and grid system can be different for ocean circulation and pollutant transport modeling. Figure 3-14 shows an example of the chosen platform locations and study area. The grid system can also be different for ocean circulation and pollutant transport as shown later in the case study conducted in this study. It is worth mentioning that the ocean circulation model and pollutant transport simulation have different vertical coordinate systems: while the ocean circulation model has sigma vertical coordinates, the pollutant transport has a Cartesian coordinate system in the vertical. During the simulation, data will be interpolated from one model to another automatically. Bottom topography, sea water temperature and

salinity, and wind data can be constant or variable data. If data are variable, pre-prepared data files are required.
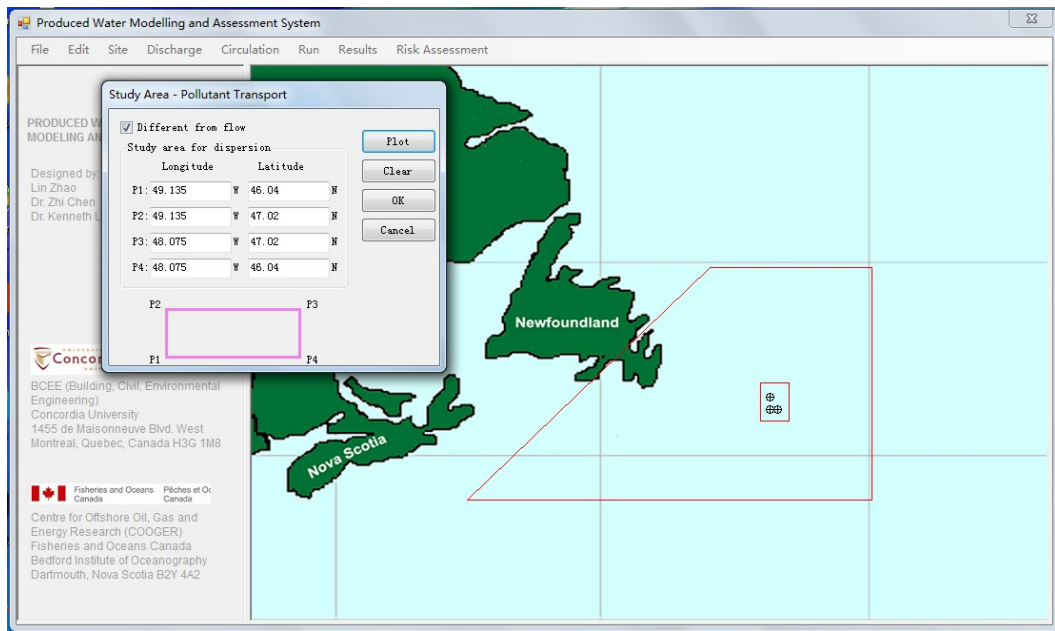
Figure 3-14 Example of the selection of platform locations and study area

Discharge menu

The <Discharge> menu includes the configuration information required for produced water discharges, including discharge depth, directions, emission rate, effluent densities, and chosen chemicals for
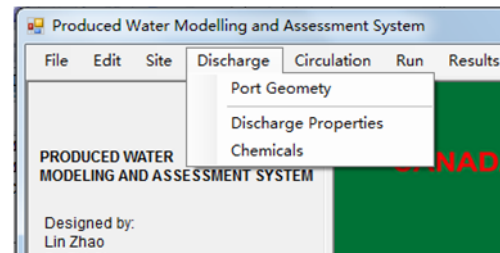
Figure 3-15 Discharge menu

the simulation. The system only can run simulation one chemical at a time and cannot run multiple chemicals simultaneously. Figure 3-16 shows an example of the Discharge Chemical Properties window. At the time of writing, only a few substances and their properties are stored in the system database, including BTEX, naphthalenes, and a

number of metals borne in produced water effluents. With future applications of the system, properties of new substances can be added.
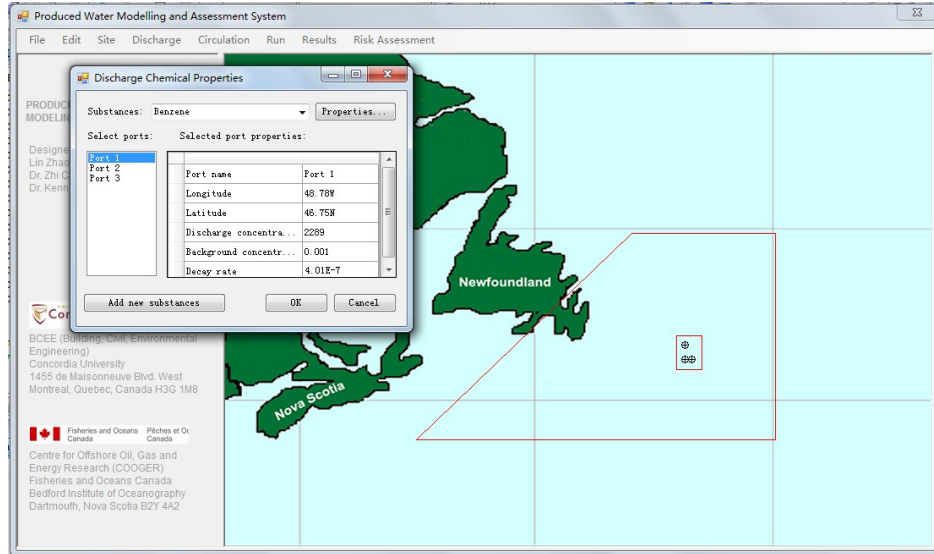
Figure 3-16 Example of inputting discharged chemical properties

Circulation menu

The <Circulation> menu as shown in Figure 3-17 are the input information required for ocean circulation simulations, including circulation mode, control parameters, initial and boundary conditions where diffusivity coefficient, viscosity, reference density, surface and bottom boundary
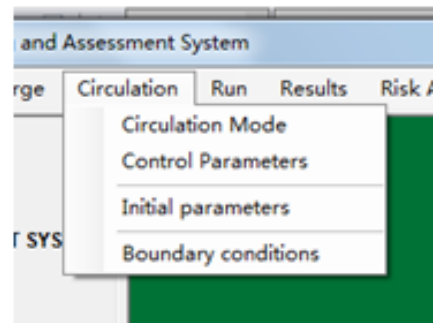
Figure 3-17 Circulation menu

conditions are required to be set up. Tips of the input information can be accessed during the application. Detailed input items and windows will not be presented in this thesis report.

Run menu

Figure 3-18 shows configurations for the system simulation. Different running modes can be selected for the simulation. No matter which running mode is selected, configuration for the ocean circulation must be filled out, even for the running mode of pollutant fate and transport only, because simulations of pollutant fate and transport require ocean circulation data as input. Simulation results are stored in data files in

Figure 3-18 Configurations for the simulation

a designated directory. The generated file names are the prefix strings following by circulation (velocities, temperature or salinity, etc.) or pollutant (near field plume, far field plume, etc.) information and time intervals.

Results menu

In the current stage, only data files are generated as simulation results. Data can be extracted for specified locations or modeling times and exported to be used in Surfer (developed by Golden Software) or Tecplot (developed by Tecplot Inc.) to plot 2D and 3D vectors and contours.

Figure 3-19 Identification of uncertainty parameters window

Risk Assessment menu

Risk assessment functions basically follow the procedures described in Section 3.6.2, including identification of uncertainty parameters, regression model computation, and Monte Carlo method. Figure 3-19 shows an example of the 'Identification of Uncertainty Parameters' window. Only random numbers from uniform distribution and normal distribution can be generated in the system as it currently stands. After Monte Carlo simulation, statistical data such as mean and standard deviation can be calculated and exported to data files.

3.7.2 Data management

As depicted in the previous sections of this chapter and Figure 3-1, the developed modeling system involves the integration of different models and approaches. A large amount of data are inputted, generated, stored, and transferred between models. Data generated by the system simulations, such as hydrodynamics, pollutant concentration distribution, statistical data from Monte Carlo method are stored as data files which can be interpolated and exported for the use of simulation and analysis. Some of the input data such as wind data and temperature and salinity of ocean waters are pre-prepared in data files as well. So far, only chemical properties and some of observed data are stored in the database developed. With continuous improvement of the system interface and future applications, further improvement of data transfer and data management is also needed.

3.8 Summary

This chapter introduces the detailed methodologies of the developed produced water modeling and assessment system. A system framework pictures the major components of the system and their relationships, where ocean circulation modeling, pollutant fate and transport simulation and risk assessment approach are integrated together as a complete system. Detailed methodologies used in this thesis study are summarized as follows.

1)   An existing three dimensional estuarine and coastal ocean circulation model POM is used for the ocean circulation modeling to provide ocean currents, sea water density, surface elevation information.

2)   An extended buoyant jet model is developed to simulate the near field plume trajectories under three dimensional cross flow conditions, and in supporting the far field fate and transport simulation.

3)   The far field transport model is developed using a finite difference method to solve the traditional advection-diffusion equation. Improvements of modeling stability and accuracy are made in the simulation.

4)   Degradation rates of non-conservative compounds associated with produced water discharges are incorporated with pollutant transport modeling. First order reaction rates are considered in the system.

5)   A dynamic integration of the ocean circulation model, near field and far field pollutant fate and transport simulation is performed. "Two-way" coupling of the physical models is introduced to ensure mass balance and a full consideration of the interactions between discharged plumes and surrounding water body.

6) Considering the uncertainty parameters in the system, a modified Monte Carlo method has been integrated to quantify system uncertainties and to provide the probability distribution of predicted concentrations for each grid square. The results from the Monte Carlo approach will serve as the basis for the environmental risk assessment.

7) Two methods for quantifying risks have been presented and incorporated with the physical modeling system: probabilistic risk and exposure risk. Risk assessment analysis based on these two methods is conducted in a study case located off the East Coast of Canada, and described in the following chapters.

8) At the end, the development of a graphic user interface is briefly introduced. Major functions to perform modeling and risk assessment studies are developed.

CHAPTER
4

STUDY CASE
AND FIELD INVESTIGATION

In order to test and evaluate the integrated modeling and assessment system (see Chapter 3), a study site around an offshore oil platform on the Grand Banks of Newfoundland, Canada, is chosen for the environmental assessment of produced water discharges in offshore areas. Detailed information of the study site, the surrounding sea water conditions, field sampling and sample analysis conducted on a research cruise are presented in the current chapter. All data collected for initializing the ocean circulation modeling and produced water dispersion simulation in the study area are described in details in this chapter.

4.1 Overview of the Study Site

Hibernia is located near the northeast corner of the Grand Banks, approximately 315 km east-southeast of St. John's, Newfoundland and Labrador. The Hibernia production platform, a Gravity Base Structure (GBS), located atop an 80 m depth of sea water accounts for the largest volume of produced water currently discharged into the waters of Atlantic Canada (CAPP, 2001). The chosen study area is a roughly 50 km × 50 km square with the Hibernia GBS at its centre as shown in Figure 4-1.

Since there is no existing ocean flow monitoring stations around the study area's four boundaries, numerical radiation open boundary conditions (OBCs) are performed in the ocean circulation model (POM) to simulate the ocean current. However, no matter which type of OBCs were chosen, numerical errors could exist that would create an unrealistic flow across the boundary, thus affecting simulation results. To eliminate such errors, ocean currents were simulated for an area almost 200-fold that of the chosen study area (Figure 4-1). Only the partial results for the middle of the larger area are used for the simulation of pollutant dispersion. A detailed consideration of the ocean circulation model setting is discussed in Chapter 5.

Temperatures at the Hibernia site range from -8 ºC to 7 ºC in the winter and can go as high as 20 ºC in the summer. The ocean surface temperature varies from -3 ºC in the winter to above 15 ºC in the summer. The average wind speed is 37 km hr^{-1} in the winter and 22 km hr^{-1} in the summer. The Guinness World Book of Records calls the Grand Banks the foggiest place on Earth. During winter, there is 40% fog coverage and up to 84% during June and July.
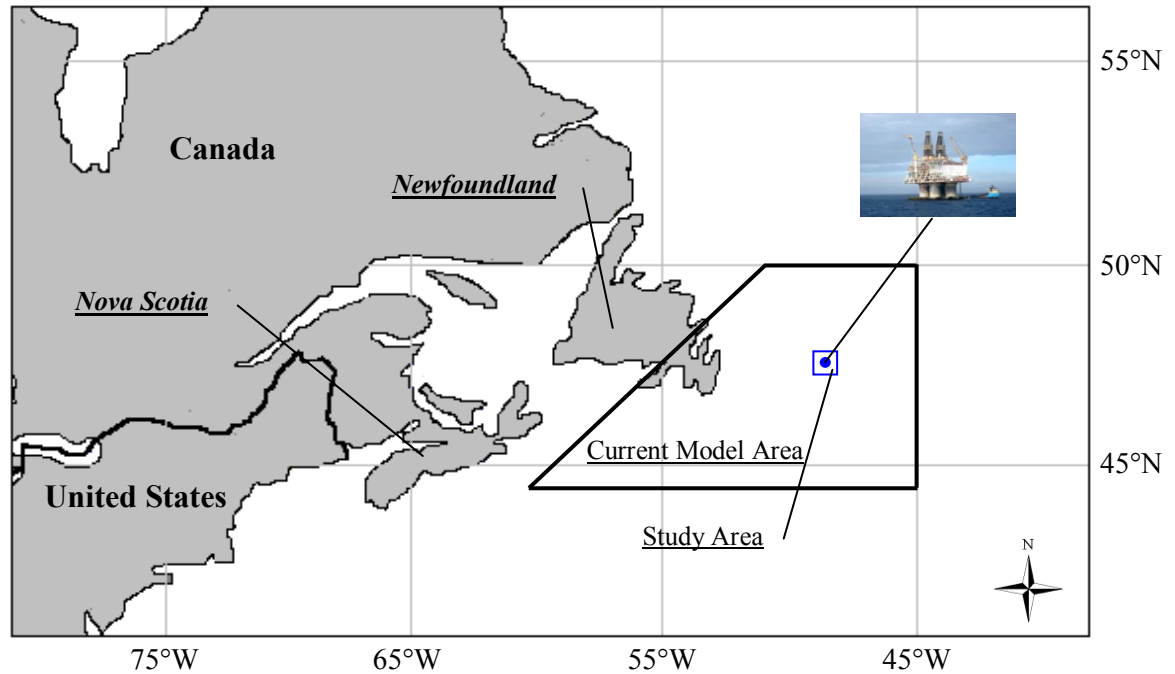
Figure 4-1 Study site and modeling area

The Hibernia oil field was discovered in 1979. The completed platform was towed to the Hibernia oil field and positioned on the ocean floor in June of 1997. The first production from the massive Hibernia platform began in November 1997. The Hibernia platform has a design capacity of approximately 2.3×10^5 barrels (4×10^4 m^3) of crude oil production per day (bpd) – the maximum annual production rate for the platform under Labrador Offshore Petroleum Board (C-NLOPB) regulations is 2.2×10^5 bpd (3.5×10^4 m^3 d^{-1}). In June 2006, Canada-Newfoundland and C-NLOPB increased its reserve estimates for the Hibernia field. Now total oil reserves are estimated at 1,395 – $1,864 \times 10^6$ barrels ($221.85 – 296.4 \times 10^6$ m^3) (C-NLOPB, 2011). Cumulative production at Hibernia from the first oil in November 1997 up to September 30, 2011 has been 765×10^6 barrels (121.7×10^6 m^3) – leaving approximately 630 - 1099×10^6 barrels ($100.2 – 174.7 \times 10^6$ m^3) of reserves yet to be extracted. Based on the oil production of 2010

(about 8.96×10^6 m^3 based on BASIN (2011)), the Hibernia field may still have 11 to 19 years of production life remaining.

4.2 Sea Water Density Profiles

Sea water temperature and salinity data for June 2005 were obtained from the Fisheries and Oceans Canada Oceanographic database. Figure 4-2 shows sea water temperature, salinity, and density profiles at a location about 20 km away from the Hibernia GBS center. The temperature, salinity, and density profiles may show slight changes in different locations over the study area. During June 2005, the sea water temperature was about 5°C - 6°C from the ocean surface to a depth of 20 m and then rapidly dropped to 0°C from 20 m to 40 m depth (Figure 4-2). Then it remains below 0°C with small changes from 40 m to 80 m depth, followed by a constant temperature to the bottom. The salinity is less than 32.5 ppt for the top 30 m, then increases rapidly to 32.8 ppt from 30 m to 40 m. After a small increase between 40 m and 70 m, the salinity show another rapid increase to 33.2 ppt from 70 m to 80 m depth, then remains at about 33.2 ppt to the bottom

Densities are calculated from temperature and salinity data based on relationships between water temperature/salinity and density presented in Martin and McCutcheon (1998) (Equation 3.37). The density profile is similar to temperature and salinity profiles. For the top 20 m, densities show small changes around 1025.6 kg m^{-3}, then increased rapidly to 1026.3 kg m^{-3} from 20 m to 40 m forming a slightly stratified layer in the

ocean water, following with a gradual increase with depth until reaches 1026.7 kg m^{-3} near the bottom.
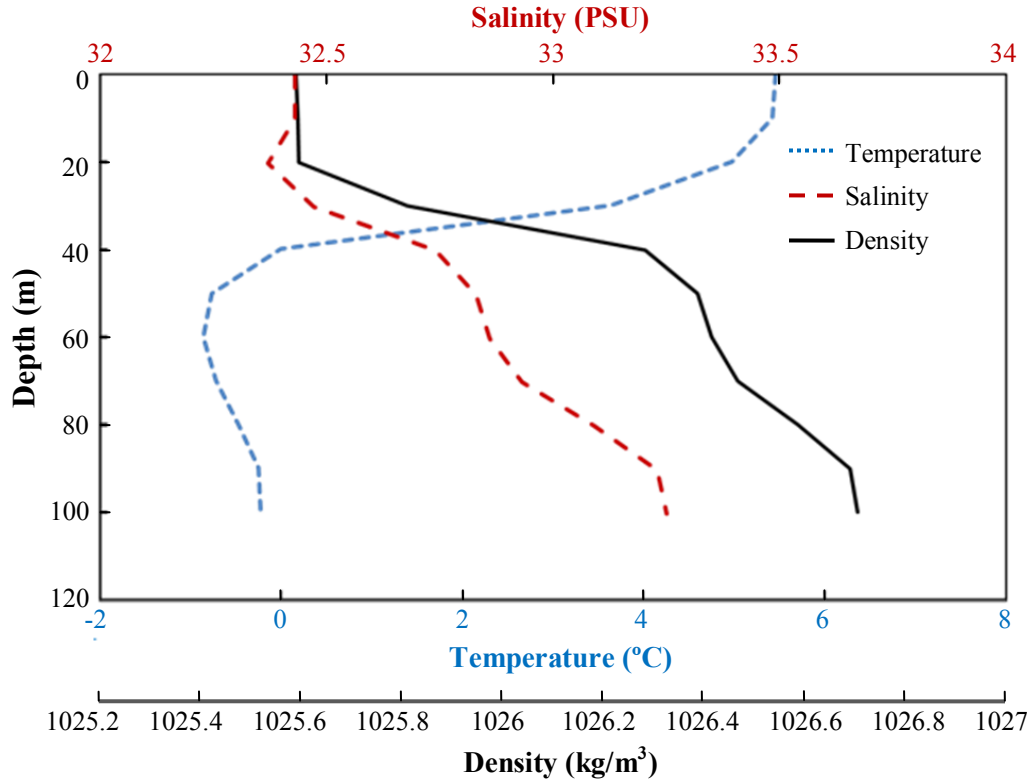
Figure 4-2 Sea water temperature, salinity, and density profiles at locations of 20,000 m away from the Hibernia GBS center (data obtained from the Fisheries and Oceans Canada Oceanographic database)

4.3 Structure of Hibernia Platform

Hibernia consists of two separate components: the Gravity Base Structure (GBS) and the Top sides. The Hibernia platform is uniquely designed to resist the impact of sea ice and icebergs. It can withstand the impact of a one-million ton iceberg with no damage.

The GBS houses the ballast control system that maintains platform buoyancy. When moored to the ocean floor, the GBS is almost completely submerged. The ice wall of Hibernia GBS consists of 16 concrete teeth designed to absorb the impact of

Gravity Base Structure

icebergs. Each tooth of the 1.4 meter-thick ice wall is designed to distribute the impact of an oncoming iceberg evenly throughout the entire structure.

All the discharge outlets are on the outside wall of the GBS, including produced water, storage displacement water, platform drainage water, sea water return, etc. Figure 4-3 presents the cross sections of Hibernia GBS with sea water inlet and discharge locations. The produced water of the Hibernia platform is discharged through a horizontally oriented 30.48 cm diameter port located 40 m above the seafloor and oriented in a southwesterly direction (Figure 4-3).

4.4 Produced Water Discharges

Produced water is defined as all water separated from crude oil or gas during the primary processing of oil and gas on offshore production platforms (Environment Canada, 1990). Based on the definition, produced water consists of formation water, injection water (sea water injected to enhance oil recovery) and production and injection water treatment chemicals (HMDC, 1994). Produced water discharged from Hibernia platform contains traces of metals, a variety of hydrocarbon fractions, as well as naturally occurring radionuclide (JWSL, 2007). Produced water discharges are only regulated with respect to their mean oil concentrations, with a regulatory daily upset limit of 60 mg L^{-1} 24-hour

average oil concentrations, and regulatory limit for the volume weighted 30-day rolling average oil discharge of 30 mg/L (JWSL, 2007).
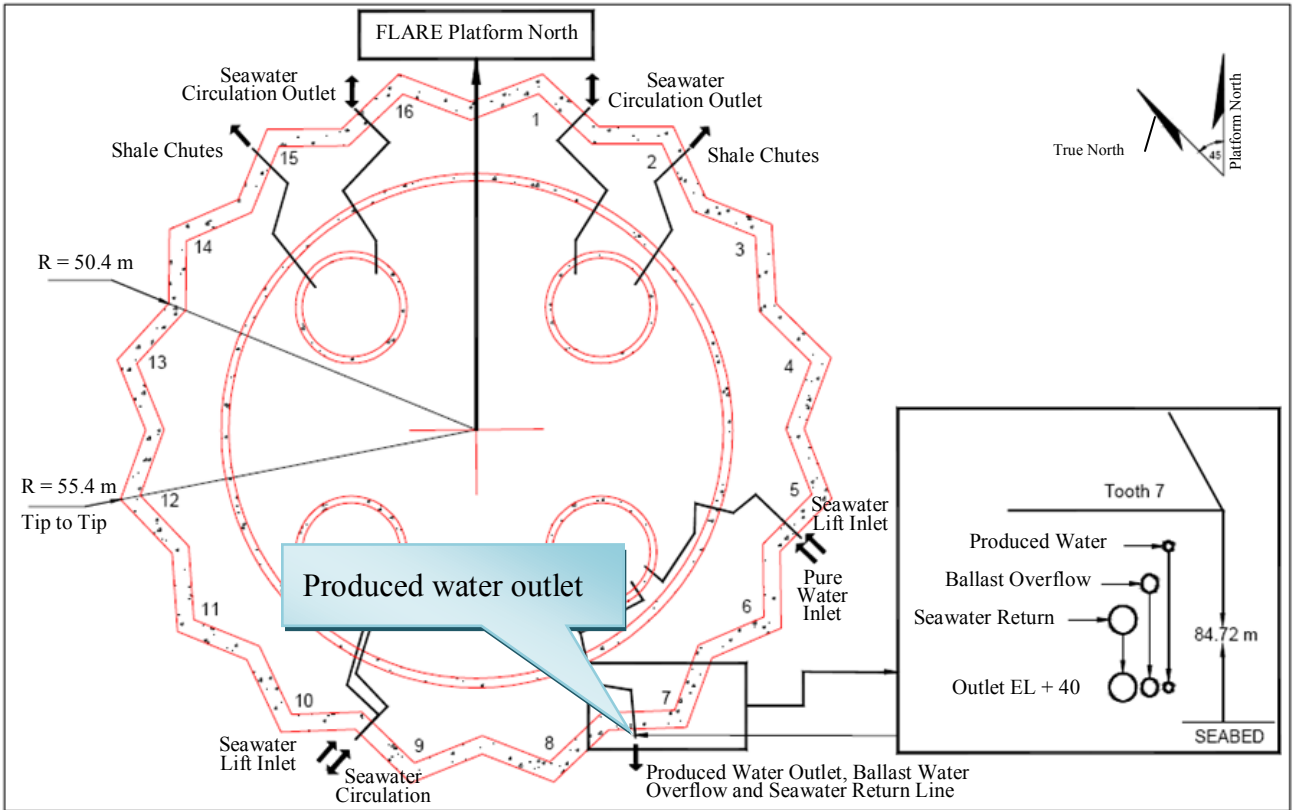
Figure 4-3 Hibernia platform: cross sectional sea water inlet and discharge locations (JWSL, 2007)

Discharge volume data for Hibernia produced water were obtained from BASIN (2011) (Natural Resources Canada). The BASIN database provides monthly production information for oil/gas platforms off the East Coast of Canada. Table 4-1 and Figure 4-4 show annually Hibernia Platform oil/gas production and produced water volume since 1997. Though produced water discharges increase rapidly with the oil/gas production after 2002, at present the production of oil still exceeds that of produced water. The

cumulative produced oil is almost 2.4-fold that of produced water generated. However, when approaching the end life of an oil field, production of produced water may be much higher than that of oil/gas (Stephenson, 1992; Shaw *et al.*, 1999).

Table 4-1 Hibernia Platform oil/gas production and produced water discharge volume (BASIN, 2011)

Year	Oil Production (10^3 m^3)	Produced Water (10^3 m^3)	Gas Production (10^6 m^3)
1997	202	0	46
1998	3784	0	904
1999	5786	15	1435
2000	8394	201	2393
2001	8631	599	2596
2002	10472	448	2445
2003	11785	2447	2686
2004	11854	4885	2742
2005	11541	7076	2808
2006	10350	6559	2495
2007	7826	5896	2065
2008	8066	7464	2414
2009	7290	7086	2445
2010	8957	5811	2556
Total	114938	48487	30030
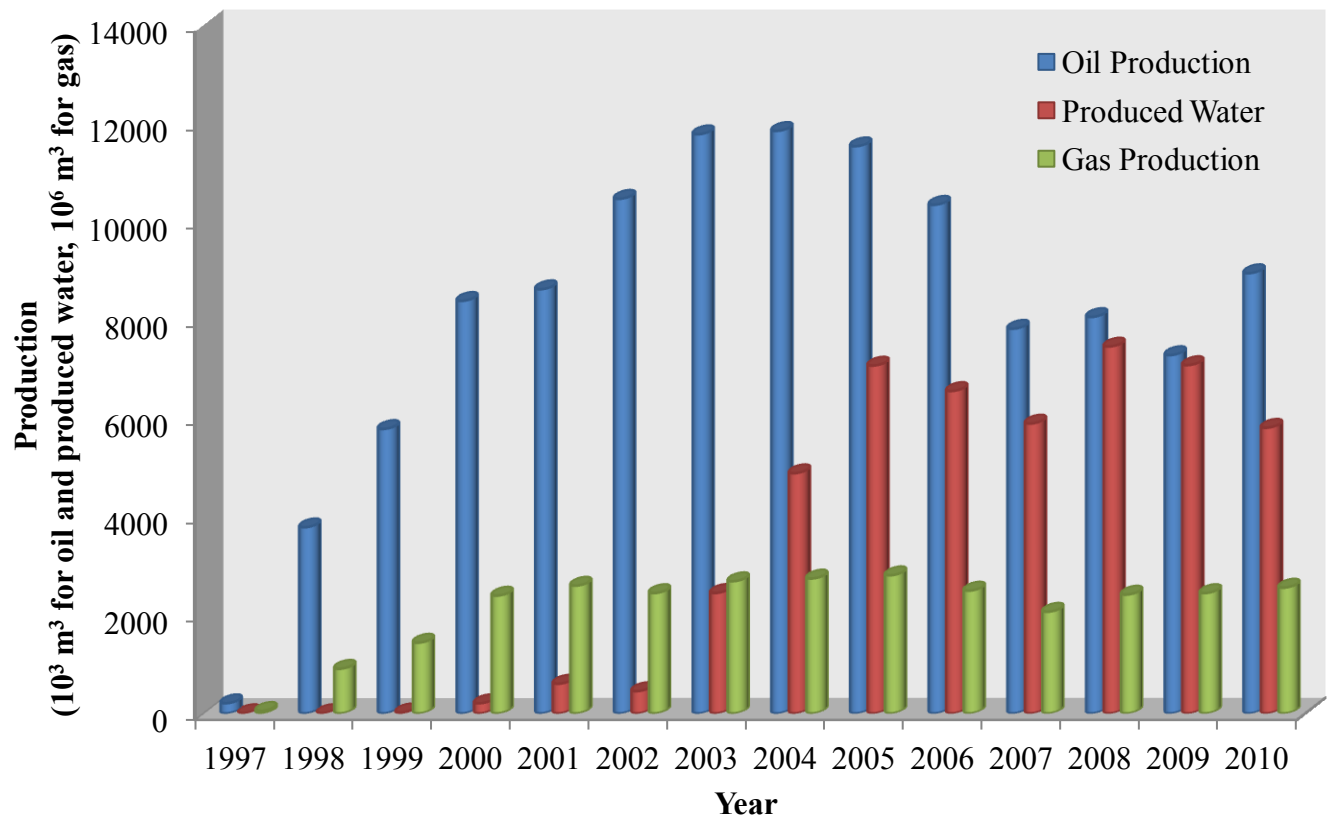
Figure 4-4 Hibernia Platform oil/gas production and produced water discharges (data were obtained from BASIN (2011))

4.5 Field Investigation and Sampling

In response to the great concern that the produced water discharges may impact the marine environment at greater distances from operational platforms due to the anticipated growth of offshore oil and gas industry in Canada, both regulators and habitat/resource managers are required to identify the acceptable disposal limits that would support changes to the regulatory waste treatment guidelines in order to protect the quality of the

ocean's environment in Canada. To carry out the necessary research, several major oceanographic expeditions to the major offshore oil production fields in the East Coast of Canada were conducted with the CCGS Hudson through years under the PERD (Program of Energy Research and Development) research program (Ecological Risk of Produced Water Discharges from East Coast Oil and Gas Operations) by BIO (Bedford Institute of Oceanography) and COOGER (Centre for Offshore Oil and Gas Environmental Research) scientific team. Since the sample analysis results for both sea water and produced water are available for the late June 2005 expeditions, the present case study was carried out for the month of June, 2005.

4.5.1 Sampling equipment

I joined DFO staff and the crew of the Hudson on the mission to Hibernia during the summers of 2006 to 2008. Based on the observations made from my research cruise trip, all the sampling equipment had been pre-installed on the Hudson research ship. A temporal lab was established for sub-sample and to preserve samples collected from the field. The sampling equipment included:

- **CTD/ROSETTE**: CTD instruments measure three important parameters directly – conductivity, temperature and pressure. This instrument has been installed and connected to the ROSETTE system. The ROSETTE

CTD + ROSETTE (taken by Lin Zhao)

system samples water from different depths. Each Niskin bottle can be closed at a

different depth, thus sampling water from many different depths at one time. This 21 × 10-L bottles ROSETTE has two component systems: 1) a computer-directed surface control interface/power supply and 2) a logic-controlled submersible sampler mounting array that selects and remotely closes water sampling bottles.

- **BOB**: BOB is the latest version of a mechanically operated device for sampling water and suspended particulate material at several heights within 0.5 m of the seabed, in the benthic boundary layer (BBL). BOB is capable of collecting larger

BOB (taken by Lin Zhao)

water samples than is the BOSS (Benthic Organic Seston Sampler), but fewer samples are collected per deployment.

- **CAMPOD**: is a light-weight, three-legged platform equipped with a video system similar to that installed on the Video Grab. It is used for very high resolution colour imagery

CAMPOD (taken by Lin Zhao)

of the sea floor. It is designed primarily for making images of the benthic environment.

- **SLO – CORER**: is a hydraulically dampened gravity corer used to take sediment cores (with an undisturbed sediment-water interface) from the ocean floor.

- **Niskin Bottle Casts**: Inorganic samples (metal analysis) were collected using Lever-Action Niskin bottles (General Oceanics) attached to a ¼" stainless-steel wire cable with a 25 kg stainless-steel weight at its end. To reduce the possibility of metals contamination, these bottles for metals analysis are specially designed with all operating mechanisms on the outside of the bottle, and the inside being coated with Teflon. The messenger weight to trip the bottles closed at the desired depth was fabricated from Teflon. Water samples for inorganic analyses were collected at 10m, 35 m and 60 m depths.
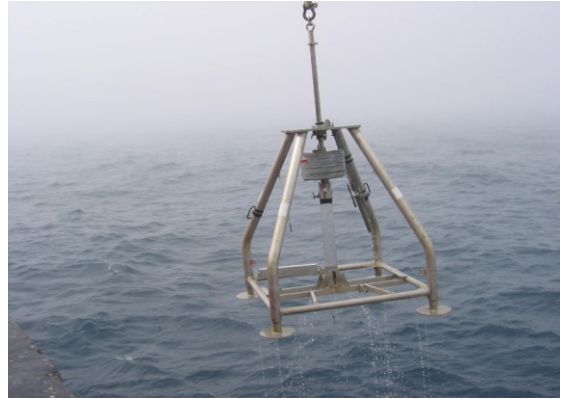
SLO-CORER (taken by Lin Zhao)

4.5.2 Sample Categories

The sample locations (called stations) include West, North, South, South-West, South-East, North-West, and North-East. In 2005, samples from almost 30 stations were collected. The nearest station is 500 meters away from the Hibernia platform; the farthest station (R100) is 100 km away from the Hibernia site. After samples were collected from each location, samples were labeled and put into different bottles for analyses. They were then sent to the lab for sub-sampling and to be preserved. The sample categories include:

- Produced water samples
- Organic samples
- Nutrient samples

- Salinity samples

- Micro biological samples

- Fluorometry samples

- DNA samples

- Sediment samples

- Inorganic samples (metals)

4.6 Sample Analysis

Samples of produced water were collected directly from the process lab on the Hibernia Gravity Base Structure in 2005. These samples were collected immediately prior to discharge and are representative of the production water that is discharged into the ocean. All sample containers were filled to overflowing to eliminate a headspace in the container.

Samples were processed according to analyses, and sent to the laboratory RPC (Research & Productivity Council, Fredericton, New Brunswick) and BIO for measurements, analysis and experiments. The metals/inorganic analyses of *seawater* were conducted at RPC. The inorganic analysis (heavy metals) of *produced water* was conducted at TAF (Trace Analysis Facility) at the University of Regina. The organic chemistry analyses were conducted at BIO. All samples were treated in the Lab according to standard procedures.

Temperature of the produced water collected in 2005 was about 80ºC with a standard deviation of 2ºC, while the salinity was 40.2 ppt to 43.2 ppt. In the present thesis study, constant temperature and salinity for produced water discharges were used for the

simulation, with values of 80ºC and 41.4 ppt, respectively. Based on 2005 production data (BASIN, 2011), an average daily discharge of 21,700 m^3 was adopted. In consideration of data availability for both sampled produced water and seawater, the dissolved concentrations of Pb and benzene were simulated to test the system's ability for simulation and analysis for both conservative and non-conservative substances. Validations of simulation results for Pb and benzene in the study area are presented in Chapter 6.

4.7 Data Preparation for Ocean Circulation Modeling

Topography and climatic information are required for the ocean circulation simulations. The observed ocean current data were also prepared for model validation. Table 4-2 lists all the information and the sources needed for ocean circulation simulation and validation. Detailed data sets are described as follows:

◆ **Topography**: topography data are collected from the Fisheries and Oceans Canada Oceanographic database, which includes the depths in 45950 locations from (78W, 35N) to (40W, 60N). The locations with zero depth are along the shorelines of Nova Scotia and Newfoundland. The deepest location is about 5000 m beneath the surface water.

◆ **Temperature and Salinity of Sea Water**: temperature and salinity data are monthly mean data, which are also from the Fisheries and Oceans Canada Oceanographic database. The data were collected from about 530 locations at 39 different depths.

- **Wind**: wind data are hourly mean data from different sources (Table 4-2). The wind data were collected from 28 locations, including the Hibernia platform. Most of the locations are distributed along the west and south boundaries of the large scale area (Figure 4-1).

- **Current**: the observed current data are the velocity vector data at the Hibernia site. Comparison of modeled ocean currents with observed velocity vector is presented in Chapter 5.

Table 4-2 Model input and validation data preparation

Data Category	Source
Topography	• Fisheries and Oceans Canada Oceanographic database • Data are modified to .csv file
Temperature	• Fisheries and Oceans Canada Oceanographic database • Data are modified to .csv file
Salinity	• Fisheries and Oceans Canada Oceanographic database • Data are modified to .csv file
Wind	• Environment Canada Climatic database • National Data Buoy Centre database • Hibernia Annual Environmental Data Summary (2005) supplied by COOGER • Data are modified to .csv file
Current	• Hibernia Platform Annual Current Measurement Report (2005) collected from COOGER • Data are presented in Chapter 5

4.8 Summary

A case study was conducted on the East Coast of Canada to test and evaluate the integrated modeling and assessment system of solving real world environmental problems. Information collected for this study case is presented in this chapter. All data set are prepared ready for modeling uses. Modeling results, validations, and risk assessment are presented in the following chapters.

CHAPTER

5

3D OCEAN CIRCULATION MODLEING IN THE STUDY AREA

Produced water continuously interacts with the surrounding ocean water after release. Therefore, in order to fully picture the produced water dispersion process, ocean circulation model plays a major role in the simulation and assessment of the fate and transport of pollutant resulting from produced water discharges. Based on information described in Chapter 4, the ocean circulation model POM is initialized and configured to simulate ocean current fields in the study area. Detailed model configurations and validation results are presented as follows.

5.1 Setup of the Modeling Area for the Study Case

The ocean hydrodynamic condition is the major factor affecting the dispersion of the contaminants of produced water discharges in the offshore area. Therefore, the results from the ocean current model directly affect the simulations of the fate and transport of contaminants in produced water discharges. The major issue involved in the ocean current simulation in the present research is that the Hibernia platform is located in an open sea; four lateral boundaries are completely unbounded in the study area (see Figure 4-1). There are no existing current monitoring stations (or existing field observation data) for each lateral boundary. Thus, the situation leaves no choice but to use numerical open boundary conditions (OBCs) for each lateral boundary as described in Section 3.2.3. However, no matter which kinds of OBCs have been chosen, numerical errors will exist and may create an unrealistic flow across the boundary, consequently affecting the simulation results. In order to eliminate the numerical errors that may be caused by numerical OBCs, simulating ocean current on a larger scale covering the study area at the centre is proposed. When the area is large enough, the boundary conditions can hardly influence the inner study area; thus the numerical errors resulting from the OBCs in four lateral boundaries could be minimized to a level that one can ignore. Therefore, in the present research, a large scale area that includes the study area at the middle was used for the ocean current simulations conducted.

The large scale area for ocean current simulation was chosen, extending from (60W, 44N) to (45W, 45N) as shown in Figure 4-1. The left boundary is along the shore of Canada's east coast. A portion of the ocean circulation modeling results related to the

study area is used for pollutant dispersion simulation, which is about 50 km × 50 km with the Hibernia site as the centre. The large scale area is almost 200 times the study area, which is located in the center of the larger area. Therefore, this solution should be enough to achieve our purpose of minimizing the influences of numerical boundary condition on the simulation of velocity components for the study area.

5.2 Model Configuration for Simulating the Ocean Current Field in the Study Region

5.2.1 Grid configuration

The model grid and bottom topography are shown in Figure 5-1. The solution of the horizontal grid is modified into Cartesian coordinate grids, which have 90 × 93 nodes for the large scale area. The size of the model grids is generated as $\Delta x \approx \Delta y \approx 2$ km in the study area. Outside the study area, the size of the model grids is designed to be larger than the inside study area, where the grids vary between $\Delta x \approx 8$ km to $\Delta x \approx 50$ km, and $\Delta y \approx 12$ km (Figure 5-1). The vertical grids in sigma coordinates have 21 vertical layers with a higher resolution near the surface. For example, for a grid point where the water depth is 80 m, Δz is about 2 m at the surface and 4 m in the other layers.

The water depth in the whole large-scale area extends from the deep ocean (3000 m) to 10 m on the continental shelf. The small study area inside is in shallow water, ranging in depth from 60 to 120 m across the area, and 80 m at the Hibernia site.
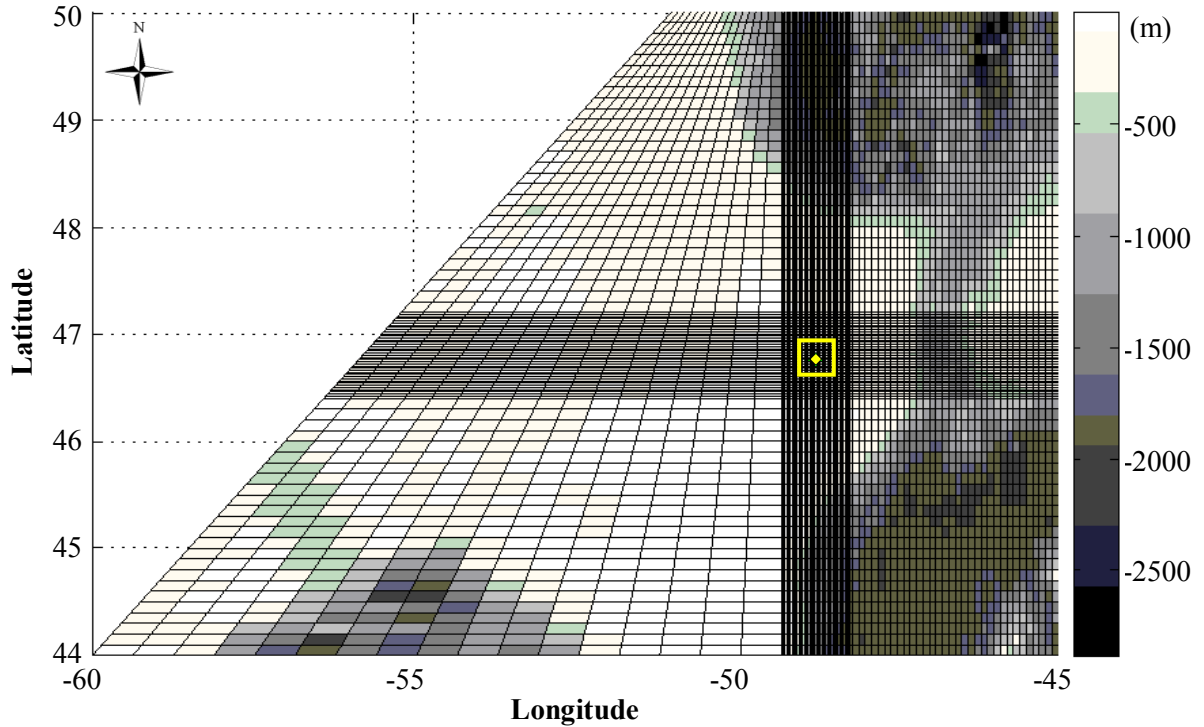
Figure 5-1 Model grid and bottom topography contour map (The diamond point is the location of Hibernia, the square around the Hibernia platform is the study area)

5.2.2 Initial conditions and parameter configuration

The initial conditions for the current model are set to zero, that is, when time is zero, the components of the velocity are zero. The horizontal time differencing is explicit, whereas the vertical differencing is implicit. The latter eliminates time constraints for the vertical grid and permits the use of fine vertical resolution near the surface and in shallow regions. The model has a split time step: a two-dimensional external mode that uses a short time step of 6 s and a three-dimensional internal mode time step of 180 s. At stable thermocline depths, the turbulence closure submodel yields vanishingly small values of vertical viscosity and diffusivity to which is added, however, a constant background value of 2×10^{-5} m^2 s^{-1} (Ezer and Mellor, 1997). A Smagorinsky-type horizontal

diffusion is used here such that the diffusion coefficient is calculated (Smagorinsky *et al.*, 1965):

$$A_M = C_A \Delta x \Delta y \left[\left(\frac{\partial U}{\partial x} \right)^2 + \frac{1}{2} \left(\frac{\partial V}{\partial x} + \frac{\partial U}{\partial y} \right)^2 + \left(\frac{\partial V}{\partial y} \right)^2 \right]^{1/2} \tag{5.1}$$

where U and V are the horizontal velocity components (m s^{-1}) and C_A is a coefficient taken here as 0.2 (Ezer and Mellor, 1997; Ezer, 2001). Table 5-1 lists the major parameters considered in the model.

Table 5-1 Main parameters data used in current modeling for the Hibernia region

Parameter	Value
External mode (2-D) time step (dte)	6 s
Internal (3-D) time step / External (2-D) time step (dti/dte)	30 (dimensionless)
Reference density for seawater (rhoref)	1025 kg m^{-3}
Von Karman's constant (kappa)	0.4
Bottom roughness (z0b)	0.01 m
Minimum bottom friction coefficient (cbcmin)	0.0025
Maximum bottom friction coefficient (cbcmax)	1.0
Smagorinsky diffusivity coefficient (horcon)	0.2
Background vertical viscosity and diffusivity (umol)	2×10^{-5} m^2 s^{-1}

At the four lateral open boundaries (the locations where the water depths are inferior to 10 m are considered as closed boundaries in the model), Sommerfeld-type radiation conditions are used (see Section 3.2.3). The monthly temperature and salinity data of ocean waters from the Fisheries and Oceans Canada Oceanographic database are implemented in the study area. Upwind advection boundary conditions allow the

advection of the temperatures and salinities into the model domain under inflow conditions. This type of boundary condition has been used successfully in the applications of POM (Ezer and Mellor, 1992, 1994; Ezer *et al.*, 1995).

The current model was mainly initialized by using climatological data for June 2005 and running the model for 30 days. Surface forcing includes sea surface temperature obtained from the Fisheries and Oceans Canada Oceanographic database and includes the hourly wind speed and directions for June 2005 from the Environment Canada climatic database, the National Data Buoy Centre database and Hibernia Platform Annual Environmental Data Summary (2005). The topography, temperature, salinity, and hourly wind data for the larger domain containing the study site were interpolated into Cartesian horizontal grids and vertical sigma coordinate layers.

5.3 Validation with Field Data for the Modeling of the Ocean Current in the Study Area

Observed ocean current data in the area close to the Hibernia platform was obtained from the Hibernia Platform Annual Current Measurement Report (2005). The observed velocity vectors were reproduced for comparisons with modeling results at different depths: the surface, 10 m below the surface and 40 m below the surface.
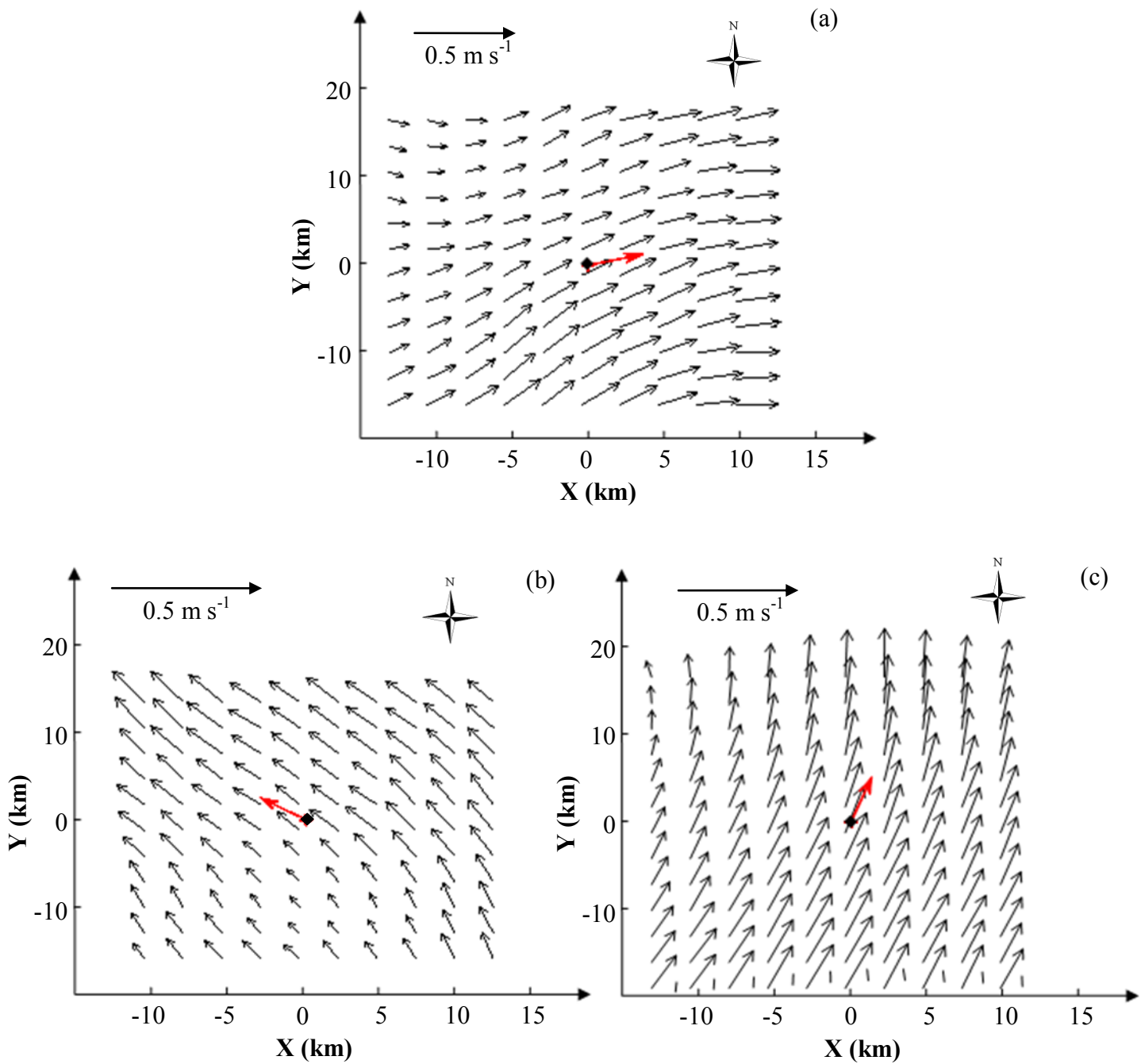
Figure 5-2 Comparison of surface current velocity field: (a) after a model run of 5 days; (b) after a model run of 10 days; and, (c) after a model run of 15 days (the point is the location of Hibernia, and the bolded red vector is the observed velocities at the Hibernia site. The observed velocity is reproduced from the Hibernia Platform Annual Current Measurement Report (2005))

Figures 5-2 (a) (b) (c) are the surface current comparisons for model runs of 5 days, 10 days and 15 days, respectively. Corresponding to each day, the field observations are real-time velocities, which are measured by a MIROS Directional Wave and Current Radar installed on the Hibernia Platform. The observation data are collected from the Hibernia Platform Annual Current Measurement Report (2005). The modeled velocity appears slightly smaller than the observations within 10 days, whereas it shows good agreement with the observed data at 15 days. The directions are generally the same.

Figures 5-3 to 5-4 are the vector comparisons between simulations and observation data reproduced from the Hibernia Platform Annual Current Measurement Report (2005) at 10 and 40 m depths. The observed velocities are instantaneous velocities measured by Acoustic Doppler Current Profiler during different periods of time of June 2005. In Figures 5-3 and 5-4, modeling results within the observation period wer chosen for the validation. The continuous changes of the magnitude and directions of ocean current with time make model validations very difficult. Though the modeling periods may not be in the same period of the observations, the current speed and directions are basically within the range of measurements (Figure 5-3 and 5-4). Comparisons between simulation and monitoring results in different depths indicate that the modeling of ocean currents in the study area is satisfactory using POM, and that it accounts for local hydrodynamic effects and is in direct support of assessing the dispersion of pollutants resulting from the offshore petroleum production process.
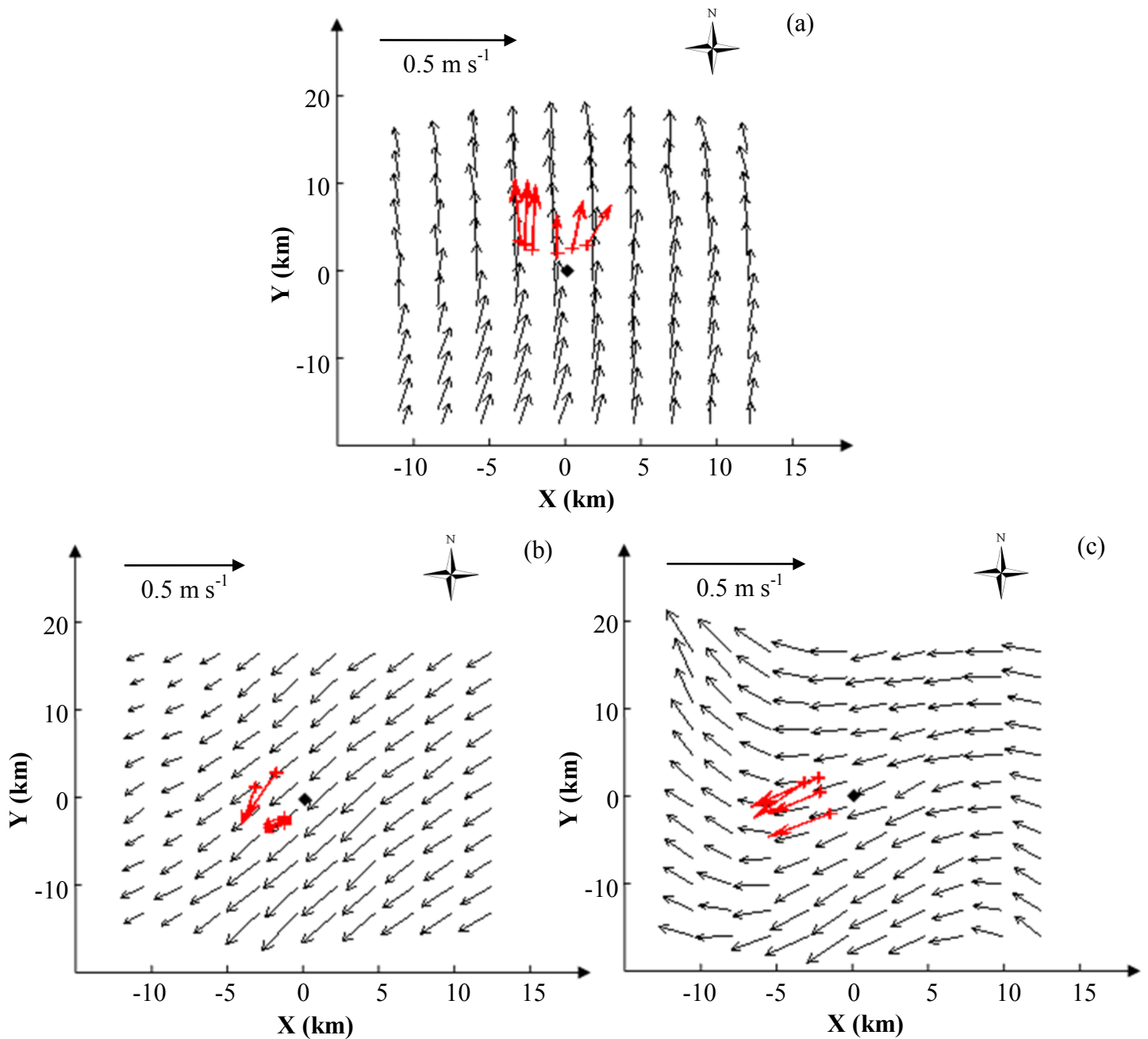
Figure 5-3 Comparison of current vectors at 10m of depth in the water: (a) after a model run of 16 days (the observed velocity was obtained during the period from June 16, 2005 to June 24, 2005); (b) after a model run of 23 days (the observed velocity was obtained during the period from June 16, 2005 to June 24, 2005; and, (c) after a model run of 25 days (the observed velocity was obtained during the period from June 24, 2005 to June 28, 2005. The point is the location of Hibernia. The observed velocities are reproduced from Hibernia Platform Annual Current Measurement Report (2005))
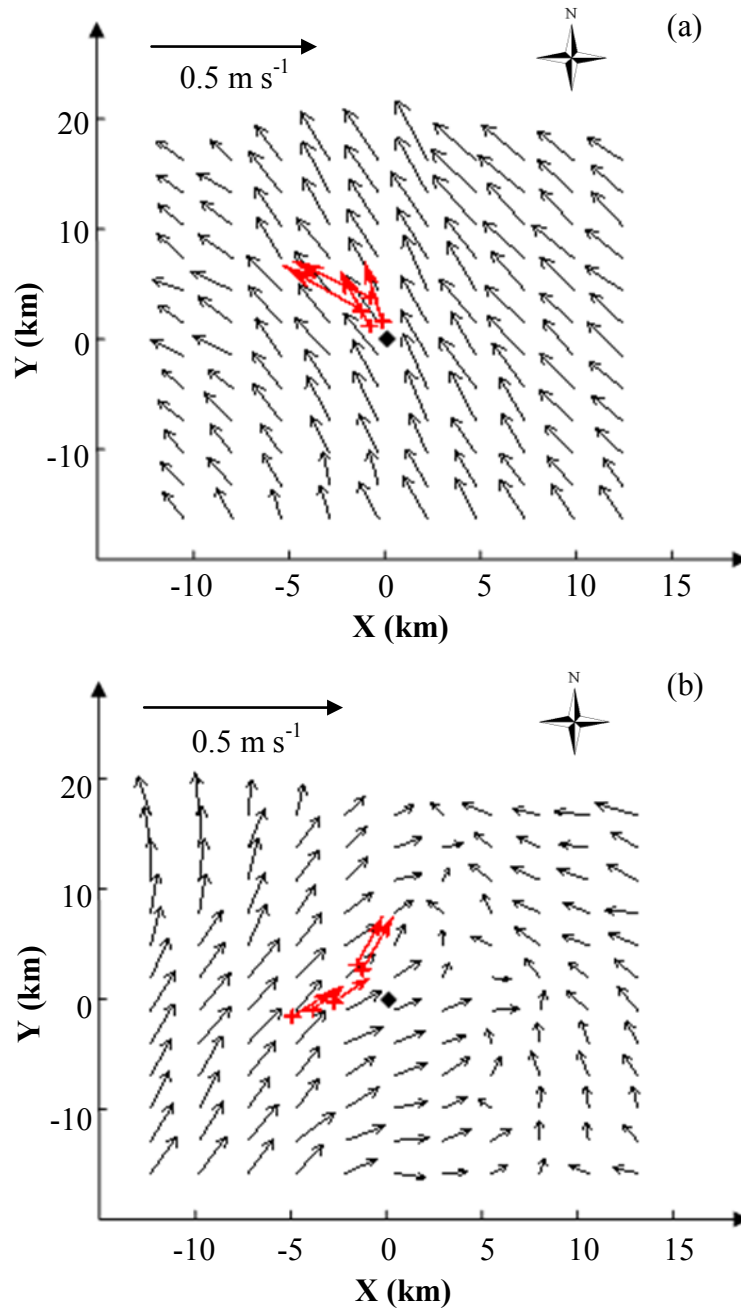
Figure 5-4 Comparison of current vectors at 40m of depth in the water: (a) after a model run of 16 days (the observed velocity was obtained during the period from June 16, 2005 to June 24, 2005; (b) after a model run of 23 days (the observed velocity was obtained during the period from June 16, 2005 to June 24, 2005. The point is the location of Hibernia. The observed velocities are reproduced from the Hibernia Platform Annual Current Measurement Report (2005))

5.4 Summary

Ocean currents in the study area were simulated using the Princeton Ocean Model (POM). In order to minimize the influences of numerical open boundary conditions existing in the study area, a large scale area over 200 times the expanse of the study area covered was chosen to simulate the regional ocean current field. The modeling results at different depths were validated against field data obtained from areas close to the Hibernia platform. The validation of 3D current velocity field simulations indicates that POM can, for the Hibernia region, provide satisfactory current simulations, which will serve as hydrodynamic inputs to the dispersion model. By integrating POM with pollutant fate and transport models, the pollutant dispersion of produced water discharges and potential risk assessment are investigated in the following chapters.

CHAPTER

6

EVALUATION AND FIELD VALIDATION OF POLLUTANT FATE AND TRANSPORT MODELS

Models for the simulation of pollutant fate and transport resulting from produced water discharges are developed as described in Chapter 3. Before using the integrated physical models to simulate produced water dispersion processes in the study area, evaluation and field validations were conducted for near field and far field models individually. Specifically, validations of the near field model were conducted using field data from a survey of literature, while the far field model was evaluated through test cases in

comparison with concentration predictions generated from an analytical solution and a RWPT method. Then, using the integrated modeling system, a field validation was performed in the study area of East Coast of Canada.

6.1 Validation of Near Field Modeling Results against Field Experiments

Because of the complex marine environment, produced water is transported and dispersed in different directions in time based on the local current and water density conditions which are highly variable in open ocean waters. Such factors make it difficult to validate the simulated jet and (or) plume profiles against field data, if there are any, which would also be collected at different periods of time. Unfortunately, there are no detailed experimental data of near field plumes available for the study site at the time of writing of this thesis. In order to verify the near field plume results, validations of the near field model against field experimental data from a published study was carried out in the following sections.

6.1.1 Site description for the validation of near field modeling results

The validation of near field results was carried out against a field study presented in Smith *et al*. (1994, 2004). The field sampling program was performed at the USA platform Eugene Island 314A located about 100 miles SSE of New Orleans Louisiana, and 82 m above the sea floor. Detailed site and sampling descriptions can be found in Smith *et al*. (1994). The major experimental parameters are summarized as follows:

The experiments were conducted on four days, May 19-22, 1992, which are presented as Day 1 to Day 4 in the following context. Produced water was discharged through a 15 cm diameter pipe placed 3 m below the sea surface. The discharge port was pointed at an approximate bearing (clockwise from North) of 105º, and at an angle of 80º below horizontal. The temperature and salinity of discharged produced water was 32ºC and 85 ppt, respectively. The discharge rates are shown in Figure 6-1 with the highest rate being 773.5 m^3 d^{-1} on Day 1 and the lowest, 342.5 m^3 d^{-1} on Day 4. The density of produced water is computed based on the temperature and salinity of produced water (Equation 3.37), having a value of 1059.08 kg m^{-3}. A fluorescent tracer was added at a fixed rate to yield a tracer concentration in the effluent of 18-36 ppm.
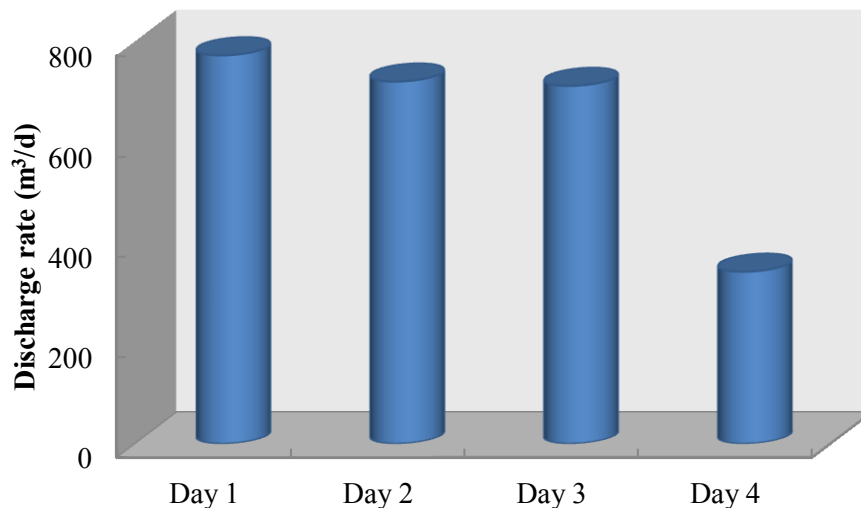
Figure 6-1 Produced water discharges of the near field validation case (reproduced from Smith *et al*. (1994))

Two dimensional ambient currents and water temperature and salinity were measured at different depths during all test discharges (data from Smith *et al*. (1994)).

Full profiles of ambient currents, water temperature and salinity are used as model input for each of the four days of model simulations. The profile of ambient densities is shown in Figure 6-2. The water column was slightly stratified during the four days of experiments, where the stratified layer was basically between 11 and 18 m depth. The water column densities were lesser than those of the produced water, with a range of 1022.65 to 1023.85 kg m^{-3} for the four days of discharge sampling.
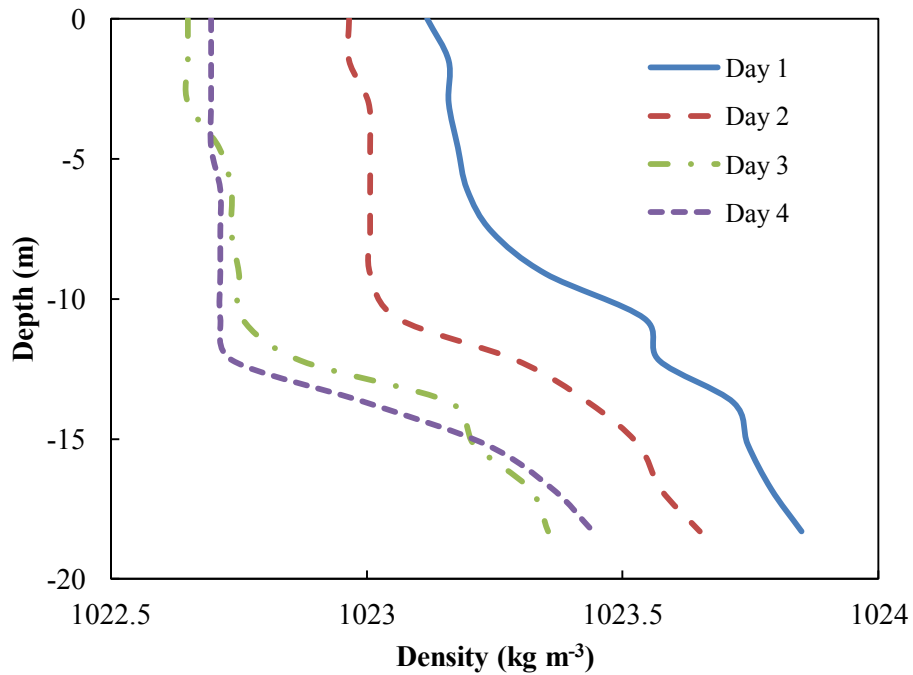
Figure 6-2 Ambient density profiles of near field validation case

6.1.2 Comparisons of near field modeling results with field experimental data

After initial set up of the near field model based on discharge information and local ambient conditions described above, we predicted the near field plume trajectories and concentration profiles, and compared these with the four days of experimental data. During the field experiment, a diver made visual observations of plume depth and

direction throughout the study. The visual observations showed that the plume reached a depth of neutral buoyancy at depths of approximately 8-12 m.

Figure 6-3 shows the predicted plume centerline from Day 1 to Day 4. The predicted maximum concentrations basically lie between 8.7 m and 12.2 m. Though the visual observations only provided an approximate indication of the depth of maximum concentrations, the overall trajectory predictions are in good agreement with observations. Figure 6-3 also presents different dispersion behaviour and trajectory of the plume during these four days. For example, on Day 1, because the discharge rate is higher than on the other days, the plume is basically headed in the discharge direction right after produced water is released. However, since the water column has higher densities (Figure 6-2) on Day 1 (smaller density difference to discharged produced water), the plume is trapped sooner and the trapping levels are higher than the other days. Day 4 has lowest discharge rate (less than half of the discharge rate of day 1, Figure 6-1) and densities (Figure 6-2), the plume is deviated from the discharge direction almost right after the release, and the trapping distance from the source is further than the others.

During the experiments performed by Smith et al. (1994), the diver also instantly collected samples during discharge sampling from Day 2 to Day 4 at various distances along the plume when visual observations confirmed the location of the plume. Figure 6-4 shows the comparison between the modeling results and sampling concentrations in these three days. The predicted average concentrations on Day 3 (Figure 6-4b) showed the best fit with an R^2 of 0.92 whereas R^2 was only 0.45 on Day 2 (Figure 6-4a). Even though the predictions on Day 2 has the lowest R^2 value among these three days (Figure 6-4a), the predicted average concentration can generally capture the concentration

profiles along the distances from source. Considering the large variability of measured parameters (e.g. ambient currents, temperature and salinity, concentration) during the experiments, the overall modeling results have an excellent agreement with the observations.
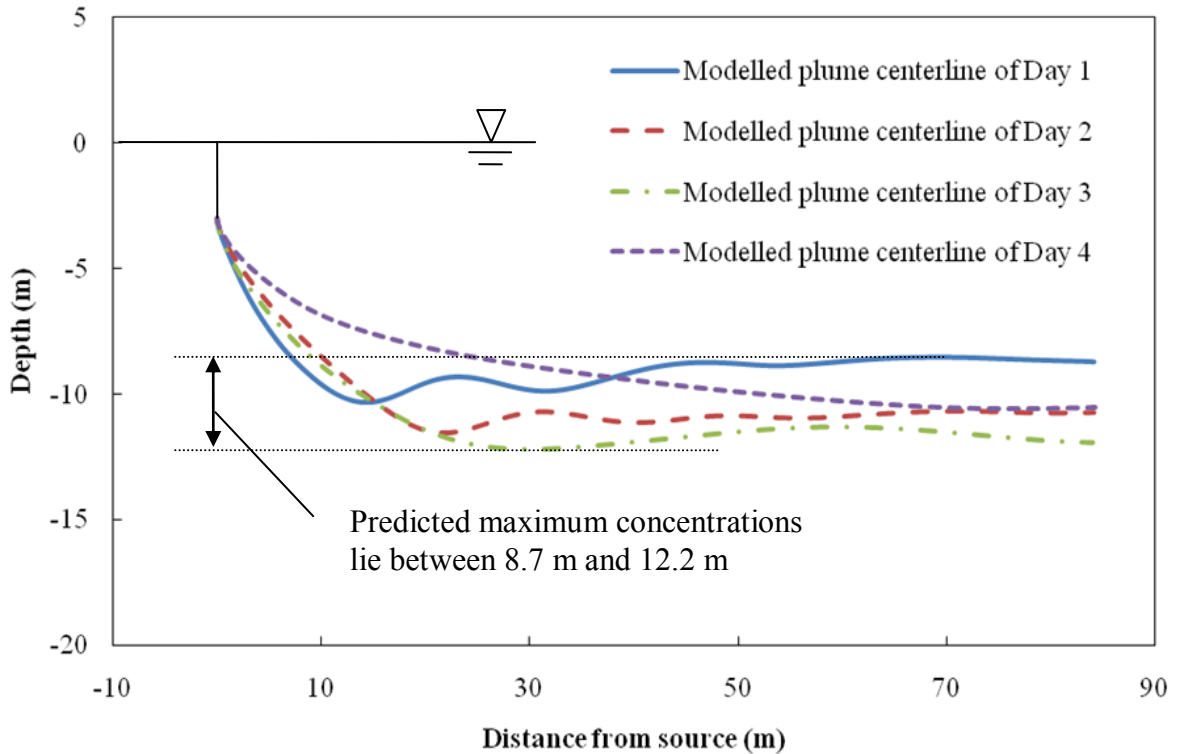
Figure 6-3 Predicted plume maximum concentration profiles for the near field validation case
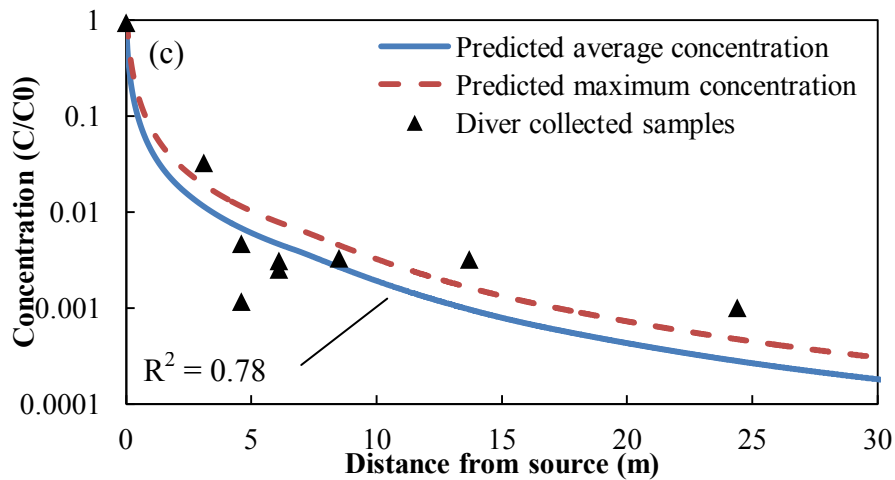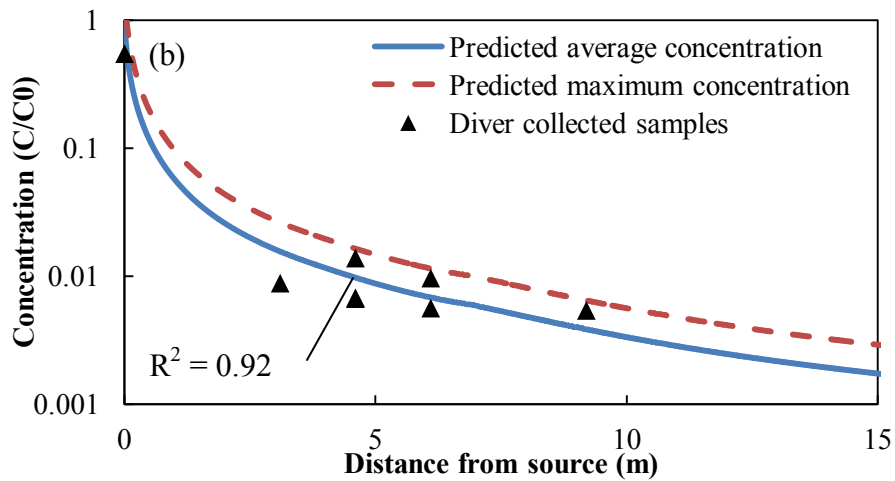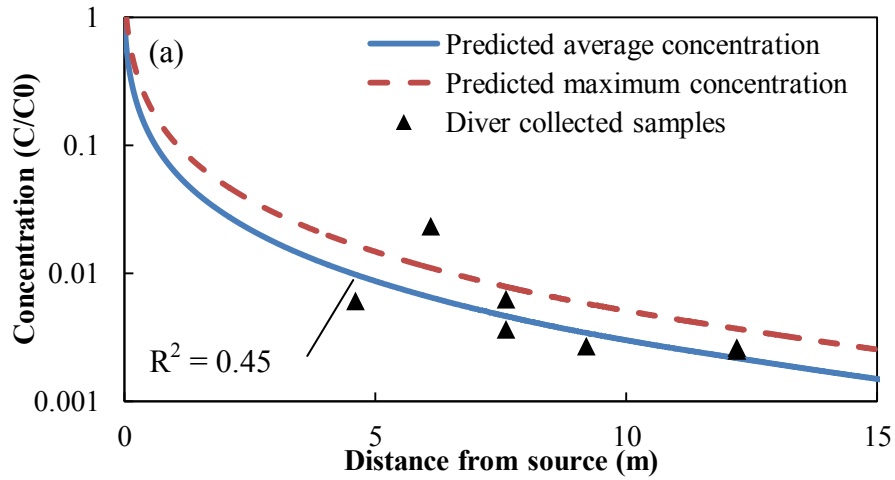
Figure 6-4 Comparison of predicted concentrations with diver-collected samples at a) Day 2, b) Day 3, and c) Day 4 of the near field validation case

6.2 Efficiency Evaluation of Far Field Models through Test Cases

To examine the computational efficiency and accuracy of the far field model developed, test cases were analyzed to compare the concentration distribution results generated with the far field model against an exact analytical solution and a RWPT method. The test cases were selected to reproduce the analytical solution with constant velocity field and dispersion coefficients. The RWPT method has been widely used to simulate pollutant dispersion in offshore areas (e.g. Riddle *et al.*, 2001; Argall *et al.*, 2003; Periáñez, 2006). In order to fully evaluate the efficiency and accuracy of our developed modeling system, the RWPT method was also chosen for the evaluation of the developed far field model.

6.2.1 Analytical solution

The advection-diffusion equations (Equation 3.48) are solved analytically for instantaneous pulses and for continuous sources during the years; for example, models for instantaneous pulses developed by Baetsle (1969) and Hunt (1978), along with three dimensional analytical solutions for continuous sources (Hunt, 1978). In order to test the performance of the developed FDM method (far field model solution described in Section 3.4), a continuous release of pollutant in a uniform current with homogeneous, anisotropic diffusion is considered in the current study. The exact analytical solution takes the following form (modified from Israelsson *et al.* (2006) and Suh (2006)):

$$C(x,y,z,t) = \frac{q \exp((x-x')U/2D_x)}{8\pi a \sqrt{D_y D_z}} \left[\exp(-\frac{aU}{2D_x})\text{erfc}(\frac{a-Ut}{2\sqrt{D_x t}}) + \exp(\frac{aU}{2D_x})\text{erfc}(\frac{a+Ut}{2\sqrt{D_x t}}) \right] \quad (6.1)$$

where $a = \sqrt{(x-x')^2 + (y-y')^2 D_x / D_y + (z-z')^2 D_x / D_z}$; q is the discharge rate (M T^{-1}); U is the current flow (L T^{-1}); t is total simulation time; x, y, z are the coordinates (L); and x', y', z' are the location of the continuous discharge source.

6.2.2 Random walk particle tracking (RWPT) method

The RWPT method can employ many different calculation schemes. For example, a RWPT method scheme may contain more complex models that introduce the pollutant particle velocity and acceleration, correlated in time (e.g. Thomson, 1987; Berloff and McWilliams, 2002). In the present study, basic calculation schemes were used for the RWPT methods because they were sufficient for simulation of pollutant dispersion, and might be used to illustrate the computational efficiency and accuracy issues relevant to more advanced methods. Detailed computational schemes are described as follows.

The RWPT method is a Lagrangian-based approach which has been widely applied in various ocean pollutant dispersion simulations. This method avoids solving the transport equation directly, and instead deals with the dispersion of a solute mass via a large number of particles. A typical particle tracking equation can be expressed as in Equation 6.2, where the local fluid velocity field is translated to the velocities of individual particles, and turbulent diffusion is simulated by a random walk process (Israelsson *et al*., 2006; Periáñez and Elliott, 2002).

$$
\begin{aligned}
\Delta x &= U\Delta t + \frac{\partial D_x}{\partial x}\Delta t + \sqrt{2D_x \Delta t}\, R_x \\
\Delta y &= V\Delta t + \frac{\partial D_y}{\partial y}\Delta t + \sqrt{2D_y \Delta t}\, R_y \\
\Delta z &= W\Delta t + \frac{\partial D_z}{\partial z}\Delta t + \sqrt{2D_z \Delta t}\, R_z
\end{aligned}
\tag{6.2}
$$

where Δx, Δy and Δz represent the movement of a particle from the start to the end of a model timestep (L); Δt is the timestep (T); and R_x, R_y, and R_z are random numbers obtained from a standard normal distribution with mean 0 and variance 1. Equation 6.2 is only one example of RWPT formulation; alternative or more complex formulations can be found in other studies (e.g. Hunter *et al.* 1993; Berloff and McWilliams 2002; Ross and Sharples 2004). Since the diffusivities are assumed to be constant in test cases, the second terms (spatial variation of diffusivities) in the right side of Equation 6.2 are dropped from the calculation.

Boundary conditions are also applied for the RWPT method. Particles which move beyond the study domain are discarded from the calculation. When the calculated elevation of a particle is across surface or bottom, the elevation of the particle is automatically set to surface or bottom elevation and the particle is retained in the calculation for next time step.

As one can see, the computational results based on Equation 6.2 are particle locations instead of concentration profiles. However, in the current study, concentration results are required to compare with the developed far field model and analytical solution. Therefore, conversion of particle distributions into concentration profiles is necessary. The conversion to concentration is straightforward. If N number of particles is moved simultaneously, and a number N_g of particles are inside a small volume V_g, then, the concentration can be expressed as:

$$C(\mathrm{X},t) = m \frac{N_g}{V_g}$$
(6.3)

where m is the mass of each particle.

Since the original concept of the RWPT method was to compute particle trajectories and introduce particle distributions in the final step of computations, in order to avoid confusion with the original concept of the RWPT method, RWPT-concentrations are used to present the final concentration distributions resulting from the conversion from particle distributions to concentrations in the following sections.

6.2.3 Model configuration for the test cases

The test cases were conducted over a study area of 50 km×50 km and up to a depth of 100 m with a steady one dimensional flow field ($U = 0.2$ m s^{-1}) and homogeneous, anisotropic diffusion ($D_x = D_y = 10$ m^2 s^{-1}, $D_z = 0.0001$ m^2 s^{-1}). A steady continuous pollutant point discharge of 10 g s^{-1} at a depth of 40 m below the surface was simulated, and concentration profiles were predicted for a distance of 50 km downstream. Three horizontal grid resolutions of 1, 0.5, and 0.1 km are evaluated with a vertical grid spacing of 2 m (only horizontal spacing is varied for evaluation purposes). For the RWPT-concentration, the grid resolution and particle resolution (number of particles released per unit time) are considered together: three particle release frequencies (1.44×10^4, 1.44×10^5, and 1.44×10^6 particles per day) were arbitrarily chosen for the purpose of examining a low, medium and high level of particle resolutions, respectively, and the same three different grid resolutions were analyzed (1.0, 0.5, and 0.1 km) as well. A simulation consisting of a 5-day model run was performed for each model under each grid and (or) particle resolution to make sure that the simulation was fully developed over the study domain.

6.2.4 Results analysis and model efficiency evaluation

Figure 6-5 shows the pollutant concentration profiles obtained with FDM results compared to the analytical solution (Figure 6-5a) using three different grid resolutions. For the 1 km grid spacing (Figure 6-5b), the FDM concentration profile is a poor match for the analytical solution. The high concentration gradients near the source are not properly simulated and concentrations at some distances (between 30km and 40km in Figure 6-5b) downstream are overestimated. In addition, artificial oscillations caused by numerical dispersion occur in areas with high concentration gradients, such as in the vicinity of the discharge point. Using the finer grid resolutions of 0.5 km and 0.1 km, visual observation shows, the FDM pollutant concentration profiles (Figures 6-5c and 6-5d, respectively) are almost identical to the analytical solution. Both improved the accuracy of the FDM simulation results compared to the 1.0 km grid, and also diminished the problem of numerical dispersion. The small artificial oscillations close to the discharge points were observed with the 0.5 km grid spacing, but not with 0.1 km grid spacing, demonstrating that choosing a finer grid resolution eventually eliminated the numerical dispersion problem, smoothed the concentration profile, and yielded an accurate simulation.

Figure 6-6 shows the pollutant concentration profiles obtained using the RWPT-concentration method with three particle resolutions and with the same three grid resolutions as used above with the FDM. The combination of grid resolutions and particle resolutions are: 1 km and 0.5 km grid spacing with 1.44×10^6 particles d^{-1} and the 0.1 km grid spacing with three particle resolutions (1.44×10^4, 1.44×10^5, and 1.44×10^6 particles per day). All of the RWPT-concentration results exhibited noise in the

concentration profiles. For the 1 km grid spacing (Figure 6-6a), the concentration profile of RWPT-concentration was a poor match to the analytical solution (Figure 6-5a), but compared to the 1 km FDM result (Figure6-5b), the overall concentration profile of RWPT-concentration was better. The concentration profile (Figure 6-6b) is improved by reducing the grid spacing to 0.5 km, but the high concentration gradients near the source are also not properly simulated. By comparing with 0.5 km FDM results (Figure 6-5c), this may suggest that in order to properly simulate the concentration near the source, RWPT-concentration require a finer grid resolution than FDM in the area close to the source.
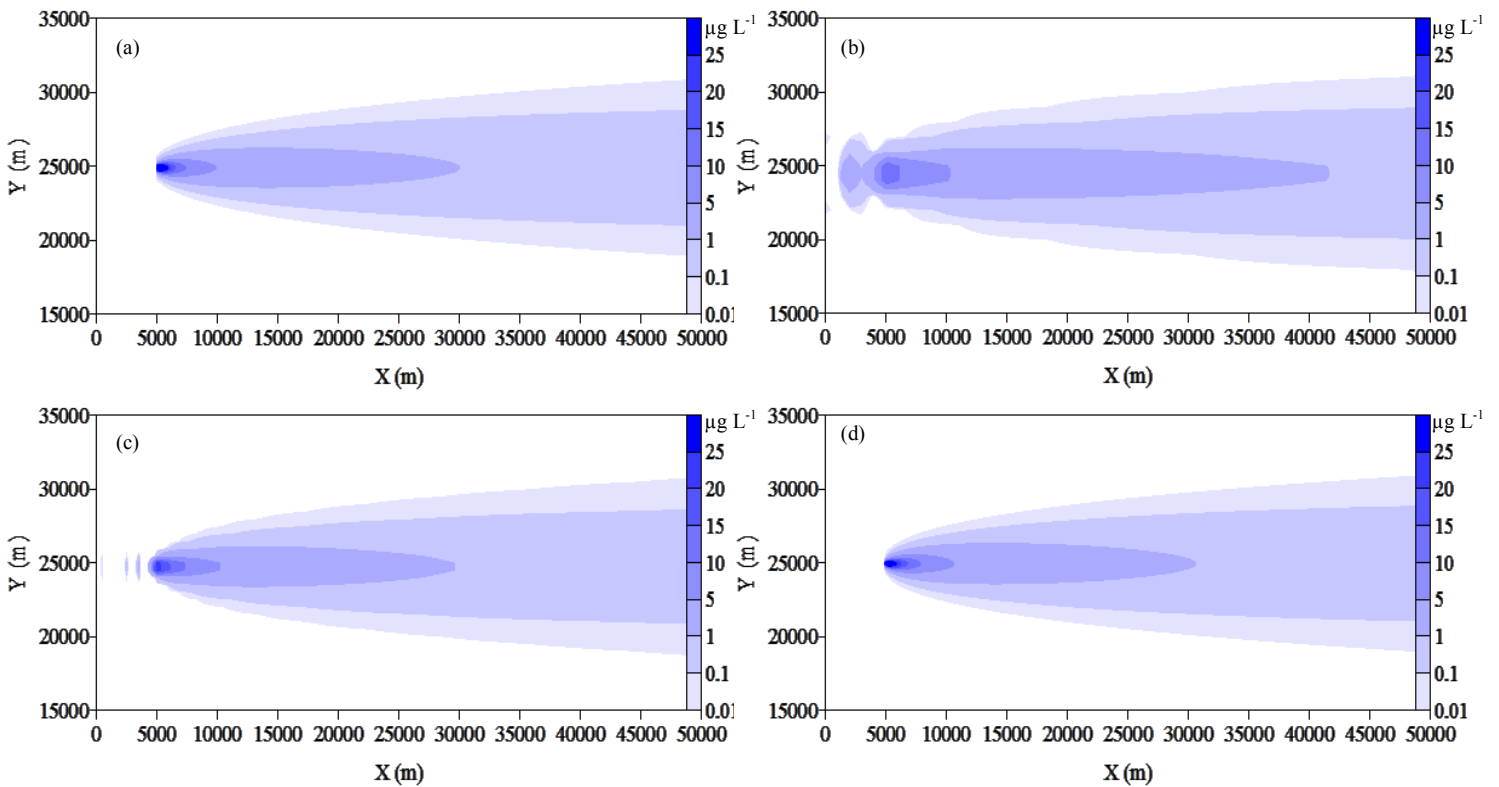
Figure 6-5 Pollutant concentration ($\mu g\ L^{-1}$) profiles at a depth of 40 m in a steady flow condition, using: (a) the exact analytical solution; and FDM method with three different grid resolutions of $\Delta x = \Delta y =$: (b) 1km; (c) 0.5km; and (d) 0.1km.

The effect of varying the particle resolution by three orders of magnitude while keeping the grid spacing constant at 0.1 km, is shown in Figures 6-6c, d, e. The quality of the concentration profiles obtained by the RWPT-concentration method depends on the particle density per grid cell (Israelsson *et al.*, 2006). When the number of particles per grid cell is too low, (*e.g.*, Figure 6-6c), the pollutant concentration profile is scattered because there are not enough particles in each grid cell. The RWPT-concentration results improve with increasing particle resolution, as shown in Figures 6-6d and 6-6e, and the larger number of particles smooth the overall concentration profile, but at increased computational expenses.

Table 6-1 shows the computational expenses for test cases, in which the ratio of the computational time of each case to the total computational time of all cases are calculated. The computational time is collected by means of actual CPU time (the time measured only accounts for the amount of time that the program is actually running, and not the time that a program is suspended or waiting) under basically the same conditions, and the average of three runs for each case is used (Table 6-1). The computational cost of finite difference algorithms with regular grid is proportional to the cube of the grid size and increases steeply when a finer grid resolution is applied (Hao and Varshney, 2006). In our cases, since only the horizontal grid resolutions are changed during the simulation, the computational cost increased quadratically with grid resolutions as shown (Table 6-1). The computation expenses of RWPT method vary linearly with particle resolutions (Israelsson *et al.*, 2006). The computational time of RWPT-concentration does not change much for different grid resolutions under the same particle resolution as shown in the table because the grid resolutions are only involved during the final step of the
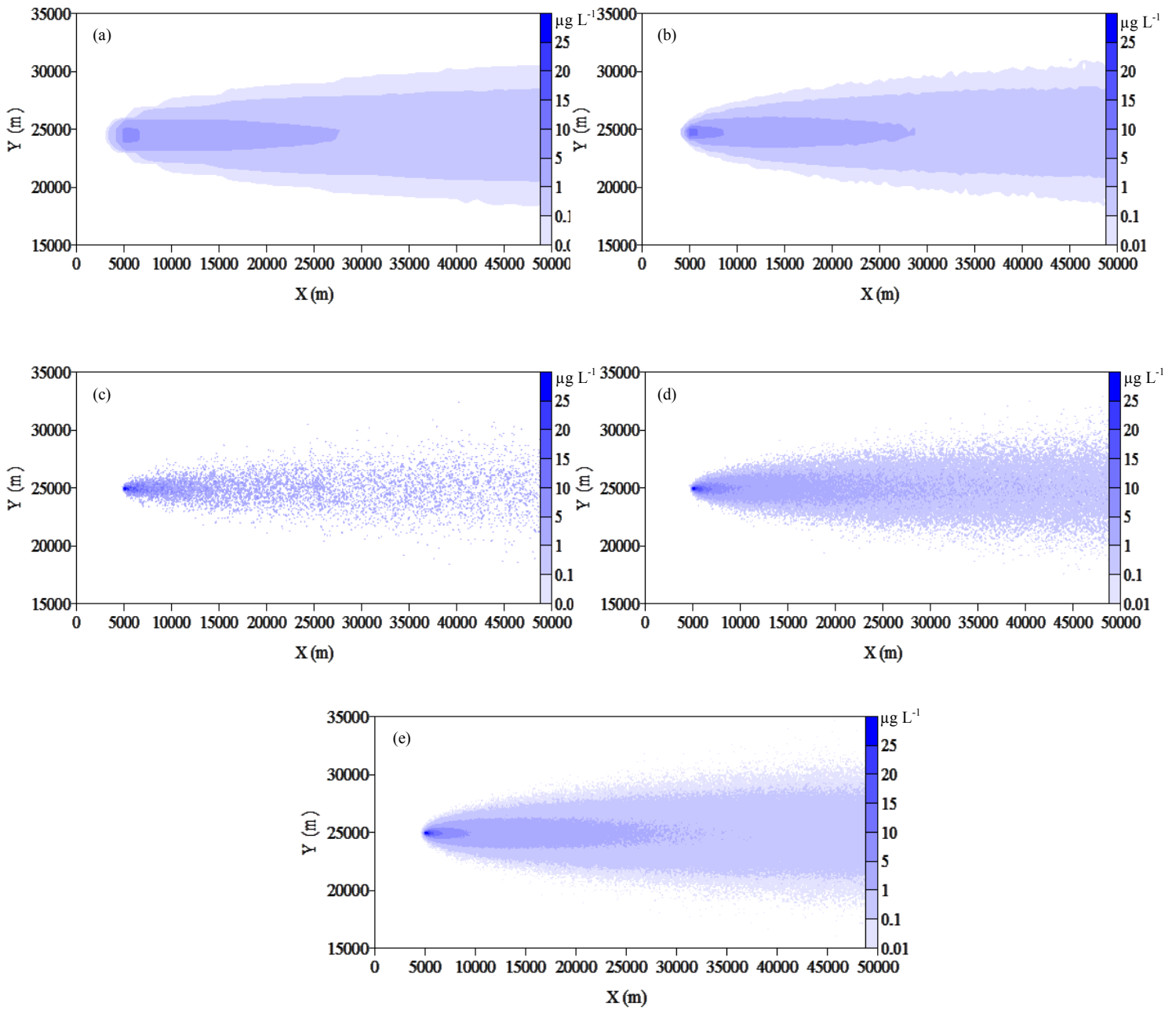
Figure 6-6 Pollutant concentration ($\mu g\ L^{-1}$) profiles at a depth of 40 m in a steady flow condition using the RWPT method with different grid resolutions and different numbers of released particles: (a) $\Delta x = \Delta y = 1$ km with 1.44×10^6 particles d^{-1}; (b) $\Delta x = \Delta y = 0.5$km with 1.44×10^6 particles d^{-1}; and $\Delta x = \Delta y = 0.1$km for: (c) 1.44×10^4 particles d^{-1}; (d) 1.44×10^5 particles d^{-1}; (e) 1.44×10^6 particles d^{-1}.

simulation when converting particle distributions to concentrations. FDM computational costs for the grid resolutions of 1 km and 0.5 km were smaller than for the RWPT-concentration with a particle resolution of 1.44×10^6 particles d^{-1}, whereas FDM computational time for a 0.1 km grid resolution was higher than for all the RWPT-concentration results.

Table 6-1 Computational expenses (%) for test cases (values are the ratio of the computational time of each case to the total computational time of all cases)

Grid resolution	FDM	RWPT-concentration		
		(14,400 par d⁻¹)	(144,000 par d⁻¹)	(1,440,000 par d⁻¹)
1 km	0.44	0.13	1.27	12.54
0.5 km	1.91	0.16	1.27	12.58
0.1 km	50.86	1.75	2.87	14.21

Note: par presents particles

Figure 6-7 shows a comparison of the centerline concentration profiles predicted using the analytical solution, FDM, and RWPT-concentration method, again with three different particle resolutions (only for RWPT-concentration method) and three different grid resolutions (for all three methods). Quality of the concentration profiles improve with increasing grid resolution, especially for the FDM, which generates a centerline concentration curve that is almost identical to the analytical solution for the 0.1 km grid spacing (Figure 6-7c), demonstrating that FDM is a highly grid dependent method and with appropriately configured spatial and temporal resolution accurate results can be obtained. For the RWPT-concentration method, increasing the particle numbers under the

same grid resolution smoothed the solution at each grid resolution; however, the finer grid resolution increased the amount of noise in the results.

It is also observed that the concentrations of RWPT-concentration are low near the source for all three figures in Figure 6-7. This is most likely caused by improper grid resolution, which can be explained by an example point 1 km away from the source. The concentrations at this point from RWPT-concentration (1.44×10^6 particles d^{-1}) for 1 km, 0.5 km, and 0.1 km grid resolution are 6.10 µg L^{-1}, 11.05 µg L^{-1}, and 14.52 µg L^{-1}, respectively, while the result of the analytical solution for this point is 25.16 µg L^{-1}. Apparently when the grid spacing is smaller, the result of the RWPT-concentration is closer to the exact solution. It should be noted that reducing the grid spacing to increase the result accuracy may only be adapted in the area close to the source, but may not be suitable for areas further away from the source. In addition, when the grid resolution increase to certain level, the results will no longer be improved, instead higher noisiness will occur because of the decrease of particle density in each grid cell. This phenomenon is further discussed in the following context.

The noisiness of RWPT-concentration results is clearly depicted in Figure 6-8, where the absolute relative error along the center line for the FDM and RWPT-concentration method vs. the analytical solution is plotted. Within 5 km downstream from the source, the RWPT-concentration results for all particle and grid resolutions are relatively smooth, and then become noisier along the distance (Figure 6-8). The finer the grid resolution, the more severe the noisiness of the results. FDM generates smooth concentration results. Basically, the relative errors of FDM results increase to a point at about 2-3 km downstream from the source and then decrease with increasing distance
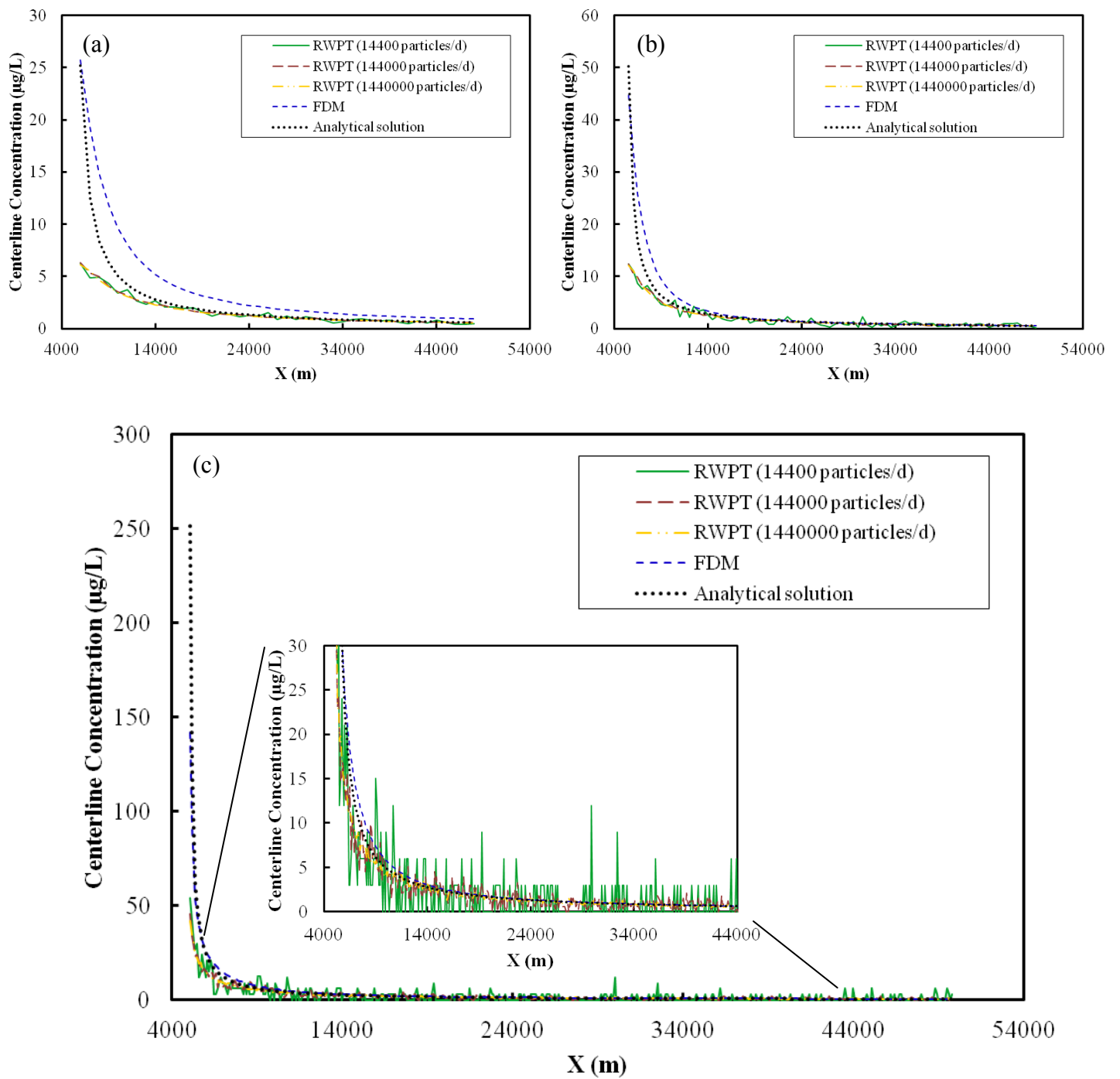
Figure 6-7 Centerline pollutant concentration comparison using different horizontal grid resolutions of Δx = Δy =: (a) 1 km; (b) 0.5 km; (c) 0.1 km.
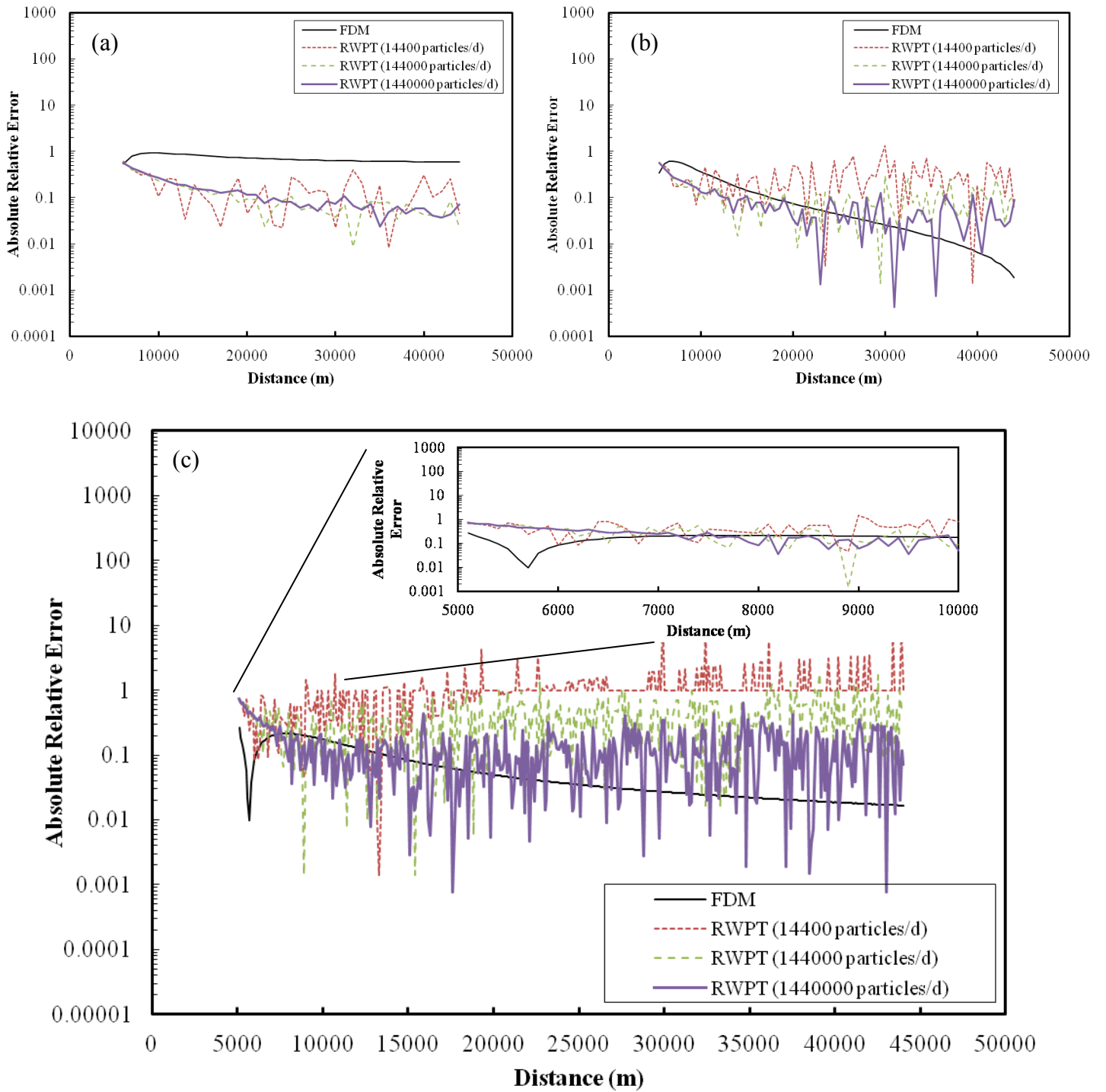
Figure 6-8 Absolute relative error along the center line for FDM and RWPT method vs. the analytical solution using different horizontal grid resolutions of Δx = Δy =: (a) 1 km; (b) 0.5 km; (c) 0.1 km.

from the source. The trend of relative errors resulting from RWPT-concentration solutions slightly decrease from the source to about 10 km downstream, and then remain relatively stable with increasing distance from the source. For the 1 km grid resolution (Figure 6-8a), the overall RWPT-concentration results are better than 1 km FDM results as pointed out in the previous discussion. For the 0.5 km grid resolution (Figure 6-8b), the relative errors from both methods are close to each other, within 15 km downstream from the source, where errors from RWPT-concentration are slightly lower than errors from FDM. After this distance, FDM generates better results than RWPT-concentration. For 0.1 km grid resolution (Figure 6-8c), the relative errors of FDM results are generally lower than all the RWPT-concentration results (three particle resolutions of RWPT method). In the area close to the source, the errors of RWPT-concentration results decrease slightly with increasing grid resolution. However, in the area away from the source, increasing grid resolution not only cause higher noisiness, but also causes large errors along the distance from the source.

In summary, if low grid resolution (e.g. 1 km) was applied, RWPT-concentration would be the better choice for the simulation than FDM, though the overall concentration profile is a poor representation of the exact situation. If a finer grid resolution (e.g. 0.1 km) can be adapted in the simulation, FDM will have obvious advantages over RWPT-concentration, but with more computational costs. For the RWPT-concentration method, the quality of the results depends on the combination of grid resolution and particle resolution. In order for RWPT-concentration to achieve smooth results in such finer grid resolution (e.g. 0.1 km), increasing particle resolution ($>1.44 \times 10^6$ particles d^{-1}) or using projection functions in which the mass of each particle is partially distributed over

adjacent grid cells (Bagtzoglou *et al*. 1992; Moeller and Adams 1993) would be needed, but both will increase the computational expenses as well. Therefore, grid resolutions (for both FDM and RWPT-concentration) and particle resolutions (for RWPT-concentration) should be chosen carefully for different study cases.

6.3 Field Validation of Modeling Results in the Study Area

Field validation of integrated modeling results was conducted for the study case of Hibernia field as introduced in Chapter 4. In order to simulate a more detailed distribution of produced water dispersion, a higher grid resolution was adopted for pollutant transport than that of the ocean circulation simulation in the study area. Since the mass of discharged produced water is relatively small compared to the surrounding ocean waters, and the grid resolution for ocean circulation in this study case is about 2 km × 2 km, produced water discharges basically did not influence the velocity fields. Therefore, for computational efficiency, the ocean circulation model was treated as standalone model to provide ocean circulation information pollutant transport model in the following case study. Dynamic integration was performed between near field and far field pollutant transport models, where ocean currents, densities, and surface elevations were updated at each time step based on POM results.

6.3.1 Model setup for the pollutant fate and transport in the study area

The modeling area is about 50 km × 50 km with the Hibernia GBS in the center, such that the location of GBS center is $x = 0$ and $y = 0$. Based on analysis conducted in the test cases (Section 6.2), a grid resolution between 0.5 km to 0.1 km should be the proper choice for FDM method to conduct simulation under similar study site conditions with appropriate accuracy and computational costs. Therefore, a grid resolution of 200m × 200m × 2m was chosen for the following field case study.

Based on the availability of data for both produced water and sea water in the study site, a produced water plume bearing the chemicals of lead and benzene was chosen for the simulation to present conservative and non-conservative substances, respectively. The pollutant fate and transport simulations were based on the discharge conditions and local hydrodynamic conditions of June 2005, and then validated with field observations collected during the expedition to the Hibernia field in June 2005 by BIO (Bedford Institute of Oceanography). The collected samples of produced water and sea water were analyzed by COOGER (Centre for Offshore Oil and Gas Environmental Research) and TAF (Trace Analysis Facility) laboratories at the University of Regina.

Detailed field investigation information is presented in Chapter 4. The main parameters used in the pollutant fate and transport modeling are summarized as follows: Produced water is discharged from the Hibernia GBS through a port horizontally oriented at an angle of 225º in a counter clockwise direction from due east. The port is 30.48 cm in diameter and located 40 m above the seafloor. Daily average effluent flow for June 2005 was about 21,700 m^3 d^{-1}. The average temperature and salinity of produced water during the summer of 2005 were about 80°C and 41.4 ppt, respectively, based on COOGER analysis.

Helmers (1996) reported the dissolved lead concentration in North Atlantic surface water to 0.002 to 0.029 µg L^{-1}. For precautionary purposes, a constant background concentration of 0.002 µg L^{-1} was used for produced water dispersion simulations for dissolved lead. A large number of monocyclic aromatic hydrocarbons are present in crude and refined petroleum products, of which the greatest concern in the environment are BTEX (benzene, toluene, ethylbenzene, and xylenes) (Neff *et al*., 1994). Concentrations of individual BTEX in seawater generally are very low, ranging from 0.001 µg L^{-1} to about 0.2 µg L^{-1} (Neff, 2002). In the present case study, a concentration of 0.001 µg L^{-1} was used as background concentration for benzene simulation. Because of their chemical/physical properties, BTEX are not persistent in seawater, bind only weakly to marine sediments, and are not bioaccumulated to high concentrations by marine organisms (Neff, 2002). Half lives for BTEX compounds in marine mesocosms are in the range of a few days to a few weeks, depending on temperature (Wakeham *et al*., 1983, 1985, 1986). Howard *et al*. (1991) reported that the half life of benzene in water is in the range of 120 h to 384 h based on river die-away data (Vaishnav and Babeu, 1987) and sea water die away test data (Van der Linden, 1978). In the current study, a half life of 384 h was used for the simulation of biodegradation mechanisms of benzene in marine water.

In the far field model, horizontal and vertical shears in the ocean current field contribute to advection of contaminants in modeled water columns. Modeling of pollutant diffusion processes is mainly determined by the set of dispersion coefficients as shown in the advection-diffusion equation (Equation 3.48). The computation of dispersion coefficients is difficult, generally requiring a large number of constants and empirical

functions which are not always well known (Ridge, 2002). Talbot and Talbot (1974) reported a number of diffusion experiments in offshore and estuarine waters around the British Isles and pointed out that the horizontal dispersion deferred from one area to another and it was difficult to draw general conclusions. They also found that, although diffusion coefficients appeared to increase during the early stages of pollutant release, coefficients tended towards a constant value at longer times. Since the dispersion coefficients were only used in the far field modeling, the horizontal and vertical dispersion coefficients were assumed to be constant for this case study. Based on Rye *et al*. (1998), the upper bound of the horizontal dispersion coefficient is normally chosen to be between 10 and 100 m^2 s^{-1}. A value of 80 m^2 s^{-1} for horizontal dispersion coefficient is used for this case study. The vertical dispersion coefficient is generally in the range of 5 $\times$ 10^{-4} m^2 s^{-1} under weaker currents and stably stratified conditions up to 0.01 m^2 s^{-1} for a fairly strong tidal current. A value of 0.007 m^2 s^{-1} was chosen for the vertical dispersion coefficient. The effects of different values of dispersion coefficients along with other uncertainty parameters on modeling results are evaluated and discussed later in the risk assessment analysis (Chapter 7).

6.3.2 Field validation of integrated modeling results at study site

Based on model configuration information (see Section 6.3.1), by dynamically integrating near field and far field transport models, and using ocean circulation simulations as input at each time step, the modeling system ran 30-day simulations for the produced water dispersion at the Hibernia site for June of 2005. Because field samples were collected during late June of 2005, the average modeling results of a 28th
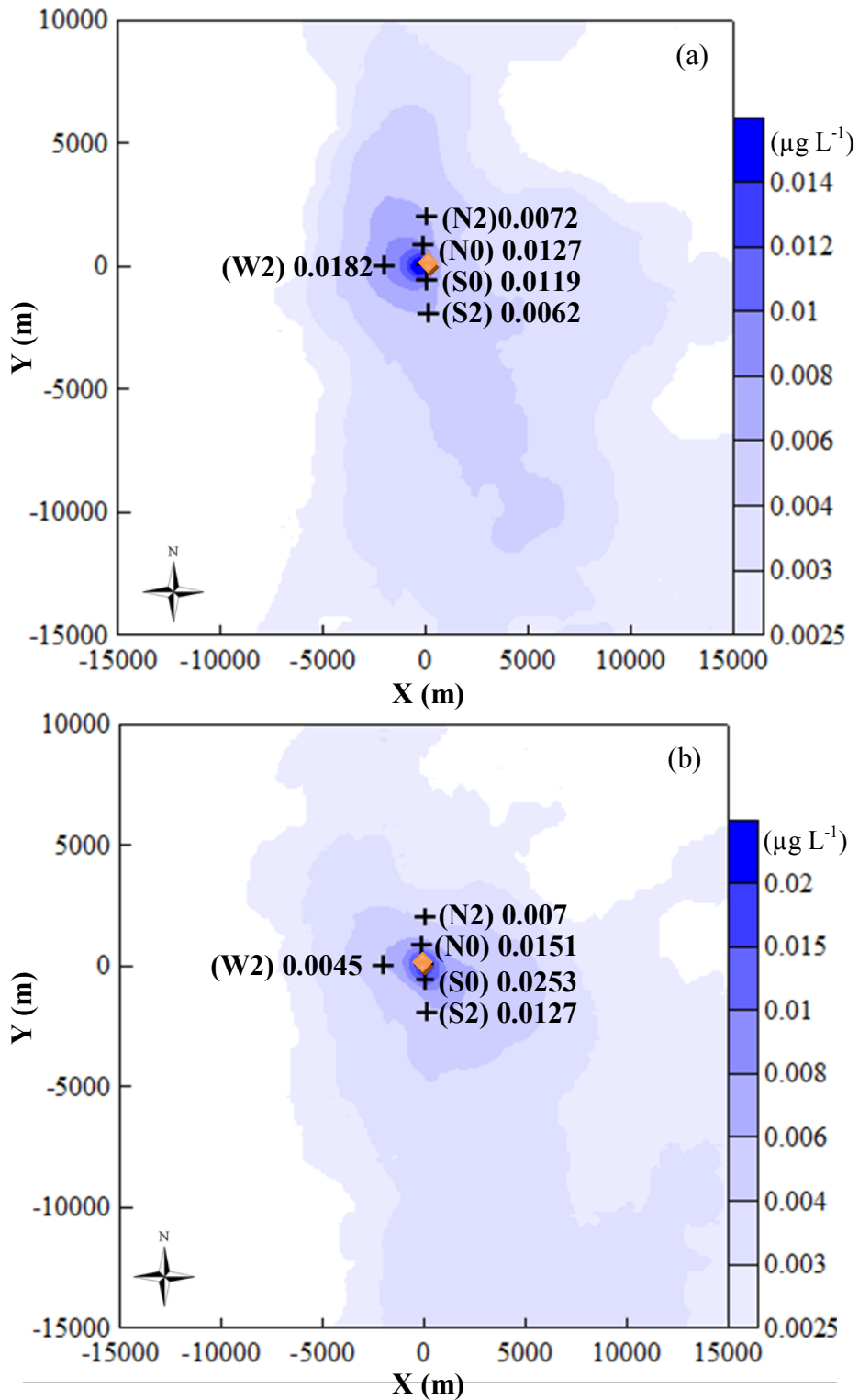
Figure 6-9 Validation of lead dispersion modeling results in the study site at a) 10 m of depth, b) 35 m of depth (the diamond sign is the location of Hibernia platform, the cross signs are the locations of sampling stations)

day model run were chosen for validation, so that the ambient flow conditions would be similar to the time period of sample collections. A discussion of validation results follows.

6.3.2.1 Validation of lead simulation results

The predicted Pb dispersion results were compared with the field data obtained at 10 m and 35 m depth, respectively (Figure 6-9). Modeling results generally correlated well with the field observations. As expected, high concentrations (low dilution) occurred around the platform at both depths. Concentrations within a few hundred meters from the source in 35 m layer (Figure 6-9b) exceeded those at a 10 m depth (Figure 6-9a), which agrees with observations. This may be because the layer at a 35 m depth is closer to the emission source (5 m above the discharge layer) and the plume trapping level (Figure 7-1b).

It should be pointed out that samples were instantly collected at different days during expeditions to the Hibernia site from late June to early July of 2005. At a sampling station, concentrations of one sample collection are different from the other because the complex marine environment causes the discharge plume to vary spatially and temporally, and so do the simulation results. This makes the comparison of field data and modeling results very difficult. Figure 6-9 only presents one example of such comparisons. The modeling results at different modeling times may have better fit for the observation data at a sampling station.

Table 6-2 analyzes the relative errors between field data and modeling results at locations presented in Figure 6-9. The mean error is 18.3% at a 10 m depth and 32.8% at 35 m depth. Modeling results are generally close to sampled concentrations at these

locations. The discrepancy of modeling results and observations may be attributable to several reasons: 1) the modeling period is different from sampling period at certain locations as discussed above. Because ocean currents are highly variable in time in a fixed location, so are the pollutant concentrations, this may cause better results at one location but not at the other; 2) taking the south two points as example, results may be affected by the transition from near field simulation to far field modeling. Produced water was discharged in a south-westerly direction. The 35 m depth layer is only 5 m above the emission source and very close to the trapping levels (Figure 7-1b) as well. The sampling station S0 is about 500 m away from the platform, which is very close to the intermediate zone (transition from near field to far field). When a near field plume reaches its terminal level, it is assumed that the diluted pollutant instantly mixes in the far field grid cells. However, the large far field grid cell (200 m× 200 m in horizontal) in the current study may not capture the details of the intermediate zone, causing lower modeling concentrations in this area. Errors at a 10 m depth for the two south points (lower than 10%) may confirm the above intermediate zone theory that a 10 m depth is less affected by the transition from near field to far field because it is further away from the plume trapping level than the 35 m depth; 3) Several parameters are assumed constant, such as dispersion coefficient and background concentration, which may also affect the simulation results as well.

Table 6-2 also presents the far field-only modeling results without coupling plume model where undiluted produced water is instantaneously mixed in the cell of the discharge location (about 40 m depth). Comparing the results of the integrated model and far field-only, the integrated modeling results are better than the results of far field-only,

especially at the 10 m depth where mean relative error is 18.3% for the integrated model and 42.6% for the far field-only. The mean relative errors at a 35 m depth were similar to each other with slightly higher errors of far field-only results. At a 10 m depth, the far field-only is basically unable to capture the pollutant dispersion because it does not account for the buoyancy effects of the discharged plume, demonstrating the ability and good performance of the integrated model.

Table 6-2 Validation of modeling results against sampling results in the study site

Depth (m)	Sampling station	Sampling results ($\mu g\ L^{-1}$)	Integrated modeling results ($\mu g\ L^{-1}$)	Far field-only ($\mu g\ L^{-1}$)	Absolute relative error (%)	
					Integrated	Far field-only
		A	B	C	|(B-A)/A|	|(C-A)/A|
10	W2	0.0182	0.0086	0.0056	52.7	69.2
	N0	0.0127	0.0107	0.0059	15.7	53.5
	N2	0.0072	0.0063	0.0052	12.5	27.8
	S0	0.0119	0.0108	0.0060	9.2	49.6
	S2	0.0062	0.0061	0.0054	1.6	12.9
	Mean				*18.3*	*42.6*
35	W2	0.0045	0.0060	0.0080	33.3	77.8
	N0	0.0151	0.0152	0.0125	0.7	17.2
	N2	0.0070	0.0043	0.0063	38.6	10.0
	S0	0.0253	0.0163	0.0123	35.6	51.4
	S2	0.0127	0.0056	0.0075	55.9	40.9
	Mean				*32.8*	*39.5*

6.3.2.2 Validation of hydrocarbon simulation results

Concentrations of individual and total BTEX compounds decreased sharply with distance from the discharges. In more open marine environments, BTEX concentrations rarely

exceeded 0.1 µg L^{-1}. In the current study, there were no experimental field data for benzene for the surrounding sea water during the study period of June 2005 to support model validations. Fortunately, an Environmental Effects Monitoring (EEM) program presented in JWSL (2007) was employed to detect changes in the quality of the receiving environment during Hibernia's production phase. A produced water column chemistry program was conducted as part of the 2007 Hibernia EEM program, during which sea water samples were collected, conjunction with the sediment sampling cruise in August 2007. Though sample collections were in different period of time compared to our case study, they may present a similar water column chemistry conditions in the receiving environment as in the study case presented in the current report.
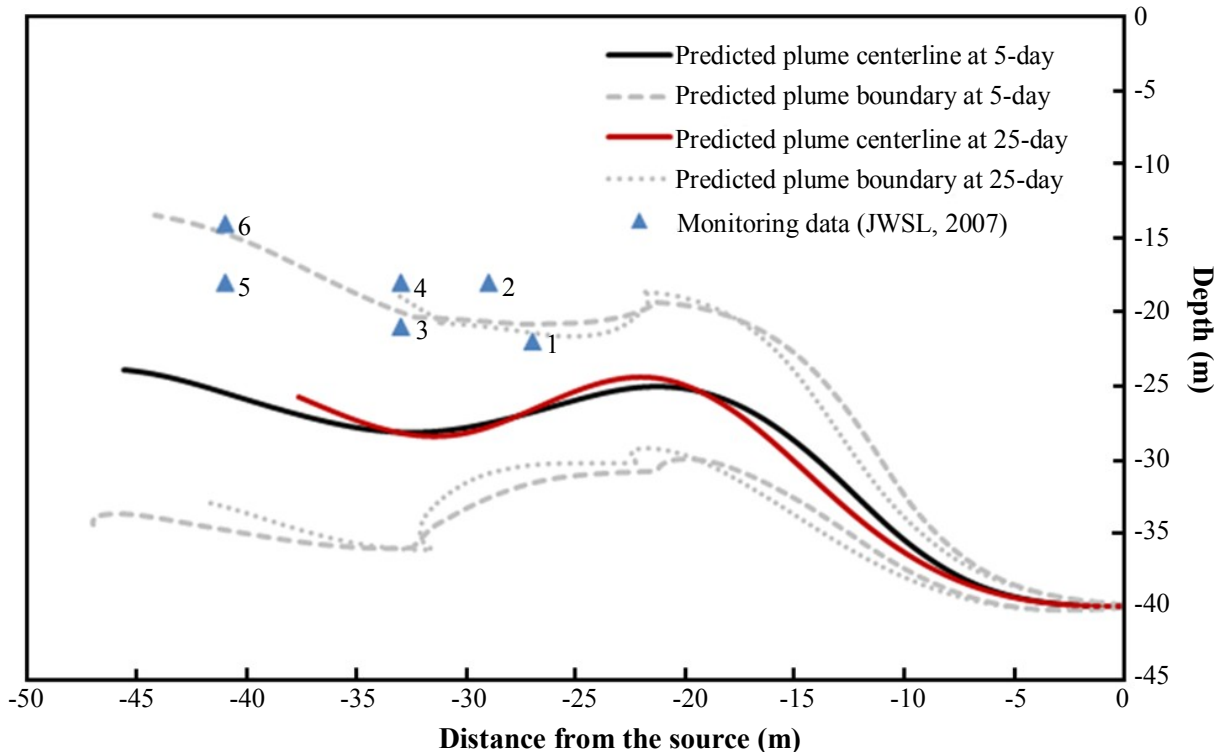
Figure 6-10 Predicted near field plumes of produced water discharges and locations of sample stations (sample stations are from JWSL (2007))

During the 2007 Hibernia EEM program, sea water samples were collected at stations located approximately 25 to 200 m from the produced water outlet in the discharge direction (southwest of GBS), and reference stations located 16 km from the GBS. Based on sample analysis, benzene concentrations for all water column stations at distances beyond 50 m from the discharge outlet were inferior to 1 µg L^{-1}, which is consistence with our modeling results for the simulation period of 2005 (3D benzene simulation results in the study area are presented in Chapter 7).

Table 6-3 Comparison of predicted average concentration of benzene and monitoring data

Monitoring point[*]	Distance (m)	Depth (m)	Sampled Benzene[*] (µg L^{-1})	Modeled average concentration at 5-day (µg L^{-1})	Modeled average concentration at 25-day (µg L^{-1})
1	27	22	11	13.79	16.62
2	29	18	10	12.29	14.75
3	33	21	12	10.37	12.61
4	33	18	19	10.37	12.61
5	41	18	0.5	6.82	<1
6	41	14	3	6.82	<1

[*] Monitoring data are collected from JWSL (2007)

For sample stations located 25 to 50 m from the discharge outlet, predicted near field plumes at 5-day and 25-day model run were compared with sampling analysis data at different locations as shown in Figure 6-10 and Table 6-3. Most of the samples were collected from water columns above 25 m depth. Sample stations located close to the modeled plume trajectories were chosen for comparison as shown in Figure 6-10. Concentrations of benzene at sample stations were in the range of 0.5 to 19 µg L^{-1}, while

predicted benzene concentrations were in the range of < 1 to 16.62 μg L^{-1} (Table 6-3). The modeling results generally match with the observations considering the different discharge and hydrodynamic conditions between modeling and monitoring, and the high variability of measurement and simulation parameters.

6.4 Summary

Field validations and model inter-comparisons of near field model, far field simulation, and the integrated modeling system were presented in this chapter. Excellent results were obtained from the near field model when comparing the predicted produced water discharge plumes in the near field (within 100 m away from the source) with a field experimental study presented in the literature. The examination of computational efficiency and accuracy of the far field model were conducted by model inter-comparisons with an analytical solution and RWPT method through test cases. With proper configuration of grid resolutions, the developed far field model was shown to be able to generate good simulation results, very close to the exact solution and with reasonable computational expenses.

The integrated modeling system was used to predict produced water dispersion processes in the study area of East Coast Canada. Field validations are performed for both lead and benzene concentration distributions resulting from produced water discharges to represent simulations of both conservative and non-conservative substances. Results show good agreement with observations. The predicted lead concentration results

also show improvement over the results of uncoupled model, demonstrating the good performance of the integrated modeling system.

CHAPTER

7

MODELING AND ASSESSMENT OF POLLUTANT DISPERSION RESULTING FROM PRODUCED WATER DISCHARGES AT STUDY SITE

Three dimensional modeling results of produced water discharges and risk assessment analysis at the study site are presented in this chapter. Since low concentration of discharged contaminants in the sea water is associated with the present discharge rate in the study site, future produced water discharges are predicted for the use of risk assessment. Other uncertainty parameters are also identified in the modeling system. Based on methodologies of risk assessment analysis described in Section 3.6.2, a multiple

linear regression model is constructed at first to approximate the output concentrations using limited model runs, then a Monte Carlo method is adopted using the regression model constructed. Both lead and benzene concentrations in the study area were evaluated.

7.1 Modeling of the Dispersion of Produced Water Discharges at study Site

Modeling results of both lead and benzene concentrations resulting from produced water discharges at the study site are presented in this section. Predicted near field plume trajectories are closely linked to produced water discharge rate and density, along with marine currents and densities. As these influencing factors are the same for simulations of lead and benzene, only the results for lead dispersion will be presented in near field simulations (Section 7.1.1). Simulations in the far field zone are discussed for both lead and benzene concentration distributions.

7.1.1 3D lead dispersion simulation results

7.1.1.1 Lead simulation of near field plume at study site

The near field plume can be highly variable depending on the interactions between ambient conditions and plume characteristics at a given point in time. Figure 7-1 shows predicted plume centerline profiles at three different days (10-day, 20-day, and 28-day) in horizontal plane and vertical cross section. In the horizontal plane (Figure 7-1a), the discharge momentum dominates the plumes in the range close to the discharge point, the

plume closely following the discharge direction (south-west direction). Because the plume momentum was weakened by the entrainment of ambient flows along the plume trajectory (Figure 7-1a), the plume centerlines began to be affected by the cross flows, thus generating different plume profiles with time, according to ambient flow conditions.
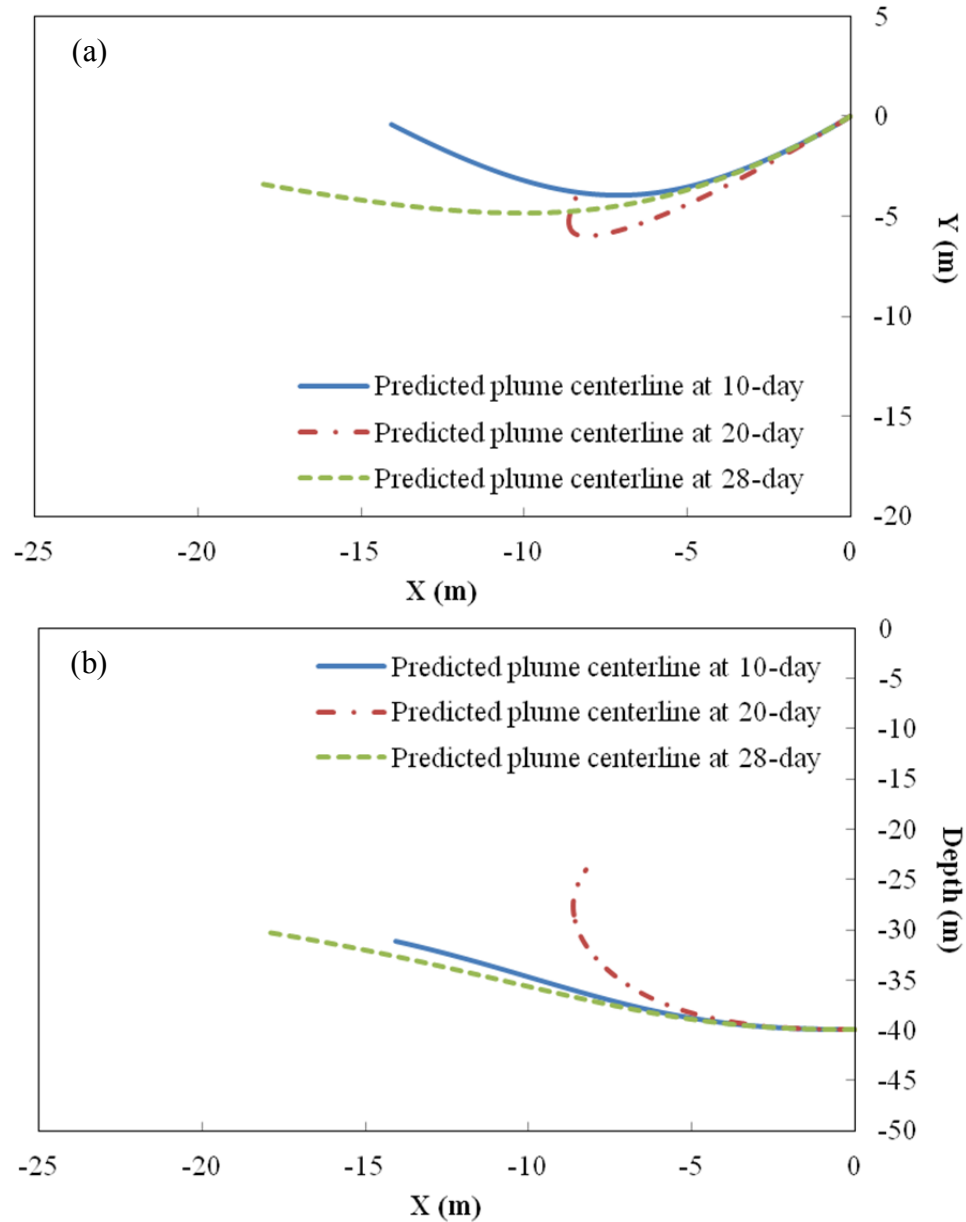
Figure 7-1 Predicted near field plume centerlines in a) horizontal plane, and b) vertical profiles.

Based on the produced water samples collected in 2005, the density of produced water (approximately 1005 kg m^{-3}) is less than that of the ambient water (e.g. Figure 4-2), and hence there exists positive buoyancy effects. Vertical cross sections (Figure 7-1b) show released produced water to flow horizontally (the discharge port is horizontally oriented) in the area close to the discharge point due to the strong discharge momentum. With the weakening of jet velocities after a short distance, buoyant density differences starts to affect the jet and (or) plume trajectories and the plume moves upward until it reaches a neutral buoyancy level. Because of the slightly stratified local marine waters, the plumes are basically trapped between 20 m and 35 m depth (Figure 7-1b), which is reasonable given the density profiles (Figure 4-2). The terminal levels are different at each time step, depending on the interaction between ambient conditions and plume characteristics.

7.1.1.2 Lead simulation of integrated modeling results at study site

The far field pollutant dispersion is mainly influenced by local hydrodynamic conditions which vary in time, resulting in different dispersion patterns. By dynamically integrating with the near field model, the 3D lead concentration patterns in the study area can be visualized for conditions after a 10-day, 20-day, and 28-day model run (Figures 7-2, 7-3, and 7-4, respectively). The plumes flowed in the same basic direction as the local current. Higher concentrations (e.g. above 0.02 µg L^{-1}) generally occurred within several hundred meters horizontally from the source. Though the discharge port is located roughly 40 m deep, the highest dissolved lead concentrations occurred between depths of 20 to 35 m,
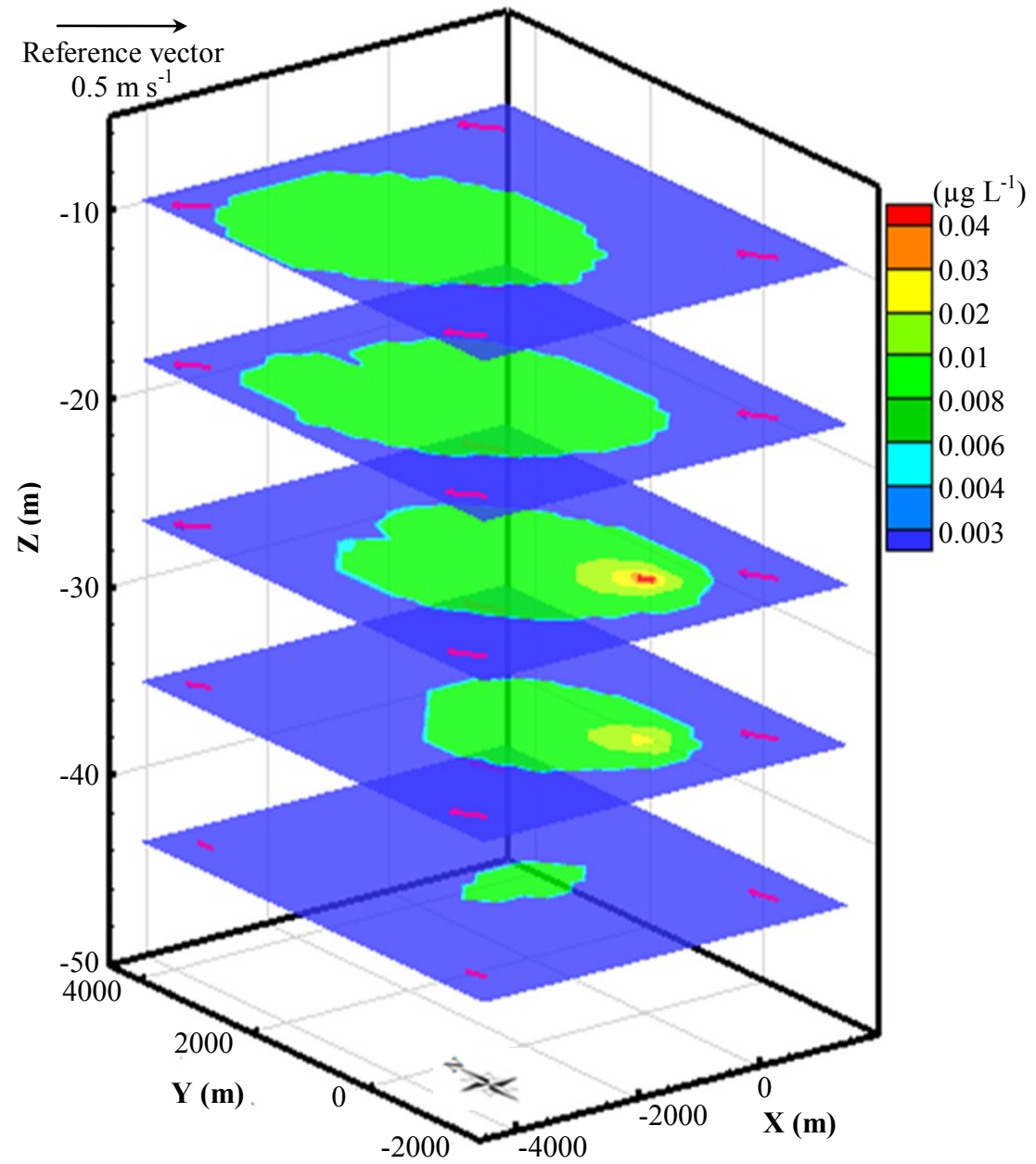
Figure 7-2 Three dimensional concentration pattern of lead dispersion modeling results after 10-day model run
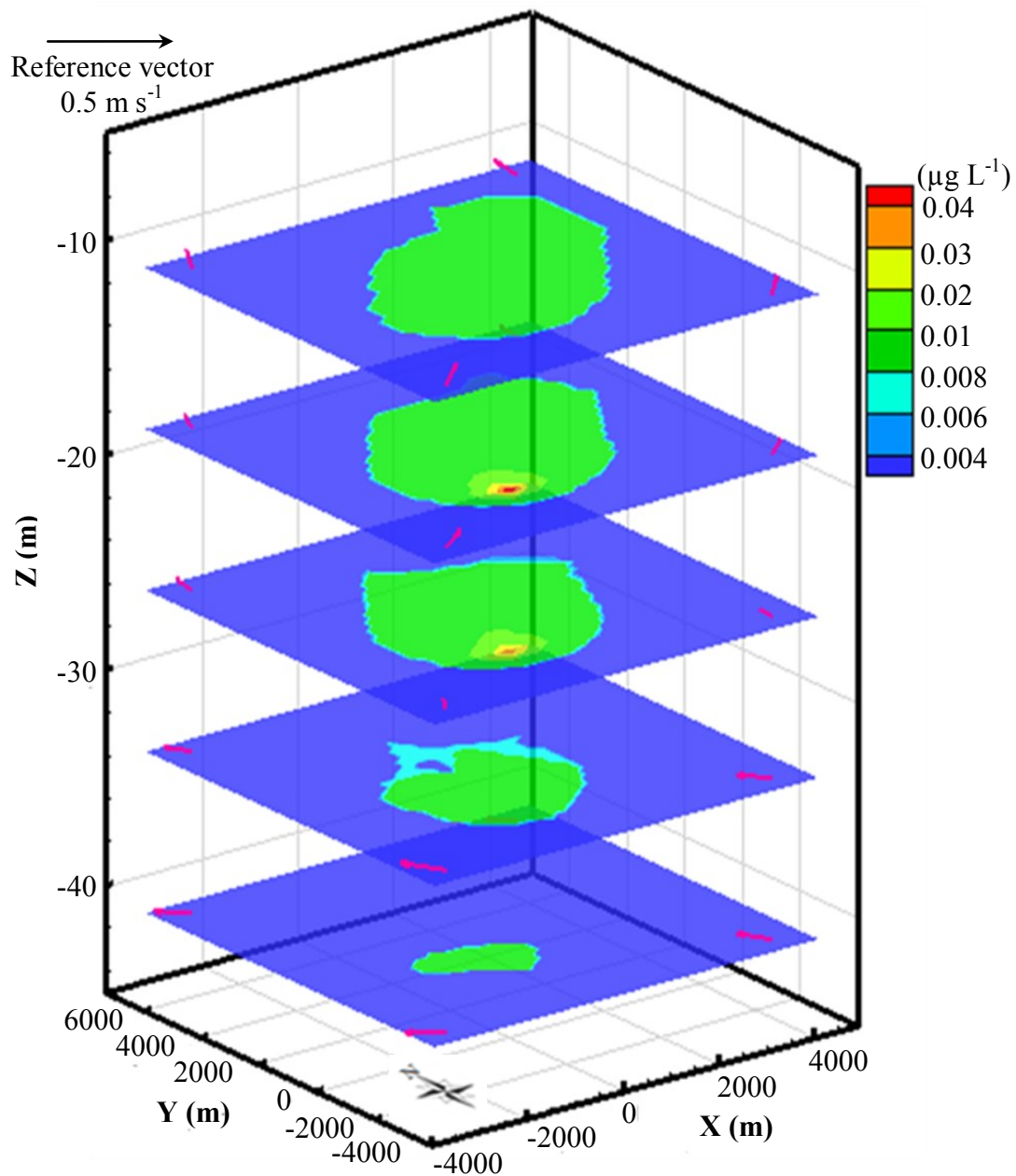
Figure 7-3 Three dimensional concentration pattern of lead dispersion modeling results after 20-day model run
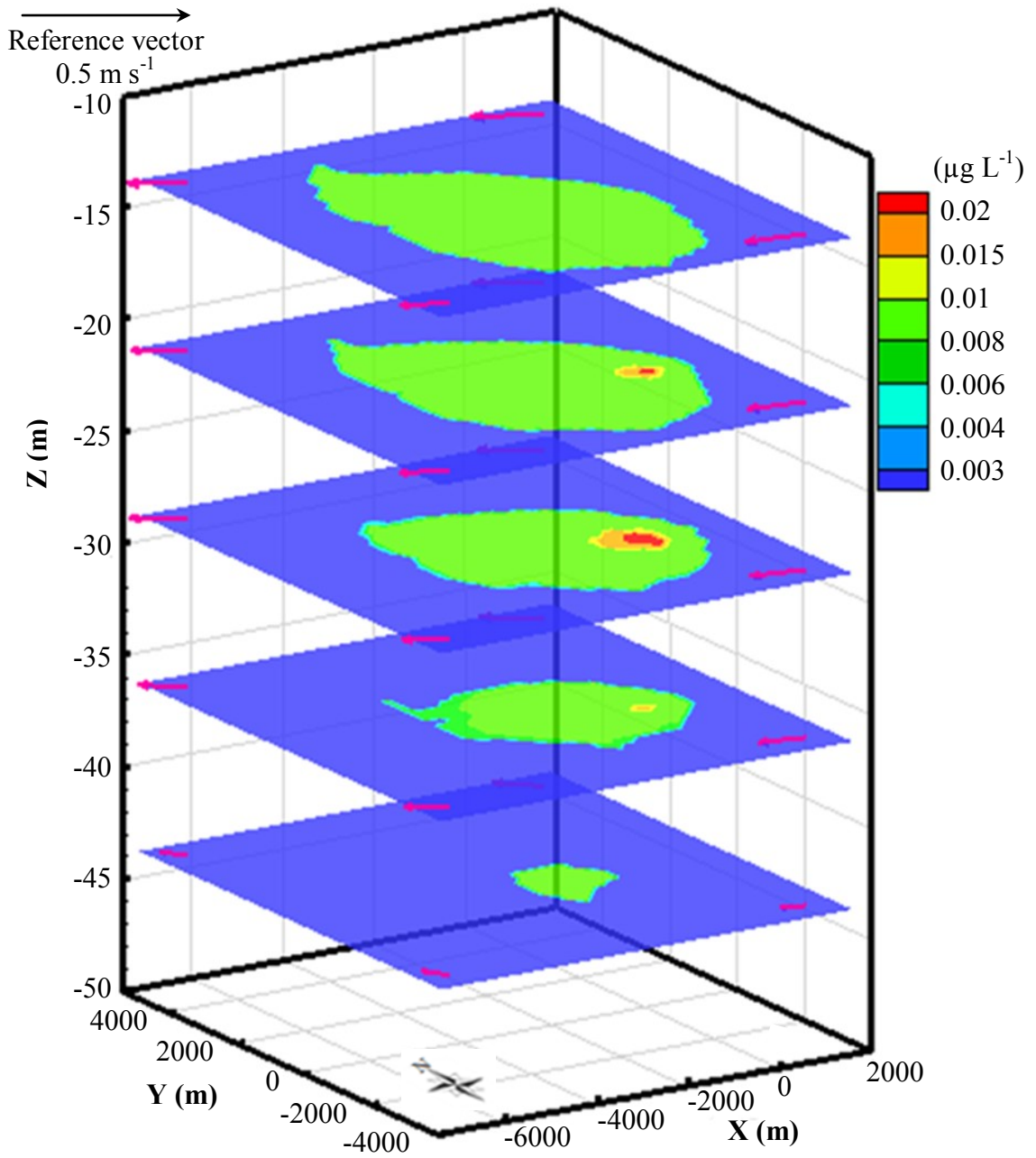
Figure 7-4 Three dimensional concentration pattern of lead dispersion modeling results after 28-day model run

depending on the trapping levels of near field plume and local hydrodynamic conditions. Horizontally, the instant plume profile in the far field zone changes with time due to the changes of local ambient conditions (Figures 7-2, 7-3, 7-4). Areas of higher concentrations located a few hundred meters from the source in the plume direction, were larger after a 10-day and 28-day model run, compared to a 20-day run. As illustrated in the figures, this may be attributable to the different ocean current profiles, where the currents at 10-day and 28-day model run were slightly greater and less turbulent than that at 20-day model run, causing substances dispersed further away from the source. Water columns with concentrations exceeding the background concentration can be found within the plume, whereas areas outside the plume basically fall into (or close to) background concentrations, demonstrating that substances do not appear to accumulate with time in areas a few thousand meters away from the source.

7.1.2 3D benzene dispersion simulation results

The 3D concentration profiles of benzene in the study area after model runs of 10-day, 20-day, and 28-day (Figure 7-5, 7-6, 7-7, respectively), show predicted benzene to range between 0.008 and 0.1 µg L^{-1}, concentration distribution patterns similar to those for lead (Figure 7-2 to Figure 7-4). The benzene concentration profiles were significantly influenced by local hydrodynamic conditions, generating distinctly different concentration distributions for these three model run durations. The higher concentrations appeared at depths between 20 m and 30 m for all these model run durations. The concentration distributions in the vicinity area of the outlet basically follow the direction of local currents. However, areas, such as those located a few thousand meters from the
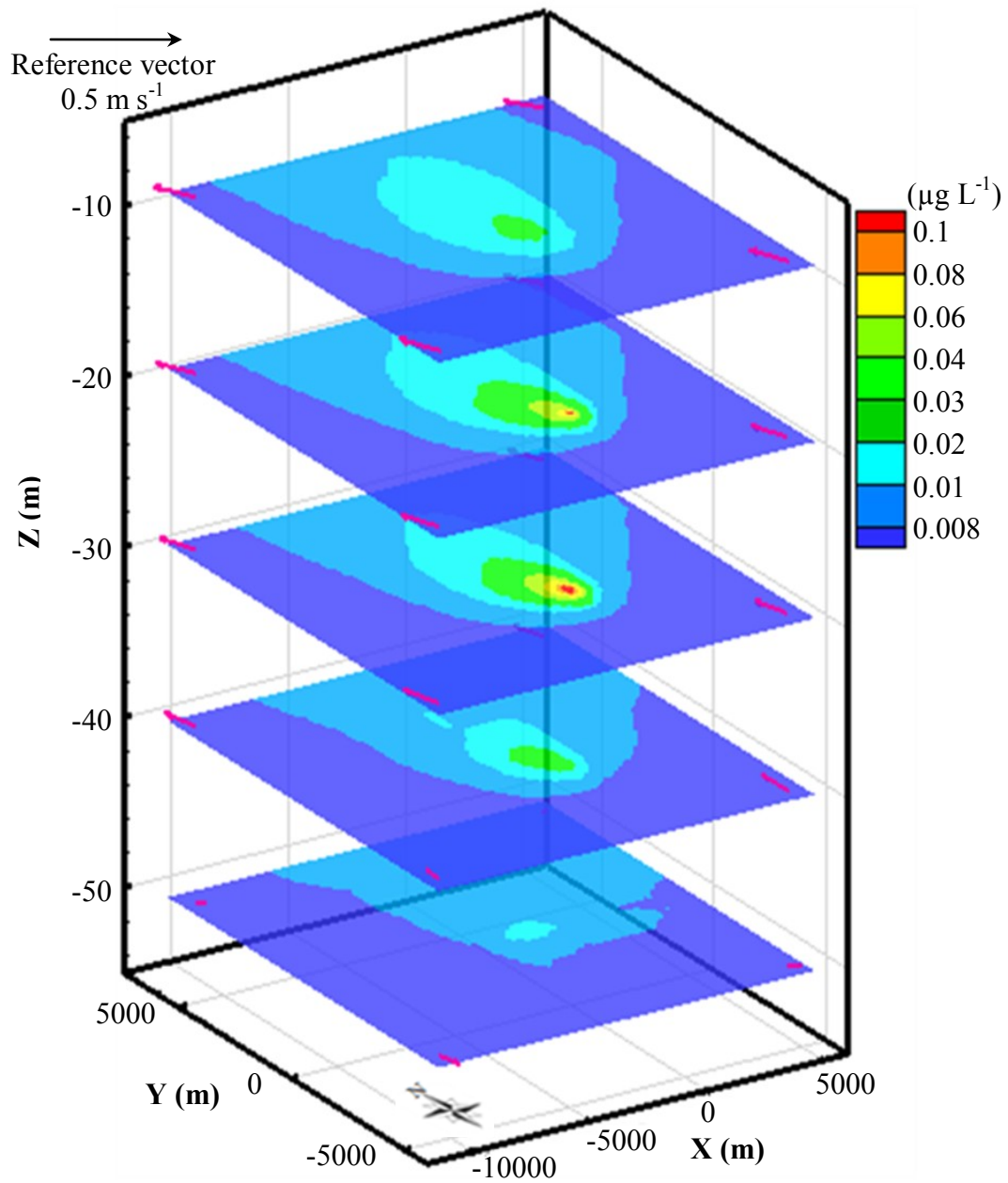
Figure 7-5 Three dimensional concentration pattern of benzene dispersion modeling results after 10-day model run
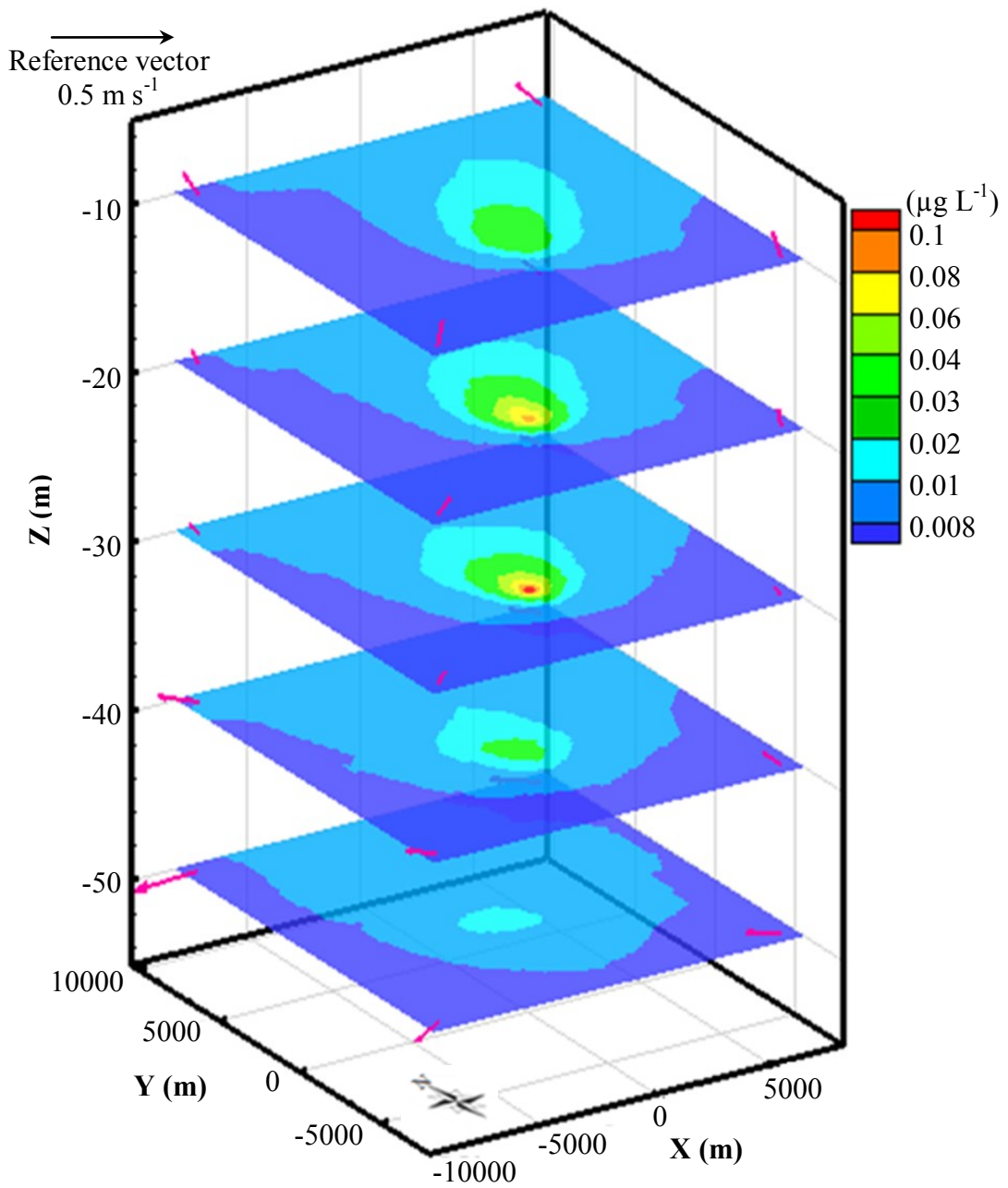
Figure 7-6 Three dimensional concentration pattern of benzene dispersion modeling results after 20-day model run
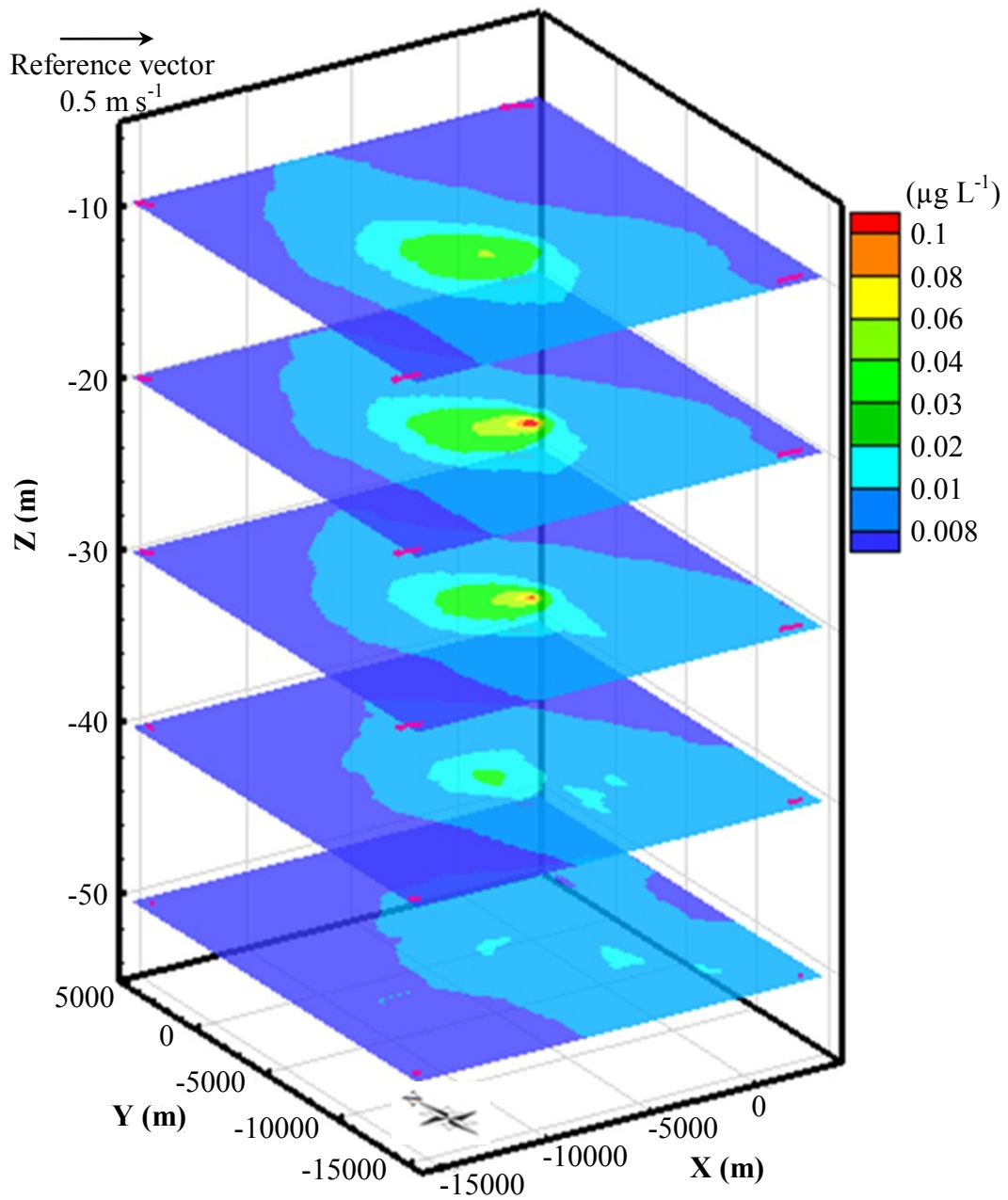
Figure 7-7 Three dimensional concentration pattern of benzene dispersion modeling results after 28-day model run

source, which show low concentrations (e.g. 0.008 μg L^{-1}) may not follow the instant current direction (e.g. Figure 7-7). Because the benzene concentration is low in these areas (*i.e.*, close to the background concentration), the dispersion processes are slowing down as well. Therefore, low concentrations may persist longer in the receiving marine water and the concentration distribution patterns in such areas may be influenced by the distributions in the previous time steps (*e.g.*, Figure 7-7).

7.2 Integrated Risk Assessment for Produced Water Discharges at Study Site

Modeling results presented in Section 7.1 showed the concentration distributions associated with the current produced water discharge rates in the study area. However, volumes of produced water discharges are time dependent and usually increase during the production process (Utivik, 1999; Neff, 2002). In addition, presence of uncertainties in the estimation of discharge rate, transport parameters, chemical decay rate, etc. in the modeling system may result in different simulation results and therefore affect estimates of related environmental risks. Therefore, in the following sections, the developed modeling system is integrated with risk assessment methods to quantify risks associated with produced water discharges. Future emission rates of the Hibernia platform are predicted based on produced and estimated productions from official records. A modified Monte Carlo method (detailed method descriptions are presented in Section 3.6.2) is used to exam system uncertainties associated with dissolved lead and benzene concentration distributions resulting from produced water discharges in the study area. Two risk

characterization methods – probabilistic risk and exposure risk combined with uncertainty analysis provide a spatial and temporal assessment of the risks from the produced water discharges at the Hibernia site.

7.2.1 Predictions of future produced water discharges at study site

Over the life of an oil well, the volume of produced water may change significantly. In nearly depleted fields, production may be 98% produced water and 2% fossil fuel (Stephenson, 1992; Shaw *et al.*, 1999). CAPP (2001) reported that by the time it ceased production in 1999 the Cohasset field, off Nova Scotia had produced nearly twice as much water as oil over its life. The authors suggested that this was a very common situation with regard to produced water volumes.

Table 7-1 presents the estimated oil productions of the Hibernia field, based on data obtained from C-NLOPB (2011). As suggested in CAPP (2001), the estimated total amount of produced water is calculated as twice the estimated total oil reserves. Deducting the cumulative amount produced as of September 30, 2011, the estimated future produced water discharges would range from 391.6×10^6 m^3 to 540.7×10^6 m^3. As stated in Chapter 4, assuming that the yearly oil production of Hibernia field remains the same as in 2010, namely 8.96×10^6 m^3, it has a remaining production life of 11 to 19 years. Produced water generated may reach 28×10^6 m^3 to 36×10^6 m^3, therefore, a uniform emission rate (Q_{prw}) distribution between these figures was chosen to present possible future produced water discharges and to quantify the potential risks which may arise from the dissolved toxicants associated with produced water discharges at the study site.

Table 7-1 Estimated future oil productions and volume of produced water discharges from Hibernia field

	Produced (10^6 m^3)	Proven and Probable (10^6 m^3)	Proven Probable and Possible (10^6 m^3)
Estimated total oil reserves[1]		221.85	296.4
Cumulative oil production (as of September 30, 2011)[1]	121.7		
Estimated remaining oil reserves[1]		100.15	174.7
Estimated total amount of produced water (estimated total oil reserves ×2)		443.7	592.8
Cumulative amount of produced water (as of September 30, 2011)[2]	52.1		
Estimated remaining amount of produced water		391.6	540.7

[1] Data were obtained from C-NLOPB (2011)
[2] Data were obtained from BASIN (2011)

7.2.2 Monte Carlo simulation for uncertainty analysis

Besides the produced water emission rate Q_{prw}, other parameters identified as uncertainty parameters in this study case included background concentration C_B; horizontal dispersion coefficients D_x, D_y, and vertical dispersion coefficients D_z (Equation 3.48); and the decay rate k for the hydrocarbon simulation. Since we assumed the two horizontal dispersion coefficients to be identical in the present case, the two parameters were treated as one parameter D_h. Other model configurations retain the same values as given in Section 6.3.1.

In this study, uncertainty parameters represent a set of standardized random variables (*srvs*) which are selected from a set of independent, identically distributed random variables. The distributions of these uncertainty parameters are determined as follows: *i*) the produced water emission rate Q_{prw} is drawn from a uniform distribution between 28×10^6 and 36×10^6 m^3 yr^{-1} (see in Section 7.2.1); *ii*) the background concentration C_B values are drawn from a uniform distribution ranging from 0.002 to 0.029 µg L^{-1} for lead (Helmers, 1996), and from 0.001 to 0.2 µg L^{-1} for benzene (Neff, 2002) respectively; *iii*) the horizontal dispersion coefficient D_h is specified from a uniform distribution spanning a range of values from 10 to 100 m^2 s^{-1} adopted from Rye *et al*. (1998); *iv*) the vertical dispersion coefficient D_z is drawn from a normal distribution with a mean of 0.005 m^2 s^{-1} and standard deviation of 0.004 m^2 s^{-1} adopted from Riddle *et al*. (2001); and, *v*) the degradation rate k is drawn from a uniform distribution ranging from 0 to 1.6×10^{-6} s^{-1}, which represents a range of benzene half-lives from 5 days (Howard *et al*., 1991) to infinity (Riddle *et al*., 2001). The decay rate is only used for hydrocarbon simulations and considered as zero for the assessment of lead dispersion.

As described in Section 3, a traditional Monte Carlo analysis can be computationally intensive, requiring hundreds or thousands of model runs in many cases. For a complex modeling system, especially a real world case study such as presented in the previous sections, it is inefficient or even unfeasible to perform a traditional Monte Carlo analysis. Therefore, a statistical method is adopted to interpolate the uncertainties from a small number of model runs. A detailed description of this uncertainty analysis methodology, as applied to both lead and benzene dispersion simulations within the current case study (East Coast, Atlantic Ocean), is presented below.

Table 7-2 Parameter values used for model runs in uncertainty analysis of lead dispersion simulation

Model Runs	Emission Rate (m^3 s^{-1}) Q_{prw}	Background Concentration (µg L^{-1}) C_B	Horizontal Dispersion Coefficient (m^2 s^{-1}) D_h	Vertical Dispersion Coefficient (m^2 s^{-1}) D_z
1	1.142	0.029	10	0.0001
2	1.142	0.029	100	0.0001
3	0.902	0.029	10	0.0001
4	0.902	0.029	100	0.0001
5	1.142	0.002	100	0.0001
6	0.902	0.002	100	0.0001
7	1.142	0.002	10	0.0001
8	0.902	0.002	10	0.0001
9	1.142	0.029	10	0.01
10	1.142	0.029	100	0.01
11	0.902	0.029	10	0.01
12	0.902	0.029	100	0.01
13	0.902	0.002	10	0.01
14	1.142	0.002	100	0.01
15	0.902	0.002	100	0.01
16	1.142	0.002	10	0.01

7.2.2.1 Uncertainty analysis for lead simulation

Initially 16 model runs were undertaken for lead dispersion simulation using parameter values selected as indicated in Table 7-2. Model outputs of dissolved lead concentration values for each grid square were collected after 16 model runs. Then a multiple linear regression model using least squares approach (Section 3.6.2.2) was carried out to approximate the output concentrations:

$$C_{Pb} = \beta_0 + \beta_1 Q_{prw} + \beta_2 C_B + \beta_3 D_h + \beta_4 D_z \tag{7.1}$$

where C_{pb} is the predicted lead concentration (M L^{-3}); β_i are the regression coefficients to be determined via the parameters in Table 7-2 and the results from the 16 model runs.

Table 7-3 Estimated regression coefficients from lead dispersion simulation

Parameters	Locations within 100 m away from the source		Locations about 1000 m away from the source	
	Regression coefficients	Percent contribution to the total sum of squares for each parameter (%)	Regression coefficients	Percent contribution to the total sum of squares (%)
Emission rate (Q_{prw})	-0.678	0.02	0.065	0.03
Background concentration (C_B)	1.878	0.12	1.442	13.12
Horizontal dispersion (D_h)	-0.015	1.0×10^{-5}	-2.42×10^{-4}	3.7×10^{-7}
Vertical dispersion (D_z)	-55.208	99.62	3.710	86.84
β_0	2.765	0.25	-0.0392	0.01
Coefficient of determination (R^2)	0.903		0.782	

Note that in Equation 7.1, regression coefficients represent independent contributions of each independent parameter to the predicted concentration. Table 7-3 shows the estimated regression coefficients β_i in two locations, where the percent contribution to the total sum of squares for each parameter is calculated. The vertical dispersion coefficient was dominant in determining the concentrations in both locations. The horizontal dispersion coefficient had a lesser effect on the output concentrations than the other parameters. The contribution of the ratio of background concentration to the predicted concentration increased with the distance from the source. On average, the coefficient of determination (R^2) calculated to estimate the equation's quality of fit,

averaged 0.9 in areas close to the source, and about 0.7 in areas further away from the source. This demonstrated the good fit of Equation 7.1, and its capacity for use in predicting the concentration distributions in the study area. After the establishment of the regression equations for each grid cell, a Monte Carlo simulation is then performed using the regression equations, resulting in the computation of 1000 estimates of lead concentration in the study area. Results from the Monte Carlo simulation were used for risk assessment.

7.2.2.2 Uncertainty analysis for benzene simulation

Twenty-four model runs were undertaken for benzene dispersion simulation using selected parameter values as shown in Table 7-4. Decay rate was also selected as an uncertainty parameter for benzene simulation, therefore, five uncertainty parameters were chosen to construct the multiple linear regression model in the prediction of the output concentrations,

$$C_{benzene} = \beta_0 + \beta_1 Q_{prw} + \beta_2 C_B + \beta_3 D_h + \beta_4 D_z + \beta_5 k \tag{7.2}$$

where $C_{benzene}$ is the predicted benzene concentration (M L^{-3}); β_i are the regression coefficients to be determined via the parameters in Table 7-4 and results from the 24 model runs.

Since benzene is non-conservative compound, its degradation rate is implemented in the concentration distribution simulation. Table 7-5 shows the estimated regression coefficients β_i and the percent contribution to the total sum of squares for each parameter in two locations. Unlike with the lead simulation results, degradation rate was the dominant parameter in determining benzene concentrations. The second dominant

Table 7-4 Parameter values used for model runs in uncertainty analysis of benzene dispersion simulation

Model Runs	Emission Rate (m³ s⁻¹) Q_{prw}	Background Concentration (μg L⁻¹) C_B	Horizontal Dispersion Coefficient (m² s⁻¹) D_h	Vertical Dispersion Coefficient (m² s⁻¹) D_z	Degradation Rate (s⁻¹) k
1	1.142	0.2	10	0.01	0
2	0.902	0.001	10	0.01	0
3	1.142	0.001	10	0.0001	0
4	0.902	0.2	10	0.0001	0
5	1.142	0.2	100	0.01	0
6	0.902	0.001	100	0.01	0
7	1.142	0.001	100	0.0001	0
8	0.902	0.2	100	0.0001	0
9	1.142	0.001	10	0.01	4.01E-07
10	0.902	0.2	10	0.01	4.01E-07
11	1.142	0.2	10	0.0001	4.01E-07
12	0.902	0.001	10	0.0001	4.01E-07
13	1.142	0.001	100	0.01	4.01E-07
14	0.902	0.2	100	0.01	4.01E-07
15	1.142	0.2	100	0.0001	4.01E-07
16	0.902	0.001	100	0.0001	4.01E-07
17	1.142	0.2	10	0.01	1.60E-06
18	0.902	0.001	10	0.01	1.60E-06
19	1.142	0.001	10	0.0001	1.60E-06
20	0.902	0.2	10	0.0001	1.60E-06
21	1.142	0.2	100	0.01	1.60E-06
22	0.902	0.001	100	0.01	1.60E-06
23	1.142	0.001	100	0.0001	1.60E-06
24	0.902	0.2	100	0.0001	1.60E-06

parameter was the vertical dispersion coefficient, whose percent contribution greatly

exceeded that of the other parameters. The average R^2 was about 0.9 in areas close to the

source, and about 0.8 in areas further away from the source. After constructing the

regression equations, a Monte Carlo simulation was performed using the regression

equations to compute 1000 estimates of benzene concentration in the study area. Results

from the Monte Carlo simulation were used for risk assessment.

Table 7-5 Estimated regression coefficients from benzene dispersion simulation

Parameters	Locations within 100 m away from the source		Locations about 1000 m away from the source	
	Regression coefficients	Percent contribution to the total sum of squares for each parameter (%)	Regression coefficients	Percent contribution to the total sum of squares (%)
Emission rate (Q_{prw})	-3.51	0.0012	0.247	0.00036
Background concentration (C_B)	2.25	0.00051	1.46	0.012
Horizontal dispersion (D_h)	-0.077	1.0×10^{-6}	-0.00132	1.0×10^{-8}
Vertical dispersion (D_z)	-279.006	7.80	17.317	1.76
Degradation rate (k)	959.5	92.2	-129.44	98.23
β_0	13.96	0.02	-0.107	6.7×10^{-5}
Coefficient of determination (R^2)	0.903		0.827	
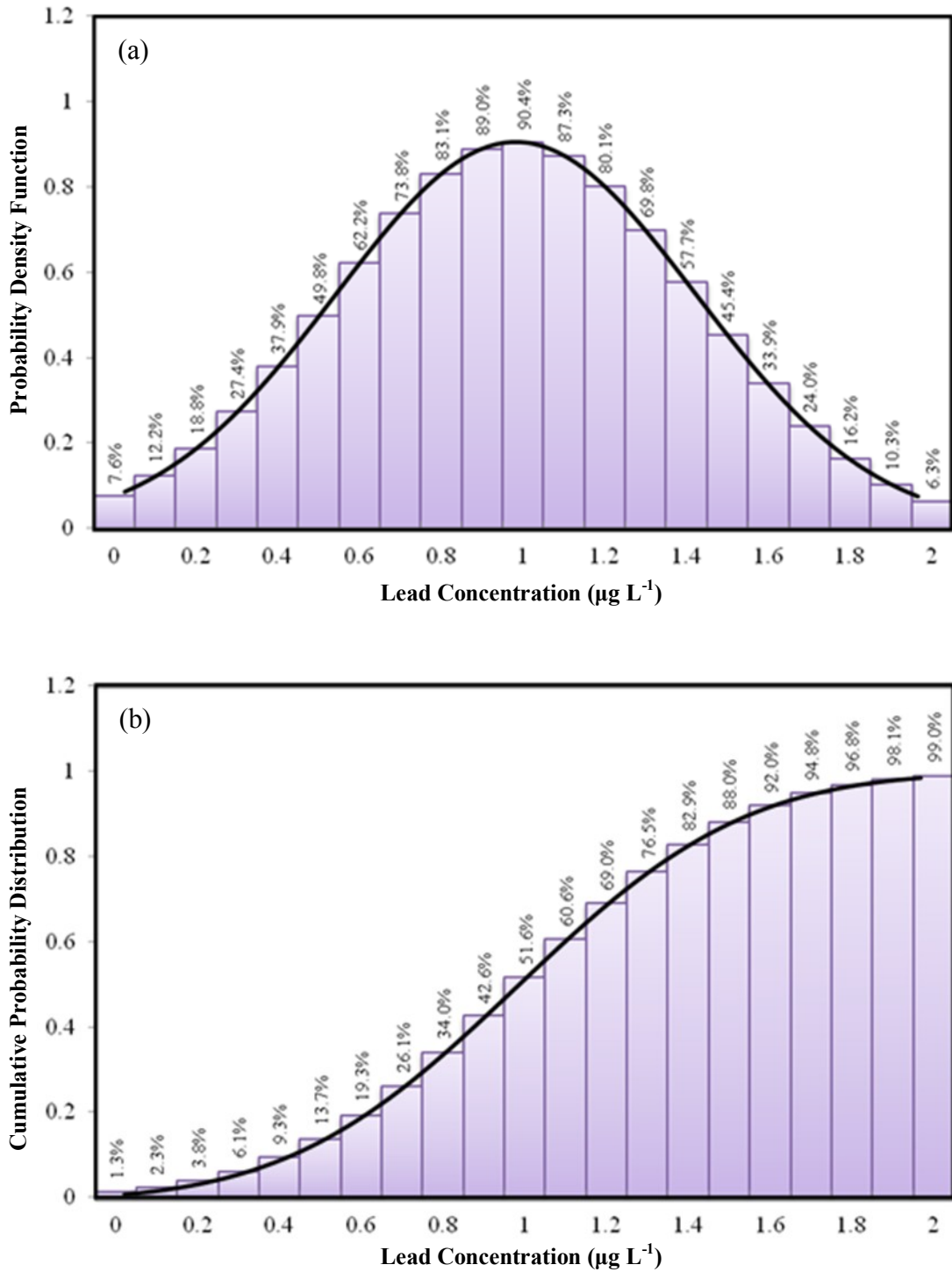
Figure 7-8 Probability distribution of predicted lead concentration for possible future produced water discharges at locations within 100 m away from the source at 24 m depth: (a) probability density function, and (b) cumulative probability distribution.

7.2.3 Risk assessment for lead concentration distribution

In order to quantify risks, an environment threshold, i.e. local environmental criteria, or a predicted no effect concentration (PNEC) is required. However, such standards can vary widely from one location to another. For example, the Canadian Water Quality Guideline (CWQG, 2006)'s protection of aquatic life criteria for 4-day mean [Pb] are 1, 2, 4, or 7 μg L^{-1} for freshwater bearing 0-60, 60-120, 120-180, or >180 mg L^{-1} CaCO$_3$ (hardness), respectively. However, there are no [Pb] criteria for seawater in Canadian guidelines. The USEPA has established a seawater protection standard for aquatic life of 5.6 μg [Pb] L^{-1} (4-day mean; Eisler, 2000), while the State of California (COP, 2001) has mandated a more stringent standard of 2 μg [Pb] L^{-1} (6-month median).

Lead adversely affects the survival, growth, reproduction, development, and metabolism of most species under controlled conditions, but its effects are substantially modified by numerous physical, chemical, and biological variables. A waterborne [Pb] above 10 μg L^{-1} is expected to cause increasingly severe long-term effects on fish and fisheries (Ruby *et al*., 1993). Borgmann *et al*. (1978) noted no deaths of the snail *L. palustris* when exposed to a [Pb] of 3.8 μg L^{-1} over its entire lifetime. Eisler (2000) reported adverse effects of [Pb] on daphnid reproduction at a [Pb^{2+}] of 1.0 μg L^{-1}. Based on Smit *et al*. (2011) and Reed and Rye (2011), a predicted no-effect concentration of 0.182 μg [Pb] L^{-1} was used in the Environmental Impact Factor (EIF) for marine environmental risk assessment in the North Sea. In the current case study, the concentration of 0.182 μg [Pb] L^{-1} and 1.0 μg [Pb] L^{-1} were used as PNEC to evaluate the risks of predicted lead concentrations in the study area.

Based on the results obtained from the Monte Carlo methods, probability functions of output concentrations can be generated for each grid cells in the study area. Figure 7-8 shows the probabilistic analysis of [Pb] within 100 m away from the source (point 1 in Figure 7-10 and point 1-3 in Table 7-6) for possible future produced water discharges. The probability of [Pb] exceeding 0.182 μg L^{-1} is 96.5%, and of exceeding 1 μg L^{-1} is 48.4%, indicating a high probability of ecological injury in this area. The 5th and 95th percentile [Pb] (i.e. 95% of all sample concentrations are less than this concentration) for this location are 0.26 μg L^{-1} and 1.71 μg L^{-1}, respectively, well above the PNEC value of 0.182 μg [Pb] L^{-1}. The risk quotient (RQ) factor is 9.38 for the 0.182 μg L^{-1} criteria, and 1.71 for the 1 μg L^{-1} criteria, for the 95th percentile concentration. Given that both values exceed a value of 1, there is a high probability that ecological injury caused by produced water discharges bearing [Pb] within 100 m away from the platform during future oil productions in the study area. It should be noted that the predicted values represent the concentration within a 200 m × 200 m × 2 m grid cell, concentrations in areas closer to the point of discharge would obviously be higher.

Figure 7-9 shows the probability distributions at a location about 700 m away from the source (point 5 in Figure 7-10 and Table 7-6). The mean dissolved lead concentration in this location is 0.13 μg L^{-1} with a standard deviation of 0.04 μg L^{-1}. About 88% of the predicted [Pb] concentrations are lower than 0.18 μg L^{-1}, in other words, the probability of [Pb] concentration exceeding 0.182 μg L^{-1} is 11.1%. None of the predicted [Pb] concentrations exceeded 1 μg L^{-1}. The 95th percentile concentration is 0.20 μg L^{-1}, only marginally above 0.182 μg L^{-1}, giving RQ factor of 1.10. The [Pb]
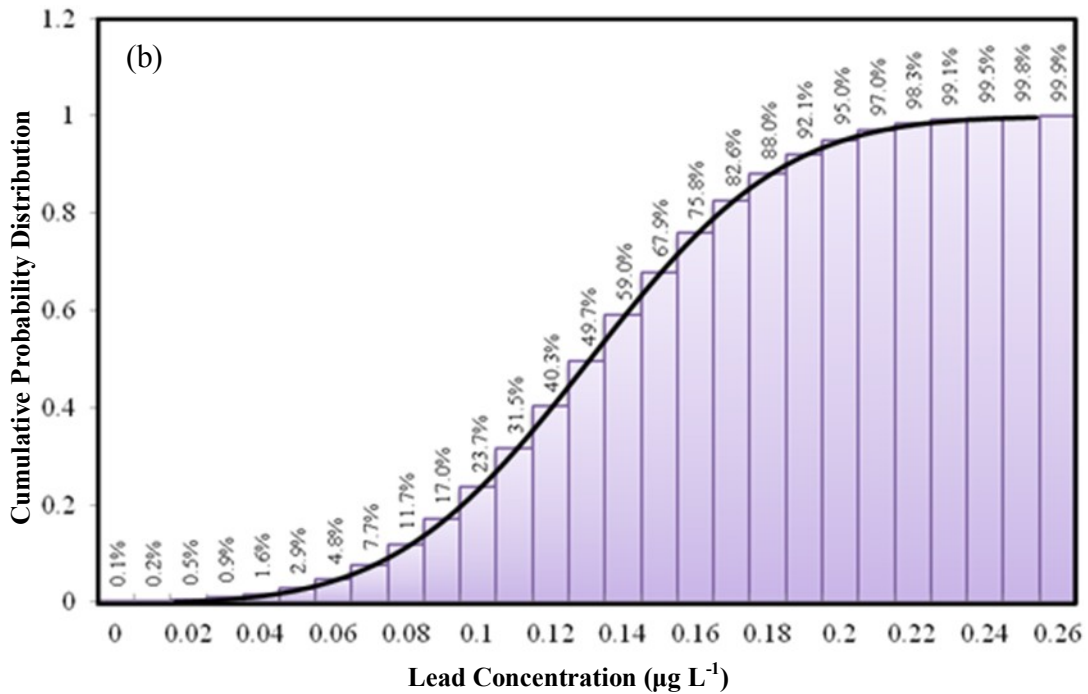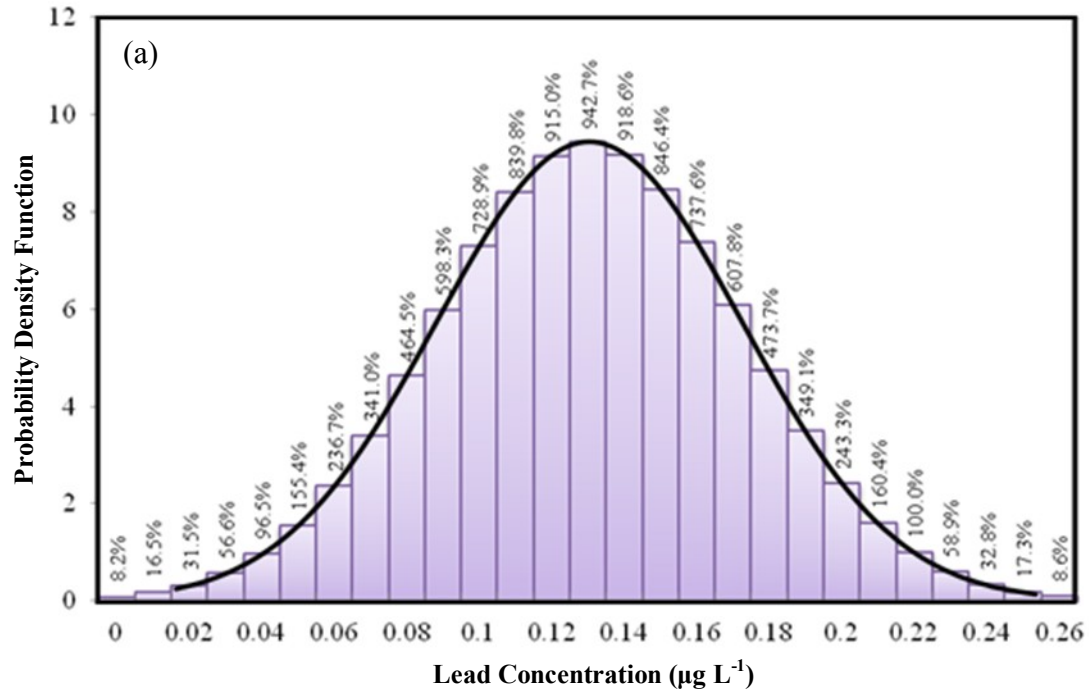
Figure 7-9 Probability distribution of predicted lead concentration for possible future produced water discharges at locations about 700 m away from the source: (a) probability density function, and (b) cumulative probability distribution.

concentration decreases 8-fold over a 600 m distance, demonstrating the rapid dilution after release from the source due to hydrodynamic effects (Figure 7-8).

Table 7-6 Summary of risk assessment results for predicted lead concentrations

Point	Distance from source (m)	Depth (m)	Mean (μg L^{-1})	Standard deviation (μg L^{-1})	Percentiles		Risk level			
					5%	95%	P (C>0.182) (%)	P (C>1) (%)	RQ (C>0.182)	RQ (C>1)
1-1		20	0.13	0.102	0	0.30	30.17	0	1.63	0.30
1-2		22	0.50	0.18	0.21	0.80	96.41	0.28	4.39	0.80
1-3	0-100	24	0.98	0.44	0.26	1.71	96.52	48.36	9.38	1.71
1-4		26	0.78	0.30	0.29	1.26	97.68	22.51	6.95	1.26
1-5		28	0.41	0.16	0.15	0.67	92.52	0.01	3.67	0.67
1-6		30	0.21	0.09	0.06	0.36	60.04	0	1.95	0.36
2	200		0.51	0.23	0.13	0.89	92.22	1.66	4.88	0.89
3	300		0.40	0.19	0.08	0.71	87.07	0.07	3.88	0.71
4	500	26	0.20	0.08	0.06	0.34	59.34	0	1.87	0.34
5	700		0.13	0.04	0.06	0.20	11.13	0	1.10	0.20
6	1000		0.07	0.02	0.04	0.09	0	0	0.51	0.09

Table 7-6 shows the overall risk assessment results for predicted lead concentrations at different depths and distances from the source. Within 100 m from the source, the mean concentration over a 10 m depth is in the range of 0.13 to 0.98 μg L^{-1} with a standard deviation of 0.09 to 0.44 μg L^{-1}. The probability risk level of exceeding the threshold concentration of 0.182 μg L^{-1} ranges from 30.17% to 97.68% with a greater than 90% probability of this occurring between 22 and 28 m in depth. The probabilistic risk level of exceeding 1 μg L^{-1} ranges from 0.01% to 48.36% over a 6 m depth, with the highest probability risk level (48.36%) occurring at a 24 m depth. The RQ factors for 95th percentile concentrations exceeding 0.182 μg L^{-1} are all above 1.0, with risk levels exceeding 3.5 between 22 and 28 m in depth. The RQ factors for exceeding 1 μg L^{-1} are

in the range of 0.30 to 1.71 with values exceeding 1.0 between 24 and 26 m in depth. Though the produced water discharge location is at about 40 m in depth, because of the buoyancy effects of the less dense effluents, the depths of greatest concern may be between 22 and 28 m below the water surface.

Table 7-6 also shows risks varies with the distance from the source, between 0 – 1000 m at 26 m depth (point 1-4 and points 2 to 6). At point 1-4 and points 2 and 3, some 300 m away from the source, the probability risk levels of exceeding the environmental threshold of 0.182 µg L^{-1} is ≥ 90%. It drops rapidly to 11.13% between 300 and 700 m from the source. At a distance of 1000 m away from the source, the probability of the predicted [Pb] concentration exceeding 0.182 µg L^{-1} is zero. An RQ factor larger than 1.0 for the [Pb] threshold of 0.182 µg L^{-1} occurs somewhere within 700 m from the source, demonstrating that there lies a risk of adverse environmental effects for aquatic lives within 700 m from the source in the study area. For the threshold concentration of 1 µg L^{-1}, the risk level is low with a probability risk level of 22.5% and RQ factor of 1.26 at point 1-4 (within 100 from the source). Beyond 100 m from the source, none of the RQ factors exceeds 1.0 for a [Pb] threshold of 1 µg L^{-1}.

In order to visually illustrate the levels of risks associated with production discharges around an offshore production platform, graphs using the values of probability risks and RQ factors are plotted in Figure 7-10 and Figure 7-11, respectively. A high risk level with [P (C>0.182) >70%] (the probability risk level of exceeding 0.182 µg L^{-1} being greater than 70%) is approximately a 400 m diameter circle with a mean [Pb] concentration exceeding 0.3 µg L^{-1} (Figure 7-10). The probability risk levels with [70%>P(C>0.182)>20%] are a ring shaped area corresponding to mean concentration of

0.1 to 0.3 µg L^{-1}. In a similar illustrative manner the 95th percentile RQ values are plotted to illustrate environmental risks (Figure 7-11). The areas of RQ exceeding 1.0 essentially correspond to the areas of probability risk levels exceeding 20% (Figure 7-10). Potential risk zones generally follow the concentration distribution. With the concentration distribution patterns varying with time, the risk distributions also change. The high risk zones (high probability risk levels or RQ > 1) are basically in a circle surrounding the platform with a radius of a few hundred meters.
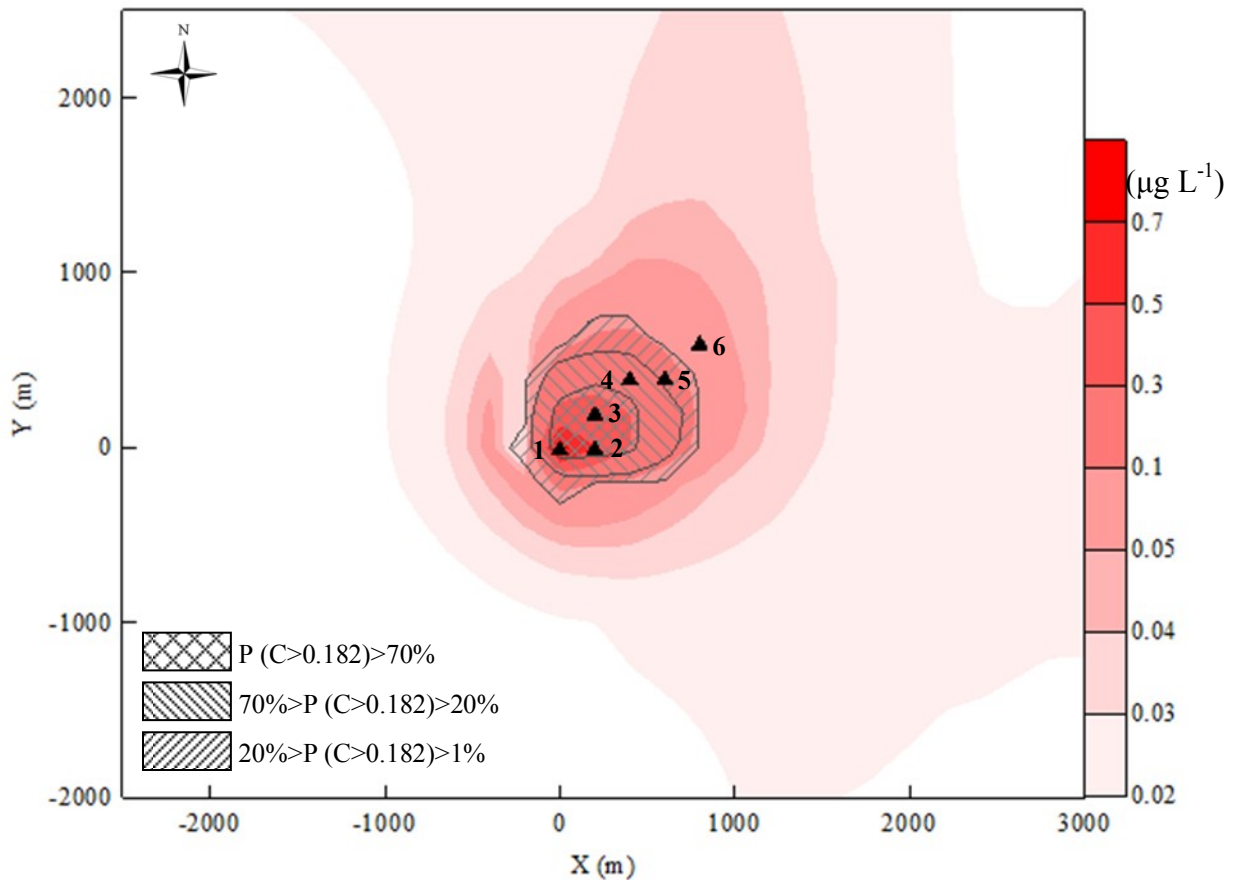
Figure 7-10 Predicted [Pb] mean concentration distribution and probability risk level of exceeding the environmental threshold of 0.182 µg L^{-1} at 26 m depth under predicted future produced water discharges.
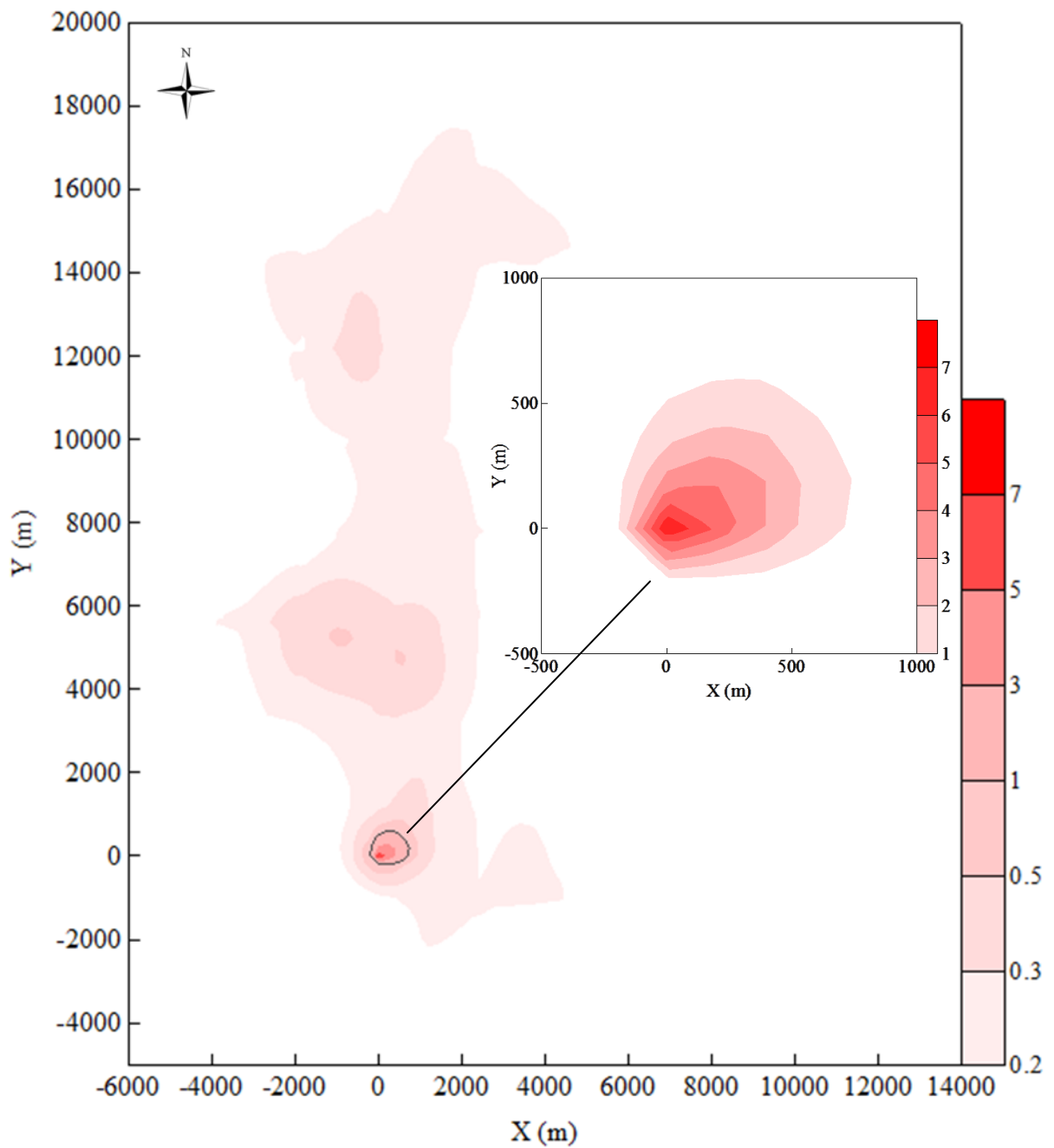
Figure 7-11 The 95th percentile risk quotient (RQ) associated with a PNEC of 0.182 μg [Pb] L[-1] at a depth of 26 m under predicted future produced water discharges. The small circle represents RQ ≥ 1.

7.2.4 Risk assessment for benzene concentration distribution

Risk assessment of benzene concentration distribution associated with produced water discharges was analyzed as an example of the evaluation of a non-conservative substance in the study area. Compounds such as BTEX (benzene, toluene, ethylbenzene, and xylenes) are diluted very rapidly in the receiving water environment following discharge of produced water to the ocean even though these compounds are often at levels as high as 10,000 μg L^{-1} in treated produced water (Neff, 2002). The marine acute water quality criterion for benzene is 5100 μg L^{-1} and the chronic criterion is 700 μg L^{-1} based on USEPA (1992, 1995) criteria designed to protect marine organisms and their consumers. Because there are insufficient data to develop criteria, these values actually are no observed effects concentration. These criteria are virtually never exceeded in marine waters near produced water discharges (Neff, 2002). In the group of compounds selected as the Environmental Impact Factor (EIF) (Smit *et al.*, 2011; Reed and Rye, 2011), a predicted no-effect concentration (PNEC) of 17 μg L^{-1} is used as an environmental criteria for benzene.

As stated in Neff (2002), it may be possible to attain a benzene concentration of 40 μg L^{-1} in solution under a slick of crude or refined petroleum for a short period of time (hours) after an oil spill, but high concentrations are not likely to persist long enough to contaminate fishery products to a level possibly harmful to human consumers. The simulation and risk assessments results performed in this thesis report agree with such statement. Detailed risk assessment results for benzene are described below.
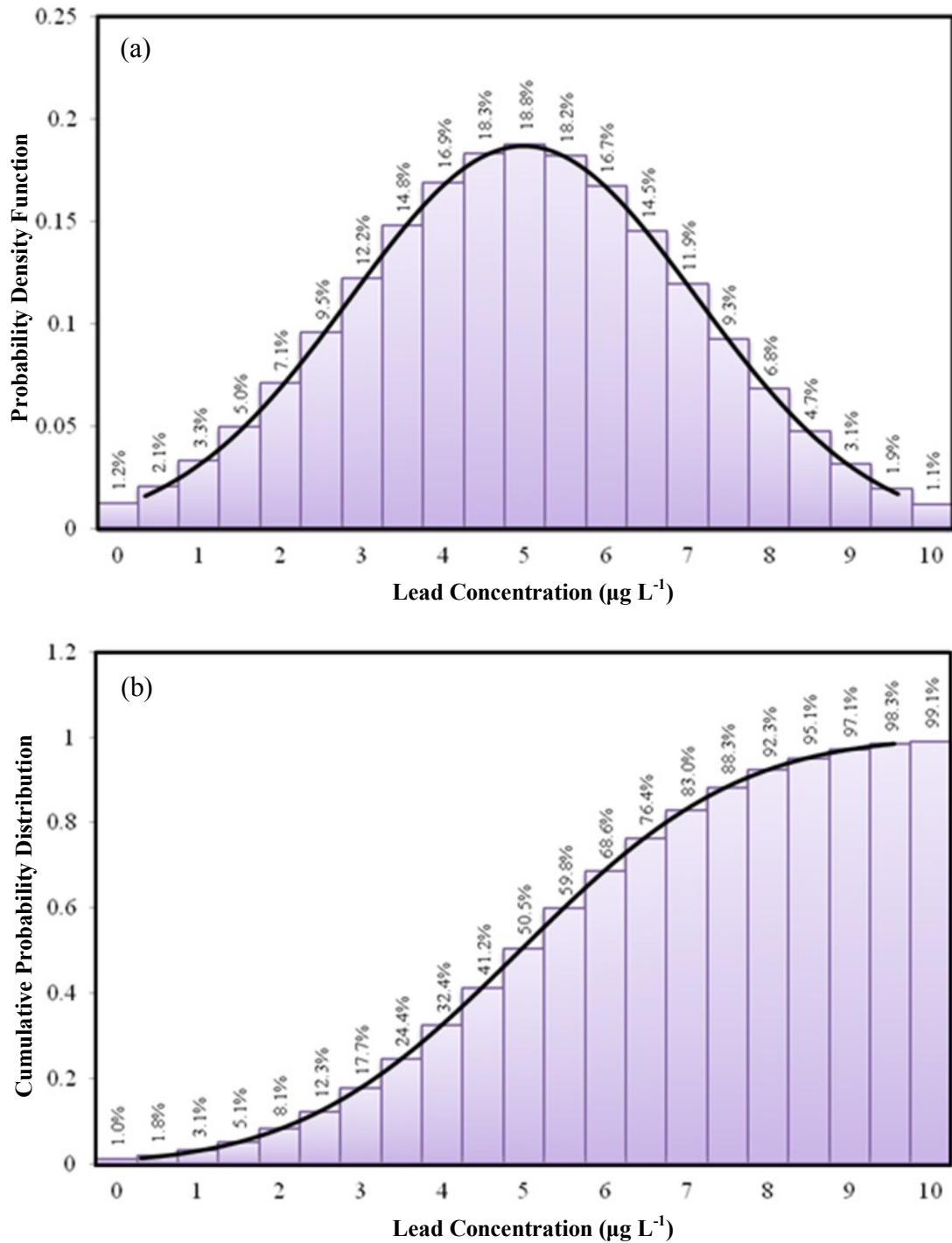
Figure 7-12 Probability distribution of predicted benzene concentration for possible future produced water discharges at locations within 100 m away from the source at a depth of 24 m: (a) probability density function, and (b) cumulative probability distribution.
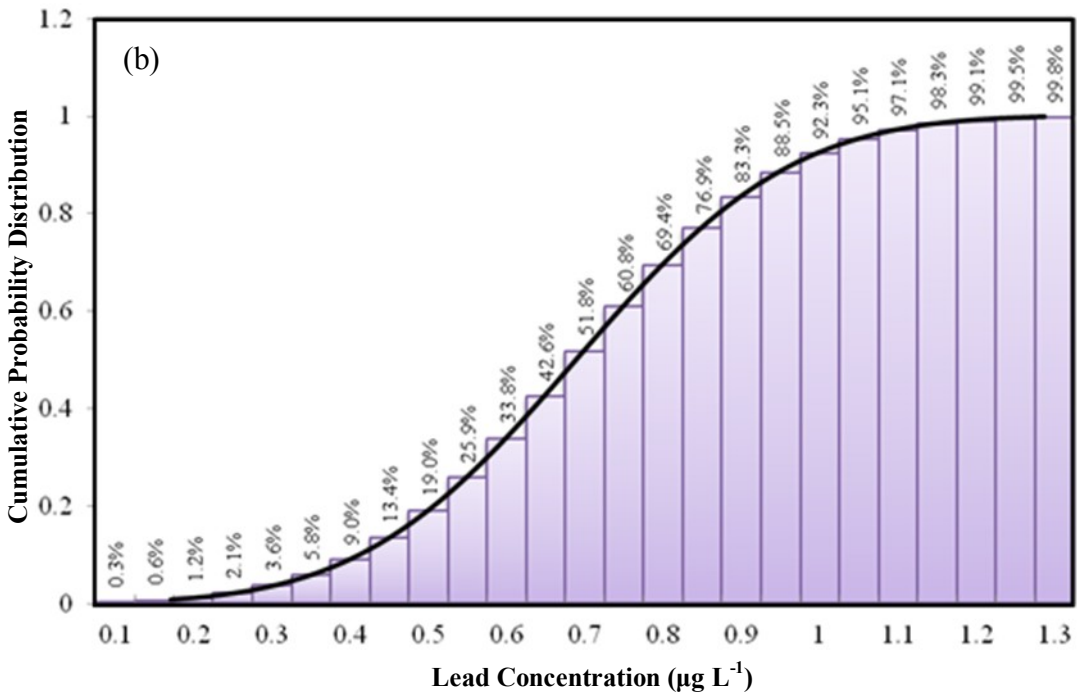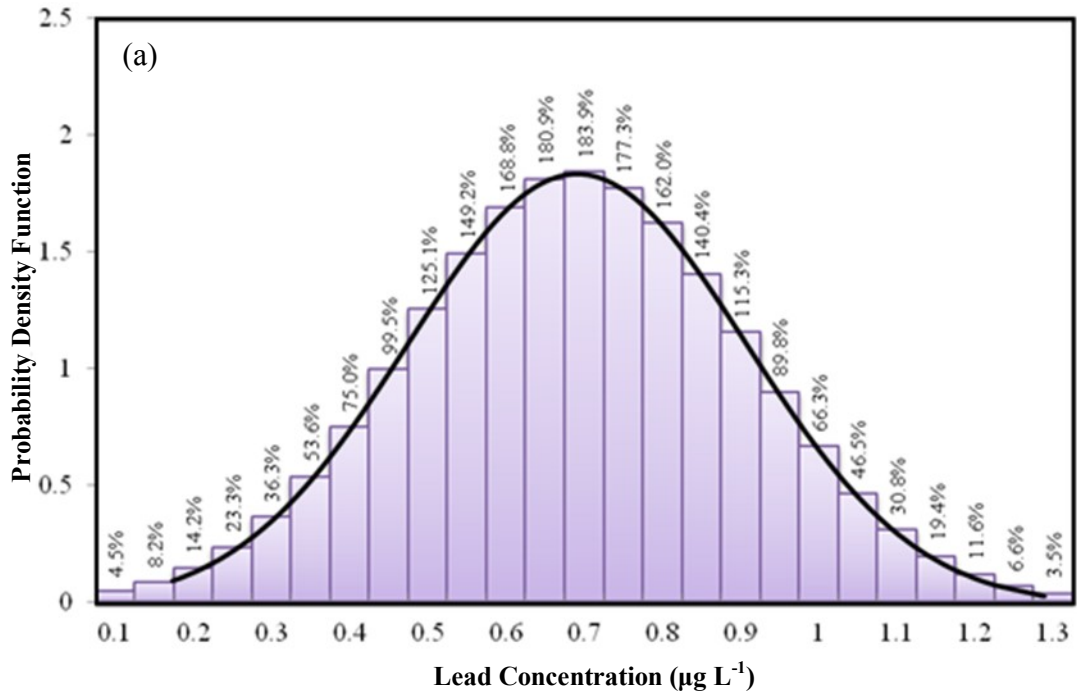
Figure 7-13 Probability distribution of predicted benzene concentration for possible future produced water discharges at locations about 700 m away from the source at a depth of 26 m: (a) probability density function, and (b) cumulative probability distribution.

Figure 7-12 shows the probabilistic analysis of benzene within 100 m from the source (point 1-2 in Table 7-7 and point 1 in Figure 7-10), under possible future produced water discharge conditions. The mean benzene concentration is 4.97 μg L^{-1} with a standard deviation of 2.13. The 5th and 95th percentile concentration are 1.47 μg L^{-1} and 8.47 μg L^{-1}, respectively. None of the predicted benzene concentrations exceed 17 μg L^{-1}. In the near field plume (within 50 m from the source), there is a possibility that the predicted benzene concentration may exceed the criteria of 17 μg L^{-1} within 30 m to 40 m away from the source along the plume (see Figure 6-10). However, because plume trajectories vary with emission rate, it is difficult to obtain risk levels in a fixed location in the near field zone. The benzene concentrations drops to 700 μg L^{-1} within a few seconds after discharge. Figure 7-13 shows the probabilistic analysis of benzene at the location about 700 m from the source (point 5 in Table 7-7 and in Figure 7-10). The mean concentration drops to 0.69 μg L^{-1} with a standard deviation of 0.22 μg L^{-1}. The 5th percentile concentration (0.33 μg L^{-1}) is close to the background concentration (0.001 μg L^{-1} to 0.2 μg L^{-1}).

Table 7-7 shows the overall risk assessment results for predicted benzene concentrations at different depths and distances from the source. At locations within 100 m from the source, the mean benzene concentration across a 6 m depth range varies from 2.11 to 4.97 μg L^{-1} with a standard deviation of 0.82 to 2.13 μg L^{-1}. The 95th percentile concentration may reach over 8 μg L^{-1} at a depth of 24 m. At a depth of 26 m, mean benzene concentrations in 200 to 300 m from the source is within a narrow range of 2.01 to 2.58 μg L^{-1} with a standard deviation of 0.92 μg L^{-1} to 1.12 μg L^{-1}. Then it drops

rapidly to 0.37 µg L^{-1} at a distance of 1000 m from the source, a value very close to the background concentration.

Table 7-7 Summary of risk assessment results for predicted benzene concentrations

| Point | Distance from source (m) | Depth (m) | Mean (µg L^{-1}) | Standard deviation (µg L^{-1}) | Percentiles | |
					5%	95%
1-1	0-100	22	2.6	0.88	1.15	4.05
1-2	0-100	24	4.97	2.13	1.47	8.47
1-3	0-100	26	3.93	1.44	1.56	6.30
1-4	0-100	28	2.11	0.82	0.76	3.46
2	200	26	2.58	1.12	0.74	4.42
3	300	26	2.01	0.92	0.50	3.52
4	500	26	1.05	0.43	0.34	1.76
5	700	26	0.69	0.22	0.33	1.05
6	1000	26	0.37	0.09	0.22	0.52

The 95th and 5th percentile benzene concentration distributions at a depth of 26 m are plotted in Figures 7-14 and 7-15. The 95th percentile benzene concentration distribution may represent a "worst case" scenario because the parameters contributing to one grid location's 95th percentile benzene concentration may differ significantly from those prevailing at another location. Predicted 95th percentile benzene concentrations are of the order of 0.2 - 5 µg L^{-1}. A benzene concentration exceeding 1 µg L^{-1} occurrs within several hundred meters from the source; however, beyond that, benzene concentration quickly falls to near background concentration, with perhaps, a few patches with benzene values of 0.3 to 0.5 µg L^{-1} scattered in different locations. The 5th percentile benzene concentrations are low, being in the order of 0.006 to 1 µg L^{-1}. Only areas within 100 m

of the outlet have benzene values exceeding 1 μg L^{-1}. The benzene concentrations fall to background levels (0.001-0.2 μg L^{-1}) within a few hundred meters from the source.
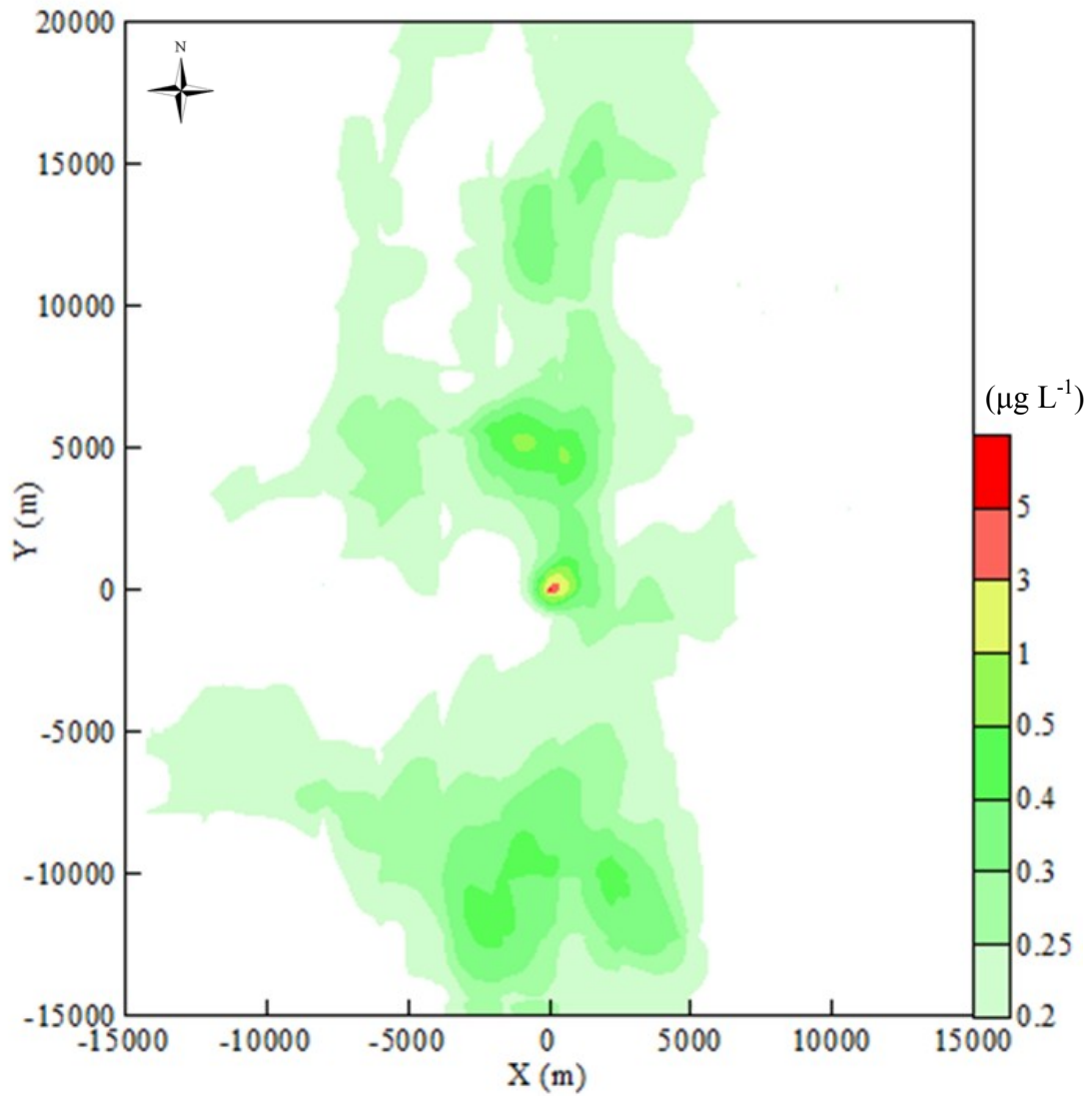
Figure 7-14 Predicted 95th percentile benzene concentration distribution at a depth of 26 m resulting from produced water discharges in the study area
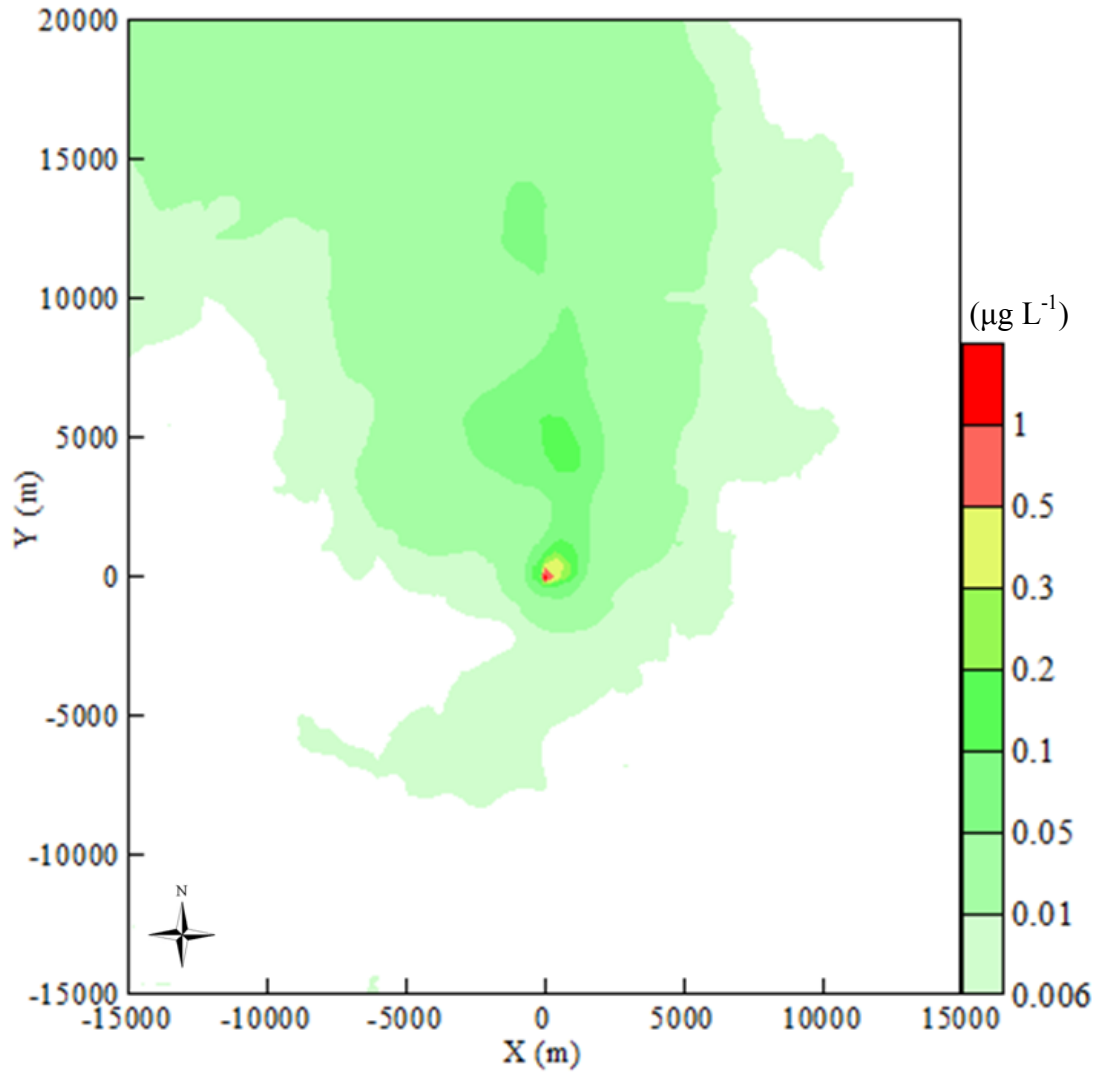
Figure 7-15 Predicted 5th percentile benzene concentration distribution at a depth of 26 m resulting from produced water discharges in the study area

7.3 Summary

A case study of modeling and assessment of produced water discharges off the East Coast of Canada was presented in this chapter. Three dimensional pollutant dispersion results show that pollutant concentration distributions vary in time in both near field and far field zones, as controlled by local hydrodynamic conditions. Because of the buoyancy effects, high concentrations may appear at depths between 20 to 30 m below the water surface. Basically, pollutants borne in the produced water are rapidly diluted after discharge. After a certain distance, the dilution processes slow down and low concentrations of substances may persist longer in the marine waters.

Risk assessment was conducted under the predicted future emission rates of produced water discharges of the Hibernia platform. Uncertainty parameters and environmental threshold were identified to support the quantification of risks associated with produced water discharges in the study area. Uncertainty analysis reveals that the vertical dispersion coefficients and degradation rate are the main parameters contributing to the output concentrations in the simulation. Risk assessment results for lead concentration distributions show that a high risk of ecological injury may occur within a few hundred meters from the platform. Comparatively, Benzene concentration levels in the produced water plumes are low comparing to the identified environmental threshold, demonstrating that benzene in produced water discharge plume may pose a minimal risk to the marine environment.

CHAPTER

8

DISCUSSION

Discussions regarding to the developed modeling system, model validation and application, and risk assessment approaches and results are presented in this chapter. The main contents in the following are mainly related to the methodologies in Chapter 3 and case study and validation results described in Chapters 5-7.

8.1 Integrated Physical Models

Determination of boundary conditions is critical for a successful simulation of the ocean current field. Modeling and verification results in this study confirm that the development

of a radiation-type open boundary condition is appropriate for modeling the ocean current fields in the study area. Additionally, a much larger and wider area (about 200 times the study area: Figure 4-1) containing the study region is considered to minimize the influence of boundary conditions for the study region. A dynamic integration effort was made towards 3D field sampling and measurements which would directly support the field validation of the developed modeling and assessment system. More regular monitoring of the local ocean current conditions will further help to configure the complex model boundary conditions.

Buoyant jet-type plume models can generally provide accurate and reliable representations of buoyant jet motions. However, one drawback of such models is that it is difficult to assign profile shapes and determine entrainment rates in boundary interactions when integral models are applied to finite receiving domains. Moreover, numerical methods such as FDMs are limited by stability or accuracy considerations to relatively larger spatial and temporal resolutions, which make them difficult to use in simulating the near field mixing process. Therefore, a hybrid method of integrating near field plume model and numerical far field methods would be a better solution for modeling pollutant discharge problems. The modeling studies and field validation results presented in this thesis report further confirm that improved overall results were obtained from the modeling system developed.

The combined centered second order spatial differences and leapfrog differencing schemes of FDM method were used in developing the modeling system. Though the relative standard formulation was implemented, test cases and field case study proved it to be sufficient to conduct a simulation of pollutant dispersion behavior with proper

configuration of grid resolution and time steps. Alternative methods such as the finite element method (FEM) or finite volume method (FVM) could be used as a replacement for FDM. However, for such integrated system to simulate large-scale case studies, the computational cost involved in solving the linear equation system from the finite element discretization of the problem, especially in time-dependent and three dimensional problems, can become impractical (Liou and Tezduyar, 1990). The finite volume methods (FVMs) may requires more CPU time than the finite element methods (FEMs), and almost twice the computational cost as the FEM in some cases (Tylor *et al.*, 2003). Appendix B shows a finite element method and a simple test case result. The application of the developed FEM confirms that more accurate results can be generated from FEM than FDM and RWPT, but much more (impractical) computation time is required for FEM than FDM. Since the proposed integrated system in this thesis study is developed to be implemented on personal computers, the developed FEM was not integrated in the system at the time of writing this thesis, but future studies under consideration will target the improvement of computational efficiency.

Though the computational expenses of FEM and FVM are the major drawback, for complex domain problems, these methods have advantages over FDM, when applied on an unstructured mesh system. The calculation time may be shortened by splitting calculation domains and using parallel computers. In parallel computations, a large-scale problem can be solved by partitioning it into several smaller problems, which are then solved by many separate processors simultaneously (Wai and Lu, 2000). Currently, parallel computation is widely used for ocean circulation modelling systems and for coastal sediment transport modelling. For example, Wai and Lu (2000) introduced a

three-dimensional (3D) parallel model for efficient simulation of sediment–water transport processes in offshore regions. Wang *et al*. (2005) explored parallel computation of the Regional Ocean Modeling System (ROMS) using the MPI programming model. Fringer *et al*. (2006) presented a parallelized finite volume formulation to simulate nonhydrostatic processes in the ocean running on parallel computers. Sørensen *et al*. (2010) reported the parallelization of MIKE by DHI's[1] flexible mesh modelling system with MPI. These studies demonstrate that efficient and accurate predictions of largescale CFD problems are possible using parallel computations. Parallel computations may be a new aspect to improve the current modeling and assessment system.

The integration method used in the present study was inspired by Choi and Lee (2007), and fully accounts for the interactions between discharge fluids and the receiving water body in order to represent near field mixing in the far field model and simultaneously ensure conservation of mass. However, the transition from near field simulation to far field model should be carefully handled. As discussed in previous sections, one problem is that if grid resolutions in the far field model are low, the areas close to the transition zone may not be properly simulated. Consequently, high grid resolutions close to the source or a subgrid system may be needed. Further studies to improve the overall far field results will be conducted in the future.

The plume profile is affected or controlled by the local ambient conditions in both near field and far field of the offshore waters. Small changes in ambient currents and densities as input into the model may have large effects on the modeling results. Most field studies in the offshore area collect instant water samples over a period of days or weeks. However, concentrations at a fixed location are highly variable over time because

---

[1] http://www.mikebydhi.com/

of the changes of local ambient conditions. The water samples collected in a given location may or may not be inside the plume, and the same goes for modeling results. These factors make field validations in the ocean environment very difficult. The validation results presented in this paper could only show one example of comparison between modeling results and field observations. Further analysis will be needed on the basis of more field experimental data collected in future studies.

Produced water discharges into the Canadian Atlantic offshore region is currently limited, as offshore oil and gas production is in the early stages of development. However, its volume is expected to be increased as new oil and gas fields are developed in the future (Lee *et al*., 2005). It is thus necessary to develop and validate new modeling tools to support effective management of our ocean environment and its living resources. The results obtained for produced water dispersion in the present study may provide fundamental knowledge for further assessment and management of produced water discharges in offshore areas.

8.2 Integrated Risk Assessment

Results from a physical modeling system are often affected by the presence of uncertainties, such as the estimates of discharge rates, pollutant fate and transport parameters, etc., which may impact the estimated outputs associated with environmental risks. Evaluation of such uncertainties is of great importance in the assessment of potential regulatory options; for example, with respect to the selection of a strategy for the control of pollutant levels (Isukapalli, 1999). The integration of uncertainty analysis

into physical modeling process could provide means to conduct risk assessment and ultimately provide information useful in decision-making.

Many techniques, including the probabilistic approach and mathematical and numerical modeling, are available to characterize the uncertainties in the natural processes. The most widely used approach to characterize uncertainty in risk assessment studies is the Monte Carlo simulation (USEPA, 1996). Focused on parameters that are naturally variable and difficult to characterize, conducting risk assessment by means of the Monte Carlo approach is appropriate and provides more details of potential risks that may occur in the natural environment.

However, employing a conventional Monte Carlo method for uncertainty propagation typically requires hundreds or thousands of model runs, resulting in significant computational demands. For the environmental modeling system described in the present thesis, it is basically impossible to estimate uncertainties using a traditional Monte Carlo method. Therefore, a modified Monte Carlo method based on Riddle *et al.* (2001) is incorporated with the physical modeling system to conduct uncertainty analysis thus only requiring a limited number of model runs (on the order of 10). The development and application of the modified Monte Carlo method not only allows fast and accurate estimates of the uncertainties associated with model outputs, but also identifies the relative contribution of individual input parameters to output uncertainties.

To evaluate the risks associated with waste water discharges, local environmental guidelines or standards are often used as evaluation criteria. However, the criteria for the protection of natural resources and human health differ greatly from one another. For example, in Canada the freshwater aquatic life protection criterion for lead ranges from 1

to 7 μg total waterborne [Pb] L^{-1} (CWQG, 2006). Within this range, high accumulations and adverse effects on growth and reproduction were recorded among sensitive species (Eisler, 2000). Moreover, certain organolead compounds are lethal to some species of aquatic biota within this range, but no criteria have yet been formulated for this highly toxic group of chemicals, especially for seawater. Current environmental surveys and regulations suggest the need for a quantitative risk-based approach in developing environmental protection policies (Benedetti *et al*., 2008). The evaluation of existing standards, and of the scale of potential deleterious impacts on ecosystems and human health, requires a consultative risk assessment approach.

In the present study, risks are calculated for individual chemicals only through the selection of a proper environmental threshold for that substance. Smit *et al*. (2011) presented a risk based management tool for the produced water discharges on the Norwegian Continental Shelf. The environmental impact factor (EIF) was developed to quantify and document the environmental risks from produced water discharges. In the EIF methodology, the risks are calculated by combining the risk due to each component in a group of 14 naturally occurring, reservoir-related substances, and component-based information on added process chemicals. However, the calculation of EIF factor is based on the produced water composition and toxicity studies in the North Sea, which may not be suitable for other areas of the world, for example, the north Atlantic. Therefore, the development of a risk based management tool associated with produced water discharges based on toxicity studies in Canadian ocean waters is recommended in future studies.

CHAPTER
9

CONCLUSION
AND RECOMMENDATION

9.1 Conclusions

Produced water, the largest volume waste stream discharged from offshore oil and gas production activities, is a mixture of a number of toxic pollutants at low concentration including heavy metals and soluble hydrocarbons. The growing importance and interest in the ocean environmental assessment has urged further evaluation of produced water impacts on the marine ecosystem. In this thesis report, an integrated system for the

modeling and assessment of produced water discharges is developed and implemented in offshore area.

The system integrates ocean circulation simulation, pollutant fate and transport modeling including both near field mechanisms and far field processes. A dynamic coupling technique is employed to integrate these modeling components. The coupling method introduced entrainment sinks to ocean circulation and far field model along the plume trajectories, and diluted source term at the terminal level, which ensure the mass balance during the transition as well as dynamic interactions between effluents and the receiving water body.

To reflect uncertainties associated with modeling inputs and conduct risk assessment for produced water discharges into marine environment, a modified Monte Carlo approach is incorporated with the modeling system, which substantially improves the computational efficiency for system uncertainty analysis. The modified Monte Carlo method also provides sensitivity information and individual contributions of input uncertainties to output uncertainties, which would require significantly large numbers of simulations to provide such information using traditional Monte Carlo method. Two risk characterization methods – probabilistic risk and exposure risk, were integrated into the modified Monte Carlo method to quantify and map the potential risk levels in areas of interest.

At first, validations of individual model components were performed. Based on the consideration of boundary conditions, the results of the flow field obtained from the ocean circulation model show good agreement with the field observations. Evaluation and field validations of pollutant fate and transport models were conducted as well. The

results from the near field model were validated against field experimental data in a USA platform. Considering the large variability of experiments on the complex ocean environment, the overall near field modeling results showed excellent agreement with the observations. The far field model was evaluated through test cases against a RWPT method and an exact analytical solution in a steady one dimensional flow condition. Test cases show that with proper configuration of the grid resolution, the finite difference method developed could provide a good presentation of pollutant dispersion processes in the far field.

A field case study was conducted on the Grand Banks of Newfoundland, Canada using the integrated system. The overall integrated modeling results were compared with field data obtained from field experiments in the study area. Concentrations of both lead and benzene were simulated and validated to test the system's ability to simulate and analyze conservative and non-conservative substances. Results for predicted lead concentrations were compared with field data in two vertical layers in the far field. Results showed good agreement with observations and also showed an improvement over the results from the far field model alone, especially in the vertical layer furthest from the source, demonstrating the good performance of the integrated modeling system. Validations of predicted benzene concentration were conducted in the near field, which show reasonable results, giving the limited observations available for benzene concentrations in the study area. Finally, risks associated with predicted lead and benzene concentrations resulting from potential future produced water discharges in the offshore waters were evaluated. Results revealed potential for ecological injury associated with

high lead concentrations in areas a few hundred meters from the discharge point, under the predicted future rates of produced water generated.

This study has demonstrated the utility of an integrated three-dimensional modeling and risk assessment system for the environmental assessment of produced water discharges in the ocean. The developed system provides a quantitative means of examining the dispersion of toxic components of produced water effluent on a regional spatial scale, and also its use for addressing the long term environmental risks associated with the produced water discharges.

9.2 Research Contributions

Scientific contributions of this Ph.D. thesis include:

- The development of a functional modeling and risk assessment system which integrates ocean hydrodynamics, near field and far field physical transport processes, chemical characteristics, and risk assessment methods.

- The major contributions in system development include:

  ➢ The development of finite difference method for far field modeling. Though a relatively standard scheme is used, improvements of modeling stability and accuracy were made in the simulation.

  ➢ Extension of a Lagrangian near field model to three dimensional cross flow conditions, which allows the model's application to field study cases in offshore areas.

- ➢ Dynamic integrations of ocean circulation, near field and far field models to ensure mass balance during the transition as well as dynamic interactions between effluents and the receiving water body.

- ➢ A modified Monte Carlo method for system uncertainty analysis. A multiple linear regression model using least squares was established to present the relationship between uncertainty parameters and output concentrations, and the contribution of individual uncertainty parameters to outputs.

- ➢ Incorporation of both probabilistic risks and exposure risks, providing the ability of an assessment of environmental impacts in a current and future time frame.

- ➢ Advanced GUI system to provide easy applications.

- • Extensive validations were performed in the research study through test cases and comparison with field experimental data to evaluate the efficiency and accuracy of the system for the simulation of produced water discharges resulting from offshore oil and gas operations.

- • The system may also be applicable to simulations of municipal waste water discharges from shoreline areas. The system will be a useful tool for research groups, government agencies and industries to provide insights into pollutant dispersion processes and to assess their potential adverse effects.

- • A case study is conducted for the modeling and assessment of offshore oil and gas activities in Atlantic Canada.

9.3 Recommendations for Future Work

Future studies may focus on:

1. A Finite element method (FEM) or finite volume method (FVM) can be developed and integrated in the system to improve simulations in a more complex domain problem in conjunction with the application of parallel computation to improve computational efficiency.

2. The fate and transport of suspended materials and other mechanisms such as evaporation and adsorption may be integrated in the system in future studies to fully represent the physical and chemical processes associated with waste water discharges in the marine environment.

3. In an attempt to present the ecotoxicological effects of discharges of produced water in Atlantic Canada, it is important to establish a set of evaluation criteria suitable for local ecosystem in conjunction with future toxicity studies conducted on the east coast of Canada.

4. Validations in the present thesis study consisted of instant samples collected in marine waters. In the future, more tests and validations can be expected, in accordance with mean sample concentrations collected during a period of time in a fixed location.

5. Complicated chemical reactions are expected in the produced water dispersion processes. However, most current modeling studies including this thesis report only consider the individual chemical kinetics. Taking reactions between

chemicals into account may provide a new perspective towards improving the system developed in this thesis.

6. The graphical user interface will need continuous improvement along with the application of model to new case studies.

REFERENCES

Abbaspour, M., Javid, A.H., Moghimi, P., Kayhan, K. 2005. Modeling of thermal pollution in coastal area and its economical and environmental assessment. International Journal of Environmental Science and Technology 2 (1), 13-26.

Abulaban, A., Nieber, J.L., Misra, D. 1998. Modeling plume behaviour for nonlinearly sorbing solutes in saturated homogeneous porous media. Advances in Water Resources 21, 487-498.

Argall, R., Sanders, B.F., Poon, Y.K. 2003. Random-walk suspended sediment transport and settling model. Proceedings of the Eighth International Conference on Estuarine and Coastal Modeling, 713-730.

Agrawal, A., Prasad, A.K. 2003. Integral solution for the mean flow profiles of turbulent jets, plumes, and wakes. Journal of Fluids Engineering 125, 813-822.

AMEC. 2006. Revision of the Physical Environmental Assessment for Deep Panuke Production Site – Oceanographic Component: Produced Water, Cooling Water, Drilling Wastes. Report prepared by AMEC for Jacques Whitford (November 2006). 50 pp.

Argall, R., Sanders, B.F., Poon, Y.K. 2003. Random-walk suspended sediment transport and settling model. In: M.L. Spaulding (ed.), Estuarine and Coastal Modeling: Proceedings of the 8th International Conference on Estuarine and Coastal Modeling, Monterey, California, November 3-5, 2003, American Society of Civil Engineers, pp. 713-730.

Asselin, R.A. 1972. Frequency filter for time integrations. Monthly Weather Review 100, 487-490.

Bagtzoglou, A.C., Tompson, A.F.B., Dougherty, D.E. 1992. Project functions for particle-grid methods. Numerical Methods for Partial Differential Equations 8, 325-340.

Banton, O., Porel, G., Delay, F. 1997. Coupling of the time domain random walk method with the finite fragment method to simulate flow and transport in 1-D heterogeneous media. Journal of Hydrology 201, 49-61.

Bardossy, A., Duckstein, L. 1995. Fuzzy Rule-Based Modeling with Applications to Geophysical, Biological and Engineering Systems. CRC Press, Boca Raton, Florida.

BASIN, 2011. Offshore Eastern Canada hydrocarbon database. Available at: Nature Resources Canada Website. http://basin.gsca.nrcan.gc.ca/index_e.php (Access date: December 20, 2011).

Batchelder, H.P. 2002. Spatial and temporal distributions of mesozooplankton in idealized models using individual based particle tracking simulations. ICES.GLOBEC workshop on transport of cod larvae, Hillerod, Denmark.

Baumgartner, D.J., Frick, W.E., Roberts, P.J.W. 1994. Dilution Models for Effluent Discharges. US Environmental Protection Agency Report EPA/600/R-94/086, US Environmental Protection Agency, Washington, D.C.

Baetsle, L.H. 1969. Migration of radionuclides in porous media. In: A.M.F. Duhamel (ed.), Progress in Nuclear Energy, Series XII, Health Physics, Pergamon Press, Elmsford, NY, pp. 707-730.

Benedetti, L., Bixio, D., Claeys, F. Vanrolleghem, P.A. 2008. Tools to support a model-based methodology for emission/immission and benefit/cost/risk analysis of wastewater systems that considers uncertainty. Environmental Modelling & Software 23(8), 1082-1091.

Berloff, P.S., McWilliams, J.C. 2002. Material transport in oceanic gyres. Part II: hierarchy of stochastic models. Journal of Physical Oceanography 32, 797-830

Bleninger, T. 2006. Coupled 3D Hydrodynamic Models for Submarine Outfalls: Environmental Hydraulic Design and Control of Multiport Diffusers. Ph.D. Thesis, University Karlsruhe.

Bleninger, T., Jirka, G.H. 2004. Near- and far-field model coupling methodology for wastewater discharges. In: J.H.W. Lee, K.M. Lam (eds.), Environmental Hydraulics and Sustainable Water Management, Proceedings of the 4th International Symposium on Environmental Hydraulics and 14th Congress of Asia and Pacific Division, International Association of Hydraulic Engineering and Research, Hong Kong, China, Taylor and Francis, pp. 447-453.

Blumberg, A.F., Mellor, G.L. 1978. A coastal ocean numerical model. In: J. Sunderman, K.-P. Holtz (eds.), Mathematical modeling of Estuarine Physics, Proceedings of International Symposium, Hamburg, Springer, Berlin, pp. 203-214.

Blumberg, A.F., Mellor, G.L. 1987. A description of a three-dimensional coastal ocean circulation model. Geophysical Fluid Dynamics Program, Princeton University, Princeton, New Jersey 08544.

Borgmann, U., Kramar, O., Loveridge, C. 1978. Rates of mortality, growth, and biomass production of Lymnaea palustris during chronic exposure to lead. Journal of the Fisheries Research Board of Canada 35, 1109-1115.

Boufadel, M.C., Du, K., Kaku, V., Weaver, J. 2007. Lagrangian simulation of oil droplets transport due to regular waves. Environmental Modelling & Software 22, 978-986.

Brandsma, M.G. 2001. Near-Field Produced Water Plume, Platform Irene. Report submitted to Arthur D. Little, Inc. Santa Barbara, California.

Brandsma, M.G., Sauer, T.C., Jr. 1983a. The OOC model: prediction of short term fate of drilling fluid in the ocean. Part 1: model description. In: Proceedings of MMS Workshop on An Evaluation of Effluent Dispersion and Fate Models for OCS Platforms, February 7-10, 1983, Santa Barbara, California, Minerals Management Service, Contract No. 14-21-0001-29122, pp. 58-84.

Brandsma, M.G., Sauer, T.C., Jr. 1983b. The OOC model: prediction of short term fate of drilling fluid in the ocean. Part 2: model results. In: Proceedings of MMS Workshop on An Evaluation of Effluent Dispersion and Fate Models for OCS Platforms, February 7-10, 1983, Santa Barbara, California, Minerals Management Service, Contract No. 14-21-0001-29122, pp. 86-106.

Brandsma, M.G., Davis, L., Ayers, R., Sauer, T. 1980. A computer model to predict the short-term fate of drilling discharges in the marine environment. In: Symposium on Environmental Fate and Effects of Drilling Fluids and Cuttings, January 21-24, 1980, Lake Buena Vista, FL.

Brandsma, M.G., Smith, J.P., O'Reilly, J.E., Ayers, R.C., Jr., Holmquist, A.L. 1992. Modeling offshore discharges of produced water. In: J.P. Ray, R. Englehardt (eds.),

Produced Water: Technological/Environmental Issues and Solutions, Plenum Press, NY, pp. 59-71.

Brouwer, R., Blois, C.D. 2008. Integrated modeling of risk and uncertainty underlying the cost and effectiveness of water quality measures. Environmental Modelling & Software 23, 922-937.

Budgell, W.P. 2005. Numerical simulation of ice-ocean variability in the Barents Sea region towards dynamical downscaling. Ocean Dynamics 55, 370-387.

Burns, K.A., Codi, S., Furnas, M., Heggie, D., Holdway, D., King, B., McAllister, F. 1999. Dispersion and fate of produced formation water constituents in an Australian northwest shelf shallow water ecosystem. Marine Pollution Buletin 38, 593-603.

CAPP. 2001. Offshore Produced Water Waste Management. Publication by the Canadian Association of Petroleum Producers (CAPP), Technical Report, Docs# 29125.

Chapman, D.C. 1985. Numerical treatment of cross-shelf open boundaries in a barotropic coastal ocean model. Journal of Physical Oceanography 25, 1060-1075.

Chen, Z., Huang, G.H., Chakma, A., Tontiwachwuthikul, P. 1998. Environmental risk assessment for aquifer disposal of carbon dioxide. Proceedings of the 4th International Conference on Greenhouse Gas Control Technologies, Interlaken, Switzerland.

Chen, Z., Zhao, L., Lee, K. 2010. Environmental risk assessment of offshore produced water discharges using a hybrid fuzzy-stochastic modeling approach. Environmental Modelling & Software 25, 782-792.

Cheung, V., Lee, J.H.W. 1999. Discussion of "Simulation of oil spills from underwater accidents I: Model development" by Yapa P.D. and Li Z. in Journal of Hydraulic Research 35(5): 673-687. Journal of Hydraulic Research 37(3), 425-429.

Choi, K.W., Lee, J.H.W. 2007. Distributed entrainment sink approach for modeling mixing and transport in the intermediate field. Journal of Hydraulic Engineering 133(7), 804-815.

Chowdhury, S., Husian, T., Veitch, B., Bose, N., Sadiq, R. 2004. Human health risk assessment of naturally occurring radioactive materials in produced water – a case study. Human and Ecological Risk Assessment 10, 1155-1171.

Chung, T.J. 2002. Computational Fluid Dynamics. Cambridge University Press, Cambridge, UK.

C-NLOPB. 2011. Estimates of Recoverable Reserves/Resources – Hibernia Field. Canada-Newfoundland and Labrador Offshore Petroleum Board. Available at: http://www.cnlopb.nl.ca/ (Access date: January 2012).

Courant, R., Friedrichs, K.O., Lewy, H. 1967. On the partial difference equations of mathematical physics. IBM Journal of Research and Development 11, 215-234.

Croucher, A., O'Sullivan, M. 1998. Numerical methods for contaminant transport in rivers and estuaries. Computers and Fluids 27(8), 861-878.

COP. 2001. California Ocean Plan. Ocean Quality Control Plan: Ocean Waters of California. State Water Resources Control Board, Resolution No. 2000-108. California Environmental Protection Agency.

CWQG. 2006. Canadian Environmental Quality Guidelines for the Protection of Aquatic Life. Canadian Council of Ministers of the Environment. The guidelines were

originally published in CCREM 1987, Chapter 3. Available at:
http://www.ccme.ca/assets/pdf/ e1_06.pdf (Access date: April 2007).

Daily, J.W., Harleman, D.R.F. 1966. Fluid Dynamics. Addison-Wesley Publishing Co. Inc., Reading, MA.

Date, A.W. 2005. Introduction to Computational Fluid Dynamics. Cambridge University Press, Cambridge, UK.

Davidson, M.J., Pun, K.L. 1998. Hybrid model for prediction of initial dilutions from outfall discharges. Journal of Hydraulic Engineering 124(12), 1188-1197.

Davis, L.R. 1999. Fundamentals of Environmental Discharge Modeling. CRC Press LLC, Boca Raton, Florida.

Delft3D. 2009. Simulation of multi-dimensional hydrodynamic flows and transport phenomena, including sediments. Delft3D-FLOW User Manual. Available at: http://delftsoftware.wldelft.nl/index.php?option=com_docman&task =cat_view&gid=39&Itemid=61 (Access date: July 2009).

DHI. 2007. MIKE 21 & MIKE 3 Flow Model FM: Transport Module. DHI, Denmark. Available at: http://www.dhigroup.com/Software/Marine/MIKE3/Details/ WaterQualityAndEcology/ADAdvectionDispersionModule.aspx (Access date: July 2009).

Di Lorenzo, E. 2003. Seasonal dynamics of the surface circulation in the Southern California Current System. Deep-Sea Research II 50, 2371-2388.

Doneker, R.L., Jirka, G.H. 2007. CORMIX User Manual: A Hydrodynamic Mixing Zone Model and Decision Support System for Pollutant Discharges into Surface Waters. EPA-823-K-07-001. US EPA, Washington, DC.

Durell, G., Utvik, T.R., Johnsen, S., Frost, T., Neff, J. 2006. Oil well produced water discharges to the North Sea. Part I: Comparison of deployed mussels (Mytilus edulis), semi-permeable membrane devices, and the DREAM model predictions to estimate the dispersion of polycyclic aromatic hydrocarbons. Marine Environmental Research 62, 194-223.

Durran, D.R. 1991. The third-order Adams-Bashforth method: an attractive alternative to leapfrog time differencing. Monthly Weather Review 119, 702-720.

Edelvang, K., Kaas, H., Erichsen, A.C., Alvarez-Berastegui, D., Bundgaard, K., Jørgensen, P.V. 2005. Numerical modeling of phytoplankton biomass in coastal waters. Journal of Marine System 57(1-2), 13-29.

Eisler, R. 2000. Handbook of Chemical Risk Assessment: Health Hazards to Humans, Plants and Animals: VI Metals. Lewis Publishers, New York, NY, USA.

Environment Canada. 1990. Environmental Code of Practice for Treatment and Disposal of Waste Discharges from Offshore Oil and Gas Operations. Report No. EPS 1/PN/2.

Ezer, T. 1999. Decadal variabilities of the upper layers of the subtropical North Atlantic: An ocean model study. Journal of Physical Oceanography 29, 3111-3124.

Ezer, T. 2001. Can long-term variability in the Gulf Stream transport be inferred from sea level? Geophysical Research Letters 28, 1031-1034.

Ezer, T., Arango, H., Shchepetkin, A.F. 2002. Developments in terrain-following ocean models: intercomparisons of numerical aspects. Ocean Modelling 4, 249-267.

Ezer, T., Mellor, G.L. 1992. A numerical study of the variability and the separation of the Gulf Stream induced by surface atmospheric forcing and lateral boundary flows. Journal of Physical Oceanography 22, 660-682.

Ezer, T., Mellor, G.L. 1994. Diagnostic and prognostic calculations of the North Atlantic circulation and sea level using a sigma coordinate ocean model. Journal of Geophysical Research 99, 14159-14171.

Ezer, T., Mellor, G.L. 1997. Simulations of the Atlantic Ocean with a free surface sigma coordinate ocean model. Journal of Geophysical Research 102(C7), 15647-15657.

Ezer, T., Mellor, G.L. 2004. A generalized coordinate ocean model and a comparison of the bottom boundary layer dynamics in terrain-following and in z-level grids. Ocean Modelling 6, 379-403.

Ezer, T., Mellor, G.L., Greatbatch, R.J., 1995. On the interpentadal variability of the North Atlantic ocean: Model simulated changes in transport, meridional heat flux and coastal sea level between 1955-1959 an 1970-1974. Journal of Geophysical Research 100, 10559-10566.

FAO. 1997. Seawater Intrusion in Coastal Aquifers: Guidelines for Study, Monitoring and Control. Food and Agriculture Organization of the United Nations, Rome, Italy.

Frick, W.E., Roberts, P.J.W., Davis, L.R., Keyes, J., Baumgartner, D.J., George, K.P. 2003. Dilution Models for Effluent Discharges. EPA/600/R-03/025, US EPA, National Exposure Research Laboratory, Athens, GA.

Frick, W.E., Sproul, C.A., Stuart, D. 1997. Bacterial impacts of ocean outfalls: legal challenges. Journal of Environmental Engineering 123(2), 191-196.

Fringer, O.B., Gerritsen, M., Street, R.L. 2006. An unstructured-grid, finite-volume, nonhydrostatic parallel coastal ocean simulator. Ocean Modelling 14, 139-173.

Glass, J., Rodi, W. 1982. A higher order numerical scheme for scalar transport. Computer Methods in Applied Mechanics and Engineering 31, 337-358.

Glover, D., Jenkins, B., Doney, S. 2010. Modeling, Data Analysis and Numerical Techniques for Geochemistry, Woods Hole Oceanographic Institution, available at:http://w3eos.whoi.edu/12.747/ (Access date: January 2012).

Gray, W.G., Pinder, G.F. 1976. On the relationship between the finite element and finite difference methods. International Journal for Numerical Methods in Engineering 10(4), 893-923.

Gresho, P.M., Sani, R.L., Engelman, M.S. 2000. Incompressible Flow and the Finite Element Method Volume 1: Advection-Diffusion, West Sussex: John Wiley & Sons Ltd.

Hakkinen, S., Mellor, G.L. 1992. Modeling the seasonal variability of a coupled Arctic ice-ocean system. Journal of Geophysical Research 97, 20285-20304.

Haidvogel, D.B., Arango, H., Hedstrom, K., Beckmann, A., Malanotte-Rizzoli, P., Shchepetkin, A.F. 2000a. Model evaluation experiments in the North Atlantic Basin: simulations in nonlinear terrain-following coordinates. Dynamics of Atmospheres and Oceans 32, 239-282.

Haidvogel, D.B., Blanton, J., Kindle, J.C., Lynch, D.R. 2000b. Coastal ocean modeling: processes and real-time systems. Oceanography 13(1), 35-46.

Hamrick, J.M. 1992. A Three-Dimensional Environmental Fluid Dynamics Computer Code: Theoretical and Computational Aspects. Special Report 317, the College of William and Mary, Virginia Institute of Marine Science.

Hao, X., Varshney, A. 2006. Geometry-guided computation of 3D electrostatics for large molecular datasets. Computer Aided Geometric Design 23(6), 545-557.

Hasse, L., Smith, S.D. 1996. Local sea surface wind, wind stress, and sensible and latent heat fluxes. Journal of Climate 10 (11), 2711–2724.

Helmers, E. 1996. Trace metals in suspended particulate matter of Atlantic Ocean surface water (40°N to 20°N). Marine Chemistry 53, 51-67.

Hibernia Platform Annual Current Measurement Report, 2005. Hibernia Management and Development Company Limited (HMDC), St John's, Newfoundland. Submitted by: Oceans Ltd., March 2006.

Hillebrand, G. 2003. Coupling of Near- and Far-field Models for Prediction of Treated Sewage Effluent Discharges into the Coastal Ocean. Thesis Report, Institut für Hydromechanik, Universität Karlsruhe, Karlsruhe, Germany.

HMDC. 1994. Hibernia Development Project Environmental Compliance Monitoring Plan (Draft). Hibernia Management and Development Company Ltd., St. John's NL.

Hodgins, D.O., Hodgins, S.L.M. 1998. Distribution of Well Cuttings and Produced Water for the Terra Nova Development. Report prepared by Seaconsult Marine Research Ltd. For Terra Nova Alliance. August, 1998.

Hodgins, D.O., Hodgins, S.L.M. 2000. Modelled Predictions of Well Cuttings Deposition and Produced Water Dispersion for the Proposed White Rose Development. Report

prepared by Seaconsult Marine Research Ltd. For Husky Oil Operations Limited. June, 2000.

Howard, P.H., Boethling, R.S., Jarvis, W.F., Meylan, W.M., Michalenko, E.M. 1991. Handbook of Environmental Degradation Rates. Lewis Publishers, Chelsea, MI.

Hunt, B. 1978. Dispersive sources in uniform groundwater flow. Journal of the Hydraulic Division (ASCE) 104, 75-85.

Hunter, J.R.; Craig, P.D.; Phillips, H.E. 1993. On the use of random walk models with spatially variable diffusivity. Journal of Computational Physics 106, 366-376.

HydroQual. 2002. A Primer for ECOMSED, Users Manual, Version 1.3. HydroQual Inc, Mahwah, NJ.

Ilyina, T., Pohlmann, T., Lammel, G., Sundermann, J. 2006. A fate and transport ocean model for persistent organic pollutants and its application to the North Sea. Journal of Marine Systems 63, 1-19.

Israelsson, P.H., Kim, Y.D., Adams, E.E. 2006. A comparison of three Lagrangian approaches for extending near field mixing calculations. Environmental Modelling & Software 21, 1631-1649.

Isukapalli, S.S. 1999. Uncertainty Analysis of Transport-Transformation Models. Ph.D. Thesis report of Graduate School-New Brunswick, Rutgers, the State University of New Jersey.

James, I.D. 2002. Modeling pollution dispersion, the ecosystem and water quality in coastal waters: a review. Environmental Modelling & Software 17, 363-385.

Jirka, G.H. 1982. Multiport diffusers for heat disposal: a summary. Journal of the Hydraulic Division 108(HY 12), 1423-1468.

Jirka, G.H. 2004. Integral model for turbulent buoyant jets in unbounded stratified flows: part I: single round jet. Environmental Fluid Mechanics 4, 1-56.

Jirka, G.H. 2006. Integral Model for Turbulent Buoyant Jets in Unbounded Stratified Flows Part 2: Plane Jet Dynamics Resulting from Multiport Diffuser Jets. Environmental Fluid Mechanics 6, 43-100.

Jirka, G.H. 2007. Buoyant surface discharges into water bodies II: jet integral model. Journal of Hydraulic Engineering 133(9), 1021-1036.

Jirka, G.H., Doneker, R.L., Hinton, S.W. 1996. User's Manual for CORMIX: A Hydrodynamic Mixing Zone Model and Decision Support System for Pollutant Discharges into Surface Waters. Tech. Rep., DeFrees Hydraulics Laboratory, Cornell University (also published by U.S. Environmental Protection Agency, Tech. Rep., Environmental Research Lab, Athens, Georgia).

Johansen, O. 2000. DeepBlow- a Lagrangian plume model for deep water blowouts. Spill Science & Technology Bulletin 6(2), 103-111.

Johnsen, S., Frost, T.K., Hjelsvold, M., Utvik, T.R. 2000. The Environmental Impact Factor – A proposed tool for produced water impact reduction, management, and regulation. In: Proceedings of the SPE International Conference on Health, Saftety and Environment in Oil and Gas Exploration and Production, June 25-28, 2000, Stavanger, Norway, Society of Petroleum Engineers, SPE paper 61178.

JWSL. 2007. Hibernia Production Phase Environmental Effects Monitoring Program – Year Six (2007) Volume I – Interpretation. Jacques Whitford Stantec Limited, St. John's NL, pages 63.

Kikkert, G.A., Davidson, M.J., Nokes, R.I. 2007. Inclined negatively buoyant discharges. Journal of Hydraulic Engineering 133(5), 545-554.

Kim, Y.D., Seo, I.W., Kang, S.W., Oh, B.C. 2002. Jet integral-particle tracking hybrid model for single buoyant jets. Journal of Hydraulic Engineering 128, 753-760.

Klir, G.J., Yuan, B. 1995. Fuzzy Sets and Fuzzy Logic: Theory and Applications. Prentice-Hall, Englewood Cliffs, NJ, USA.

Koh, R.C., Chang, C. 1973. Mathematical Model for Barged Ocean Disposal of Waste. Report to Office of Research and Development, US Environmental Protection Agency, Washington DC.

Korotenko, K.A., Mamedov, R.M., Kontar, A.E., Korotenko, L.A. 2004. Particle tracking method in the approach for prediction of oil slick transport in the sea: modeling oil pollution resulting from river input. Journal of Marine Systems 48, 159-170.

Koziy, L., Maderich, V., Margvelashvili, N., Zheleznyak, M. 1998. Three-dimensional model of radionuclide dispersion in estuaries and shelf seas. Environmental Modelling & Software 13, 413-420.

Krause, P.R. 1995. Spatial and temporal variability in receiving water toxicity near an oil effluent discharge site. Archives of Environmental Contamination and Toxicology 29, 523-529.

Lai, T.L., Robbins, H., Wei, C.Z. 1978. Strong consistency of least squares estimates in multiple regression. Proceedings of the National Academy of Sciences USA 75(7).

Lee, H.M. 1996. Applying fuzzy set theory to evaluate the rate of aggregative risk in software development. Fuzzy Sets and Systems 26, 1182-1191.

Lee, K., Azetsu-Scott, K., Cobanli, S.E., Dalziel, J., Niven, S., Wohlgeschaffen, G., Yeats, P., 2005. Overview of Potential impacts from produced water discharges in Atlantic Canada. In: S.L. Armsworthy, P.J. Cranford, K. Lee (eds.), Offshore Oil and Gas Environmental Effects Monitoring Approaches and Technologies, Battelle Memorial Institute, pp. 319-342.

Lee, J.H.W., Cheung, V. 1990. Generalized Lagrangian model for buoyant jets in current. Journal of Environmental Engineering 116(6), 1085–1105.

Lee, J.H.W., Cheung, V., Lai, C. 2008. JETLAG2008 – An Update. Technical Note, Croucher Laboratory of Environmental Hydraulics, the University of Hong Kong.

Lee, J.H.W., Chu, V.H. 2003. Turbulent Jets and Plumes. Kluwer Academic Publishers, Massachusetts, USA.

Lee, J.H.W., Neville-Jones, P. 1987. Initial dilution of horizontal jet in crossflow. Journal of Hydraulic Engineering 113(5), 615-629.

LeVeque, R.J. 2002. Finite Volume Methods for Hyperbolic Problems. Cambridge University Press, Cambridge, UK.

Lewis, R.E. 1997. Dispersion in Estuaries and Coastal Waters. John Wiley & Sons, Chichester.

Li, S., Hodgins, D.O. 2004. A dynamically coupled outfall plume-circulation model for effluent dispersion in Burrard Inlet, British Columbia. Journal of Environmental Engineering and Science 3, 433-449.

Liou, J., Tezduyar, T.E. A clustered element-by-element iteration method for finit element computations. In: R. Glowinski, Y.A. Kuznetsov, G. Meurant, J. Périaux,

O.B. Widlund (eds.), Proceedings of the 4th International Conference on Domain Decomposition Methods in Moscow, Russia, May 21-25, 1990, pp. 140-150.

Lomborg, U., Windelin, A. 2003. Hydrography and cohesive sediment modelling: application to the Rømø Dyb tidal area (MIKE 21 MT). Journal of Marine Systems 38(3-4), 287-303.

Lowrance, W.W. 1976. Of Acceptable Risk, William Kaufmann, Inc., Los Altos, CA.

Luhar, A.K., Britter, R.E. 1992. Random-walk modeling of buoyant-plume dispersion in the convective boundary layer. Atmospheric Environment 26A(7), 1283-1298.

Marchesiello, P., McWilliams, J.C., Shchepetkin, A. 2001. Open boundary conditions for long-term integration of regional oceanic models. Ocean Modelling 3, 1-20.

Marsaleix, P., Auclair, F., Estournel, C. 2006. Notes and correspondence – Considerations on open boundary conditions for regional and coastal ocean models. Journal of Atmospheric and Oceanic Technology 23, 1604-1613.

Martin, J.L., McCutcheon, S.C. 1998. Hydrodynamics and Transport for Water Quality Modeling. Lewis Publishers, New York, USA.

McCutcheon, S.C. 1990. Water Quality Modeling: Transport and Surface Exchange in Rivers. CRC Press, Inc., Boca Raton, Florida.

McDaniels, T., Small, M.J. 2004. Risk Analysis and Society. Cambridge University Press, New York, USA

Meinhold, A.F., Holtzman, S., DePhillips, M.P. 1996. Risk assessment for produced water discharges to Open Bays in Louisiana. In: M. Reed, S. Johnsen (eds.), Produced Water 2: Environmental Issues and Mitigation Technologies, Plenum Press, New York.

Mellor, G.L. 2004. Users Guide for a Three-dimensional, Primitive Equation, Numerical Ocean Model. Princeton University, Princeton, NJ 08544-0710.

Mellor, G.L., Ezer, T. 1995. Sea level variations induced by heating and cooling: An evaluation of the Boussinesq approximation in ocean model. Journal of Geophysical Research 100, 20565-20577.

Mellor, G.L., Ezer, T., Oey, L.-Y. 1994. The pressure gradient conundrum of sigma coordinate ocean models. Journal of Atmospheric and Oceanic Technology 11, 1126-1134.

Mellor, G.L., Kantha, L. 1989. An ice-ocean coupled model. Journal of Geophysical Research 94, 10937-10954.

Mellor, G.L., Oey, L.-Y., Ezer, T. 1998. Sigma coordinate gradient errors and the seamount problem. Journal of Atmospheric and Oceanic Technology 12, 1122-1131.

Mellor, G.L., Yamada, T. 1982. Development of a turbulent closure model for geophysical fluid problems. Review of Geophysics 20, 851-875.

Meteorological Institute, 2007. Numerical ocean models: MI-POM. Available at: http://www.met.no/english/r_and_d_activities/method/num_mod/ocean_mod/mi_pom.html (Access date: April 2007)

Moeller, J.C., Adams, E.E. 1994. Comparison of Eulerian-Lagrangian, random walk and hybrid methods of modeling pollutant transport. In: Proceedings of the Third International Conference on Estuarine and Coastal Modeling, Oak Brook, Illinois, September 8-10, 1993, pp. 609-623.

Mofarrah, A., Husain, T. 2010. Modeling for uncertainty assessment in human health risk quantification: a fuzzy based approach. In: D.A. Swayne, W. Yang, A.A. Voinov, A. Rizzoli, T. Filatova (eds), International Environmental Modelling and Software Society (iEMSs) 2010 International Congress on Environmental Modeling and Software modeling for Environment's Sake, Fifth Biennial Meeting, Ottawa, Canada.

Moore, A.M., Arango, H.G., Miller, A.J., Cornuelle, B.D., Di Lorenzo, E., Neilson, D.J. 2004. A comprehensive ocean prediction and analysis system based on the tangent linear and adjoint components of a regional ocean model. Ocean Modelling 7, 227-258.

Mukhtasor, Lye, L.M, Sharp, J. 2002. Methods of compliance evaluation for ocean outfall design and analysis. Environmental Management 30(4), 536–46

Mukhtasor, Husain, T., Veitch, B., Bose, N. 2004. An ecological risk assessment methodology for screening discharge alternatives of produced water. Human and Ecological Risk Assessment 10, 505-524.

Nakano, M., Povinec, P.P. 2003. Oceanic general circulation model for the assessment of the distribution of 137Cs in the world ocean. Deep-Sea Research II 50, 2803-2816.

Neff, J.M. 2002. Bioaccumulation in Marine Organisms, Effects of Contaminants from Oil Well Produced Water. Elsevier, Amsterdam, 452pp.

Neff, J.M., Langseth, D.E., Graham, E.M., Sauer Jr., T.C., Gnewuch, S.C. 1994. Transport and Fate of Non-BTEX Petroleum Chemicals in Soil and Groundwater. API Publication 4593. American Petroleum Institute, Washington, DC.

Neff, J.M., Lee, K, DeBlois, E.M. 2011. Produced water: Overview of composition, fates, and effects. In: J.M. Neff, K. Lee (eds.), Produced Water: Environmental Risks and Advances in Mitigation Technologies, Springer, pp. 3-54.

Neff, J.M., Johnsen, S., Frost, T.K., Utvik, T.I.R., Durell, G.S. 2006. Oil well produced water discharges to the North Sea. Part II: Comparison of deployed mussels (Mytilus edulic) and the DREAM model to predict ecological risk. Marine Environmental Research 62, 224-246.

Niu, H., Lee, K., Husain, T., Veitch, B., Bose, N. 2009. The PROMISE model for evaluation of the mixing of produced water in marine environment. Proceedings of the 20th IASTED international conference on modeling and simulation, MS 2009, July 6-8, 2009, Banff, AB, Canada.

Niu, H., Lee, K., Husain, T., Veitch, B., Bose, N. 2011. Experimental and modeling studies on the mixing behavior of offshore discharged produced water. In: J. Neff, K. Lee (eds.), Produced Water: Environmental Risks and Advances in Mitigation Technologies, Springer, pp. 223-234.

Noye, J. 1987. Numerical methods for solving the transport equation. In: J. Noye (ed.), Numerical Modelling: Applications to Marine Systems, Elsevier Science Publishers B.V., pp. 195-230.

Oey, L.-Y. 2005. A wetting and drying scheme for POM. Ocean Modelling 9, 133-150.

Oey, L.-Y. 2006. An OGCM with movable land-sea boundaries. Ocean Modelling 13, 176-195.

Oey, L.-Y., Ezer, T., Forristall, G., Cooper, C., DiMarco, S., Fan, S. 2005. An exercise in forecasting loop current and eddy frontal positions in the Gulf of Mexico. Geophysical Research Letters 32, L12611.

OGP (International Association of Oil and Gas Producers). 2004. Environmental Performance in the E&P Industry. 2003 Data. Report No. 359. OGP, London, UK, 32pp.

O'Reilly, J.E., Sauer, T.C., Jr., Ayers, R.C., Jr., Brandsma, M.G., Meek, R.P. 1988. Field verification of the OOC mud discharge model. In: Drilling Wastes, Proceedings of the 1988 International Conference on Drilling Wastes. Calgary, Alberta, Canada, April 5-8, 1988, Elsevier Applied Science Publishers Ltd., London, England, 1989.

Orlanski, I. 1976. A simple boundary condition for unbounded hyperbolic flows. Journal of Computational Physics 21, 251-269.

Palma, E.D., Matano, R.P. 1998. On the implementation of passive open boundary conditions for a general circulation model: The barotropic mode. Journal of Geophysical Research, January, 1319-1341.

Periáñez, R. 2006. Modeling surface radioactive spill dispersion in the Alboran Sea. Journal of Environmental Radioactivity 90, 48-67.

Periáñez, R., Elliott, A.J. 2002. A particle-tracking method for simulating the dispersion of non-conservative radionuclides in coastal waters. Journal of Environmental Radioactivity 58, 13-33.

Poulter, S.R. 1998. Monte Carlo simulation in environmental risk assessment - science, policy and legal issues. Risk, Health, Safety Environment 9(1), 7-13.

Ramaswami, A., Milford, J.B., Small, M.J. 2005. Integrated Environmental Modeling: Pollutant Transport, Fate, and Risk in the Environment. John Wiley & Sons, Inc., Hoboken, New Jersey.

Reed, M., Hetland, B., Ditlevsen, M.K., Ekrol, L. 2001. DREAM Version 2.0. Dose Related Risk Effect Assessment Model, Users Manual. SINEF Applied Chemistry, Environmental Engineering, Trondheim, Norway.

Reed, M., Rye, H. 2011. The DREAM model and the environmental impact factor: decision support for environmental risk management. In: J. Neff, K. Lee (eds.), Produced Water: Environmental Risks and Advances in Mitigation Technologies, Springer, pp. 189-203.

Reichardt, H. 1941. Über eine neue Theorie der freien Turbulenzen. ZAMM 21, 257-264.

Riddle, A.M., Beling, E.M., Murray-Smith, R.J. 2001. Modeling the uncertainties in predicting produced water concentrations in the North Sea. Environmental Modelling & Software 16, 659-668.

Ridge, M.M. 2002. Three Dimensional Simulation of Pollutant Dispersion in Coastal Waters. Ph.D. Thesis, Universitat Politecnica de Catalunya, Barcelona.

Robert, A.J. 1966. The integration of a low-order spectral form of the primitive meteorological equations. Journal of the Meteorological Society of Japan 44, 237-244.

Roberts, P.J.W. 1999. Modelling Mamala Bay outfall plumes. Parts I and II. Journal of Hydraulic Engineering 125, 564-583.

Roberts, P.J.W., Snyder, W.H., Baumgartner, D.J. 1989a. Ocean outfalls I: submerged waste field formation. Journal of Hydraulic Engineering 115, 1-25.

Roberts, P.J.W., Snyder, W.H., Baumgartner, D.J. 1989b. Ocean outfalls II: spatial evolution of submerged waste field. Journal of Hydraulic Engineering 115, 26-48.

Roberts, P.J.W., Snyder, W.H., Baumgartner, D.J. 1989c. Ocean outfalls III: effect of diffuser design on submerged waste field. Journal of Hydraulic Engineering 115, 49-70.

Robertson, R., Beckmann, A. 2001. A Comparison of POM and ROMS for Modeling Internal Tides in Weak Stratification. Second joint biannual Terrain-following modeling communities (POM, ROMS, SCRUM, SPEM) meeting, Boulder, Colorado, USA.

Ross, O.N.; Sharples, J. 2004. Recipe for 1-D Lagrangian particle tracking models in space-varying diffusivity. Limnology and Oceanography: Methods 2, 289-302.

Ruby, M.V., Davis, A., Link, T.E., Schoof, R., Chaney, R.L., Freeman, G.B., Bergstrom, P. 1993. Development of an in vitro screening test to evaluate the in vivo bioaccessibility of ingested mine-waste lead. Environmental Science &Technology 27 (13), 2870-2877.

Rye, H., Reed, M., Ekrol, N. 1998. The PARTRACK model for calculation of the spreading and deposition of drilling mud, chemicals and drill cuttings. Environmental Modelling & Software 13, 431-441.

Sabeur, Z.A., Tyler, A.O. 2004. Validation and application of the PROTEUS model for the physical dispersion, geochemistry and biological impacts of produced waters. Environmental Modelling & Software 19, 717-726.

Sabeur, Z.A., Tyler, A.O., Hockley, M.C. 2000. Development of a new generation modeling system for the prediction of the behaviour and impact of offshore

discharges to the marine environment. In: Proceedings of the Fifth International Conference on Health, Safety and Environment in Oil and Gas Exploration and Production, Society of Petroleum Engineers, Stavenger, Norway.

Salamon, P., Fernandez-Garcia, D., Gomez-Hernandez, J.J. 2006. A review and numerical assessment of the random walk particle tracking method. Journal of Contaminant Hydrology 87, 277-305.

Shaw, D.G., Farrington, J.W., Connor, M.S., Trippm, B.W., Schubel, J.R. 1999. Potential Environmental Consequences of Petroleum Exploration and Development on Grand Banks. New England Aquarium Aquatic Forum Series Report 99-3, Boston, 64.

Shchepetkin, A.F., McWilliams, J.C. 1998. Quasi-monotonic advection schemes based on explicit locally adaptive dissipation. Monthly Weather Review 126, 1541-1580.

Shchepetkin, A.F., McWilliams, J.C. 2003. A method for computing horizontal pressure-gradient force in an oceanic model with a nonaligned vertical coordinate. Journal of Geophysical Research 108(C3), 3090.

Shchepetkin, A.F., McWilliams, J.C. 2005. The Regional Ocean Modeling System: A split-explicit, free-surface, topography following coordinates ocean model. Ocean Modelling 9, 347-404.

Skåtun, H.M. 1996. A buoyant jet/plume model for subsea releases. In: M. Reed, S. Johnsen (eds), Produced Water 2: Environmental Issues and Mitigation Technologies. Plenum Press, New York and London, pp. 247-255.

Smagorinsky, J., Manabe, S., Holloway, J.L. 1965. Numerical results from a nine-level general circulation model of the atmosphere. Monthly Weather Review 93, 727-768.

Smit, M.G.D., Jak, R.G., Holthaus, K.I.E., Karman, C.C. 2003. An Outline of the DREAM Project and Development of the Environmental Impact Factor for Produced Water Discharges. Technical report R2003/376. Den Helder (NL): Netherlands Organisation for Applied Scientific Research (TNO), pages 36.

Smit, M.G.D., Jak, R.G., Rye, H., Frost, T.K., Singsaas, I. Karman, C.C. 2008. Assessment of environmental risks from toxic and nontoxic stressors; a proposed concept for a risk-based management tool for offshore drilling discharges. Integrated Environmental Assessment and Management 4, 173-183.

Smit, M.G.D., Frost, T.K., Johnsen, S. 2011. Achievements of risk-based produced water management on the Norweigian Continental Shelf (2002-2008). Integrated Environmental Assessment and Management 7(4), 668-677.

Smith, J.P., Brandsma, M.G., Nedwed, T.J. 2004. Field verification of the Offshore Operators Committee (OOC) mud and produced water discharge model. Environmental Modelling & Software 19, 739-749.

Smith, J.P., Mairs, H.L., Brandsma, M.G., Meek, R.P., Ayers, R.C. Jr. 1994. Field verification of the Offshore Operators Committee (OOC) produced water discharge model. In: Society of Petroleum Engineers Paper 28350 presented at the SPE 69th Annual Technical Conference and Exhibition, New Orleans, LA, September 25-28.

Sommerfeld, A. 1949. Partial differential equations. Lecture notes on Theoretical Physics, vol. 6. Academic Press, San Diego, CA.

Song, Y.T., Haidvogel, D. 1994. A semi-implicit ocean circulation model using a generalized topography following coordinate system. Journal of Computational Physics 115, 228-248.

Sørensen, O.R., Sørensen,L.S., Carlson, J. 2010. Parallelization of the flexible mesh modeling systems with MPI. In: International MIKE by DHI Conference 2010, Copenhagen, Denmark, pp. 30.1-30.8.

Stephenson, M.T. 1992. A Survey of produced water studies. In: J.P. Ray, R.F. Engelhardt (eds), Produced Water: Technological/Environmental Issues and SolutionsPlenum Press, New York, pp. 46.

Stolwijk, S., Villars, M.T., Laane, R., Baart, A., Dick, S., Svendsen, E. Tappin, A., De Vries, A. 1998. Comparison of the performance of five different water quality models of the North Sea. Environmental Modelling & software 13, 455-460.

Suh, S.W. 2006. A hybrid approach to particle tracking and Eulerian-Lagrangian models in the simulation of coastal dispersion. Environmental Modelling & Software 21, 234-242.

Talbot, J.W., Talbot, G.A. 1974. Diffusion in shallow seas and in English coastal and estuarine waters. Rapp. Proc. Verb., Cons. Int. Explor. Mer. 167, 93-110.

Tang, Y., Grimshaw, R. 1996. Radiation boundary conditions in barotropic coastal ocean numerical models. Journal of Computaional Physics 123, 96-110.

Thatcher, M., Robson, M., Henriquez, L.R. 1999. A User Guide for the Evaluation of Chemicals Used and Discharged Offshore, Version 1.0. A CIN revised CHARM III report. Netherlands Ministry of Transportation, The Netherlands.

Thatcher, M., Robson, M., Henriquez, L.R., and Karman, C.L. 2001. A User Guide for the Evaluation of Chemicals Used and Discharged Offshore, Version 1.2. A CIN revised CHARM III Report, Charm Implementation Network (CIN), European Oilfield Speciality Chemicals Association (EOSCA).

Thomson, D.J. 1987. Criteria for the selection of stochastic models of particle trajectories in turbulent flows. Journal of Fluid Mechanics 180, 529-556.

Tomicic, B., Lützen, A., Mark, O. 2001. Integrated modeling of the sewer system and the receiving water for the island of Ischia. In: R.W. Brashear, C. Maksinovic (eds.), Urban Drainage Modeling, Proceedings of the Specialty Symposium Held in Conjunction with the World Water and Environmental Resources Congress, Orlando, Florida, May 20-24, 2001, American Society of Civil Engineers, pp. 548-557.

Tompson, A.F.B., Schafer, A.L., Smith, R.W. 1996. Impacts of physical and chemical heterogeneity on contaminant transport in a sandy porous medium. Water Resources Research 32(4), 801-818.

Taylor, G.A., Bailey, C., Cross, M. 2003. A vertex-based finite volume method applied to non-linear material problems in computational solid mechanics. International Journal for Numerical Methods in Engineering 56, 507-529.

USEPA. 1992. Quality Criteria for Water 1992. U.S. Environmental Protection Agency, Office of Water, Criteria and Standards Division, Washington, DC.

USEPA. 1995. Water Quality Standards; Establishment of Numeric Criteria for Priority Toxic Pollutants; States' Compliance-Revision of Metals. Interim Final Rule, Notice of Data Availability and Request for Comments. FR60, No. 86, Thursday, May4, 1995, 22229.

USEPA. 1996. Summary Report for the Workshop on Monte Carlo Analysis Risk Assessment Forum. U.S. Environmental Protection Agency, Washington, DC. EPA-630-R-96-010.

USEPA. 2002. User's Manual for Environmental Fluid Dynamics Code, Hydro Version (Draft). US EPA, Region 4, Atlanta, Georgia.

Utivik, T. 1999. Chemical characteristics of produced water from four offshore oil production platforms in the North Sea. Chemosphere 39, 2593-2606.

Vaishnav, D.D., Babeu, L. 1987. Comparison of occurrence and rates of chemical biodegradation in natural waters. Bulletin of Environmental Contamination and Toxicology 39, 237-244.

Vanderborght, J.-P, Folmer, I.M., Aguilera, D.R., Uhrenholdt, T., Regnier, P. 2007. Reactive-transport modelling of C, N, and O2 in a river–estuarine–coastal zone system: Application to the Scheldt estuary (MIKE 21 and ECOLab). Marine Chemistry 106(1-2), 92-110.

Van der Linden, A.C. 1978. Degradation of oil in the marine environment. Dev. Biodegradation Hydrocarbons 1, 165-200.

Van Genuchten, M.Th. 1976. On the accuracy and efficiency of several numerical schemes for solving the convective-dispersive equation. In: Proceedings of the First International Conference on Finite Elements in Water Resources, Princeton University, Princeton, New Jersey, pp. 1.71-1.90.

Wai, O.W.-H., Lu, Q. 2000. An efficient parallel model for coastal transport process simulation. Advances in Water Resources 23,747-764.

Wakeham, S.G., Canuel, E.A., Doering, P.H. 1986. Geochemistry of volatile organic compounds in seawater: mesocosm experiments with ^{14}C-model compounds. Geochimica et Cosmochimica Acta 50, 1163-1172.

Wakeham, S.G., Canuel, E.A., Doering, P.H., Hobbie, J.E., Helfrich, J.V.K., Lough, G.R.G. 1985. The biogeochemistry of toluene in coastal seawater: radiotracer experiments in controlled ecosystems. Biogeochemistry 1, 307-328.

Wakeham, S.G., Davis, A.C., Karas, J.L. 1983. Mesocosm experiments to determine the fate and persistence of volatile organic compounds in coastal seawater. Environmental Science & Technology 17, 611-617.

Wang, P., Song, Y.T., Chao, Y., Zhang, H. 2005. Parallel Computation of the Regional Ocean Modeling System. The international Journal of High Performance Computing Applications 19(4), 375-385.

Webb, A.T., Mansour, N.N. 2000. Towards LES models of jets and plumes. Center for Turbulence Research, Annual Research Briefs 2000, 229-240.

Wendt, J.F. 2009. Computational Fluid Dynamics: an Introduction. Springer, Berlin, German.

Westerink, J.J., Shea, D. 1989. Consistent higher degree Petrov-Galerkin methods for the solution of the transient convection-diffusion equation. International Journal for Numerical Methods in Engineering 28(5), 1077-1101.

Wu, J. 1980. Wind-stress coefficient over sea surface near neutral conditions-a revisit. Journal of Physical Oceanography 10, 727-740.

Yang, X.S. 2008. Introduction to Computational Mathematics. World Scientific Publishing Co. Pte. Ltd., Singapore.

Yao, T., Tang, C.L., Peterson, I. 2000. Modeling the seasonal variation of sea ice in the Labrador Sea with a coupled multi-category ice model and the Princeton Ocean Model. Journal of Geophysical Research 105, 1153-1165.

Yapa, P.D., Zheng, L. 1997. Simulation of oil spills from underwater accidents I: Model development. Journal of Hydraulic Research 35(5), 673-687.

Zhang, X.Y. 1995. Ocean Outfall Modeling - Interfacing Near and Far Field Models with Particle Tracking Method. Ph.D. Thesis, Massachusetts Institute of Technology.

Zhang, X.Y., Adams, E.E. 1999. Prediction of near field plume characteristics using far field circulation model. Journal of Hydraulic Engineering 125(3), 233-241.

Zhang, A., Parker, B., Wei, E. 2002. Assimilation of water level data into a coastal hydrodynamic model by an adjoint opticmal technique. Continental Shelf Research 22, 1909-1934.

Zhao, L. 2007. Modeling and Assessment of Produced Water Discharges Emitted from Offshore Petroleum Plat forms in the East Coast of Canada. M.A.S. Thesis, Concordia University, Montreal.

Zhao, L., Chen, Z., Lee, K. 2008. A risk assessment model for produced water discharge from offshore petroleum platforms-development and validation. Marine Pollution Bulletin 56, 1890-1897.

Zimmermann, H.J. 2001. Fuzzy Set Theory and Its Application, fourth ed. Kluwer Academic Publishers, Norwell, MA, USA.

APPENDIX
A

PUBLICATIONS

Journal papers

- <u>Lin Zhao</u> *et al*. (2011). Modelling the dispersion of wastewater discharges from offshore outfalls: a review. Environmental Review 19, 107-120.

- Zhi Chen, Amir M.Y., <u>Lin Zhao</u>, Zetian Mi (2011) A review of environmental effects and management of nanomaterials. Toxicological & Environmental Chemistry 93, 1227-1250.

- Zhi Chen, <u>Lin Zhao</u>, Kenneth Lee (2010). Environmental risk assessment of offshore produced water discharges using a hybrid fuzzy-stochastic modeling approach. Environmental Modelling & Software 25, 782-792.

- <u>Lin Zhao</u> *et al*. (2008). A risk assessment model for produced water discharge from offshore petroleum platforms-development and validation. Marine Pollution Bulletin 56, 1890-1897.

- Zhi Chen, <u>Lin Zhao</u>, Kenneth Lee, Charles Hannath (2007). Modeling and assessment of the produced water discharges from offshore petroleum platforms. Water Qual. Res. J. Canada 42(4), 303-310.

Book chapter

- Zhi Chen, Lin Zhao, Kenneth Lee (2011). Fuzzy-Stochastic Risk Assessment Approach for the Management of Produced Water Discharges. In: Lee K., Neff J. (Eds.), Produced Water: Environmental Risks and Advances in Mitigation Technologies. Springer, pp 493-509.

Conference papers

- Zhao, L., Chen, Z., Lee, K., 2009. An extended study of three dimensional mass advection-dispersion modeling for ocean discharges. 2009 International Conference on Scientific Computation and Differential Equations (SciCADE09), Beijing, China.

- Zhao, L., Chen, Z., Lee, K., 2007. Integrated modeling and risk assessment for the management of produced water discharges. International Association of Science and Technology for Development, The 16th IASTED International Conference on Applied Simulation and Modelling, Palma de Mallorca, Spain, p.440-445.

APPENDIX
B

DEVELOPMENT OF THREE DIMENSIONAL FINITE ELEMENT METHOD (FEM) FOR FAR FIELD POLLUTANT TRANSPORT MODELING

Historically, the finite element method originates from the field of structural mechanics. In 1960s, Zienkiewics and Cheung (1965) first developed FEM for the application of simple flow problems. After that, many studies have developed the finite element method in fluid dynamics. One of the standard FEM is the Galerkin finite element method (GFEM). Though many new approaches have been developed using modified Galerkin principle in various ways to deal with specific simulation problems (e.g. stability, numerical diffusion), most of these methods still require finer mesh to achieve better results which could be done with GFEM (Gresho *et al.*, 2000). Therefore, in the following context, the GFEM is used for space discretization, and the Crank-Nicolson scheme which is semi-implicit with second-order accuracy is used for time differencing.

Weak forms of the advection-diffusion equation

A standard weighted residual approach with Galerkin-type weighting functions is used to determine approximate solutions of the advection-diffusion equation (Equation 3.48). With a properly selected test functions $W(x, y, z)$, Equation 3.48 can be formed as:

$$\left(\frac{\partial C}{\partial t} + \frac{\partial(UC)}{\partial x} + \frac{\partial(VC)}{\partial y} + \frac{\partial(WC)}{\partial z} - \frac{\partial}{\partial x}\left(D_x \frac{\partial C}{\partial x} \right) - \frac{\partial}{\partial y}\left(D_y \frac{\partial C}{\partial y} \right) - \frac{\partial}{\partial z}\left(D_z \frac{\partial C}{\partial z} \right) - S \right) W = 0 \quad (D1)$$

By integrating and rearranging, Equation (3.57) becomes:

$$\int W \frac{\partial C}{\partial t} + \int W \left(\frac{\partial(UC)}{\partial x} + \frac{\partial(VC)}{\partial y} + \frac{\partial(WC)}{\partial z} \right) = \int WS + \int W \left(\frac{\partial}{\partial x}\left(D_x \frac{\partial C}{\partial x} \right) + \frac{\partial}{\partial y}\left(D_y \frac{\partial C}{\partial y} \right) + \frac{\partial}{\partial z}\left(D_z \frac{\partial C}{\partial z} \right) \right) \quad (D2)$$

For the second order diffusion terms, we have obtained the following result via integration by parts:

$$\int W \nabla \cdot (\vec{D} \cdot \nabla C) = \int_\Gamma W \vec{n} \cdot (\vec{D} \cdot \nabla C) - \int \nabla W \cdot (\vec{D} \cdot \nabla C) \quad (D3)$$

where $\vec{n}$ is the outward pointing unit normal vector. Γ denotes the boundary of the whole domain Ω. Substituting Equation D3 to Equation D2, leads to the weak form of the governing equation, which provides the natural boundary conditions of the solution in regard to diffusive fluxes.

$$\int_\Omega W \frac{\partial C}{\partial t} + \int_\Omega W \left(\frac{\partial(UC)}{\partial x} + \frac{\partial(VC)}{\partial y} + \frac{\partial(WC)}{\partial z} \right) + \int_\Omega \left[\frac{\partial W}{\partial x}\left(D_x \frac{\partial C}{\partial x} \right) + \frac{\partial W}{\partial y}\left(D_y \frac{\partial C}{\partial y} \right) + \frac{\partial W}{\partial z}\left(D_z \frac{\partial C}{\partial z} \right) \right]$$
$$= \int_\Omega WS + \oint_\Gamma W \left[\left(D_x \frac{\partial C}{\partial x} \right) + \left(D_y \frac{\partial C}{\partial y} \right) + \left(D_z \frac{\partial C}{\partial z} \right) \right] \quad (D4)$$

Discretization of the weak form

The FEM is based upon the weak form to obtain a set of ordinary differential equations for the unknown variables (e.g. the nodal values of concentration C). Once the weak form is established, the standard Galerkin approximation can now be employed for solving Equation D4. For computer efficiency, we chose a linear element fulfilling the minimal global and local continuity requirement. The hexahedral isoparametric element with eight nodes is used, which permits the global solutions to be applicable for both regular and irregular meshes. To obtain the finite element equations, it is required that suitable functions for the variable can be approximated locally within an element. Suppose that the variable C can be approximated linearly within an element *e*, we can express the variable as

$$C^e = \sum_N \Phi^e_N C^e_N = \langle \boldsymbol{\Phi} \rangle \{ \mathbf{C} \} \tag{D5}$$

where Φ^e_N are the local element shape functions; N is the number of element nodes, here $N = 8$ for a hexahedron element; $< >$ and $\{ \ \}$ represent matrix sets with a row and a column vector, respectively.

The standard Galerkin method approximate the solution using the same functions for both test functions W and the shape functions Φ over the elements. Therefore, substituting Equation D5 into Equation D4, we obtain the global algebraic system of equations for the state variable C, expressed in matrix-vector form as

$$\mathbf{M} \frac{\partial \{C\}}{\partial t} + \mathbf{N(u)}\{C\} + \mathbf{K}\{C\} = \mathbf{S} + \mathbf{F}\{C\} \tag{D6}$$

The components of Equation D6 are expressed as follows in terms of the elementary weak form *e*, and [ ] represents a matrix set.

The mass matrix is

$$[\mathbf{M}]_\Omega = \sum_e \int_{\Omega^e} \{\mathbf{\Phi}\}\langle\mathbf{\Phi}\rangle d\Omega$$

(D7)

The convection matrix is

$$[\mathbf{N(u)}]_\Omega = \sum_e \int_{\Omega^e} \{\mathbf{\Phi}\}\langle\mathbf{\Phi}\rangle\{\mathbf{u}\}\langle\frac{\partial\mathbf{\Phi}}{\partial x}\rangle d\Omega + \sum_e \int_{\Omega^e} \{\mathbf{\Phi}\}\langle\mathbf{\Phi}\rangle\{\mathbf{v}\}\langle\frac{\partial\mathbf{\Phi}}{\partial y}\rangle d\Omega + \sum_e \int_{\Omega^e} \{\mathbf{\Phi}\}\langle\mathbf{\Phi}\rangle\{\mathbf{w}\}\langle\frac{\partial\mathbf{\Phi}}{\partial z}\rangle d\Omega \quad \text{(D8)}$$

The diffusion matrix is

$$[\mathbf{K}]_\Omega = \sum_e \int_{\Omega^e} \{\frac{\partial\mathbf{\Phi}}{\partial x}\}\langle\mathbf{\Phi}\rangle\{\mathbf{D_x}\}\langle\frac{\partial\mathbf{\Phi}}{\partial x}\rangle d\Omega + \sum_e \int_{\Omega^e} \{\frac{\partial\mathbf{\Phi}}{\partial y}\}\langle\mathbf{\Phi}\rangle\{\mathbf{D_y}\}\langle\frac{\partial\mathbf{\Phi}}{\partial y}\rangle d\Omega + \sum_e \int_{\Omega^e} \{\frac{\partial\mathbf{\Phi}}{\partial z}\}\langle\mathbf{\Phi}\rangle\{\mathbf{D_z}\}\langle\frac{\partial\mathbf{\Phi}}{\partial z}\rangle d\Omega \quad \text{(D9)}$$

The source vector is

$$[\mathbf{S}]_\Omega = \sum_e \int_{\Omega^e} \{\mathbf{\Phi}\}\langle\mathbf{\Phi}\rangle\{\mathbf{S}\} d\Omega$$

(D10)

The forcing vectors along the boundary edges are

$$[\mathbf{F}]_\Omega = \sum_e \oint_{\Gamma^e} \{\mathbf{\Phi}\}\langle\mathbf{\Phi}\rangle\{\mathbf{D_x}\}\langle\frac{\partial\mathbf{\Phi}}{\partial x}\rangle n_x d\Gamma + \sum_e \oint_{\Gamma^e} \{\mathbf{\Phi}\}\langle\mathbf{\Phi}\rangle\{\mathbf{D_y}\}\langle\frac{\partial\mathbf{\Phi}}{\partial y}\rangle n_y d\Gamma + \sum_e \oint_{\Gamma^e} \{\mathbf{\Phi}\}\langle\mathbf{\Phi}\rangle\{\mathbf{D_z}\}\langle\frac{\partial\mathbf{\Phi}}{\partial z}\rangle n_z d\Gamma$$

(D11)

where in the forcing matrix, (n_x, n_y, n_z) are the direction cosines of the outward pointing normal to the boundary. Integration of the items in [$\mathbf{F}$] matrix is performed along the boundaries in two dimensions.

The isoparametric element was first studied by Zienkiewicz and his associates (Zienkiewicz, 1971). The isoparametric element utilizes a nondimensionalized coordinate and therefore is one of the natural coordinate elements. As shown in Figure D-1, the isoparametric coordinates (ξ, η, ζ) whose values range from 0 to ±1 are established at the centroid of the element. In the isoparametric element for a linear variation of the geometry and variable, the shape functions $\mathbf{\Phi}$ can be expressed as
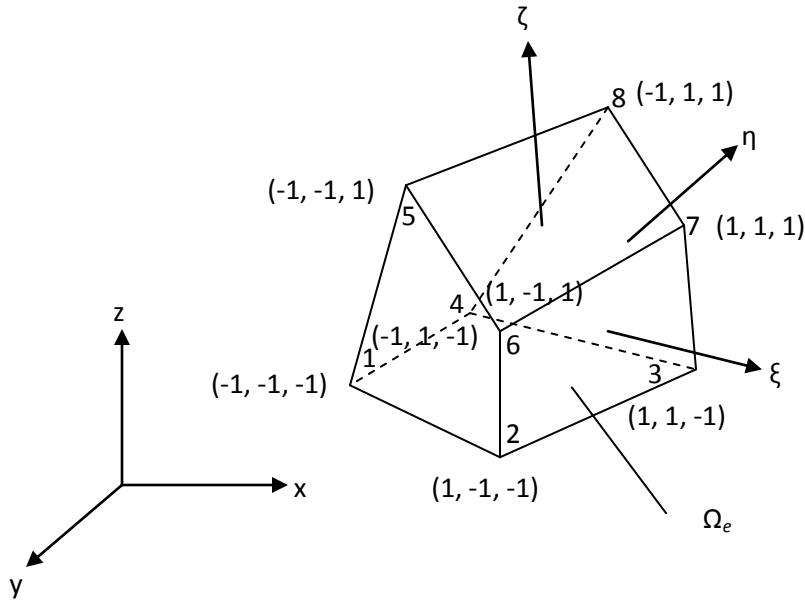
Figure D-1 Hexahedral isoparametric element – 8 nodes linear variation (reproduced from Chung (2002))

$$\{\boldsymbol{\Phi}\} = \begin{Bmatrix} \dfrac{1}{8}(1-\xi)(1-\eta)(1-\zeta) \\[2mm] \dfrac{1}{8}(1+\xi)(1-\eta)(1-\zeta) \\[2mm] \dfrac{1}{8}(1+\xi)(1+\eta)(1-\zeta) \\[2mm] \dfrac{1}{8}(1-\xi)(1+\eta)(1-\zeta) \\[2mm] \dfrac{1}{8}(1-\xi)(1-\eta)(1+\zeta) \\[2mm] \dfrac{1}{8}(1+\xi)(1-\eta)(1+\zeta) \\[2mm] \dfrac{1}{8}(1+\xi)(1+\eta)(1+\zeta) \\[2mm] \dfrac{1}{8}(1-\xi)(1+\eta)(1+\zeta) \end{Bmatrix} \qquad (D12)$$

The coordinate transformation is straightforward. The global x, y, z coordinate system certainly varies linearly on the physical domain Ω_e, hence,

$$X^e = \sum_N \Phi_N^e X_N^e = \langle\mathbf{\Phi}\rangle\{\mathbf{X}\} \tag{D13}$$

$$Y^e = \sum_N \Phi_N^e Y_N^e = \langle\mathbf{\Phi}\rangle\{\mathbf{Y}\} \tag{D14}$$

$$Z^e = \sum_N \Phi_N^e Z_N^e = \langle\mathbf{\Phi}\rangle\{\mathbf{Z}\} \tag{D15}$$

The integration over the domain referenced to the Cartesian coordinates must be changed to the domain now referenced to the isoparametric coordinates

$$\iiint dxdydz = \int_{-1}^{1}\int_{-1}^{1}\int_{-1}^{1} |J| d\xi d\eta d\zeta \tag{D16}$$

where J is called Jacobian matrix given by

$$[J] = \begin{vmatrix} \dfrac{\partial x}{\partial \xi} & \dfrac{\partial y}{\partial \xi} & \dfrac{\partial z}{\partial \xi} \\[2mm] \dfrac{\partial x}{\partial \eta} & \dfrac{\partial y}{\partial \eta} & \dfrac{\partial z}{\partial \eta} \\[2mm] \dfrac{\partial x}{\partial \zeta} & \dfrac{\partial y}{\partial \zeta} & \dfrac{\partial z}{\partial \zeta} \end{vmatrix} \tag{D17}$$

The integration of the main matrices from Equation D7-D11 is performed by means of the Gaussian quadrature (Hildebrand, 1956). For the three dimensional case we carried out here, the general form of integration is written as follows:

$$\int_{-1}^{1}\int_{-1}^{1}\int_{-1}^{1} g(\xi,\eta,\zeta) d\xi d\eta d\zeta = \sum_{i=1}^{n}\sum_{j=1}^{n}\sum_{k=1}^{n} w_i w_j w_k g(\xi_i,\eta_j,\zeta_k) \tag{D18}$$

where w_i, w_j, w_k are the weight coefficients, and $g(\xi_i,\ \eta_j,\ \zeta_k)$ denote the abscissa representing the values of the functions $g(\xi,\eta,\zeta)$ corresponding to the n Gaussian points.

Solution Method

For time dependent problems, the matrix equation (Equation D6) can be expressed as

$$(\mathbf{M} + \alpha\Delta t(\mathbf{N(u)} + \mathbf{K} - \mathbf{F}))\{C^{n+1}\} = (\mathbf{M} - (1-\alpha)\Delta t(\mathbf{N(u)} + \mathbf{K} - \mathbf{F}))\{C^n\} + \Delta t\mathbf{S} \qquad \text{(D19)}$$

With $\alpha = 0.5$, the scheme is called Crank-Nicolson scheme which is semi-implicit and second order accurate. In general, the resultant space-time Crank-Nicolson-Galerkin method gives better solutions for most types of equations (Padilla *et al.*, 1997; Noorishad *et al.*, 1992).

In order to solve Equation D19, assembling global matrices are required for many iteration methods which need a large amount of computational costs and storage. Such methods will not be suitable for the three dimensional FEM introduced above to conduct large system case studies. Therefore, the Generalized Minimal Residual (GMRES) algorithm is used to solve the time dependent problems as in Equation D19. The GMRES iterative algorithm is based on the property of minimizing the norm of the residual vector over a Krylov space. Detailed discussions of Krylov space can be found in Householder (1964). The GMRES algorithm has been proved to be efficient for non-systematic nonlinear, time dependent problems, and indefinite matrices (Saad and Schultz, 1986; Saad, 1996; Chung, 2002). The method does not need computation and storage of the global matrix and therefore it is very suitable for mesh refinement and large system simulation.

For time dependent problems like Equation D19, preconditioning of the matrix is necessary in order to obtain the convergence of the iterative method. In the present study, the main diagonal of the mass matrix is used as the preconditioning matrix.

A testing example

A test case as described in Section 6.2 is conducted using the developed FEM method. Only grid resolution of 1 km and 1-day simulation run is evaluated in comparison with analytical solution, FDM, RWPT method in consideration of the unbearable computational cost using FEM for the test case. Simulations using FDM or RWPT method for such test case only take a few minutes, while computational costs using FEM under basically the same conditions are days by using a personal computers.

Other than the computational results, FEM can generate much better results even with a relatively coarse grid resolution than FDM and RWPT method. The case example results are shown in Figure D-2 and D-3. Figure D-2 shows the concentration distribution pattern at the discharge depth. The result from FEM (Figure D-2b) is very close to the exact solution (Figure D-2a), though numerical diffusions are spotted in the vicinity area (upstream) of the source which is similar to result from FDM, suggesting that higher resolutions may be required in areas with high concentration gradients. Figure D-2b also shows that in areas a little further away from the source, results are almost identical to the exact solution, demonstrating that adaptable grid resolutions, such as high grid resolution in areas close to the source and relatively lower grid resolution in areas further away would be plausible for FEM. Figure D-3 shows the comparison of pollutant centerline concentration. Except the concentration at the discharge point, result of FEM is basically the same as the analytical solution, demonstrating the high accuracy of FEM. For the problem of computational costs, parallel computation should be helpful to improve the computational efficiency in future studies. The developed FEM method can also be used

on an unstructured grid system. Such advantage is especially helpful for a complex domain with shoreline along boundaries.
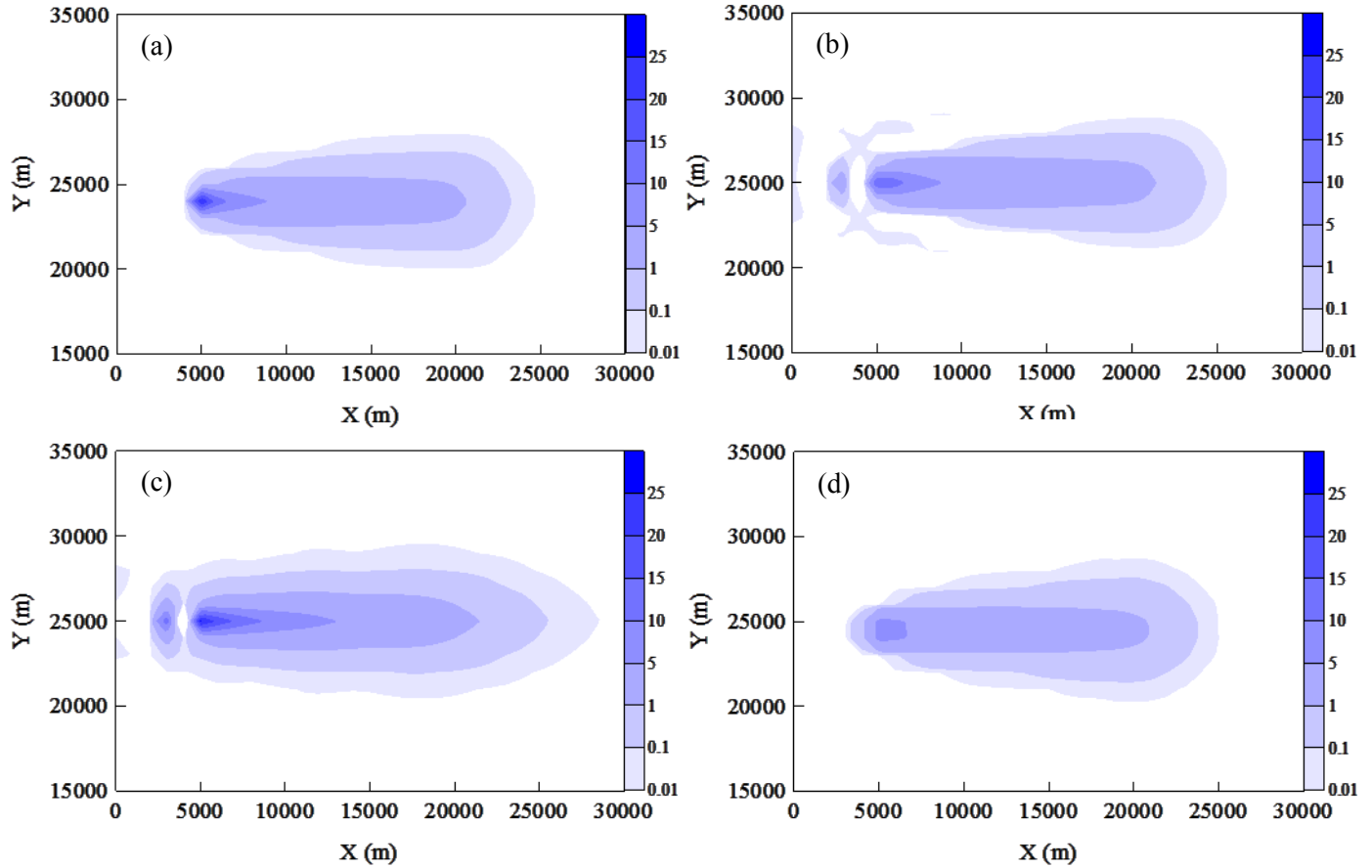

Figure D-2 Pollutant concentration ($\mu g \ L^{-1}$) profiles at a depth of 40m in a steady flow condition, 1 km grid resolution after 1-day model run, using: (a) the exact analytical solution; (b) FEM; (c) FDM; and (d) RWPT with a particle resolution of 144000 particles d^{-1}
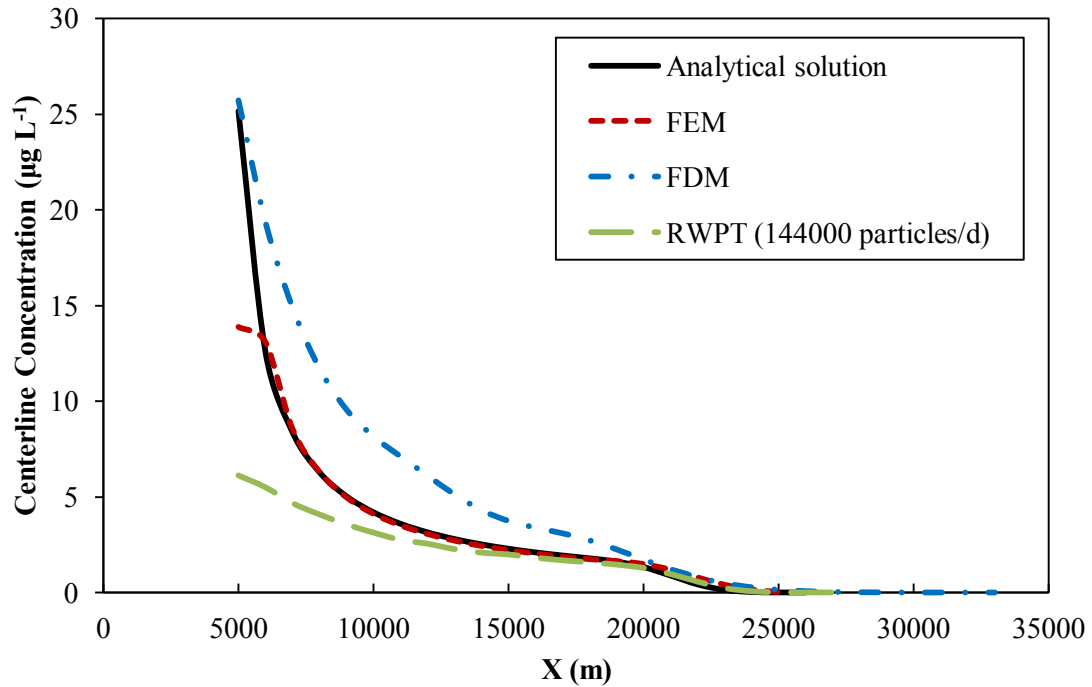
Figure D-3 Centerline pollutant concentration comparison

References

Chung, T.J. 2002. Computational Fluid Dynamics. Cambridge University Press, Cambridge, UK.

Gresho, P.M., Sani, R.L., Engelman, M.S. 2000. Incompressible Flow and the Finite Element Method Volume 1: Advection-Diffusion, West Sussex: John Wiley & Sons Ltd.

Hildebrand, F.B. 1956. Introduction to Numerical Analysis, New York: McGraw-Hill.

Householder, A.S. 1964. Theory of Matrices in Numerical Analysis. Johnson, CO: Blaisdell.

Noorishad, J., Tsang, C.F., Perrochet, P., Musy, A. 1992. A perspective on the numerical solution of convection-dominated transport problems: a price to pay for the easy way out. Water Resources Res. 28, 551-561.

Padillar, F., Secretan, Y., Leclerc, M. 1997. On open boundaries in the finite element approximation of two-dimensional advection-diffusion flows. International Journal for Numerical Methods in Engineering 40, 2493-2516.

Saad, Y. 1996. Iterative Methods for Sparse Linear System. Boston: PWS Publishing.

Saad, Y., Schultz, M.H. 1986. GMRES: a generalized minimal residual algorithm for solving nonsymmetric linear systems. SIAM J. Sci. Stat. Comp. 7, 856-869.

Zienkiewicz, O.C. 1971. The Finite Element Method in Engineering Science, 2nd, ed. New York: McGraw-Hill.

Zienkiewics, O.Z., Cheung, Y.K. 1965. Finite elements in the solution of field problems. The Engineer, 507-510.